APRIL 15, 1990

Analytical CHEMISTRY

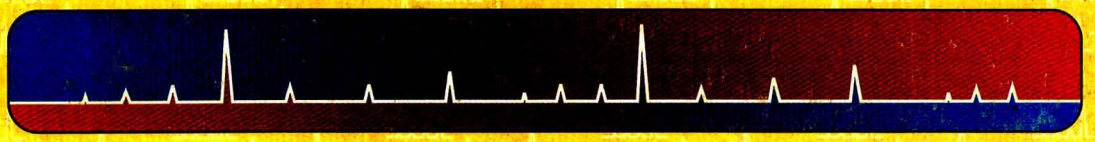

CONTINUOUS-FLOW *FAST ATOM* BOMBARDMENT MASS SPECTROMETRY

477 A

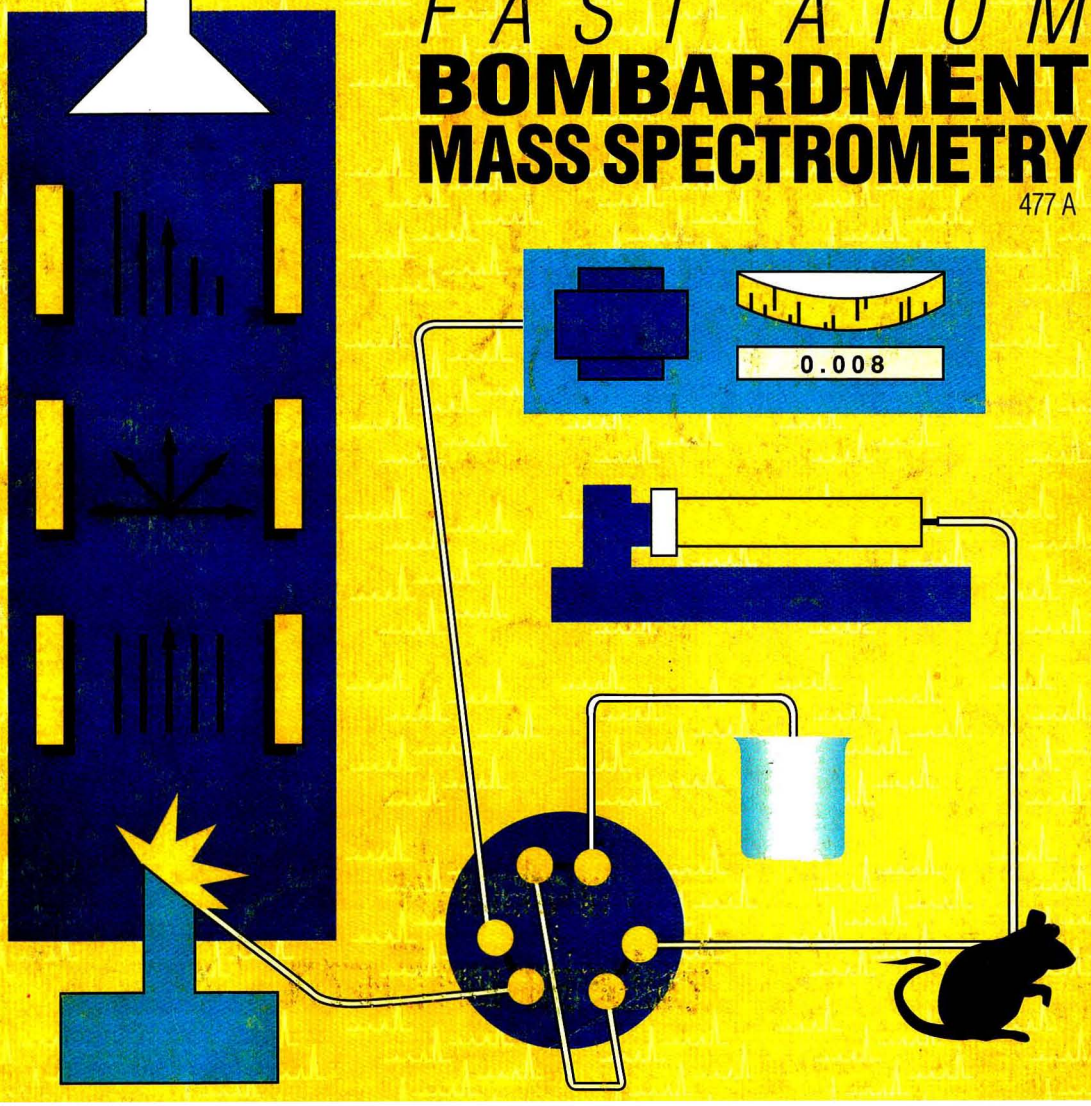

Spectroscopy for Research... SLM Leads the Way

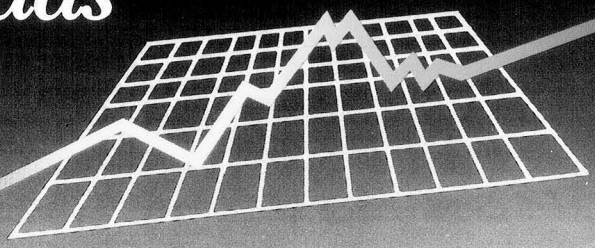

SLM Instruments is the leader in the innovative design and manufacture of spectrophotometers and spectrofluorometers for research. From our introduction of fluorescence polarization and time-resolved spectroscopy using the T-Optics™ lightpath, to our patented dual wavelength system, to the world's only multi-harmonic fast Fourier-transform fluorometer, we continue to explore and expand the frontiers of spectroscopy.

Our comprehensive line of instruments and accessories answers the demands of the widest range of research applications:

Fluorescence Polarization and Photon Counting

Highest sensitivity in its class • T-Optics polarization • Dual emission wavelengths • Simultaneous multiparameter measurements • Photon counting, analog, and millisecond kinetics on each of three channels • *SLM 8000C™ Photon Counting Spectrofluorometer*

Circle 134

Fluorescence Lifetimes

Picosecond lifetimes • Dynamic depolarization • Phase resolved spectroscopy • Three-frequency, continuous, and multi-harmonic fast Fourier-transform instruments • *SLM 4800C™ and SLM 4800S™ Lifetime Spectrofluorometers and SLM 48000MHF™ Multi-harmonic Fourier Fluorometer*

Circle 135

Fluorescence in an Integrated Package

Outstanding sensitivity and resolution • Complete scanning, ratiometric, and timebase capabilities • Keyboard or computer control • *SPF-500C™ Spectrofluorometer*

Circle 136

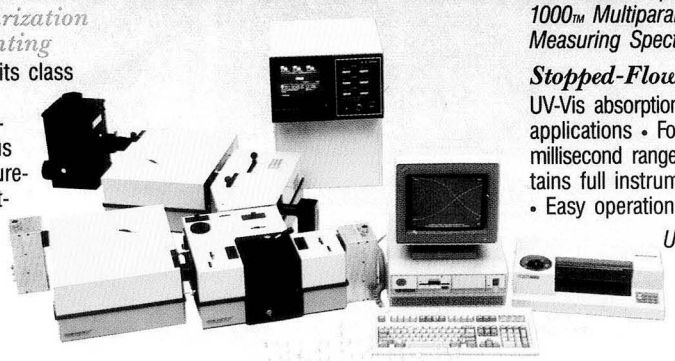

Dual Wavelength UV-Visible Spectrophotometry

Simplifies difficult analyses such as turbid samples, highly scattering samples, whole tissue preparations, and other complex systems • Dual wavelength and split beam modes • Millisecond reaction rate studies • Stand-alone operation or computer control • *DW-2000™ Dual Wavelength UV-Visible Spectrophotometer*

Circle 137

Intracellular Calcium Measurements

Designed for dual wavelength fluorescent probes • Simultaneous multiple probe measurements • Unmatched specifications • *DMX-1000™ Multiparameter Cation Measuring Spectrofluorometer*

Circle 138

Stopped-Flow Kinetics

UV-Vis absorption and fluorescence applications • For reactions in the millisecond range or longer • Maintains full instrument capabilities • Easy operation

Circle 139

Use the Reader Service Numbers, or call or write to us for more information on any SLM products.

SLM AMINCO®

SLM Instruments, Inc., 810 West Anthony Drive, Urbana, IL 61801
(217) 384-7730 • (800) 637-7689 • Telex 206079 • FAX (217) 384-7744

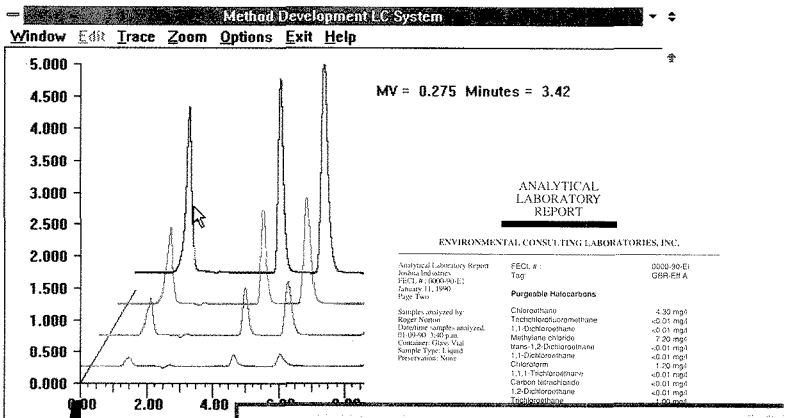

Point your way to effortless chromatography!

Finally, chromatography data management is easy with Spectra STATION.™

Fast, flexible and intuitive, Spectra STATION points the way to custom chromatography data management. Now you can develop methods for your LC or GC with just the click of a mouse.

There is no difficult learning curve. Our mouse-driven interface lets you integrate peaks and optimize parameters quickly.

Develop your chromatography method right on screen, knowing that all revisions are saved in the built-in database.

Customizing reports is easy. Select the results you want to report and Spectra STATION prints them automatically, on a form of your choice.

Effortless chromatography data management—Spectra STATION makes it automatic. For more information, call us at **800-424-7666.**

VISIT US AT F.A.S.E.B.– BOOTH 1605

Spectra-Physics

Discover the Quality

Business Partner

Circle 130 for literature. Circle 131 for a sales representative.

DIVIDE AND CONQUER

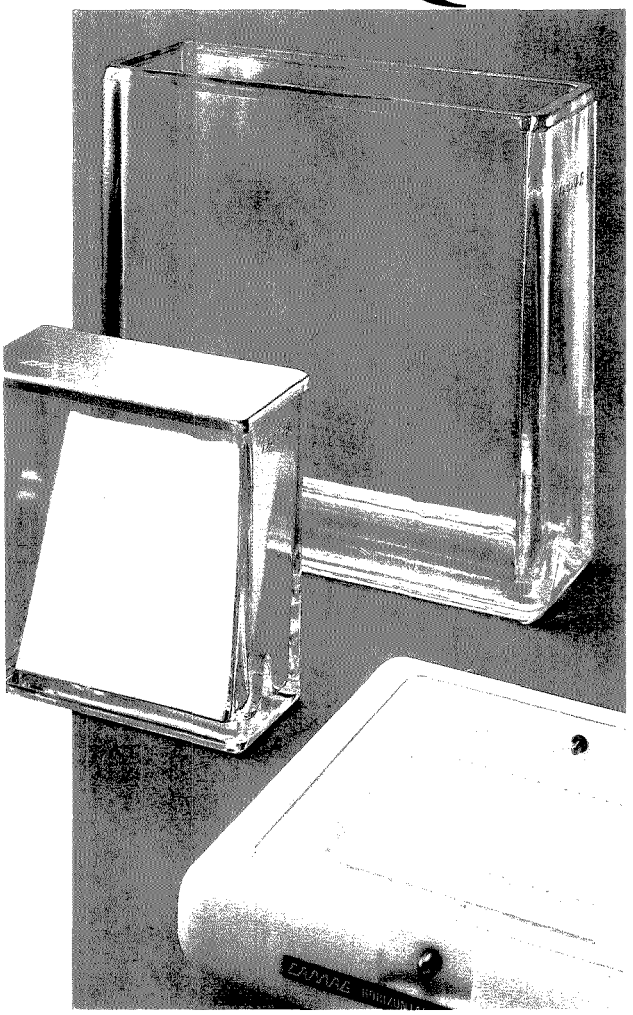

Modern Thin-Layer Chromatography combines precision, speed and versatility.

As an analyst, you face the challenge of separation. Instrumental TLC allows you to divide your analyte and conquer the result, whether in research or daily routine.

We offer you TLC separation at different levels of sophistication.

Chromatogram development in a chamber is as old as the science itself. Only CAMAG quality chambers ensure the chromatographic conditions for consistent results. **Twin Trough Chambers** – unique from CAMAG – conserve solvent, minimizing your disposal problem.

Conquering a large number of samples is easy with the **Horizontal Developing Chamber**. Since the chromatogram is developed from both sides, you double the number of samples per plate.

Even your complex sample mixtures, historically not associated with TLC, can now be separated in the **CAMAG Automated Multiple Developing System** using gradient elution.

Call us at (800) 334-3909, in NC (800) 476-1815 for technical information. Let us show you how to conquer your chromatography problems with CAMAG TLC instrumentation

CAMAG

Leading the World in Modern Thin-Layer Chromatography

CAMAG Scientific Inc. · P.O. Box 563 · Wrightsville Beach, NC 28480 · Telephone (919) 343-1830 · Fax (919) 343-1834

CIRCLE 24 ON READER SERVICE CARD

APRIL 15, 1990
VOLUME 62
NUMBER 8

The Audit Bureau
ANCHAM
62(8) 465A-514A/785-880 (1990)
ISSN 0003-2700

ANALYTICAL CHEMISTRY (ISSN 0003-2700) is published semimonthly by the American Chemical Society at 1155 16th St., N.W., Washington, DC 20036. Editorial offices are located at the same ACS address (202-872-4570; FAX 202-872-4574; TDD 202-872-8733). Second-class postage paid at Washington, DC, and additional mailing offices. Postmaster: Send address changes to ANALYTICAL CHEMISTRY Member & Subscriber Services, P.O. Box 3337, Columbus, OH 43210.

Claims for missing numbers will not be allowed if loss was due to failure of notice of change of address to be received in the time specified; if claim is dated (a) North America: more than 90 days beyond issue date, (b) all other foreign: more than one year beyond issue date, or if the reason given is "missing from files."

1990 subscription rates include air delivery outside the U.S., Canada, and Mexico

	1 yr	2 yr
Members		
Domestic	$ 29	$ 49
Canada and Mexico	64	119
Europe	96	183
All Other Countries	118	227
Nonmembers		
Domestic	59	100
Canada and Mexico	94	170
Europe	186	336
All Other Countries	208	380

Three-year and other rates contact: Member & Subscriber Services, ACS, P.O. Box 3337, Columbus, OH 43210 (614-447-3776 or 800-333-9511).

Subscription orders by phone may be charged to VISA, MasterCard, Barclay card, Access, or American Express. Call toll free 800-ACS-5558 in the continental United States; in the Washington, DC, metropolitan area and outside the continental United States, call 202-872-8065. Mail orders for new and renewal subscriptions should be sent with payment to the Business Management Division, ACS, P.O. Box 28597, Central Station, Washington, DC 20005.

Subscription service inquiries and changes of address (Include both old and new addresses with ZIP code and *recent mailing label*) should be directed to the ACS Columbus address noted above. Please allow six weeks for changes to become effective.

ACS membership information: Lorraine Bowlin (202-872-4567)

Single issues, current year, $8.00 except review issue, $14.00, and LabGuide, $49.00; **back issues and volumes and microform editions** available by single volume or back issue collection. For information or to order, call the number listed for subscription orders by phone; or write the Microform & Back Issues Office at the Washington address.

Nonmembers rates in Japan: Rates above do not apply to nonmember subscribers in Japan, who must enter subscription orders with Maruzen Company Ltd., 3-10 Nihonbashi 2-chome, Chuo-ku, Tokyo 103, Japan. Tel: (03) 272-7211.

Analytical CHEMISTRY

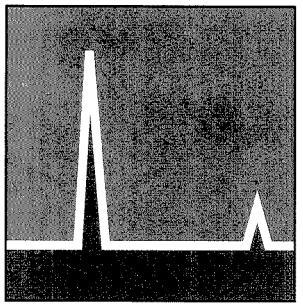

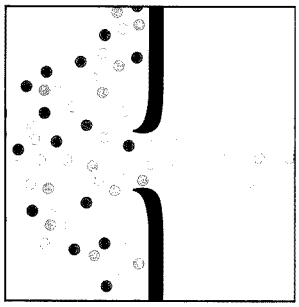

INSTRUMENTATION **477 A**

On the cover. **Continuous-flow fast atom bombardment MS** minimizes or eliminates the drawbacks of the standard FAB technique while retaining its inherent advantages. Richard M. Caprioli of the University of Texas Medical School describes the instrumentation involved and applications for biochemical and biological analyses

ANALYTICAL APPROACH **505 A**

Real-time detection of chemical agents using molecular beam laser MS. Detecting chemical warfare agents in the atmosphere is analogous to finding the proverbial needle in a haystack. Jack A. Syage of The Aerospace Corporation discusses how multiphoton ionization and MS can be combined and enhanced to detect these compounds

BRIEFS **470 A**

NEWS **475 A**

Janet Osteryoung wins **ANACHEM Award.** ▸ Undergraduates encounter the bulging drum problem. ▸ Ozone missing over the Arctic. ▸ CHESS gets five new pieces

MEETINGS **487 A**

38th ASMS Conference on Mass Spectrometry and Allied Topics. ▸ **Texas Symposium on Mass Spectrometry V.** ▸ Conferences. ▸ Short courses and workshops

BOOKS **490 A**

Critical reviews. Recently released books on sensors, drug testing, surface analysis, ICP spectrometry, ICP/MS, expert systems, electrophoresis, and NMR spectroscopy are reviewed

FOCUS **499 A**

Diagnosing sick buildings. Recent EPA studies reveal that most people are exposed to more harmful pollutants in their homes and offices than outdoors. Analytical chemists are supporting efforts to monitor toxic compounds by developing new methods for sampling and analyzing indoor air

NEW PRODUCTS & MANUFACTURERS' LITERATURE **502 A**

AUTHOR INDEX **785**

BRIEFS

Articles

Porphyrin Pyrrole Sequencing: Low-Energy Collision-Induced Dissociation of $(M + 7H)^+$ Generated in Situ during Ammonia Chemical Ionization 786

Low-energy collision-induced dissociation of $(M + 7H)^+$, produced in situ during high-pressure ammonia chemical ionization of a porphyrin, yields simple, reproducible daughter ion mass spectra from which the pyrrole sequence of the porphyrin and combined mass of the substituent groups on the individual pyrroles can be determined.

Gary J. Van Berkel*, Gary L. Glish, and Scott A. McLuckey, Analytical Chemistry Division, Oak Ridge National Laboratory, Oak Ridge, TN 37831-6365 and **Albert A. Tuinman*,** Department of Chemistry, University of Tennessee, Knoxville, TN 37996

Ultraviolet Laser Desorption/Ionization Mass Spectrometry of Proteins above 100 000 Daltons by Pulsed Ion Extraction Time-of-Flight Analysis 793

High mass UV laser-desorbed molecular ions are detected in a Wiley–McLaren-type instrument with pulsed extraction geometry. The initial kinetic energies of these ions are much smaller than previously assumed.

Bernhard Spengler and Robert J. Cotter*, Department of Pharmacology and Molecular Sciences, Middle Atlantic Mass Spectrometry Facility, The Johns Hopkins University School of Medicine, Baltimore, MD 21205

Determination of [^{3}H]-2,3,7,8-Tetrachlorodibenzo-*p*-dioxin in Human Feces to Ascertain Its Relative Metabolism in Man 796

Results of the analysis of human feces from a self-dosing experiment indicate that, at most, 50% of the radioactivity in the sample is attributed to [^{3}H]-2,3,7,8-tetrachlorodibenzo-*p*-dioxin.

Jay M. Wendling* and Robert G. Orth, Monsanto Company, 800 North Lindbergh Boulevard, St. Louis, MO 63167 and **Hermann Poiger,** Institute of Toxicology, Federal Institute of Technology and University of Zurich, Schorenstrasse 16, CH-8603 Schwerzenbach, Switzerland

Ion Chromatography/Mass Spectrometry for the Determination of Organic Ammonium and Sulfate Compounds 800

The ion spray LC/MS interface is coupled via a postsuppressor split with an ion chromatography system. Mixtures of tetraalkylammonium, alkyl sulfate, and alkyl sulfonate compounds are characterized.

J. J. Conboy and J. D. Henion*, Drug Testing and Toxicology, Cornell University, 925 Warren Drive, Ithaca, NY 14850 and **M. W. Martin* and J. A. Zweigenbaum,** Analytical Technology Division, Eastman Kodak Company, Rochester, NY 14652-3712

*Corresponding author

Extended Life for Blood Serum Analysis Columns Using Dual Zone Chromatographic Materials 807

The adsorbents display greater column lifetimes than corresponding control adsorbents. Columns are evaluated by repetitive direct serum injection analyses for drugs by HPLC.

Dwight E. Williams*, Dow Corning Corporation, Midland, MI 48640 and **Pokar M. Kabra,** Department of Laboratory Medicine, University of California, San Francisco, CA 94143

Multipoint Calibration of a Gas Chromatograph Using Cryogenic Preconcentration of a Single Gas Standard Containing Volatile Organic Compounds 810

Results indicate that the method is linear over the concentration range of 1–13 nmol/mol (ppb) for the operating conditions studied. The determination of linearity allows for the use of one calibration gas standard to develop a calibration range for an instrument.

George C. Rhoderick* and Walter R. Miller, National Institute of Standards and Technology, Center for Analytical Chemistry, Gas and Particulate Science Division, Gaithersburg, MD 20899

Calibrating Detector Responses Using Chromatographic Peak Shapes 816

A computation-based method for calibrating time-independent detector response from a series of chromatographic peak shapes is presented. The method is useful in nonlinear chromatographic studies.

Eric V. Dose and Georges Guiochon*, Department of Chemistry, University of Tennessee, Knoxville, TN 37996-1600, and Analytical Chemistry Division, Oak Ridge National Laboratory, Oak Ridge, TN 37831

Thermal Analyses of Compound Semiconductors Using Differential Scanning Calorimetry. Application to Compositional Analyses of Cathodically Electrosynthesized Cadmium Telluride 821

Differential scanning calorimetry is used for the compositional analyses of compound semiconductors such as CdTe. Changes in the composition of electrodeposited samples of this model compound are quantitated as a function of deposition potential.

Wen-Yuan Lin, Kamal K. Mishra, Erik Mori, and Krishnan Rajeshwar*, Department of Chemistry, The University of Texas at Arlington, Arlington, TX 76019-0065

Highly Stable Phospholipid/Cholesterol Electrode Coatings for Amperometric Monitoring of Hydrophobic Substances in Flowing Streams 826

Highly stable lipid coatings, prepared by doping phosphatidylcholine with cholesterol, enhance the selectivity of amperometric flow detectors toward hydrophobic compounds.

Joseph Wang* and Ziling Lu, Department of Chemistry, New Mexico State University, Las Cruces, NM 88003

Discover

System 800 FT-IR

Your best choice in a high-performance research FT-IR system.

- *Superior stability*
- *Highest sensitivity*
- *Widest versatility*

System 800 gives you superior performance to solve today's research problems with confidence—and unmatched adaptability to respond to tomorrow's challenges. System 800 frees you from the built-in limitations of past instruments.

When you choose the System 800, you're making a cost-effective investment as well as a sound scientific decision. *Write us or circle the reader's service number to receive our new 16-page System 800 brochure.*

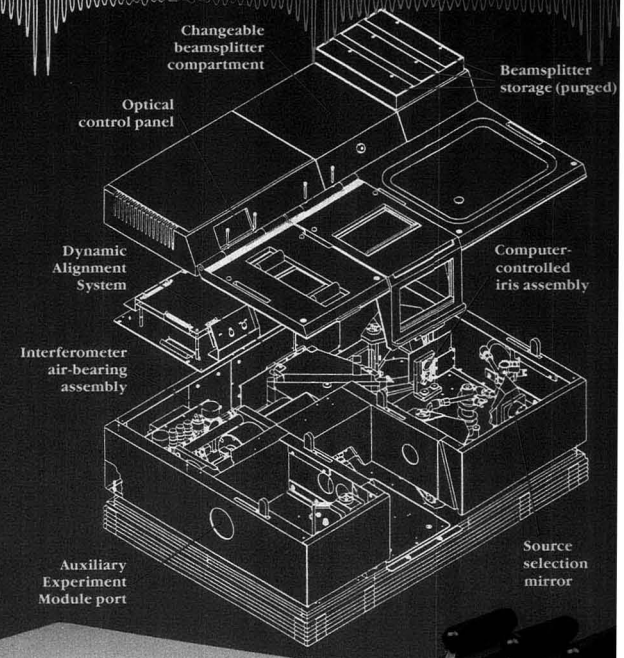

Nicolet

INSTRUMENTS OF DISCOVERY

Circle 95 for information. Circle 96 for demonstration.

Belgium 02-762-2511
Canada 416-625-8302
France 1-30-66-3330
Germany 069-837001
Japan 06-863-1550
Netherlands 03403-74754
Switzerland 01-251-6133
United Kingdom 0926-494111

Nicolet Analytical Instruments / 5225-1 Verona Rd. / Madison, WI 53711 / (608) 271-3333 / FAX (608) 273-5046

Thermal Lensing Detection of Lanthanide Ions by Solvent Extraction Using Crown Ethers 830

Solvent extraction with crown ethers is used to enhance the sensitivity and selectivity of thermal lens detection of lanthanide ions.

Chieu D. Tran* and Weifeng Zhang, Department of Chemistry, Marquette University, Milwaukee, WI 53233

Luminescence Detection of Rare-Earth Ions by Energy Transfer from Counteranion to Crown Ether–Lanthanide Ion Complexes 835

Lanthanide ions are extracted from water into the organic phase using crown ether and benzoate. The luminescence of the ions in the organic phase is measured at the excitation wavelength where excitation energy is transferred from the counteranion (benzoate) to the rare-earth ions.

Chieu D. Tran* and Weifeng Zhang, Department of Chemistry, Marquette University, Milwaukee, WI 53233

Influence of Small Amounts of Organic Solvents in Aqueous Samples on Argon Inductively Coupled Plasma Spectrometry 840

The presence of organic solvents in concentrations as low as 0.1% by volume produce large decreases in emission intensities. While the ion number density increases, the fraction of ions that are excited decreases.

John W. Olesik* and Alvin W. Moore, Jr., Department of Chemistry, Venable and Kenan Laboratories, CB 3290, University of North Carolina, Chapel Hill, NC 27599-3290

Surface-Enhanced Raman Scattering of Dopamine at Polymer-Coated Silver Electrodes 846

The surface-enhanced Raman spectra of dopamine on Nafion- and cellulose acetate-coated silver electrodes are reported. Polymer coatings are shown to eliminate surfactant effects normally encountered in protein-rich matrices.

Michael L. McGlashen, Kevin L. Davis, and Michael D. Morris*, Department of Chemistry, University of Michigan, Ann Arbor, MI 48109-1055

A Simple and Robust Flow Injection Analysis Method for Determination of Free Acid and Metal Concentrations in Hydrolyzable Metal Solutions 849

A single-line FIA system for simultaneous determination of acid and iron in highly concentrated solutions is described. The prediction error is 7% for acid and 3.8% for iron.

Walter Lindberg, Gregory D. Clark, Christopher P. Hanna, David A. Whitman, Gary D. Christian*, and Jaromir Ruzicka, Department of Chemistry, BG-10, University of Washington, Seattle, WA 98195

Helium Discharge Detector for Quantitation of Volatile Organohalogen Compounds 853

An element-selective helium discharge detector for GC provides pg detection limits and a mass-dependent response for Cl and Br in volatile organohalogen compounds. The detector is used for haloform analysis in water.

David A. Ryan, Suzanne M. Argentine, and Gary W. Rice*, Department of Chemistry, College of William and Mary, Williamsburg, VA 23185

Minimization of Interferences in Inductively Coupled Plasma Mass Spectrometry Using On-Line Preconcentration 857

A semi-automated preconcentration system for nine analytes is used to mitigate spectral and physicochemical interferences in ICP/MS. The RSD at 0.5 μg/L is 2–10%.

E. M. Heithmar* and T. A. Hinners, U.S. Environmental Protection Agency, P.O. Box 93478, Las Vegas, NV 89193-3478, **J. T. Rowan,** Lockheed Engineering and Sciences Company, 1050 East Flamingo Road, Las Vegas, NV 89119, and **J. M. Riviello,** Dionex Corporation, 1228 Titan Way, P.O. Box 3603, Sunnyvale, CA 94088-3603

Automatic Phase Correction of Fourier Transform Nuclear Magnetic Resonance Spectroscopy Data and Estimation of Peak Area by Fitting to a Lorentzian Shape 864

A method is proposed for automatically phasing NMR spectra (zero and first-order corrections). A further refinement provides a reliable estimation of peak areas.

F. Montigny, K. Elbayed, J. Brondeau, and D. Canet*, Laboratoire de Méthodologie RMN (U.A. CNRS 406-LESOC), Université de Nancy I, B.P. 239, 54506 Vandoeuvre lès Nancy Cedex, France

Laser Desorption Electron Impact: Application to a Study of the Mechanism of Conjugation of Glutathione and Cyclophosphamide 868

Laser desorption, combined with electron impact ionization, provides the ion radical fragmentation required for isotope-labeling studies of the mechanism of conjugation of glutathione with cyclophosphamide.

Zhi-min Yuan, Catherine Fenselau*, D. M. Dulik, William Martin, W. Bart Emary, R. B. Brundrett, O. M. Colvin, and R. J. Cotter, Department of Chemistry and Biochemistry, University of Maryland Baltimore County, Baltimore, MD 21228, and Department of Pharmacology and Molecular Sciences, Johns Hopkins University, Baltimore, MD 21205

Quantitative Static Secondary Ion Mass Spectrometry of Molecular Ions from 1-β-3,4-Dihydroxyphenylalanine (L-DOPA) and Indolic Derivatives 870

Linear calibration curves of L-DOPA and related indolic compounds are constructed by integrating the protonated molecular ion to silver ion peak area ratios over a known ion dosage and plotting them versus the original sample concentration (molecules/cm^2 Ag).

Michael B. Clark, Jr., and Joseph A. Gardella, Jr.*, Department of Chemistry and Surface Science Center, State University of New York at Buffalo, Buffalo, NY 14214

Correspondence

Reversible, Linear-Sweep Voltammetry of a Soluble Redox Couple: Effect of Initial Concentrations 875

John W. Weidner and Peter S. Fedkiw*, Department of Chemical Engineering, North Carolina State University, Raleigh, NC 27695

Detection of Mass 31 830 Ions with an External Ion Source Fourier Transform Mass Spectrometer 878

Carlito B. Lebrilla, Diana T.-S. Wang, Richard L. Hunter, and Robert T. McIver, Jr.*, Department of Chemistry, University of California, Irvine, CA 92717

Backed by Matheson's more than 60 years of experience.

Questionable quality of standard gases or calibration mixtures is intolerable. Purity and consistency are the by-words of the analytical chemist.

Matheson's experience and reputation as a supplier of the highest quality laboratory gases and mixtures eliminate uncertainty. Each Matheson UHP, Zero Gas, and Matheson Purity Gas is guaranteed to be exactly what the label says. Nothing more. Nothing less. Matheson Primary Standards are of the highest accuracy. Our complex calibration standards required in gas chromatography are the benchmark of the industry. And, our gas handling equipment will never jeopardize the integrity of our gases.

So whether your work is in the field of pharmaceuticals, petroleum, lasers, or aerospace. . . insist on quality. Insist on Matheson.

APPLICATIONS

Atomic Absorption Spectroscopy

Calibration Standards

Primary Standards
Certified Standards

Gas Chromatography Detectors

DID	Discharge Ionization Detector
ECD	Electron Capture Detector
FID	Flame Ionization Detector
FPD	Flame Photometric Detector
GADE	Gas Density Detector
HECD	Hall Electroconductivity Detector
HID	Helium Ionization Detector
NPD	Nitrogen Phosphorus Detector
PID	Photoionization Detector
TCD	Thermal Conductivity Detector
TID	Thermionic Ionization Detector

Supercritical Fluid Chromatography

Medical / Biological

Blood Gas Analysis
Pulmonary Function
Surgical Lasers
Biological Atmospheres

Flame Photometry

Nuclear Counters

Emissions Testing

E.P.A. Protocol

Burner Calibration (BTU Verification)

Leak Detection

Matheson®
Gas Products
World Leader in Specialty Gases & Equipment
30 Seaview Dr., Secaucus, NJ 07096-1587
FAX: (201) 867-4572

CIRCLE 90 ON READER SERVICE CARD

NEWS

Award to Janet Osteryoung

Janet Osteryoung, professor of chemistry at the State University of New York at Buffalo, has won the ANACHEM Award. The award, which is given by the Association of Analytical Chemists of Detroit, will be presented to Osteryoung at the Federation of Analytical Chemistry and Spectroscopy Societies (FACSS) meeting this October in Cleveland.

Osteryoung is being honored for her electroanalytical research, which includes development and application of pulsed voltammetric techniques and microelectrode studies. Currently she is employing electrochemical techniques to develop corrosion-resistant coatings that can be applied to metals without toxic cyanide baths.

Osteryoung received her B.A. degree (1961) from Swarthmore College and her Ph.D. from the California Institute of Technology (1967). She joined the faculty at Buffalo in 1979.

Synchrotron Expansion

The Cornell High-Energy Synchrotron Source (CHESS) has completed construction of new research facilities that nearly double its size. The centerpiece is an isolation room for obtaining X-ray structures of hazardous viruses such as hepatitis or poliomyelitis. Four other lead-lined research rooms have been added, including space for studying materials at ultra-high pressures.

Three of the new CHESS stations are served by a beam line containing a wiggler—an array of 24 permanent magnets designed to oscillate the electron beam, thereby intensifying the synchrotron X-rays at least fivefold. The wiggler will produce X-ray beams with energies up to 100 kV.

Procter & Gamble Sells Industrial Analytical Chemistry

Since 1983 analytical chemists from Procter & Gamble have been presenting undergraduate chemistry majors with a glimpse of life in an industrial analytical laboratory. During a lively one-day short course, students learn how analytical chemists have solved a series of real problems (with titles like "the bulging drum problem" or "the case of the purple surfactant") and even work on their own "problem." At the same time the instructors discuss the level of training necessary to solve these problems and career opportunities for industrial analytical chemists. Organizers hope these real-life examples will encourage participants to consider an advanced degree in analytical chemistry. Students participating in the short course have commented that they were surprised to find the material so interesting.

According to one of the instructors, Alan Ullman, "The course grew out of our concern that too few [analytical chemistry] graduates were available to meet the growing needs of industry and that most science students did not know what scientists do in industry." The course has been offered at numerous U.S. colleges and universities as well as at major chemical meetings such as the recent Pittsburgh Conference in New York. Material in the course is aimed at junior- and senior-level undergraduates who have completed instrumental analysis. For further information, write to Ullman, Procter & Gamble Co., 6250 Center Hill Rd., Cincinnati, OH 45224.

Arctic Ozone Hole

Scientists participating in the Winter 1989 Airborne Arctic Stratospheric Expedition, conducted from Stavanger, Norway, report finding ozone depletions linked to chlorofluorocarbons and unique weather conditions. However, the Arctic losses are concentrated at certain altitudes, and total ozone levels—unlike those in Antarctica—still remain normal.

During January 1989 unusually cold air helped to stabilize the Arctic vortex, a swirling column of air that isolates chemicals in the atmosphere like a beaker. Inside the vortex the scientists found chlorine atoms along with chlorine and bromine oxides involved in ozone-destroying reactions. In certain regions O_3 had declined as much as 17%. From the concentrations of chlorine and bromine species, researchers calculate that during January O_3 was lost at the rate of about 1% per day. The vortex broke down in late February, allowing outside air to flow in and restore normal conditions.

The expedition members also found a layer of tiny particles in the stratosphere that they believe could contribute to the formation of polar stratospheric clouds. These clouds play a key role in the chemistry of ozone destruction. It has even been suggested that residue from solid fuel rockets and/or debris from reentering spacecraft may be contributing large particles to the stratosphere, which would also contribute to cloud formation.

For Your Information

NIST will offer a workshop May 30–31 in Gaithersburg, MD, dealing with measurement as a process, statistical considerations in the evaluation of data quality, standard reference materials, quality assurance programs, and criteria for a good laboratory. The seminar, limited to 50 participants, is directed toward analytical laboratory supervisors, experienced analytical chemists, and individuals in charge of laboratory quality control programs. For more information, contact John Taylor, A309 Chemistry Bldg., NIST, Gaithersburg, MD 20899 (301-975-3148).

CONTINUOUS-FLOW *FAST ATOM*

BOMBARDMENT MASS SPECTROMETRY

Richard M. Caprioli
Department of Biochemistry and Molecular Biology and
The Analytical Chemistry Center
University of Texas Medical School
Houston, TX 77025

Extraordinary innovations and developments in mass spectrometry (MS) literally have revolutionized its breadth and utility during the past decade. This is mainly a result of the development of new analytically useful ionization techniques, such as fast atom bombardment (FAB), secondary ion mass spectrometry (SIMS), thermospray, electrospray, laser desorption, and plasma desorption. Analytical measurements that were unheard of 15 years ago are now performed routinely by MS. They include the direct introduction of water solutions by injection or spray for the analysis of charged organic compounds and the measurement of the molecular species of proteins of molecular weight of 100,000 daltons or more by laser desorption. Each of these techniques has particular advantages and provides specific information; no single technique provides all of the mass spectrometric capabilities needed in the modern analytical laboratory.

FAB has remained one of the more commonly used desorption ionization techniques because it permits the analysis of polar and ionic compounds, often without the need for purification, isolation, and derivatization of these compounds (*1*, *2*). Moreover, it is an easy-to-use technique that can be retrofitted on virtually any mass spectrometer at minimal cost. In particular, it has had an enormous impact on the use of MS in the biological sciences and has provided the bioanalyst with the ability to obtain mass-specific detection of individual compounds in complex mixtures (*3*).

Despite its utility, FAB has many shortcomings, most of which come from the need for rather high concentrations of a viscous organic liquid matrix (usually glycerol) to maintain the liquid nature of the sample inside the ionization chamber of the mass spectrometer. Typically, one mixes a small portion of sample solution with a viscous matrix liquid so that the latter comprises 80–90% of the sample solution to be bombarded. Poor sensitivity, ion suppression effects, and extraordinarily high background are among the more serious problems.

Continuous-flow FAB (CF-FAB) MS was devised to eliminate or at least minimize the drawbacks of the standard FAB technique while retaining its inherent advantages (*4*). A related technique, frit-FAB, originally introduced as an LC/MS interface (*5*), has demonstrated similar performance advantages. Basically, in CF-FAB, a direct insertion probe containing a fused-silica capillary transfer tube is introduced directly into the mass spectrometer ion source. The capillary terminates at the target of the probe, which is bombarded by xenon atoms having a translational energy of about 8 keV. The sample solution flows through the capillary and onto the target, where ions are produced as a result of the bombardment process. Liquid samples may be introduced into the spectrometer by flow injection, a process in which sample solution is injected into a carrier solvent that is flowing into the source.

Figure 1 shows the instrumental arrangement for CF-FAB operated in the flow injection mode. The carrier solution is typically composed of 95% water and 5% glycerol. Glycerol is required to provide a nonvolatile hydrophilic coat-

INSTRUMENTATION

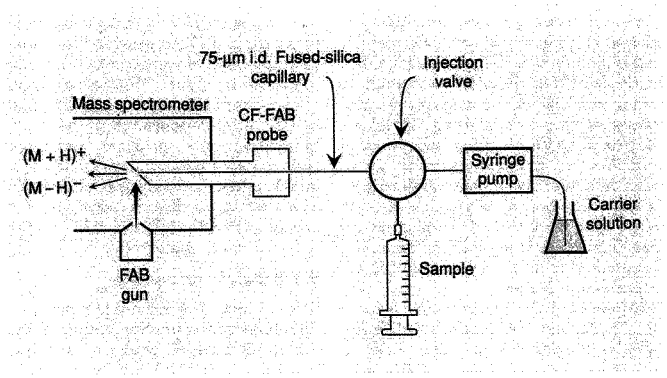

Figure 1. Instrumental arrangement for CF-FAB MS operated in the flow injection mode.

0003-2700/90/0362-477A/$02.50/0

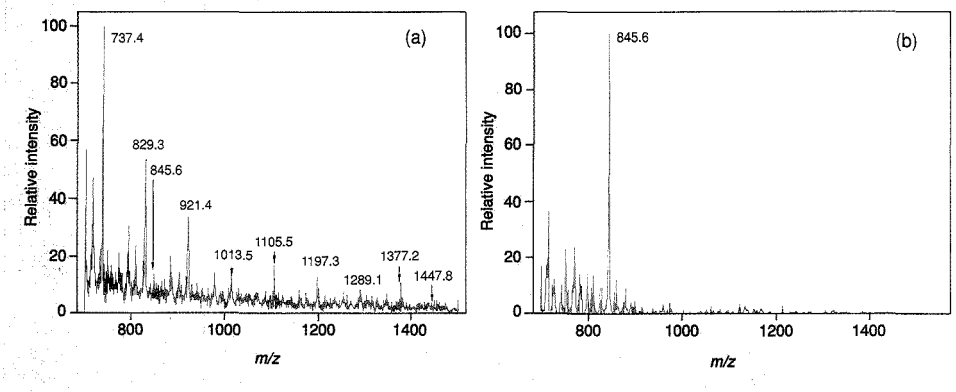

Figure 2. Mass spectra of approximately 200 pmol of an oligopeptide having an $(M + H)^+$ at m/z 845.6.
(a) Spectrum obtained with standard FAB techniques. (b) Spectrum obtained with CF-FAB by flow injection with background subtracted. Data were obtained on a Finnigan MAT 90 mass spectrometer.

ing on the target so that the sample solution flows smoothly over the surface and is either absorbed in a filter pad below the target or evaporated by gentle heating. Liquid samples are injected into this carrier solution; injection volumes range from ~0.5 to 5 μL. Of course, the larger the injection volume becomes, the longer the time the sample will persist on the target.

One of the prime benefits of CF-FAB is the capability to inject water solutions directly into the mass spectrometer ion source without the need to add glycerol or other organic modifiers to the sample itself, although the carrier solution usually contains 5% glycerol. This has enormous potential for biochemical and biological analyses where analytes are often found in low concentrations and almost exclusively in an aqueous environment.

Another benefit, derived from the reduction in the concentration of glycerol or other organic modifiers, is a significantly decreased chemical background throughout the entire mass range in mass spectra obtained using CF-FAB relative to those obtained using standard FAB (*6*). For example, with peptides in the 1500-dalton molecular weight range, sensitivity has been shown to be more than 200-fold greater than that of standard FAB when analyzing compounds in the low picomole or femtomole ranges.

Moreover, CF-FAB provides other benefits such as the capability of flow injection analysis, which adds a temporal parameter to the measurements (i.e., one observes a background before and after the sample injection and the rise and fall of the ion current produced by the sample in a specific time period.) The peak produced in the "total ion chromatogram" is composed of individual ion profiles for each mass-to-charge ratio (m/z) scanned. This allows efficient background subtraction and permits quantitative comparison of ion profiles between two or more sample injections without the use of internal standards.

The ability of CF-FAB to utilize a constant flow of an aqueous solution has made it an effective interface for chromatographic techniques as well. LC/CF-FAB MS applications have been demonstrated by a number of laboratories, and the technique has been particularly useful for the identification of peptide products in protease digestion reactions and in the analysis of drugs and their metabolites. CF-FAB can also be coupled with capillary electrophoresis (CE) to provide mass-specific detection of compounds primarily separated by charge. The combination of high-resolution separations afforded by CE, often measured in terms of 10^5 theoretical plates or more, and mass spectrometric detection makes it a formidable tool in analytical chemistry. The coupling of these separation techniques with CF-FAB MS will be discussed in more detail later.

Batch sample processing

In many analytical service laboratories, FAB mass spectrometric analysis is required for a large number of samples. Operating the CF-FAB MS interface in the flow injection mode provides an efficient method for batch sample processing because it allows sample solutions to be injected into the source as often as once every 2 min. To achieve this rate of analysis, one must use relatively small injection volumes (typically 1 μL or less) and eliminate excessive dead volumes in plumbing connections so that injected samples do not exceed a presence of approximately 1 min on the target and consequent peak tailing is minimized. Automated flow injection operation uses the same basic setup shown in Figure 1 except that an automatic injection valve and an autosampler are used instead of the manually operated valve.

The question of memory effects is always of concern in an automated analytical technique such as this. In one test, samples of 200 pmol each of two peptides, substance P (MW 1347) and renin substrate tetradecapeptide (MW 1760), were alternately injected every 2 min. After 2 h, the mass spectrum obtained from the injection of each compound showed a relative intensity of less than 0.1% for the molecular species of the other. This clearly demonstrates that only a negligible memory effect was observed. Of course, memory effects should be checked with each class of compound analyzed because, if present, they could lead to excessive peak tailing and thereby limit the sampling rate.

For solid-phase synthetic peptide preparations, use of FAB MS provides a fast and efficient means for the analysis of the products cleaved from the resin. A single mass spectrum provides important information on the distribution of peptides produced in the cou-

pling reactions and on the efficiency of the deblocking reactions, as well as an estimate of the relative amounts of each molecular species under the appropriate conditions (quantitative aspects are considered later). CF-FAB is especially useful for these analyses because of its high sensitivity and decreased ion suppression effect. The latter is a phenomenon first observed with standard FAB in the analysis of mixtures of compounds of different charges and polarities where more hydrophobic molecules tend to accumulate at the surface of the sample droplet, suppressing the ionization of more hydrophilic compounds (*7*). This effect is diminished with CF-FAB, presumably because of the mechanical mixing of the liquid as it flows over the surface of the target (*8*).

Figure 2a shows the standard FAB and Figure 2b shows the CF-FAB mass spectrometric analysis of approximately 200 pmol of a synthetic peptide of MW 844.6. The $(M + H)^+$ molecular species at m/z 845 is not observed above background in the spectrum taken with standard FAB. The major ions recorded arise from glycerol and appear at m/z $(92n + 1)$, beginning at $n = 8$ in this spectrum. In the spectrum taken with CF-FAB, the $(M + H)^+$ signal for this peptide is significantly larger because of the decreased intensity of the background and reduced ion suppression effect. Furthermore, background could be effectively subtracted in this spectrum because ions derived from the injected sample could be differentiated on the time scale from those derived from the background carrier solvent.

Quantitative analyses

The analyst often faces different types of quantitative tasks in a given analysis. Perhaps the most difficult of these for standard FAB is to compare the level of a given compound in multiple samples. Even with extreme care, it is very difficult to introduce the sample repeatedly into the ion source of the mass spectrometer with identical positioning, which is crucial for good reproducibility. When CF-FAB is used, the introduction probe remains untouched throughout a series of sample injections, and errors introduced in measured ion intensities because of nonreproducible probe orientation, size and placement of the glycerol droplet, target temperature, and ion source focusing parameters do not significantly change from sample to sample.

Peak area reproducibility on replicate injection of samples is typically ±5–10% deviation from the mean. This has important implications because the analyst can quantitatively compare sample injections without addition of an internal standard. An application of this type is exemplified by the study of rate curves for enzymic hydrolysis of polypeptide substrates, as shown in Figure 3a. Measurement of the area under the peak produced from the selected ion chromatogram of the $(M + H)^+$ ion of interest for each injection of the reaction aliquot gives the required quantitation. This particular application is described in detail in the following section.

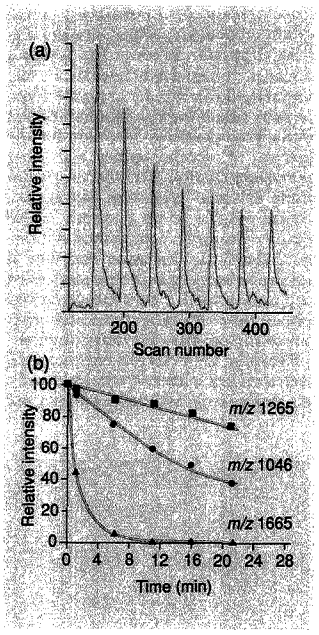

Figure 3. Monitoring the tryptic hydrolysis of a peptide mixture using automated on-line CF-FAB methods.

(a) Selected ion recording for one of the peptide substrates at m/z 1265. (b) Rate curves plotted for three of the peptides in the mixture: physalaemin, m/z 1265; angiotensin II, m/z 1046; and bombesin, m/z 1665. Data were obtained on a Kratos MS50 mass spectrometer.

A second type of quantitative analysis requires measurement of the relative intensities of several ions within a given sample. As in other mass spectrometric analyses, internal standards such as isotopically labeled analogues will provide the most accurate measurements.

Wang and co-workers (*9*) have used CF-FAB to quantitate 1-methyl-4-phenylpyridine (MPP) in biological extracts using the trideuterated species as an internal standard. To determine the precision and accuracy of the methodology, they made 10 consecutive injections of 0.5 μL of a solution containing 50 ng of MPP (m/z 170) and 125 ng of d_3-MPP (m/z 173). The individual peaks were 50 s wide at baseline and 15 s wide at half-height. The mean ratio of peak areas (m/z 170/173) was measured to be 0.3983 ± 0.002 (standard deviation) with a range of 0.3955–0.4011. This agrees very well with the theoretical ratio of 0.4. Furthermore, the standard curve was linear with a correlation coefficient of 0.999 over the range 200 pg to 200 ng. By scanning a 10-mass-unit-wide window, the detection limit of 200 pg was obtained at a signal-to-noise (S/N) ratio of 3:1. The decreased ion intensity derived from chemical background using CF-FAB, compared with standard FAB, is an important advantage for these low-mass applications, particularly when only picogram or nanogram amounts of sample are available.

On-line reaction monitoring

On-line monitoring allows the factor of time to become an integral part of the measurements of an ongoing reaction or process. MS allows the analyst to monitor many different molecular events in the same time domain even in a complex reaction mixture. Consider, for example, the reaction of the enzyme trypsin with a mixture of 10 different polypeptides, some of which contain a single arginine or lysine residue within the peptide chain. One would expect an extremely dynamic situation in which the ion intensities of the molecular species of substrate peptides would decrease as they were hydrolyzed, ion intensities for the peptide fragments formed from each substrate would increase, and molecular ion intensities for peptides that did not contain a susceptible chemical bond would remain unchanged.

Figure 3a shows the change in ion current for one such peptide substrate at $(M + H)^+ = m/z$ 1265, having the sequence pyroGlu-Ala-Asp-Pro-Asn-Lys-Phe-Tyr-Gly-Leu(NH_2). Each peak represents the automated injection of 1 μL of the reaction mixture at a given time into the reaction. Monitoring of all the molecular species then produces a series of rate curves that shows the relative rates of hydrolysis of each peptide; Figure 3b shows the results for several substrates undergoing this reaction. The intensities of the molecular ion species that did not contain a susceptible cleavage site remained constant throughout the reaction.

The ability to follow multiple molecular events almost simultaneously is a powerful tool for the investigation of biological processes. For example, if

one structurally alters an enzyme, it is important to determine the effect on the activity of the enzyme using as many different substrates as possible. MS makes it possible to present the enzyme with a single sample containing dozens of substrates and to specifically follow the fate of each. A small number of such samples could include scores of such substrates, quickly and accurately providing detailed information on the action of the enzyme and the effect of any structural alterations that had been made.

Microdialysis/MS

Microdialysis takes advantage of the process that allows compounds to diffuse through a membrane from a region of higher concentration to one of lower concentration. A commercially available microdialysis probe (Carnegie Medicin, Uppsala, Sweden) fits inside a 22-gauge hypodermic needle. It was originally devised to be implanted into nervous tissue for use in combination with electrochemical detection for the analysis of catecholamines and other neurotransmitters. The dialysis membrane will pass molecules having molecular weights of up to about 20,000 daltons. Basically, compounds of interest dialyze into the inner chamber of the probe and are subsequently swept into a detector by an aqueous carrier solvent flowing at about 5 μL/min that constantly perfuses the inner chamber.

Recently, CF-FAB MS has been connected on line with microdialysis to obtain pharmacokinetic measurements of a drug in a live animal (*10*). In one experiment, shown in Figure 4, a microdialysis probe was inserted into the jugular vein of a rat and the antibiotic penicillin G administered intramuscularly. The dialysis probe was perfused with sterile water containing 5% glycerol, and the perfusate was passed through a 2 × 10-mm C-18 column to concentrate the dialysate. At 10-min intervals, the column was eluted with a solution containing 60% acetonitrile, 35% water, and 5% glycerol and the eluate passed into the mass spectrometer via the CF-FAB interface. Negative ion MS/MS techniques were employed to follow the fragment ion at m/z 192 produced from the collisionally activated decomposition of the molecular species.

The pharmacokinetic curve obtained from this experiment is shown in Figure 5 together with curves for the metabolism of this same drug taken in humans and dogs by classical off-line techniques involving individual blood sampling at each time point. Although interspecies comparisons of such data are difficult to interpret, these data nevertheless demonstrate the effectiveness of on-line MS procedures in such studies.

The potential of MS in this field is considerable, and its use in this manner has important implications not only for medical research but also for direct patient care. It provides the capability for measuring a number of endogenous metabolites as well as administered drugs at virtually the same time. Thus one can effectively obtain details of specific biochemical changes resulting from the administration of drugs in the context of the whole body response.

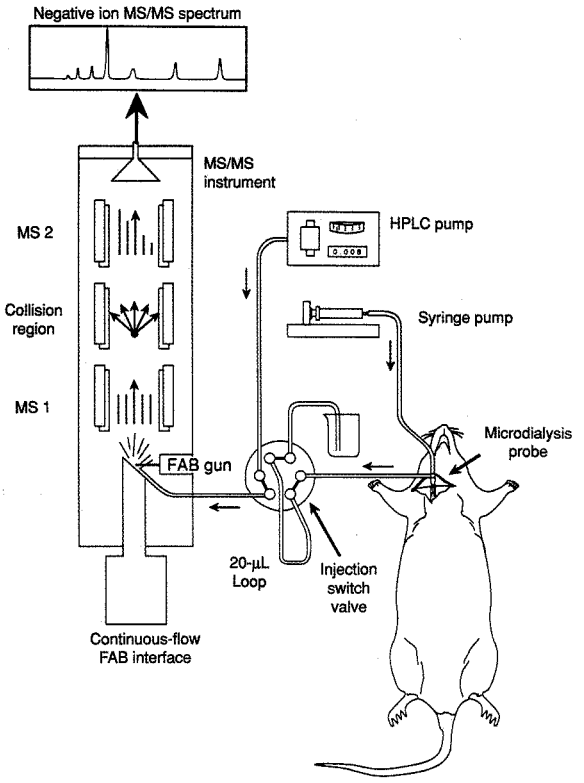

Figure 4. Experimental setup for the in vivo measurement of drug pharmacokinetics.
The microdialysis probe is placed into the jugular vein of the rat, and the compounds dialyzing into the probe are swept out into a sample loop of an injection valve via a carrier stream supplied by a syringe pump. At 10-min intervals, the sample loop is flow injected and analyzed by CF-FAB. Data were obtained on a Finnigan MAT TSQ 70 MS/MS instrument. (Adapted from Reference 10.)

Trace analysis

For many types of analytical procedures using MS, it is advantageous to maintain long sample lifetimes to achieve good S/N measurements for wide mass range scans or accurate mass ratio measurements. In trace analysis, the opposite is often advantageous in that one usually targets one or more compounds and then optimizes analytical parameters to obtain sharp, concentrated responses by narrowing the time domain. Because CF-FAB allows samples to be injected in a short-lived, concentrated pulse with a well-defined background subtraction capability, it is a useful technique for trace compound analysis.

Gaskell and Orkiszewski (*11*) have recently used CF-FAB in combination with tandem MS for the determination of platelet activating factor (PAF). The flow injection mode was used with the carrier solution of water/acetonitrile/

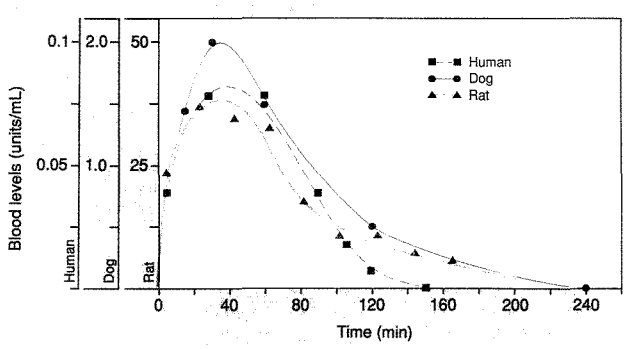

Figure 5. Pharmacokinetic curve for the metabolism of penicillin G by the rat obtained using on-line in vivo measurement techniques.

Metabolic curves in humans and dogs obtained by classical procedures are plotted for comparison. (Adapted from Reference 10.)

saturated aqueous oxalic acid/2,2′-dithiodiethanol (49/49/1/1). The instrument used was a hybrid sector/quadrupole type of the BEqQ design (i.e., the analyzer arrangement was magnet/electric sector/collision cell quadrupole/analyzer quadrupole). The transition followed was m/z 524 [$(M + H)^+$ for C-16 PAF] fragmenting to m/z 184. Thus the sectors were tuned to pass m/z 524 into the collision quadrupole where collision-activated decomposition occurred, and the analyzer quadrupole was set to pass the m/z 184 fragment.

This technique is important for trace analysis because it eliminates much of the background chemical noise (except that at m/z 524) derived from glycerol or other matrix compounds used and significantly lowers the limit of detection. To achieve greater selectivity, one can also increase the resolution of the instrument above that required to give unit mass separation to help eliminate background at m/z 524.

Figure 6 shows the first-stage MS analysis of several 50-pg injections of PAF obtained by monitoring m/z 524.37 at a resolution of 1500. This effectively eliminates a solvent background peak at m/z 524.07 that is approximately 50% of the relative intensity of the $(M + H)^+$ ion of PAF. The points marked B in the figure are blank (water) injections, which show that none of the ion current recorded for the PAF samples was the result of background or injection artifacts.

LC/MS

A number of interfaces for combining LC and MS have been described, two of which—continuous-flow and the moving belt—use FAB ionization. CF-FAB is useful because of its high sensitivity, negligible memory effect, and applicability to a wide range of compounds. Unlike most other LC/MS interfaces, CF-FAB maintains the liquid nature of the eluate inside the ion source on a target surface and uses atom bombardment of this liquid to produce ions rather than nebulization and spray formation.

A liquid flow interface for the combination of LC and FAB was first reported by Ito and co-workers (*5*) for the separation and analysis of bile acids using glycerol/acetonitrile/water (10:27:63) as the eluting solvent. They termed the technique frit-FAB because they used a stainless steel mesh or frit

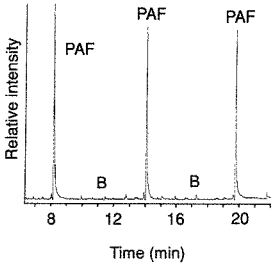

Figure 6. Analysis of C-16 platelet activating factor (PAF) at trace levels using CF-FAB and MS/MS techniques.

Approximately 50 pg of PAF were injected interspersed with blank (B) water injections. Data were obtained on a VG ZAB SEQ hybrid mass spectrometer. (Courtesy of S. J. Gaskell, Baylor University College of Medicine.)

on the target to disperse the liquid. The CF-FAB interface (*12*) uses an open capillary that delivers the eluant to the target and then, either by a combination of gentle heating and evaporation or by capillary action from a nearby absorbent pad, excess liquid is efficiently removed from the target surface.

A number of investigators have used CF-FAB as an LC/MS interface for the separation and analysis of a wide range of biological compounds, including peptides, oligosaccharides, lipids, drugs, endogenous metabolites, porphyrins, bile acids, and antibiotics. The small percentage of glycerol or other organic modifier usually required to maintain stable operating conditions may be added directly to the elution solvents or may be added postcolumn. Because the maximum flow rate for CF-FAB is about 20 μL/min for commercially available instruments, the technique is best suited for either microbore or capillary bore LC where split ratios are small, if used at all. Typically, microbore columns (1 × 50 mm) can be efficiently operated in the flow rate range of 25–50 μL/min and capillary bore (0.3 × 300 mm) at 3–5 μL/min.

The excellent resolving power of the technique using microbore columns of short length in combination with a mass spectrometer is illustrated in Figure 7 for the separation of the tryptic fragments of human apolipoprotein A1 (*13*). Figure 7a shows a portion of the total ion chromatogram where a number of peaks are overlapping; Figure 7b is the same portion of the chromatogram showing the specific mass ions detected for the various peaks. The latter chromatogram was generated by superimposing the independently normalized specific ion chromatograms for each mass of interest.

Capillary bore LC columns are now being used with CF-FAB because they operate at low flow rates and thus do not require effluent splitting and because they have high-resolution capability, thereby providing maximum signal intensities over short time intervals. Coutant and co-workers (*14*) have used a slurry packed 5-μm Spherisorb ODS capillary column (0.32 × 250 mm) for the analysis of teicoplanin A2 antibiotics, a group of glycopeptide compounds obtained from fermentation reactions.

Figure 8 shows the gradient elution

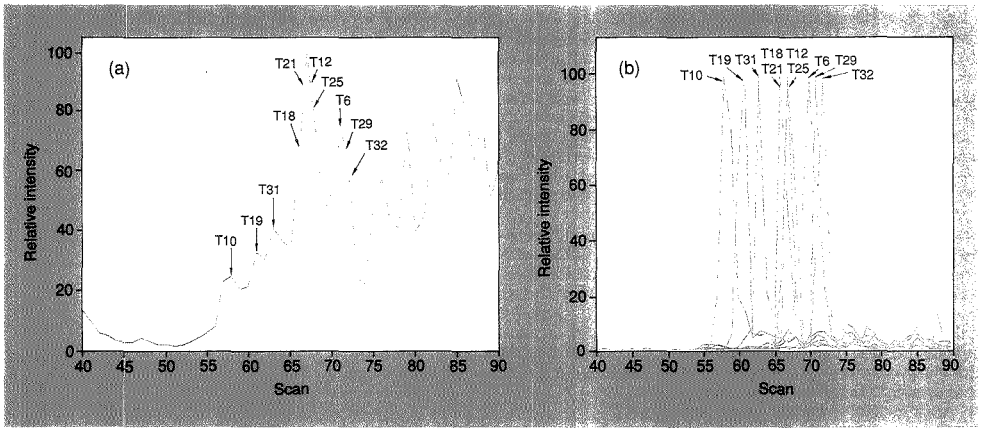

Figure 7. Separation of the tryptic fragments of human apolipoprotein A1.

(a) Portion of the total ion chromatogram for the microbore LC/MS analysis using the CF-FAB interface with a 1 × 50 mm RP-300 C-8 column (ABI). The tryptic peptides located in the region between scans 55 and 75 are noted on the chromatogram. (b) Selected ion chromatograms of the various $(M + H)^+$ ions for the peptides present in scans 55–75, shown on the left. Each selected ion chromatogram has been independently normalized. Data were obtained on a Finnigan MAT 90 mass spectrometer.

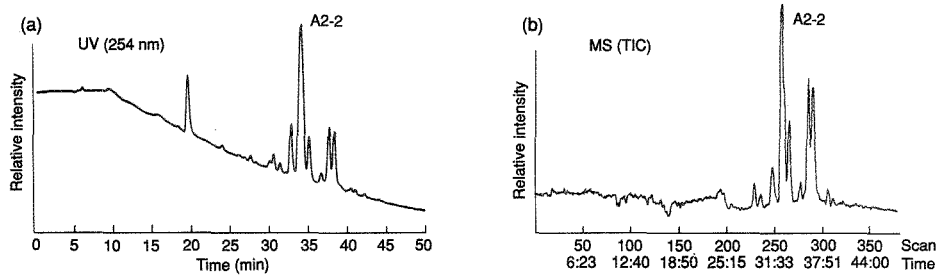

Figure 8. Gradient elution chromatogram for the analysis of the teicoplanin A2 antibiotics using a slurry packed capillary column.

(a) UV detection and (b) MS detection. The MS total ion chromatogram was obtained by on-line CF-FAB. (Adapted with permission from Reference 14.)

profile of 1 nmol of total antibiotic for both UV and MS detection. The elution rate was 2 μL/min, and a makeup solvent containing glycerol, water, and methanol (2:1:1) was added postcolumn at 1 μL/min. Six different antibiotic compounds were identified in the analysis. Teicoplanin A2-2 [$(M + H)^+ = m/z$ 1880.6] was the major component.

Although full-bore columns have been used with CF-FAB, high split ratios of 1:50 to 1:100 are generally necessary and therefore preclude their use where analyte concentrations are very low. In some cases, even the use of microbore and capillary bore columns is not a great advantage because the benefit of a splitless interface is offset by the lower injection volumes used.

Kokkonen and co-workers (*15*) have used a technique for target compound analysis, termed phase system switching, that uses full-bore columns and CF-FAB without splitting. Valving and column trapping techniques accomplish this goal. Basically, the compound of interest, which is eluted off a large-bore column, is trapped onto a short microbore column. After washing, this column is eluted with the appropriate solvent at the flow rate suitable for the MS interface. For example, these investigators determined dextromethorphan in plasma using an RP-2 analytical column (3 × 100 mm) at a flow rate of 1.0 mL/min in combination with an XAD-2 trapping column (1 × 50 mm) that was subsequently eluted into the source of the mass spectrometer at 5 μL/min. A concentration of about 0.5 ng/mL of the drug in plasma could be detected at a S/N ratio of 10:1. This procedure is best suited for target compound analysis.

CE/MS

CE is a high-resolution separation technique that is well suited for low-flow-rate liquid introduction MS. The principal advantages of the technique are its ability to achieve very high resolution separations of several hundred thousand theoretical plates or better, a very low flow rate on the order of tens of nanoliters per minute in most cases, and its ability to achieve separations based primarily on charge.

Several investigators have reported the coupling of CE and CF-FAB MS (*16–18*). An interface is needed between the end of the CE capillary and the CF-FAB probe because of flow rate incompatibility; CF-FAB requires a minimum flow rate of about 1–2 μL/min to maintain stability, whereas any pressure-driven flow through the CE capillary would lead to band broadening and a loss of resolution. Basically, interfaces are of two types: a liquid junction of the type first reported by Minard et al. (*16*) and Caprioli et al. (*17*), and the coaxial type described by Tomer et al. (*18*). The liquid junction interface is illustrated in Figure 9. In both cases, carrier solution is supplied

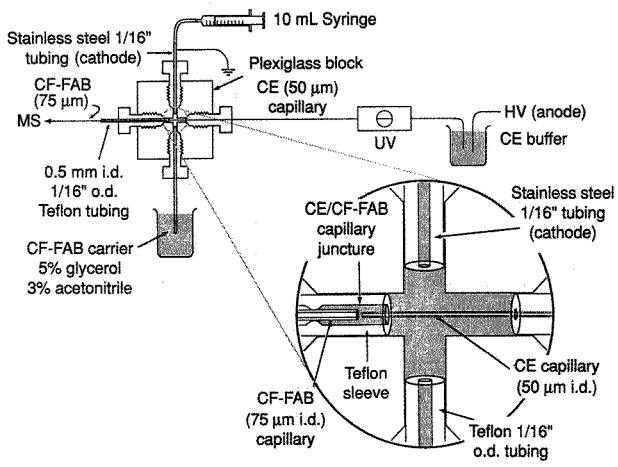

Figure 9. Instrumental setup for coupling CE and CF-FAB.

The interface, shown in the magnified area, allows 5 μL/min of solution from the CF-FAB reservoir to be supplied to the mass spectrometer without inducing mechanical flow in the CE capillary. (Adapted with permission from Reference 17.)

from an external reservoir to produce sufficient flow to stabilize the CF-FAB device without inducing mechanical flow in the CE capillary.

The CE/MS separation and analysis of peptide mixtures such as those produced from protease digestions are a major focus of this technology. Figure 10 shows a selected ion chromatogram for the peptide of m/z 693.4 from the analysis of 40 pmol of the tryptic digest of recombinant human growth hormone (*17*). The mass range scanned was m/z 600–2000 at a rate of 10 s/scan. The peak at half-height is about 12 s wide and represents the practical minimum peak width needed for a mass spectrometer scanning at this speed. The electrophoretic separation was performed at 15 keV (8 μA) with a buffer containing 40 mM sodium citrate and 40 mM NaCl, pH 2.5. The CF-FAB carrier solvent was 92% water, 5% glycerol, and 3% acetonitrile containing 2.3 mM acetic acid and 1 mM ammonium hydroxide to provide electrical conduction.

Generally, although high salt concentrations in the CE capillary tend to give optimal separations, this is not used in the anodic reservoir because it results in cationized molecular species in the FAB spectrum. Thus, at high sodium concentrations, one sees ions at $(M + H)^+$, $(M + Na)^+$, $(M - H + 2Na)^+$, and so forth. This decreases the effective sensitivity by distributing the ion current of the molecular species among several ions and complicates interpretation of the spectra, especially in complex mixtures.

The limit of detection for peptides undergoing CE was determined using the octapeptide angiotensin II (MW 1045). The mass spectrometer was scanned over a 4-mass-unit-wide window centered on the $(M + H)^+$ ion at m/z 1046. When 368 fmol of the peptide was injected, the measurement of the S/N for this ion was 12:1, and for injection of 75 fmol, about 3:1. This experiment defines only the apparent sensitivity of a single peptide under

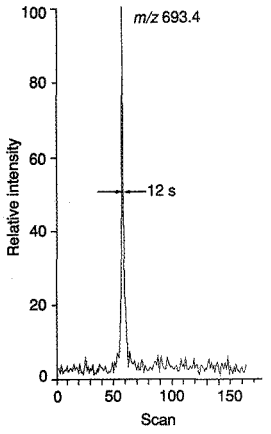

Figure 10. Selected ion chromatogram of m/z 693.4 obtained from the CE/CF-FAB separation and analysis of a tryptic digest of recombinant human growth hormone.

Data were obtained on a Finnigan MAT 90 mass spectrometer. (Adapted with permission from Reference 17.)

specific operating conditions. If wide mass range scans were required—for example, m/z 200–2000—the limit of detection would be in the high femtomole or low picomole range.

Conclusion

The appearance of direct liquid introduction systems for mass spectrometers has had a big impact on the use of these instruments for the analysis of polar and charged compounds. CF-FAB is one such technique and has been applicable for a wide range of different classes of compounds. Biologists and biochemists now have at their fingertips analytical capabilities that can directly accommodate aqueous-based samples and give mass-specific analytical data.

On-line techniques using FAB ionization are now possible, allowing the analyst to effectively add the time domain to many experiments so that changes in concentrations of multiple molecular species can be monitored virtually simultaneously. In the near future, mass-specific instruments will play an important role in health care, permitting a number of critical metabolic parameters to be monitored on line as small amounts of blood are drawn.

MS has undergone a revolution in its ability to determine compounds in aqueous-based solutions and record molecular ions at very high mass. This fact, coupled with the general trend toward simpler and less expensive instrumentation, indicates that the use of MS in both research and industrial environments should increase significantly in the coming years.

The author acknowledges the following for their efforts in the development and application of the CF-FAB technique: Annie Ballatore, Su Chang, Beverly DaGue, Per Johannson, Shen-Nan Lin, William T. Moore, William E. Seifert, Jr., Marc Suter, and Brenda Whaley. The technical assistance of Robert Amason and Tim Woodward is acknowledged, as is the help of Alice Stafford and Margaret Winkler in preparing this manuscript.

References

(1) Barber, M.; Bordoli, R. S.; Sedgwick, R. D.; Tyler, A. N. *J. Chem. Soc., Chem. Commun.* **1981**, 325–27.
(2) Barber, M.; Bordoli, R. S.; Elliott, G.; Sedgwick, R. D.; Tyler, A. N. *Anal. Chem.* **1982**, *54*, 645 A–657 A.
(3) Caprioli, R. M. *Biochemistry* **1988**, *27*, 513–21.
(4) Caprioli, R. M.; Fan, T.; Cottrell, J. D. *Anal. Chem.* **1986**, *58*, 2949–54.
(5) Ito, Y.; Takeuchi, T.; Ishi, D.; Goto, M. *J. Chromatogr.* **1985**, *346*, 161–66.
(6) Caprioli, R. M.; Fan, T. *Biochem. Biophys. Res. Commun.* **1986**, *141*, 1058–65.
(7) Naylor, S.; Findeis, F.; Gibson, B. W.; Williams, D. H. *J. Am. Chem. Soc.* **1986**, *108*, 6359–63.
(8) Caprioli, R. M.; Moore, W. T.; Fan, T. *Rapid Commun. Mass Spectrom.* **1987**, *1*, 15–18.
(9) Wang, T. L.; Shih, M.; Markey, S. P.; Duncan, M. W. *Anal. Chem.* **1989**, *61*, 1013–16.
(10) Caprioli, R. M.; Lin, S. N. *Proc. Nat. Acad. Sci.* **1990**, *87*, 240–43.
(11) Orkiszewski, R. S.; Gaskell, S. J. Baylor University College of Medicine, private communication, 1989.
(12) Caprioli, R. M.; DaGue, B.; Fan, T.; Moore, W. T. *Biochem. Biophys. Res. Commun.* **1987**, *146*, 291–99.
(13) Caprioli, R. M. In *Methods in Enzymology*; McCloskey, J. D., Ed.; Academic Press: New York, in press.
(14) Coutant, J. E.; Chen, T. M.; Ackerman, B. L. *Proc. 37th ASMS Conf. on Mass Spectrom. and Allied Topics*, Miami Beach, FL, May 21–26, 1989.
(15) Kokkonen, P.; Niessen, W. M.; Tjaden, U. R.; van der Greef, J. *J. Chromatogr.* **1989**, *474*, 59–68.
(16) Minard, R. D.; Chin-Fatt, D.; Curry, P., Jr.; Ewing, A. G. *Proc. 36th ASMS Conf. on Mass Spectrom. and Allied Topics*, San Francisco, CA, June 5–10, 1988.
(17) Caprioli, R. M.; Moore, W. T.; Wilson, K. B.; Moring, S. *J. Liq. Chromatogr.* **1989**, *480*, 247–57.
(18) deWit, J.S.M.; Deterding, L. J.; Moseley, M. A.; Tomer, K. B.; Jorgensen, J. W. *Rapid Commun. Mass Spectrom.* **1988**, *2*, 100–104.

Richard M. Caprioli received his B.S. degree (1965) and Ph.D. (1969) from Columbia University. After postdoctoral and faculty appointments at Purdue University, he joined the faculty of the University of Texas Medical School in 1975, where he is now professor of biochemistry and molecular biology and director of the analytical chemistry center. He is interested in the use of MS for the analysis of compounds in biological systems. Over the past several years, he has been involved in the use of FAB in applications of real-time on-line analysis of enzymic reactions. In November 1989, he organized a successful ASMS fall workshop on CF-FAB. Currently he serves on the editorial boards of Mass Spectrometry Reviews *and* Rapid Communications in Mass Spectrometry, *and he was recently appointed editor-in-chief (North America) of* Biomedical and Environmental Mass Spectrometry.

MEETINGS

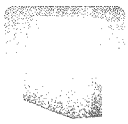

38th ASMS Conference on Mass Spectrometry and Allied Topics

The 38th ASMS Conference on Mass Spectrometry and Allied Topics will be held in Tucson, AZ, June 3–8. The meeting will consist of plenary lectures, symposia, and regular oral presentations in the mornings, Monday through Friday, and poster sessions and workshops Monday through Thursday afternoons.

Topics for the poster and regular oral sessions include biochemical applications, continuous-flow FAB, environmental applications, FT-MS and ion traps, fuels and geoscience, organic/elemental analysis, instrumentation, ion activation/dissociation, ion–molecule reactions, ionization methods, isotope ratios, LC/MS applications, LC/MS instrumentation, MS/MS, pharmacology/drugs, polymers, reaction mechanisms, and surface science. A list of the plenary lectures and symposia titles appears below.

For further information about the conference, including details on registration, housing, and transportation, contact ASMS, P.O. Box 1508, East Lansing, MI 48826 (517-337-2548).

Monday

Plenary Lecture: UV-Laser Desorption/Ionization MS of Large Biomolecules—Techniques, Promises, and Limitations. F. Hillenkamp, U of Münster
Symposium: High-Mass Ions by Electrospray and Laser Desorption. Organized by B. Chait, Rockefeller U
Symposium: LC/MS for Nonvolatile Pollutants. Organized by R. D. Voyksner, Research Triangle Institute
Symposium: Isotopic Techniques. Organized by L. W. Green, Chalk River Nuclear Laboratories

Tuesday

Plenary Lecture: FT-ICR and the Future of Cluster Surface Science. R. E. Smalley, Rice U
Symposium: Advances in Instrumental Techniques. Organized by J. Amster, U of Georgia
Symposium: State of the Art in Mass Analyzers. Organized by A. G. Marshall, Ohio State U
Symposium: Elemental MS. Organized by R. K. Marcus, Clemson U

Wednesday

Plenary Lecture: Facts and Fiction. C. Djerassi, Stanford U
Plenary Lecture: Commercializing Technology—The Competitive Challenge of the '90s. J. Young, Hewlett-Packard

Thursday

Symposium: State Selected Chemistry. Organized by M. T. Bowers, U of California, Santa Barbara
Symposium: LC/MS and Problems in Biology. Organized by R. Willoughby, Extrel Corp.
Symposium: MS/MS and Activation Methods. Organized by S. A. McLuckey, Oak Ridge National Laboratory

Friday

Plenary Lecture: Beyond Practicing Current Science. G. G. Meisels, U of South Florida
Symposium: Hybrid MS. Organized by J. A. Leary, U of California, Berkeley

Texas Symposium on Mass Spectrometry V

New Trends in Biopolymer Analysis

Texas A&M University in College Station, TX, will be the site of the Texas Symposium on Mass Spectrometry V—New Trends in Biopolymer Analysis, May 21–23. The emphasis of the meeting, which in past years has been primarily on mass spectrometry, has been expanded to include a variety of methods for the structural analysis of proteins, nucleic acids, and carbohydrates.

The program will feature invited lectures and contributed poster and oral (five-minute) presentations. Discussion periods will follow each invited lecture. To encourage debate and discussion in a relaxed atmosphere, attendance at the symposium will be limited to 125 participants.

For additional information about the symposium, contact Catherine McNeal, Department of Chemistry, Texas A&M University, College Station, TX 77843 (409-845-2355). A tentative schedule for the invited lectures follows.

Monday

The Human Genome Project. L. Hood, California Institute of Technology
DNA Sequencing. L. Smith, U of Wisconsin
Instrumentation for the Biotechnology Industry. D. Botstein, Genentech
Applications of Laser Desorption MS. F. Hillenkamp, U of Münster
X-ray Crystallography of Proteins. S. Sprang, Howard Hughes Medical Institute
Protein Structure Determination by NMR. A. Gronenborn, National Institutes of Health

Tuesday

Protein Purification and Characterization. J. Shively, City of Hope
Capillary Electrophoresis and Microcolumn LC. M. Novotny, U of Indiana
Electrospray MS. R. Smith, Pacific Northwest Laboratories
Protein Sequence Analysis by Tandem MS. D. Hunt, U of Virginia
Commercial Developments in MS. M. Story, Finnigan MAT

Wednesday

Two-Dimensional Polyacrylamide Gel Electrophoresis. R. Aebersold, U of British Columbia
Instrumental and Chemical Analyses of Carbohydrates. R. Laine, Louisiana State U and Glycomed, Inc.
Fundamentals of Laser Desorption MS. B. Chait, Rockefeller U
MS in the Protein Laboratory. P. Roepstorff, Odense U
^{252}Cf-PDMS for the Analysis of Macromolecules. R. Macfarlane, Texas A&M U

Conferences

■ **8th Annual Chemistry Graduate Student Symposium.** May 23–24. Buffalo, NY. *Contact: Cindy Burkhardt, Dept. of Chemistry, State University of New York—Buffalo, Acheson Hall, Buffalo, NY 14214 (716-831-2529)*

■ **Meeting on NMR Imaging: Recent Developments and Future Prospects.** June 6–7. London, U.K. *Contact: Scientific Meetings Secretary, The Royal Society, 6 Carlton House Terrace, London SW1Y 5AG, U.K.*

■ **3rd International Conference on Near-Infrared Spectroscopy.** June 25–29. Brussels, Belgium. *Contact: Nicole Bartiaux-Thill, Agricultural Research Center, 22, Avenue de la Faculté d'Agronomie, B-5800 Gembloux, Belgium*

■ **Meeting of the American and International Electrophoresis Societies.** June 30–July 3. Washington, DC. *Contact: American Electrophoresis Society, 27 Music Square East, Suite 134, Nashville, TN 37203 (615-327-7064)*

■ **International Symposium on Optical and Optoelectronic Applied Science and Engineering.** July 8–13. San Diego, CA. *Contact: SPIE, P.O. Box 10, Bellingham, WA 98227 (206-676-3290)*

■ **2nd International Conference on Trace Metals in the Aquatic Environment.** July 8–14. Sydney, Australia. *Contact: K. R. Brown, University of Technology, Sydney, P.O. Box 123, Broadway NSW 2007, Australia*

■ **5th International Diffuse Reflectance Conference.** Aug. 12–17. Chambersburg, PA. *Contact: David Wetzel, Kansas State University, Shellenberger Hall, Manhattan, KS 66506*

■ **International Symposium on X-ray Microscopy.** Sept. 3–7. London, U.K. *Contact: A. G. Michette, Dept. of Physics, King's College, Strand, London WC2R 2LS, U.K.*

■ **International Symposium on Gas Flow and Chemical Lasers.** Sept. 10–14. Madrid, Spain. *Contact: J. M. Orza, Instituto de Estructura de la Materia, CSIC, Seranno, 123, 28006 Madrid, Spain*

■ **6th Interdisciplinary Laser Science Conference.** Sept. 18–22. Minneapolis, MN. *Contact: Michael Scanlan, American Physical Society, 335 East 45th St., New York, NY 10017 (212-682-7341)*

■ **8th Asilomar Conference on Mass Spectrometry.** Sept. 23–27. Pacific Grove, CA. *Contact: Lazlo Tokes, Syntex Research, 3401 Hillview Ave., Palo Alto, CA 94304 (415-855-5713)*

■ **9th European Symposium on Polymer Spectroscopy.** Sept. 25–27. Cologne, F.R.G. *Contact: ESOPS 9, c/o Congress Partner GmbH, Tiefer 2 (Rhenus-Haus), D-2800 Bremen 1, F.R.G.*

Short Courses and Workshops

For information on the following courses, contact the American Association for Laboratory Accreditation, P.O. Box 200, Fairfax Station, VA 22039 (703-250-5900)

■ **Laboratory Information Management Systems.** May 2–3. Baltimore, MD

■ **Environmental Laboratory Quality Assurance and Assessment.** May 16–17. Atlanta, GA

For information on the following courses, contact Barbara Nowicki, Professional Analytical and Consulting Services, 409 Meade Dr., Coraopolis, PA 15108 (412-262-4222)

■ **EPA Environmental Analytical Chemistry.** May 7–8. Pittsburgh, PA

■ **Interpretation of IR Spectra.** May 7–9. Pittsburgh, PA

■ **EPA Organic Priority Pollutant Analyses.** May 7–11 and Nov. 5–9. Pittsburgh, PA

■ **Near-IR Principles and Applications.** May 10–11. Pittsburgh, PA

■ **Quality Assurance of Chemical Measurements.** May 24–25. Pittsburgh, PA

■ **Basics of Packed and Capillary GC.** June 11–13. Pittsburgh, PA

■ **Atomic Absorption Spectrometry.** Oct. 22–23. Pittsburgh, PA

■ **ICP/DCP Analyses.** Oct. 24–25. Pittsburgh, PA

■ **Chemometrics.** Nov. 12–13. Pittsburgh, PA

For information on the following courses, contact Tom Jupille, LC Resources, 3182C Old Tunnel Rd., Lafayette, CA 94549 (415-930-9043)

■ **Practice of Modern HPLC.** May 8–10. Saddle Brook, NJ; June 4–6. Bethesda, MD

■ **Troubleshooting HPLC Systems.** May 9. Saddle Brook, NJ; June 5. Bethesda, MD

■ **Introduction to Computer-Aided HPLC Method Development.** May 10. Saddle Brook, NJ; June 6. Bethesda, MD

■ **Sampling and Evaluating Airborne Asbestos Dust.** May 7–11. Los Angeles, CA. *Contact: University of Southern California, Institute of Safe-*

ty and Systems Management, Professional Programs, 3500 South Figueroa St., Suite 202, Los Angeles, CA 90007 (213-743-6523)

■ **Course in Experimental Design.** June 12–14, Aug. 7–9, Oct. 9–11, and Dec. 4–6. Newark, DE. *Contact: ECHIP, Hockessin Mill Plaza, Suite 6, 7460 Lancaster Pike, Hockessin, DE 19707 (302-239-5429)*

■ **Polymer Testing and Characterization.** June 14–15. Lowell, MA. *Contact: Plastics Institute of America, Stevens Institute of Technology, Castle Point Station, Hoboken, NJ 07030 (201-420-5552)*

For information on the following courses, contact Kathy Dickinson, ASTM, 1916 Race St., Philadelphia, PA 19103 (215-299-5480)

■ **Optical Emission Spectrochemical Analysis of Aluminum.** June 26–28. Indianapolis, IN

■ **Optical Emission Spectrochemical Analysis.** Oct. 16–18. St. Louis, MO

■ **Modeling, Simulation, and Optimization of Chemical Processes.** July 16–25. Cambridge, MA. *Contact: Director of the Summer Session, MIT, Room E19-356, Cambridge, MA 02139 (617-253-2101)*

■ **Environmental Applications of GC/MS.** July 30–Aug. 3. Bloomington, IN. *Contact: Executive Education Program, Indiana University, SPEA 410H, Bloomington, IN 47405 (812-855-0193)*

For information on the following courses, contact Jacob Fuchs, Dept. of Chemistry, Arizona State University, Tempe, AZ 85287

■ **Applied Molecular Spectroscopy—Infrared.** July 23–27. Tempe, AZ

■ **Modern Industrial Spectroscopy.** Aug. 6–17. Tempe, AZ

ACS Courses

■ **Polymer Characterization: Thermal, Mechanical, and Optical.** April 29–May 4. Blacksburg, VA. Thomas Ward

■ **Supercritical Fluid Extraction/Chromatography.** May 7–10. Blacksburg, VA. Larry Taylor

■ **Recombinant DNA for Chemists.** May 9–11 and June 20–22. Washington, DC. Jack Chirikjian

■ **Modern FT-NMR Spectrometry: Principles and Practice.** Blacksburg, VA. May 20–25. Harry C. Dorn

■ **Laboratory Safety and Health.** May 30–June 1. Philadelphia, PA; Oct. 15–17. Chicago, IL; Nov. 28–30. Pasadena, CA. Norman Steere, Maurice Golden, and Roger Conrad

■ **Biotechnology Separation Techniques for Chemists.** June 26–30 and July 26–28. Washington, DC. Jack Chirikjian

■ **Mass Spectrometry: Principles and Practice.** Sept. 10–14 and Dec. 10–14. East Lansing, MI. J. T. Watson

For information on these and other ACS short courses, contact the Department of Continuing Education, American Chemical Society, 1155 16th St., N.W., Washington, DC 20036 (202-872-4508)

These events are newly listed in the JOURNAL. See back issues for other events of interest.

BOOKS

Sensors, Drug Testing, Surface Analysis, and ICP/MS

Handbook of Inductively Coupled Plasma Spectrometry. M. Thompson and J. N. Walsh, Eds. xi + 316 pp. Routledge, Chapman, & Hall, 29 West 35th St., New York, NY 10001. 1989. $115

Reviewed by Diane Beauchemin, Department of Chemistry, Queen's University, Kingston, Ontario, Canada K7L 3N6

This book contains an impressive amount of valuable information on inductively coupled plasma atomic emission spectrometry (ICP-AES). It covers some fundamental aspects of the technique such as the general background (Chapter 1), analytical characteristics (Chapter 2), and instrumentation available (Chapter 3), and describes useful alternative means of sample introduction (i.e., other than nebulization) that allow the analysis of samples in the gas phase (Chapter 6) or directly as a solid (Chapter 7).

Six chapters are devoted to the application of ICP-AES to the analysis of various types of samples: silicate rocks (Chapter 4), geochemical samples (soils, sediments, etc.) (Chapter 5), water (Chapter 8), environmental samples (air, dust, animal and plant tissues, etc.) (Chapter 9), archaeological materials (Chapter 10), and metals (Chapter 12). Chapter 11 gives a good overview of inductively coupled plasma mass spectrometry (ICP/MS) and its application to geologically related samples.

However, the organization of the book would be improved if all the chapters on instrumentation appeared consecutively, followed by all those on applications, with the last chapter reserved for ICP/MS, which has similarities but is nonetheless different from ICP-AES. Except for Chapters 10 and 11 (which have been written by invited authors), cited references are not quite up to date. In too many cases, the authors omit recent references for reasons such as "reports to date have concentrated on technique rather than on routine applications," whereas they should make the latest (and logically most improved) tools available to the reader. In Chapters 8 and 9, the authors refer the reader to specialized textbooks without providing references. They give digestion procedures for biological materials and point out that they are suitable neither for oily or fatty samples nor for the accurate determination of volatile elements, yet they provide no information for these later cases. There is also no mention of microwave digestion, which is certainly an efficient means of speeding dissolution procedures. Throughout the book, the authors make some comparisons with atomic absorption techniques but do not clearly state the atomization system used (i.e., flame or electrothermal atomizer), which is somewhat misleading, given the completely different operation and analytical performances of these two techniques.

> **"...As a textbook it should prove invaluable to newcomers to the field..."**

Despite the deficiencies, this book is undoubtedly very handy. But it can only be called a handbook by specialists in the field, and certainly not by any ICP-AES user who would in most instances have to read at least a whole chapter before being able to use the information. However, as a textbook it should prove invaluable to newcomers to the field, especially those with geological interests. It is also an appropriate source of information for analytical courses on atomic emission techniques and on the variety of sampling and sample processing techniques. In general, specific information is easy to find using either the index or the table of contents. The appendices on safety precautions and on manufacturers of ICP systems certainly add a nice finishing touch to an overall impressive assessment of the wide range of applications and analytical capabilities of ICP spectrometry.

Applications of Inductively Coupled Plasma Mass Spectrometry. A. R. Date and A. L. Gray, Eds. xi + 254 pp. Routledge, Chapman, & Hall, 29 West 35th St., New York, NY 10001. 1989. $105

Reviewed by Diane Beauchemin, Department of Chemistry, Queen's University, Kingston, Ontario, Canada K7L 3N6

This book is the first to be published on inductively coupled plasma mass spectrometry (ICP/MS). It begins with a chapter by A. L. Gray (one of the main instigators of ICP/MS), which describes the historical development and theoretical basis of the technique and gives a general description of the instrumentation as well as its analytical characteristics. It constitutes a firm basis for subsequent chapters describing the applications of ICP/MS to particular types of samples or measurements. Chapters include the analysis of geological (Chapter 2), hydrological (Chapter 3), food (Chapter 6), petrological (Chapter 7), environmental (Chapter 8) and metallurgical (Chapter 9) samples, as well as isotope ratio measurements (Chapter 4) and stable isotope tracer studies (Chapter 5).

In general, the current limitations, requirements (e.g., in sample preparation) and capabilities of ICP/MS for each application are well described, with adequate references. Some inconsistencies and deficiencies, however, do exist. For instance, although the first chapter condemns using "molecular interferences" instead of "interferences from polyatomic species," other chapters in the book use the former terminology. The chapter on water resources concentrates on water samples containing relatively low levels of salt and completely omits the problems associated with saline waters such as seawater, where the very low analyte concentration and high salt level require special care in both sample preparation and analysis. In the chapter on metallurgical analyses, impressive results are presented for various samples but the precision is only reported for "clean" standard solutions.

The style of the chapters is fairly

consistent, except for Chapter 8 on environmental analysis, which resembles a journal paper and misses important details (especially on the sampling procedures) as well as some references. In many chapters, alternative sample introduction techniques for the ICP are discussed, but only once is the direct sample introduction device briefly mentioned (without even one supporting reference). The book ends with an appendix containing useful data (e.g., relative abundances, first and second ionization energies) on naturally occurring isotopes. However, no references are given for the provided data. Furthermore, the oxide bond strength of the various elements is not included. This is an unfortunate omission because, as mentioned several times in the book, isobaric interferences from polyatomic species of various elements with oxygen constitute one of the main problems in ICP/MS.

Despite the small deficiencies, this book is certainly well organized. Specific information is easy to find, using either the table of contents or the index. The book gives a very good overview of the growing range of analytical applications of ICP/MS. It makes a thorough assessment of the multielemental capability of the technique for ultratrace analysis and should therefore be welcome by analytical chemists, as well as any chemist (such as those involved in hydrology, geology, medicine, or the nuclear industry) in need of such a powerful tool. This book will prove extremely valuable to newcomers to the field. It could also be used to form the basis of a course on instrumental developments. It is undoubtedly a very nice tribute to the late Alan R. Date, who made an outstanding contribution to ICP/MS.

Methods of Surface Analysis. J. M. Walls, Ed. 342 pp. Cambridge University Press, 110 Midland Ave., Port Chester, NY 10573. 1989. $80

Reviewed by Joseph A. Gardella, Jr., National Science Foundation, Analytical and Surface Chemistry Program, Chemistry Division, Washington, DC 20550

This compact book meets a real need in the field. It is a well-organized, well-written text that is meant to introduce electron and ion spectroscopic methods of surface analysis. In a short preface, the editor points out that the plan and outline for this book resulted from short courses taught to introduce (as he puts it) "practical surface analysis" to technical personnel of all levels. Thus it presents the methodology and analytical approach necessary for problem solving, leaving the details to other, more sophisticated treatments.

This book follows a very successful treatment of the same subject (with the same title) edited by A. W. Czanderna in 1975. One of the major problems with Czanderna's book is that much of the material is terribly dated. Advances in the methodology have made many things "practical" that were not possible in 1975, so the Walls book is very timely. It is appropriate for short courses and self-study, and as a textbook for senior-level undergraduates and graduate students interested in instrumental surface chemical analysis. Unfortunately, the cost of the text ($80) limits its use as a textbook for graduate courses. This is a major drawback, in my estimation. However, this was a drawback with the Czanderna text and was partially solved by a softbound edition. I hope the publishers will consider this possibility, because it really is an excellent text.

The style is consonant throughout the book, a result of excellent editing. The content is a pleasure to read, and I consider the level of presentation more than suitable for introducing technicians to the methodology. Figures are clearly presented, and the experience of the group of authors in teaching the course together is evident.

One of the strengths is the organizational scheme. In fact, about the only complaint I have, aside from the price, is that the table of contents does not reflect the extensive work accomplished in presenting a clearly organized flow of information to the reader; it gives only the titles of the chapters. That minor point aside, the emphases in the book closely parallel those of Czanderna's text, with valuable additions. In teaching and learning this material, it is important to get away from the idea that these techniques are an unrelated group of methods—in other words, look for the unifying similarities.

In Czanderna's book, one introductory chapter dwelled on organizing the methods by schematizing by probe particles and analyzed particles. A second focused on the interaction of ion beams with solid surfaces for sputtering. Both subjects are treated in the Walls book also, including an additional excellent chapter by M. P. Seah focusing on common electron and ion energy analysis instrumentation, a subject discussed in Czanderna's book. The chapters introducing core methodologies include one each on Auger electron and X-ray photoelectron spectroscopy (XPS or electron spectroscopy for chemical analysis) and four on ion beam methodologies.

A major strength is the separate treatment of dynamic and static secondary ion mass spectrometry (SIMS) and low- and high-energy ion scattering (the latter known as Rutherford backscattering). One potential criticism is the seeming overemphasis on ion beam methods, which perhaps results from the editor's current position as head of a major surface science instrument division specializing in SIMS and (more realistically) his own research interests. However, despite the admittedly broader application of electron spectroscopies in practical surface analysis, I am delighted to find such a treatment for a text. There are many outstanding detailed books on theory, fundamentals, and applications of electron spectroscopies. Few of them give such a practical introduction to ion scattering in such an organized manner and are as up to date as this text. I was also pleased with the chapter on static SIMS; it is well written and uses specific examples to illustrate the information content of this complicated experiment.

The references are limited and critical, so there is not an exhaustive treatment of each subject. This is appropriate. Furthermore, one might complain that the examples are limited to the authors' work and are not representative of all of the leading work in the field. However, the editor and authors are to be commended for sacrificing this aspect for the consistency in presentation, and the examples given are not exclusive of any particular approach or overly restricted. There is a good index, which is short but well organized. I highly recommend this book for its intended use.

Analytical Aspects of Drug Testing. Dale G. Deutsch, Ed. xvi + 304 pages. John Wiley & Sons, 605 Third Ave., New York, NY 10158. 1989. $75.

Reviewed by Lawrence A. Pachla, Analytical Biochemistry, Sterling Research Group, 25 Great Valley Parkway, Malvern, PA 19355

Given the social–economic factor of analytical toxicology and analytical testing of drugs of abuse in today's world, this monograph should be a valuable desk reference for analytical toxicologists. Chapters provide overviews of enzyme-multiplied immunoassay techniques, solid-phase extraction, GC/MS, LC/MS, and dry reagent chemis-

tries. Additional chapters are devoted to quality assurance principles, drug screening using retention indices and LC/UV spectral analysis, direct sample analysis and microcolumn LC of therapeutic agents, pitfalls and problems associated with drug analysis using immunoassay and chromatographic assays, and methods for assaying cocaine and anabolic steroids.

Readers who expect detailed dissertations on the above-cited techniques will be disappointed. This monograph was not intended to be a definitive treatise discussing theory and providing detailed methodologies, although it does provide an overview of the available technology and methodology that are applicable to practical analytical toxicology.

Many of the chapters are written for the semi-expert. One strength of this book is that it provides literature citations for further learning. The authors have introduced how these techniques can potentially and practically be employed in the everyday analytical toxicology laboratory.

Portions of the monograph are slanted toward the theme of cooperation between physicians and laboratory supervisory scientific personnel. It is imperative that responsible individuals in the sample chain of command be aware of and understand their responsibilities so that the analytical data are properly interpreted and clinical therapy is applied. The importance of a proper quality assurance system is described in Chapters 1 and 11. Adherence to the described procedures is of paramount importance in medico-legal instances.

This book has several other strengths. It was written by a group of analytical toxicologists who wish to initiate others into the importance (and pitfalls) of applying different techniques in the analytical toxicology laboratory. Throughout the text, the authors have stressed the importance of understanding the underlying principles and ramifications of data interpretation. In addition, it is well written and easy to read. More than 600 literature references are cited that describe the various techniques and their applications. Many of the references are recent.

This book will be useful to analytical toxicologists, clinical chemists, and scientists interested in therapeutic drug monitoring and detection of drugs of abuse. The authors and editor have done an exemplary job of conveying the importance of proper data analysis and interpretation. Their efforts are commendable and should help fill a void that needs to be filled.

Introduction to NMR Spectroscopy. R. J. Abraham, J. Fisher, P. Loftus. xiii + 271 pp. John Wiley & Sons, 605 Third Ave., New York, NY 10158. 1988. $45.

Reviewed by Wolfgang G. Glasser, Department of Wood Science and Forest Products, Virginia Polytechnic Institute and State University, Blacksburg, VA 24061

The authors state in the preface to the first edition of the book that they were motivated by their desire to develop a progressive, basic text that treats the two most important nuclei, ^{1}H and ^{13}C, as an integrated whole—not as two separate phenomena. Experience with lecture courses on NMR had convinced the authors that this integrated approach was necessary for students—particularly those in organic chemistry—to gain a proper appreciation for the usefulness of NMR spectroscopy and that no adequate text was (then) available. The resulting book, published first in 1978 and adapted in the 1988 edition with only minor amendments, meets these goals with a splendid and easy-to-follow display of the basic principles and concepts of the physical phenomena underlying NMR spectroscopy, and with detailed application of these concepts to simple examples.

Following an introduction of the basic principles of NMR in Chapter 1, the book provides theoretical and practical considerations of chemical shifts and coupling constants for the ^{1}H and ^{13}C nuclei. The basic principles of the analysis of NMR spectra are covered in Chapter 4. Pulsed NMR techniques are introduced in Chapter 5, which includes a discussion of the relationship between conventional continuous-wave and pulsed experiments. Double-resonance techniques, spin relaxations, and the nuclear Overhauser effect are the subject of Chapter 6, which includes a detailed discussion of the significance and determination of spin–lattice and spin–spin relaxation times, T_1 and T_2, respectively.

The 1988 edition has been expanded by a discussion of the fundamental concepts and some applications of two-dimensional NMR and of the most common multipulse techniques. Among them are the spin–echo Fourier transform experiment (SEFT), J-resolved spectroscopy, the homonuclear and heteronuclear shift correlation, and nuclear Overhauser enhancement spectroscopy (NOESY). An extensive and highly useful Chapter 8 presents numerous applications of NMR spectroscopy with emphasis on assignment and quantitation techniques in ^{13}C NMR; biological, biochemical, and biomedical (imaging) NMR applications; and a brief mention of high-resolution, solid-state NMR.

The authors continue to meet their stated goal of providing a concise integrated introduction to ^{1}H and ^{13}C NMR spectroscopy that is well written and well illustrated. Although most of the chapters have (in the authors' words) "survived the test of time" since the first edition was published (by having had only minor changes), lack of vitality is reflected in the first six chapters: Most "recommended readings" are almost 20 years old. Despite its age, the absence of a much-needed glossary, and numerous typesetting errors, this book should nevertheless be included in the list of required readings for any serious graduate student in an organic chemistry-related field.

Expert System Applications in Chemistry. Bruce A. Hohne and Thomas H. Pierce, Eds. xi + 257 pp. American Chemical Society, 1155 16th St., N.W., Washington, DC 20036. 1989. $55

Reviewed by F. A. Settle, Jr., Department of Chemistry, Virginia Military Institute, Lexington, VA 24450

This volume supports the thesis that expert systems can be used to solve chemical problems. The development of expert systems, the most practical manifestations of artificial intelligence, is moving from the domain of the AI programmers into the domain of practicing chemists. The availability of commercial microcomputer expert system software tools is largely responsible for this development. Sixteen of the 18 total chapters describe the application of a variety of expert system development tools to a broad spectrum of chemical problems.

The introduction by the editors contains an excellent description of rule-based expert systems and a brief but informative glossary of terms associated with expert systems. An interesting philosophical discussion about the possibility of sharing knowledge bases by the chemical community follows the introduction. The applications chapters are divided into three sections: general chemical applications (seven chapters), industrial applications (five chapters), and analytical chemistry (four chapters). These applications provide examples of the major types of expert system development tools, AI programming languages (Prolog and

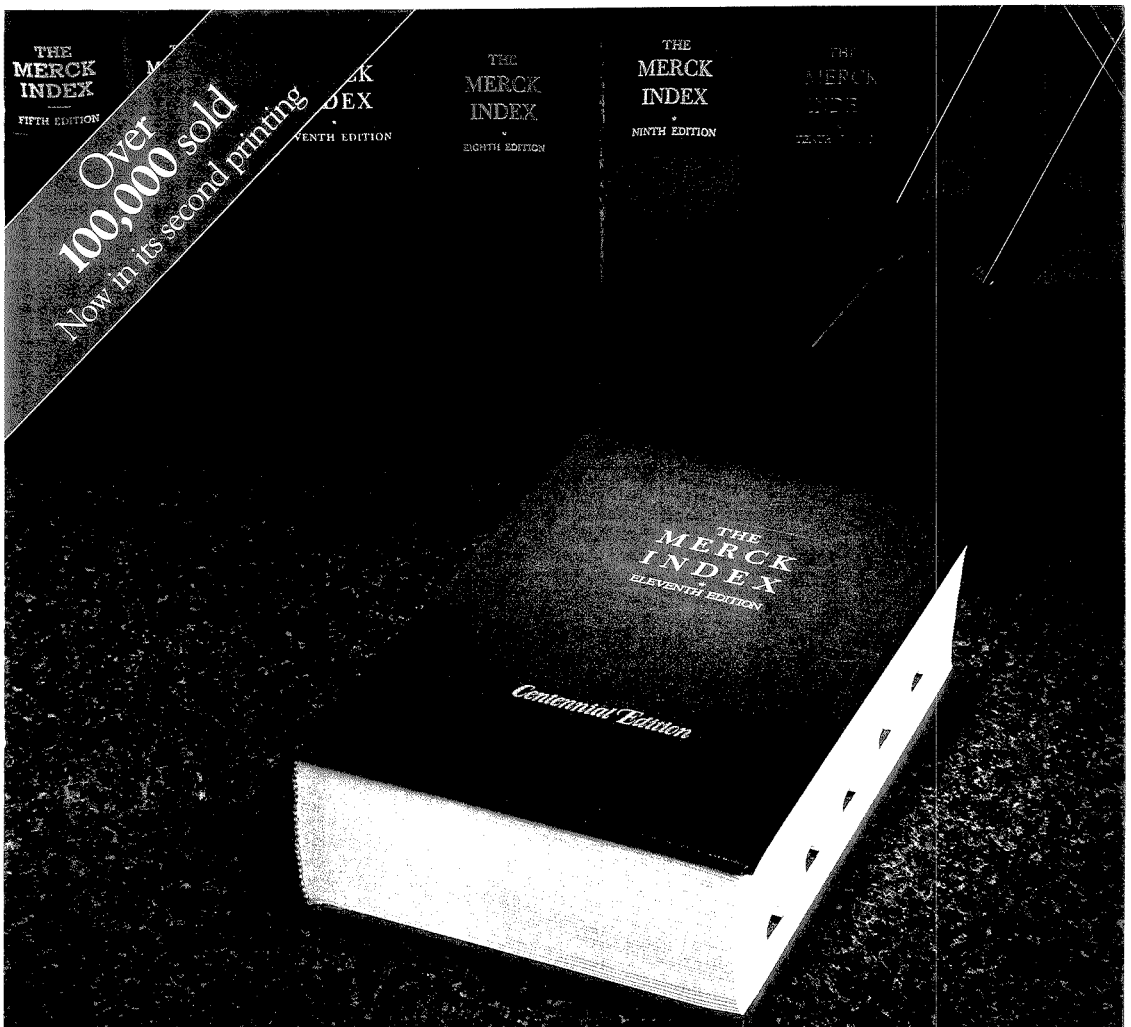

THE MERCK INDEX:
A 100-year-old classic... always contemporary

To order, call toll-free 1-800-999-3633, extension 750 (VISA or MasterCard only) or complete the coupon.

Since 1889, *The Merck Index* has kept up-to-date with the progress in science, accommodating the diverse interests of its readers. The newest edition, the Eleventh/Centennial Edition, continues this tradition with information on more than 10,000 significant drugs, chemicals and biologicals. New entries include pharmaceuticals with novel mechanisms of action, unique, naturally occurring compounds, and chemicals of environmental concern. It also features an entirely new therapeutic category/bioactivity index and CAS Registry Number indices.

Merck & Co., Inc., a research-intensive company, publishes *The Merck Index* as a non-profit service to the scientific and medical communities.

CIRCLE 92 ON READER SERVICE CARD

Enclosed is my payment for $35.00 for the Eleventh/Centennial Edition of THE MERCK INDEX. I will not be charged for shipping (U.S. only).

☐ Check enclosed. Make check payable to Merck & Co., Inc. ☐ VISA ☐ MasterCard

Card No. _____ Exp. Date _____

Signature _____

Name _____

Address _____

City _____

State _____ Zip _____

Please allow four to six weeks for delivery.

Merck & Co., Inc.
Professional Handbooks
Department 750
P.O. Box 229
Norwood, NJ 07648

LISP), tool kits (KEE), and shells (PCPLUS and KDS). Most applications involve linking the expert system to other software packages such as databases, spreadsheets, and graphics. Although the style varies considerably from chapter to chapter, most chapters are detailed enough to show why a particular tool was selected for the chemical problem and to outline the steps in the development of the application.

The analytical section contains chapters on computer-aided characterization of solids and surfaces, environmental pollutant analysis, automated metal analysis by atomic absorption, and a review of the development of PAIRS (Program for the Analysis of Infrared Spectra). The chapter on automated metal analysis details concepts that should be useful in designing expert systems for use with other analytical methods.

"...recommend this volume to any chemist wishing to explore the use of expert systems to solve chemical problems."

Each chapter contains useful references to both the literature of expert systems in general and to specific applications in chemistry. The subject and author indices are adequate. Little attention is devoted to object-oriented expert systems or semantic networks, but this appears to be an accurate representation of activity in the development of expert systems in chemistry. Although the introductory chapter provides an overview of the subject, the reader who is unfamiliar with expert systems may need to consult other references to understand the contents of the chapters that follow.

Many of the applications described in this volume are still in the prototype stage, and one wonders how many of them will emerge as mature, useful systems. This is not meant as a negative comment on this volume but as a reflection of the current state of expert system development. I feel confident that the next volume on expert systems in chemistry will contain applications illustrating successful, mature expert systems. In the meantime, I would recommend this volume to any chemist wishing to explore the use of expert systems to solve chemical problems.

Chemical Sensors and Microinstrumentation. Royce W. Murray, Raymond E. Dessy, William R. Heineman, Jiri Janata, and W. Rudolf Seitz, Eds. xii + 410 pp. American Chemical Society, 1155 16th St., N.W., Washington, DC 20036. 1989. $90

Reviewed by Otto S. Wolfbeis, Analytical Division, Institute of Organic Chemistry, Karl-Franzens-University, A-8010 Graz, Austria

---

Analytical scientists witness an impressive development of sensor technology, and this book reflects a large part of it. Improvement in existing techniques and sensing schemes, rapid development and commercialization of new methods (mainly in biomedical, biotechnology, and environmental sciences), and successful application of fundamental sensing methods to increasingly difficult analytical problems are factors that contribute to the broad interest in this field.

This book developed from a symposium with the same title and, given the recent activities in this field, is rather timely. It contains 25 chapters and is divided into sections on electrochemical sensors, mass and thermal microsensors, and optical sensors. Each section starts with an introduction and contains a representative number of authoritative papers—some more of review character, others of an original paper type. In most cases, the literature cited is both extensive and representative up to 1989.

The chemical sensors described are mainly intended for use in sensing clinical parameters such as pH, gases, cations, or anions. Attention is also paid to enzyme-based biosensors and immunosensors, and to sensors for vapors and industrial hygiene. Surprisingly, specific sensors for use in process control and environmental monitoring have not been found. Some sections cover a broad range in development, from first proof of principle up to methods of characterization of sensing membranes (with respect to aging effects and other practical considerations that are important in sensor mass fabrication).

In the Electrochemical Sensor section, eight papers give a state-of-the-art description of current problems and activities. Potentiometric and amperometric (voltammetric) methods as well as an interesting combination of electrochemistry and fiber-optic sensing (called "fiber-optic electrode") are described, with particular emphasis on the use and characterization of new materials and enzymatic techniques. Chapter 7 is an excellent contribution to the bioelectrochemistry at microelectrodes using artificial and natural mediators. However, I missed a chapter on conductometry that turned out to be so useful in FIA of biomolecules.

In the Mass and Thermal Microsensors section, an interesting article describes the measurement of enzyme reaction enthalpies via fiber optics, and four others discuss the construction and performance of piezoelectric and related resonator devices—including the characterization of new coatings and other materials. Applications include vapor sensing (or probing) and liquid-phase sensors (which virtually were unknown a couple of years ago).

In the Optical Sensors section, nine chapters cover aspects of sensor design; construction; optimization of sensing membranes and multiwaveguide structures; and new sensing schemes such as receptor-based optical transduction, pattern recognition in multiwaveguide sensing, and fluorescence lifetime measurements through fiber optics. In view of the wealth of optical sensing methods, this indeed is a very good and representative selection. Aspects of microfabrication are not treated sufficiently, however.

The individual chapters require basic knowledge of the respective field (which can be had from other books), and most offer detailed discussion of the instrumentation used. A carefully edited subject index completes the book.

Given the title of the book, I would have expected more information on the progress that has been made in microinstrumentation. As is stated in the preface, the substantial intermingling and dependence of modern chemical sensors and miniaturization ideas in physical and chemical transducers have become evident in the past years. Microinstrumentation design, which is of particular interest to people in (or close to) industry, is discussed in some depth in only a few chapters.

Aspects of material sciences that are crucial in the development of microsensors and sensing membranes for use with real samples are treated in several very useful chapters. In fact, this aspect is often ignored in related books, most of which focus only on sensing schemes and techniques.

This is a useful book for researchers active in one of the main disciplines (i.e., electrochemical, optical, resonator, and thermal sensors). It can be highly recommended because it reflects the latest developments that are of interest both for those working in their field and those who want to see what their competitors in other areas are doing.

Advances in Electrophoresis Volume 1. A. Chrambach, M. J. Dunn, and B. J. Radola. 441 pp. VCH Publishers, Suite 909, 220 East 23rd St., New York, NY 10010

Reviewed by Tom van de Goor and Frans Everaerts, Laboratory of Instrumental Analysis, Department of Chemistry, Eindhoven University of Technology, P.O. Box 513, 5600 MB Eindhoven, The Netherlands

In the vast field of chemical and biological sciences, electrophoresis has become an important tool of analysis. The use of flatbed gels for 2D electrophoresis, in combination with sensitive detection methods, offers a powerful method for characterization of biochemical compounds.

Recently capillary electrophoretic techniques have rapidly grown into an automated high-resolution technique that will even increase the field of electrophoretic techniques. Volume 1 of *Advances in Electrophoresis* can be a useful source of information for those currently using the technique or to give an overview of applications. Especially when you have limited time to follow the developments in the original literature, it offers you an interesting compilation with a large amount of valuable references. The following subjects are discussed:

- Two-Dimensional Polyacrylamide Gel Electrophoresis by M. J. Dunn (110 pp. and 587 refs.). A practical description of the powerful field of 2D analysis describing many steps in preparation of gels and samples and several methods of detection.
- Detection of Proteins Separated by Electrophoresis by C. R. Merril (30 pp. and 98 refs.). Several ways of staining proteins are described both pre- and postelectrophoretically together with the quantitative effects involved.
- Protein Blotting: A Tool for the Analytical Biochemist by J. M. Gershoni (36 pp. and 148 refs.). Blotting is used to transfer electrophoretically separated materials from their supporting gel to an immobilized matrix. Applications of this technique in the protein field are described.
- Electrophoresis of DNA in Agarose and Polyacrylamide Gels by N. C. Stellwagen (52 pp. and 155 refs.). The theory of gel electrophoresis of DNA fragments is discussed to explain their electrophoretic behavior. Several types of experiments are given to illustrate the applications.
- Affinity Electrophoresis by K. Takeo (52 pp. and 207 refs.). A very interesting survey is given on theory and applications of the very specific and powerful method of affinity electrophoresis. The extensive tabular data are impressive and most useful.
- Recent Trends in Capillary Isotachophoresis by P. Gebauer, V. Dolník, M. Deml, and P. Boček (82 pp. and 239 refs.). A review is given on capillary isotachophoresis, which for many biochemists is still an unknown field. Description of instrumentation is important in this technique where commercial equipment is hard to find, although the applications are extensive, as shown in a survey table.
- Preparative Polyacrylamide Gel Electrophoresis of Proteins by R. Horuk (19 pp. and 30 refs.). Although short, this review shows the possibilities and limitations concerned with preparative electrophoresis.
- Red Cell Enzyme Markers in Forensic Science: Methods of Separation and Some Important Applications by J. G. Sutton (50 pp. and 30 refs.). This chapter describes the electrophoretic fingerprinting of proteins in blood samples. It is a readable chapter describing the technique and applications.

To conclude, this book is a useful overview of electrophoretic techniques, with emphasis on applications. Missing, however, is the technique of isoelectric focusing, and no attention is paid to the fast-growing field of capillary zone electrophoresis.

Books Received

PCR Technology: Principles and Applications for DNA Amplification. Henry A. Erlich, Ed. x + 246 pp. Stockton Press, 15 East 26th St., New York, NY 10010. 1989. $20

Topics covered in the 19 chapters of this book include automation, sample preparation, sequencing, gene expression, and diagnosing disease. The references are from the 1980s through 1989. An index is included.

Computerized Multiple-Input Chromatography. M. Kaljurand and E. Küllik. 225 pp. John Wiley & Sons, 605 Third Ave., New York, NY 10158. 1989. $105

The five chapters in this book are entitled "Introduction," "Correlation Chromatography," "Two-Dimensional Measurements Involving Chromatography," "Instrumentation," and "Application of Multiple-Input Computerized Chromatography." The references are from the 1970s and 1980s, up to 1986. Four appendices, a list of notation and abbreviations, and an index are included.

Flow Injection Analysis: A Practical Guide. Bo Karlberg and Gil E. Pacey. xii + 372 pp. Elsevier Science Publishers, P.O. Box 1663, Grand Central Station, New York, NY 10163. 1989. $117

Topics include principles, components, detectors, modes of operation, selectivity enhancement, developing a method, and applications. The references are from the 1970s and 1980s, up to 1988. An appendix, an index, and a bibliography of almost 1400 references are included.

Clinical Chemistry. E. Howard Taylor, Ed. ix + 293 pp. John Wiley & Sons, 605 Third Ave., New York, NY 10158. 1989. $75

Chapters in this book are entitled "Preanalytical Variables," "Quality Control and Quality Assurance," "Electrolytes and Acid–Base Disorders," "Evaluation of Renal Function," "Proteins," "Enzyme Analysis," "Hormone Immunoassays," "Coagulation," "Therapeutic Drug Monitoring," and "Clinical Laboratory Evaluation of Vitamin Nutritional Status." The references are from the 1970s and 1980s, up through 1986. An index is included.

ASTM Standards on Chromatography, 2nd ed. Roberta A. Storer, Ed. xvii + 807 pp. American Society for Testing and Materials, 1916 Race St., Philadelphia, PA 19103. 1989. $69

This book contains 137 testing methods using GC, LC, TLC, steric exclusion chromatography, IR spectroscopy, and electron impact MS for paint, paper, plastics, rubber, soaps, and other materials. Four proposed methods are also included. A three-table index facilitates finding the appropriate method for the substance to be tested. An index and a membership application are also provided.

The Enzyme Catalysis Process: Energetics, Mechanism, and Dynamics. Alan Cooper, Julien L. Houben, and Lisa C. Chien, Eds. ix + 493 pp. Plenum Publishing, 233 Spring St., New York, NY 10013. 1989. $110

This book contains 30 presentations from the Proceedings of a NATO Advanced Study Institute held in Barga, Italy, in July 1988. The 25 lecturers represent Italy, Canada, the United Kingdom, France, the United States, and Germany. Most of the references are from the 1970s and 1980s, up to 1988. A list of workshops, posters, and participants, as well as an index, are included.

Diagnosing Sick Buildings

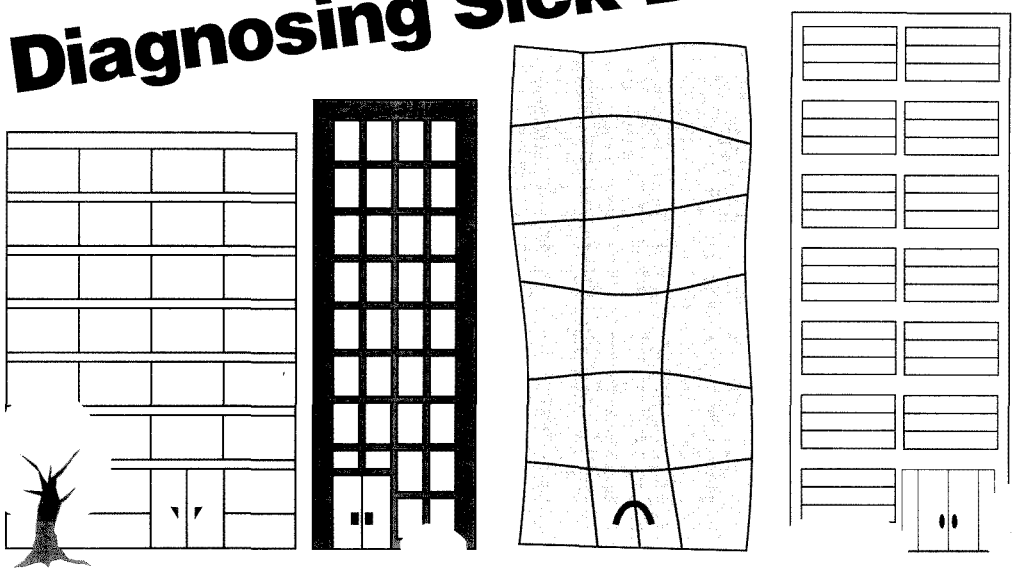

When most people think of air pollution, they picture factory smokestacks belching black smoke and cars trailing blue exhaust. Since the federal Clean Air Act was passed by Congress in 1970, billions of dollars have been spent fighting outdoor air pollution. However, recent Environmental Protection Agency (EPA) studies reveal that most people are exposed to more harmful pollutants in their homes and offices than outdoors. Because of this, EPA is now studying ways to rid indoor air of benzene and other polycyclic aromatic compounds found in tobacco smoke; formaldehyde and polychlorinated biphenyls (PCBs) from building materials; and volatile compounds often found in paints, air fresheners, and common household cleaners. Analytical chemists are supporting these efforts by developing new methods for sampling and analyzing indoor air.

The causes of indoor air pollution have been around for a long time, but it was not until the energy crisis of the early seventies, when increased emphasis was placed on energy-efficient "tight" buildings, that "sick" buildings began to attract attention. Many of these new and remodeled buildings lack windows that can be opened, resulting in poor air circulation. In fact, a recent study by the National Institute for Occupational Safety and Health indicates that as many as half of the cases of sick building syndrome (SBS) can be blamed on poor ventilation. People living or working in a sick building may exhibit symptoms such as drowsiness, nausea, sneezing, headaches, and dizzy spells. Analytical methodology has targeted these pollutants roughly according to the volatility of the compound of interest.

Volatile organic compounds

Although formaldehyde has been implicated in many cases of SBS, other volatile organic compounds (VOCs) may also be contributing to the depression, lethargy, and irritability often associated with formaldehyde exposure, according to Lance Wallace, an EPA scientist who has directed studies of total exposure to both indoor and outdoor pollutants. Furthermore, exposure to other highly reactive compounds, such as SO_2, ozone, acrolein, allyl alcohol, allyl acetate, or allyl ether, can have the same symptomatic effects as formaldehyde exposure.

According to Linda Sheldon, a member of the team of analytical chemists at the Research Triangle Institute (Research Triangle Park, NC) that has been developing indoor air monitoring methods for EPA, successful methods for measuring VOCs must be capable of detecting pollutants at ambient levels (i.e., ppt–ppb levels); use collection/measurement devices that are lightweight, compact, and quiet for use in the field; provide accurate and reproducible analysis with a minimum of artifactual and contamination problems; and allow for reasonable sampling periods that are compatible with monitoring needs.

These methods can be classified into two broad groups: analytical methods that detect and quantitate VOCs on site and methods in which VOCs are collected and concentrated on a sorbent for later analysis. Each group can

FOCUS

be further divided into active methods, in which a power source is used to pull air across a sensor or collector, and passive methods, which rely on permeation or diffusion to bring the analyte in contact with the collector or detector. Although on-site analytical methods can provide concentration profiles rather than the time-integrated averages offered by collection methods,

they are more complex and expensive and require significant calibration and maintenance in the field.

Collection methods for vapor-phase organics commonly involve collection on a solid sorbent, such as a polymeric resin (e.g., Tenax GC or XAD), activated carbon, or a carbon molecular sieve. These sorbents can be used for a wide variety of VOCs, and because they have a low affinity for water, their collection efficiency is not strongly dependent on humidity. Inorganic adsorbents (such as silica gel, alumina, and florisil) are not commonly used for collecting VOCs in air, however, because they readily adsorb water, which deactivates their surface sites.

Either thermal or solvent desorption is then used to desorb collected organic compounds from the sorbent. Because polymer resins reversibly adsorb organic compounds, thermal desorption followed by GC/MS analysis, which provides positive identification of target organics as well as broad spectrum analysis, is normally used. Activated carbon, on the other hand, chemically binds organic compounds and thus requires solvent desorption for efficient recovery of collected compounds. Solvent desorption usually precludes GC/MS analysis for low molecular weight organics because the solvent front interferes with the analysis. In these cases, solvents such as carbon disulfide or acetone are used, and GC detectors that are relatively insensitive to the eluting solvent, such as flame ionization, electron-capture, or nitrogen–phosphorus detectors, are employed. Overall, the sensitivity of the solvent desorption methods is less than that for thermal desorption because only a fraction of the sample is analyzed.

An alternative to sorbent methods involves collecting air samples in stainless steel canisters rather than on a sorbent cartridge. "Essentially," says Sheldon, "air is sucked into the canister in the field. Once the canister is brought back to the lab, about 200 mL of the collected air is cryofocused and analyzed using GC/MS with selected ion monitoring." This method has replaced the Tenax–desorption method for many very volatile compounds.

Although real-time analytical methods can provide more information than the passive collection methods, they are not commonly used for organics because of contamination problems at the ambient levels necessary for effective indoor air monitoring. Most existing real-time methods have been developed for inorganic species (e.g., NO_2 and SO_2), although instruments for monitoring formaldehyde and acrylonitrile are also available. "Although these instruments have potential," says Sheldon, "they were primarily developed for workplace monitoring, and they just don't quite have the sensitivity necessary for detecting part-per-trillion levels of organics."

Formaldehyde

Because formaldehyde from insulation and building materials is among the more common indoor pollutants, specialized methods have been developed for determining formaldehyde in air. These methods involve in situ derivatization with 2,4-dinitrophenylhydrazine (DNPH) followed by reversed-phase LC. Air samples are collected either on silica gel cartridges coated with acidified DNPH or in impingers containing acidified DNPH–acetonitrile solution. Back in the lab, the cartridges are eluted with acetonitrile while the impinger solutions are brought to volume with acetonitrile; the solutions are then analyzed for formaldehyde by LC.

Semivolatile and nonvolatile organic compounds

Semivolatile and nonvolatile organics include polycyclic aromatic hydrocarbons (PAHs), organochlorine and organophosphorous pesticides, PCBs, and chlorinated dibenzodioxins and furans. These compounds get into the air primarily from cigarette smoke, plasticizers in building materials, and the use of pesticides for insect and rodent control.

Common methods for sampling semivolatile and nonvolatile compounds involve the use of polyurethane foam (PUF) plugs or XAD resin. PUF has a number of advantages over other adsorbents, including low flow restriction, ease of purification and handling, and low cost. XAD, however, has better retention characteristics for the more volatile pesticides and PCBs, allowing lower detection limits for these compounds. PUF also forms mutagenic artifacts during sampling, reducing its usefulness as a collection medium for bioassay studies.

After sample collection, the analytical techniques used for both PUF and XAD are generally the same as for other media. The sorbent is extracted with a suitable solvent and the extractant analyzed using GC/MS or LC with fluorescence or ultraviolet detection for PAHs, chlorinated dioxins, and furans, and GC with electron capture detection for PCBs. Chromatographic cleanup is often needed to achieve the required sensitivity.

Biological factors

Indoor biological pollution is only beginning to receive the same type of at-

PROGRESS IS OUR TRADITION

In 1851 Heinrich Emanuel Merck guaranteed highest quality to his customers. This guarantee is still one of our commitments today.

The LiChroGraph® HPLC Systems are outstanding products in our chromatography line-setting new trends in analytical HPLC.

CIRCLE 88 ON READER SERVICE CARD

E. Merck, P.O. Box 4119, 6100 Darmstadt 1
Phone +49/6151/72-0

MERCK

JOURNAL OF CHEMICAL AND ENGINEERING DATA

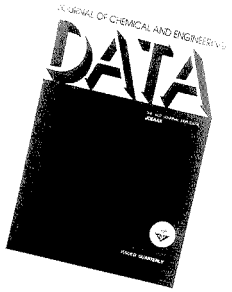

Get A World Of Precise, Accurate Data In This International, Quarterly Journal

Multidisciplinary in nature and international in scope, the *Journal of Chemical and Engineering Data* (*JCED*) features contributions by distinguished physicists, chemists, chemical engineers, mechanical engineers, biological scientists, and applied mathematicians from the world over. Their expert reports represent numerical data bases for private technical information systems, particularly in industry, that will broaden your scientific horizons and improve the quality of your work.

This unique journal offers you precise, accurate data on physical, thermodynamic and transport properties of well-defined materials. It also keeps you informed about the latest international standards on symbols, terminology and units of measurement for reporting data properly.

You'll find numerical property data measurements on:

- pure substances of defined purity
- well-defined gaseous, liquid and solid mixtures
- semi-empirical and theoretical correlations useful in interpolating, extrapolating and predicting properties of scientific and technological importance
- new substances — the physical and spectral properties of inorganic, organic, and biochemical substances and other complex substances prepared by established synthetic procedures that may have major scientific and technological applications

1990 SUBSCRIPTION INFORMATION

Volume 35
4 Issues Per Year

		U.S.	Canada and Mexico	Europe (Air Service Included)	All Other Countries (Air Service Included)
ACS Members	1 year	$ 30	$ 35	$ 37	$ 40
	2 years	$ 54	$ 64	$ 68	$ 74
Nonmembers	1 year	$207	$212	$214	$217
Supplementary Material on Microfiche		$ 12	$ 16	$ 16	$ 16

Member subscription rates are for personal use only.
For nonmember rates in Japan, contact Maruzen Co., Ltd.

Journal subscriptions start January 1990 and are based on a calendar year.

Address your orders or inquiries to:
American Chemical Society
Sales and Distribution Department
1155 Sixteenth Street, N.W.
Washington, DC 20036

Toll free (800) 227-5558
Outside U.S. (202) 872-4363
Telex: 440159 ACSPUI or
892582 ACSPUBS
Fax: (202) 872-4615

This publication is available on microfilm, microfiche, and electronically through Chemical Journals Online on STN International.

tention as indoor chemical pollution, according to Harriet A. Burge of the University of Michigan Medical School. This apparent lack of study stems from the difficulties of sampling biological aerosols and their variable health effects. The majority of biological pollutants comes from outdoors (e.g., pollen) and causes disease only in sensitized people. Outbreaks of Legionnaires' disease, caused by buildup of *Legionella pneumophila*, however, can affect a larger number of people, and have made the public more aware of indoor biological pollution.

There is no single method of choice for sampling airborne microbial particles, although there are three major sampling strategies: viable particle sampling, particulate sampling with visual assessment, and immunological sampling.

The most widely used type of viable sampling involves the use of a settle plate, in which a plate of culture medium is set out uncovered for a period of time to collect viable spores. Unfortunately, because the chance of impingement is directly related to a particle's mass (and thus its size), large particles are almost always overrepresented. As an alternative to settle plates, volumetric cultural sampling devices draw air through a defined orifice using a vacuum pump, accelerating the air to the point that most particles impact. Although this method ensures collection of all microbe sizes, only particles that will grow under the given culture parameters will be recovered.

Particulate sampling with visual assessment is useful primarily when dealing with large particles such as pollen or fungal spores. Either impaction samplers or suction traps are used to collect microorganisms, which are then identified and counted under a microscope.

For immunological sampling, samples are drawn from large volumes of air and either impinged on a filter, dissolved or suspended in a liquid, or frozen from the air on the walls of cooled containers. The samples are then used in immunoassays for antigen-specific antibodies. This method is more sensitive than either viable or visual discrimination methods, but it cannot be used for screening because it necessitates prior knowledge of a target microorganism.

Control measures

What can we do to control indoor air pollution? Probably the easiest thing to do is to remove the source of the pollutants. "This can be difficult if the source is unknown or if the pollutants are in the building materials," says Wallace, "but often getting rid of all the paint cans, aerosol spray cans, and solvents in the building will solve the problem. It's best to store such chemicals in a detached garage or in the attic rather than in the basement, so that they are out of the airflow leading into the living areas of the building."

The next step is to ensure that buildings have adequate ventilation so that toxic levels of pollutants do not accumulate. There is also evidence that ordinary house plants can help to control VOCs in indoor air. A National Aeronautics and Space Administration study found that philodendrons, spider plants, and the golden pothos are most effective in absorbing formaldehyde, while flowers like the gerbera daisy and chrysanthemums can reduce levels of benzene. English ivy, peace lily, mother-in-law's tongue, and Chinese evergreen are also effective air purifiers. Biological indoor pollution can be prevented by filtering the air entering a building, eliminating standing water in which microbes can multiply, and controlling dust in the building.

EPA is now getting firsthand knowledge of indoor air pollution. The *Washington Post* reports that workers in the Washington, DC, headquarters building have been complaining of respiratory and neurological symptoms for the past few years. Like most buildings erected 20 years ago, EPA headquarters was designed to be energy efficient, with the flow of outside air restricted and most windows sealed. Environmental monitoring revealed not only the presence of phenylcyclohexane emitted from the latex backings of newly laid carpet but also low levels of other toxic compounds as well as legionella bacteria in outdoor air conditioning cooling towers and pneumonia bacteria in a cooling system drip pan. EPA officials have promised to improve ventilation in the building to at least partially eliminate the problem.

Although EPA's budget for indoor air pollution is increasing, it may be many years before all aspects of this complex issue are under control. In the meantime, it may be wise to dispose of all unnecessary paint cans, aerosol spray cans, and solvents; stop smoking; open your windows; and keep those house plants healthy. *Mary Warner*

Suggested reading

Stammer, L. B. *Washington Post Health*, Jan. 23, 1990, p. 17.

Wallace, L. A. *Proc. APCA Ann. Meet.*; Air Pollution Control Association: Pittsburgh, PA, 1988; 88-110.6.

Indoor Air and Human Health; Gammage, R. B.; Kaye, S. V., Eds.; Lewis Publishers: Chelsea, MI, 1985.

Tejada, S. *Int. J. Environ. Anal. Chem.* **1986**, *26*, 167–85.

NEW PRODUCTS

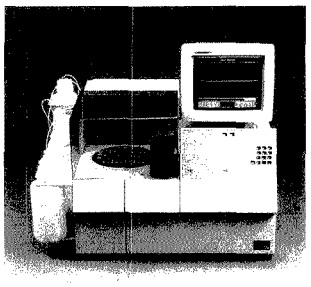

Integral 4000 liquid chromatography system features a built-in four-solvent pump, multiwavelength detector, 109-position random access autosampler, column oven, and data manipulation software. Perkin-Elmer **401**

LC. PF1C biocompatible photodiode array HPLC detector features a high-output tungsten–halogen source, 512-element diode array, data acquisition and analysis capabilities, and three nonmetallic flow cells for analytical and preparative procedures. Groton Technology **404**

Air sampling. LFS 113D is a dual-mode air sampler that provides constant flow for individual sorbent tube sampling and constant pressure for multiple sorbent tube sampling. A pneumatic control system provides pulsation-free flow in both modes. The unit is rechargeable and features a battery test LED. Gilian Instrument **405**

Calorimeter. Model 4207 differential scanning calorimeter operates over the temperature range −30 to 110 °C and detects changes in heat capacity of 10 μcal/degree. The system features four cell cavities and removable sample ampules. Hart Scientific **406**

Microanalysis. Voyager X-ray microanalysis system features a Sun Microsystems SPARC-based workstation and an X-ray detector with a diamond window and germanium crystal. Users can produce custom reports that combine entered text with tabular and spectral data as well as images from the system's screens. Tracor Northern **407**

Leak detectors. Gas leak detectors incorporate a thermistor-actuated thermal conductivity cell in a Wheatstone bridge circuit. A specially designed hand-held probe allows leaks to be detected in inaccessible places. Helium and refrigerant leaks can be detected at rates of 1.0×10^{-5} cc/s and 1.1×10^{-4} cc/s, respectively. Gow-Mac **408**

Diode array. Quickscan is a high-performance thermoelectrically cooled diode array specifically designed for multichannel detection. Applications include radiometry, plasma monitoring, colorimetry, and process control. Spex **409**

Centrifuge. KR422 high-capacity floor model centrifuge accommodates up to 6.4 L and can achieve an RCF of 7300*g*. Features include microprocessor control, refrigeration, steel guard barrier ring, imbalance detector, dual lid interlock, and four rotor systems. Jouan **410**

NMR. AdvanceTec-MRS portable NMR quality control system incorporates a spinner that does not require an external source for operation. The 42-MHz system, which weighs 75 lbs, features a 100-KHz-per-channel, 16-bit A/D converter. Advanced Techtronics **411**

LC detector. UV–VIS is a variable-wavelength UV–vis absorbance monitor with a bandwidth of 6 nm and wavelength accuracy of ±1 nm. The detector can be used with a deuterium or tungsten lamp and accommodates flow cells ranging in volume from 0 to 15 μL. Chrompack **412**

IR. FTS 60A research-grade FT-IR spectrometer, which covers the range from 15,000 to 10 cm^{-1}, features dynamic interferometer alignment, resolution of 0.25 cm^{-1}, and a sample compartment with purge protection and IR-transparent shutters. Bio-Rad, Digilab Division **413**

Software

Regulations. RegScan RCRA, designed for IBM PC-AT, PC-XT, and PS/2 computers, allows users to quickly access federal solid waste regulations. The complete text of the solid waste regulations from Title 40 CFR Parts 240–299 is provided. Regulation Scanning Technology **415**

NMR. MRPEST, Magnetic Resonance Pulse Stimuli, is a DOS-based Windows software program for the simulation of sophisticated pulsed FT-NMR experiments for groups of spin 1/2 nuclei. Intended for instructors, students, and researchers, the program allows the user to test a proposed pulse sequence without actually performing the experiment. Wisc-Ware **416**

Manufacturers' Literature

Newsletter. *Biotext*, Vol. II, No. 4, includes articles on Amberchrom resins for purification, concentration, and recovery of biomolecules; enzyme purification scale-up; and sample preparation for monitoring antipsychotic drugs. 12 pp. Supelco **418**

AA. Brochure describes the Z-8100 polarized Zeeman atomic absorption spectrophotometer, which features a tandem flame–furnace design, 60-position autosampler, and eight-lamp turret. 8 pp. Hitachi **419**

Oxygen. "Guide to the Selection of Oxygen Analyzers" includes historical information on the discovery of oxygen and the development of measurement techniques. Detailed information on a variety of oxygen analyzers is provided. Delta F **420**

For more information on listed items, circle the appropriate numbers on one of our Readers' Service Cards

Sample preparation. Brochure highlights the MilliLab workstation, which performs filtration, solid-phase extraction, evaporation, single and serial dilutions, mixing, gas purging, and addition of standards and reagents. 18 pp. Waters Chromatography Division of Millipore 421

Catalogs

Chemicals. Catalog lists research chemicals, ceramics, pure elements, alloys, analytical standards, catalysts, glassware, platinum labware, and precious metals. 1120 pp. Johnson Matthey/Alfa 425

HPLC. Catalog features fittings and accessories, including biocompatible filters, frits, and check valves. Information on solvent compatibility, material properties, and system applications is provided. Upchurch Scientific 426

Scientific products. Color-coded catalog includes compact laboratory water systems, centrifugal filter devices, blotting membranes and transfer systems, and environmental testing products. 400 pp. Millipore 427

Spectroscopy. Catalog features supplies and accessories for atomic spectroscopy systems, including lamps, burner system components, ICP torch accessories, graphite furnace tubes, sampling supplies, standards, and products for ICP/MS. 60 pp. Perkin-Elmer 428

GC. Catalog features specialty gas chromatography columns and reference standards for environmental applications. EPA 500, 600, and 8000 series methods are discussed. Quadrex 429

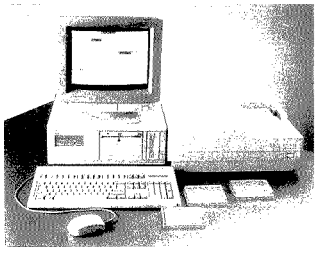

CytoFluor fluorescent measurement system is a computer-controlled scanning device for multiwell plates that can be used to quantify both soluble and cell-associated fluorescent signals. Millipore 402

NOW YOU CAN SEARCH RSC JOURNALS ONLINE

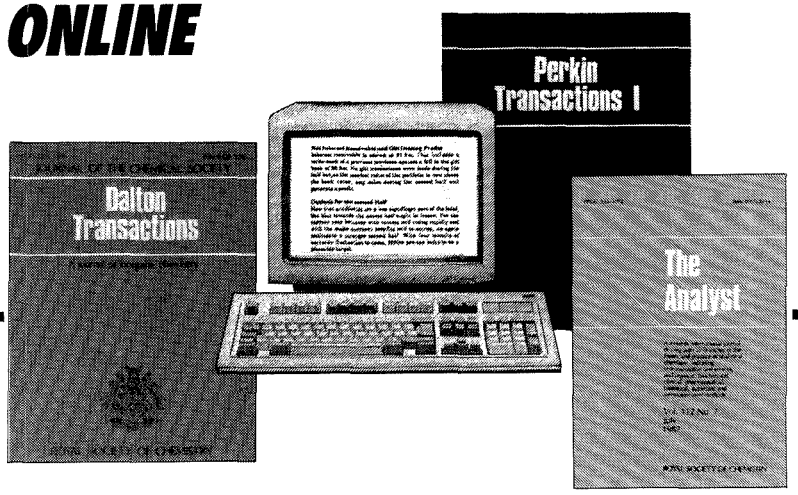

The main primary journals published by the Royal Society of Chemistry (RSC) are now searchable online via **CHEMICAL JOURNALS ONLINE (CJO)** – a family of new online files produced by the American Chemical Society and available through STN International.

The RSC journals file **(CJRSC)** includes Chemical Communications. Dalton Transactions. Faraday Transactions (I* & II). Perkin Transactions (I & II). The Analyst. Journal of Chemical Research.* Journal of Analytical Atomic Spectrometry. Faraday Discussions.
*Available from 1988

CJRSC may be searched alone or in conjunction with other components of the **CJO** database which includes ACS journals and polymer journals published by Wiley.

The unique Crossover facility from STN enables you to perform the same search on CJRSC and CAS ONLINE thereby combining the breadth of coverage of Chemical Abstracts with the depth of coverage of RSC journals.

Online access to the RSC journals provides you with a convenient, rapid and economical means of keeping up with the latest significant research in the chemical sciences.

For more information, call (614) 421-3600, or return the form below to: STN International, c/o Chemical Abstracts Service, 2540 Olentangy River Road, P.O. Box 02228, Columbus, OH 43210.

Please send me more information on CJRSC and the Chemical Journals Online data base.

Name .....

Address .....

.....

.....

CHEMICAL JOURNALS ONLINE

ANALYTICAL APPROACH

REAL-TIME DETECTION of Chemical Agents Using Molecular Beam Laser Mass Spectrometry

Jack A. Syage
Aerophysics Laboratory
The Aerospace Corporation
P.O. Box 92957
Los Angeles, CA 90009

The alleged production and use of chemical warfare agents are causes for great concern. When these agents are unleashed into the atmosphere, the physiological response is quick and dramatic. Short-term exposure can be lethal at parts-per-million levels, and even at parts-per-billion concentrations chemical warfare agents can cause serious, irreversible injury. These concerns prompted our efforts to develop a detector as a warning system for chemical warfare agents. For obvious reasons, the detector must be sensitive and have a rapid response time. Less obvious is the fact that the system must be selective and able to distinguish between poisonous molecules and those that normally exist in the atmosphere. In other words, anyone can find a needle, but finding one in a haystack poses a more challenging problem.

Our molecular detection work centers on the use of multiphoton ionization (MPI) and mass spectrometry (MS) (*1*). By enhancing MPI-MS with supersonic molecular beam expansion (*2*), resonance-enhanced excitation, and time-of-flight (TOF) mass detection, we have been able to design a suitable detection system.

MPI-MS

MPI occurs when a molecule sequentially absorbs photons until the total energy of the molecule exceeds the ionization potential. Resonance-enhanced MPI occurs when the photon wavelength chosen matches an absorbing state of the molecule. The resonance step not only substantially improves sensitivity but also provides a means for selectively ionizing molecules. If the intermediate resonance absorption lineshapes are narrow, then the likelihood of excitation frequencies overlapping for different molecules diminishes dramatically. Selective ionization for a particular molecule would occur despite the abundance of other molecules in the sample. Hence high-resolution spectroscopic techniques translate into highly selective detection (*3–6*).

In high-resolution supersonic molecular beam spectroscopy (Figure 1), the most important element is the expansion of gas at high pressure (atmospheric gas in this case) into a vacuum. Because of the dynamics of the expansion, the sample undergoes substantial cooling of the internal rotational and

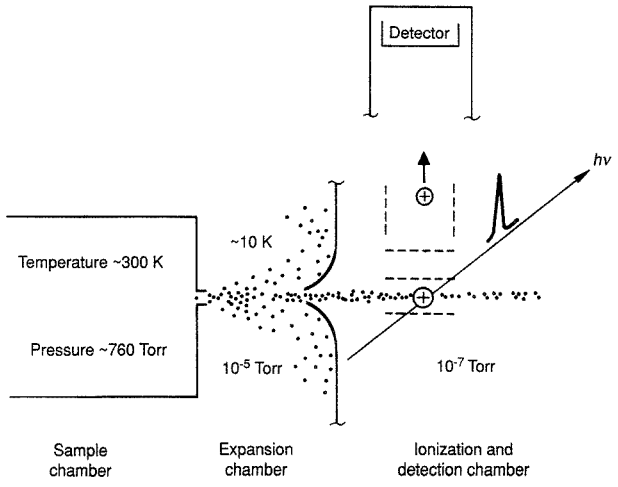

Figure 1. Pictorial view of the molecular beam laser MS technique.

0003-2700/90/0362-505A/$02.50/0

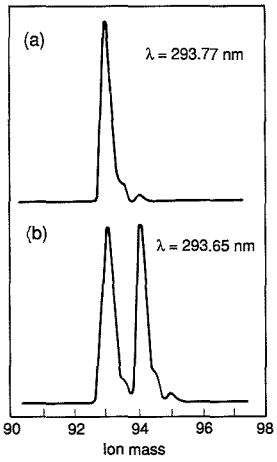

Figure 2. 1 + 1 resonance-enhanced multiphoton ionization mass spectra of aniline: (a) excitation of the nominal aniline absorption maximum and (b) enhancement of the ion signal for natural abundance aniline ^{13}C.

vibrational degrees of freedom. At a distance into the expansion chamber, when no further cooling occurs, the expanding gas pulse is skimmed to allow the central and coldest portion to enter the high-vacuum detection chamber in the form of a collimated molecular beam. Here, the molecular beam is crossed with a laser pulse that is synchronized in time with the molecular beam pulse. For specific excitation wavelengths, the molecules of interest will absorb and ionize. The ion masses are then analyzed by a TOF mass spectrometer equipped with acceleration and focusing grids, a field-free drift tube, and a sensitive ion detector (*5, 6*).

The response time for molecular detection is limited only by the time it takes for the molecules to reach the ionization region and the ions to reach the detector—considerably less than a millisecond. The TOF mass detection method has the advantage over techniques such as field-swept quadrupole detection in that complete mass spectra are obtained for a single pulse. Because of the laser repetition rate, mass spectra are updated and recorded in real time at 10 Hz. Signal averaging can be used to improve sensitivity at some expense of speed.

The selectivity of mass spectrometric detection is not always adequate for ultratrace detection at parts-per-billion levels. For this reason, high-resolution optical excitation was applied to enhance performance. A good example of optical selectivity is illustrated by using aniline and natural abundance aniline containing a single ^{13}C (Figure 2). The absorption spectra for these two species are essentially indistinguishable except for a nearly imperceptible shift in the line positions (293.77 nm vs. 293.65 nm, respectively, for the origin transition). By conventional electron impact or MPI-MS, the mass intensities would reflect the natural abundance of both species (Figure 2a). However, in the presence of a molecular beam, where high-resolution conditions prevail, it is possible to preferentially excite the less abundant species, thereby enhancing the ion signal for that mass (Figure 2b) (*7, 8*). Despite the stringent conditions imposed by the exceptionally close-lying absorption wavelengths ($\Delta\lambda$ = 0.12 nm), an optical enhancement of nearly 20 was obtained.

Detection

Chemical warfare agent detection was addressed in our labs by using molecules that have nearly identical structural and spectroscopic properties as actual agent molecules, but without the lethality. For example, we used the molecule diisopropyl methylphosphonate as an analogue for the nerve agent isopropoxymethylphosphoryl fluoride (Sarin). Other forms of organophosphonate molecules are used

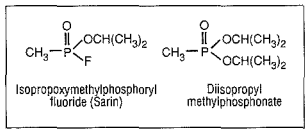

as pesticides. We also examined a class of chemical warfare agents known as blistering agents (such as the mustard agent $S(CH_2CH_2Cl)_2$) for which we used analogues consisting of various chlorinated and nonchlorinated dialkyl sulfides.

We had to answer a number of questions before the molecular beam resonance-enhanced multiphoton ionization (REMPI)/TOF-MS technique could be considered viable for chemical warfare agent detection. For example, do absorption resonances exist at wavelengths that are conveniently accessible to laser radiation? Is atmospheric air a suitable medium for obtaining supersonic expansion cooling? Are the intermediate resonance states sufficiently stable to allow further photon absorption, leading to ionization?

Little spectroscopic information existed for chemical warfare agent analogue molecules prior to this study. Therefore we began by constructing a medium-resolution, gas-phase absorption spectrometer to record survey spectra in the ultraviolet (UV) and the vacuum-UV regions. This provided the necessary database for high-resolution detection measurements. It became evident that it would be difficult to detect the organophosphonate and the organosulfide molecules by laser ionization because of the lack of strong one-photon absorptions in the near-UV region of the spectrum where adequate laser pulse energy is most readily available (i.e., $\lambda > 220$ nm). The lowest energy strong bands for both classes of molecules occur at ~200 nm. This made it necessary to resonantly ionize by the less efficient process of two-photon absorption using 400-nm laser pulses. (Recent advances in crystal technology now permit us to generate 200-nm laser pulses conveniently.) We reached our first milestone when highly resolved spectra were recorded for diisopropyl methylphosphonate by 2 + 2 REMPI excitation and for dimethyl sulfide by 2 + 1 REMPI under optimized expansion conditions (*6*).

Our second concern was whether atmospheric air would act as an effective medium for supersonic expansion cooling. The cooling of seed molecules expanded in a high-pressure carrier gas improves with increased pressure and

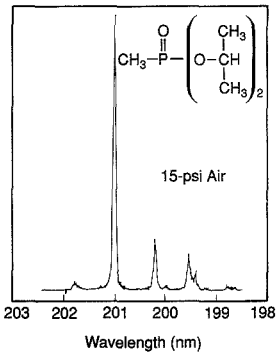

Figure 3. 2 + 2 REMPI excitation spectrum of diisopropyl methylphosphonate (0.5% diisopropyl methylphosphonate in 15-psi air).

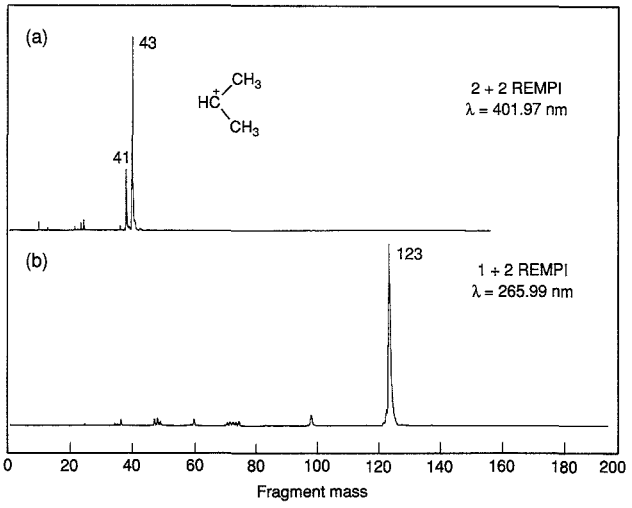

Figure 4. REMPI mass spectra of diisopropyl methylphosphonate in a supersonic beam recorded for two different excitation conditions.
(a) Predominant peak at *m/z* 43 and (b) predominant ion signal at *m/z* 123.

is most efficient for carrier gases that lack internal energy, such as the monoatomic rare gases. The suitability of atmospheric air as a carrier gas was found to compare favorably with more optimum expansion conditions (e.g., 50 psi He). The narrow-line resonance absorption ionization spectrum of diisopropyl methylphosphonate in air (Figure 3) attests to the highly selective excitation conditions obtainable for atmospheric samples. Thus supersonic molecular beam spectroscopy can be used for atmospheric sampling.

Finally, a lengthy study was undertaken to investigate the photochemical and photophysical properties of the intermediate vibronic (*vib*rational–elec*tronic*) states that serve to resonantly enhance the ionization step. Our most serious concern was that short-lived states that dissociate or decay would compete with the ionization step to diminish the ion signal (*5*, *6*, *9*). We explored several methods to overcome such problems: exciting and ionizing with laser pulses that are short (i.e., picosecond) (*10*) compared with the dissociative lifetime, ionizing and detecting a known fragment of the dissociation, and exciting through a different resonance intermediate state that is long lived.

The detection of diisopropyl methylphosphonate is an example in which the REMPI mass spectrum did not reveal a significant amount of molecular ion at 180 amu. The 2 + 2 REMPI excitation for the strong origin transition in Figure 3 gave a predominant peak at *m/z* 43 (Figure 4a). Ionization from a lower energy electronic state by 1 + 2 REMPI, on the other hand, gave a predominant ion signal at *m/z* 123 (Figure 4b). This latter electronic state was weak and diffuse and therefore not favorable for sensitive or selective detection. However, we learned that a very different dissociation and fragmentation behavior can occur by different excitation pathways.

We carried out electron impact ionization studies to establish that the 123 amu ion is a molecular ion fragmentation product. These same studies showed that the 43 amu ion is not a molecular ion fragmentation product but may instead be produced by the dissociation of diisopropyl methylphosphonate before it is ionized, followed by MPI of the neutral isopropyl radical. The selectivity of detection is still very high because detection depends on a specific ion mass and a very narrow wavelength of light; however, sensitivity is relatively poor because of the number of photons that must be absorbed per diisopropyl methylphosphonate molecule (at least four) to obtain a signal. A detection limit of 50 ppb was measured with a time response of 6 s by this excitation scheme. Recent research to extend laser wavelength ranges now makes it possible to apply direct 200-nm excitation by using a much more efficient 1 + 1 REMPI scheme.

The related organophosphonate molecule, dimethyl methylphosphonate, exhibits somewhat different spectroscopic and photochemical behavior than the structurally related molecule diisopropyl methylphosphonate. Broadband UV/vacuum-UV absorption spectra of room-temperature vapor-phase samples showed no evidence for any strong absorption bands ($\epsilon < 500$) at wavelengths longer than 140 nm, nor were any vibrationally resolved electronic state features revealed. Because optical selectivity by discrete resonance excitation was apparently not available for dimethyl methylphosphonate, we sought to obtain optical selectivity by REMPI excitation of a major photofragment.

Other investigators have reported the efficient production of PO radicals from dimethyl methylphosphonate by a variety of excitation sources (*9*). We therefore used the sharp PO vibrationless transition $\tilde{A}^2\Sigma^+ \leftarrow \tilde{X}^2\Pi$ at 247.7 to ionize the fragment by 1 + 1 REMPI. This wavelength also proved effective for photodissociating dimethyl methylphosphonate to give the characteristic fragment PO, thereby avoiding the need for a second wavelength of light (*6b*). In a related program, we have been investigating the use of two independently tunable sources of light for double-resonance detection schemes of aromatic molecules. Additional optical selectivity becomes available by this strategy, especially if one views the first resonance as the detection step and the second resonance as a verification step. Details of this work for aromatic molecules are reported elsewhere (*5*, *11*, *12*).

Our study of chemical warfare agent-type molecules also included the class of mustard simulants represented by dialkyl sulfides. We summarize this work for the case of dimethyl sulfide. The first strong electronic-state absorption for dimethyl sulfide occurs at rather high energies (195.31 nm origin transition), which necessitated the use of less efficient two-photon absorption at ~390 nm. The intermediate resonance-state absorption spectrum was very sharp in the molecular beam expansion; hence, enormous selectivity was evident by the high-resolution laser excitation and specific mass detection. The overall ionization described by 2 + 1 REMPI resulted in a predomi-

ANALYTICAL APPROACH

nantly molecular ion at 62 amu. This observation is evidence of a stable resonance intermediate state that does not dissociate in competition with ionization. Despite the inefficient two-photon absorption, the final ionizing photon was very efficient.

Performance

A major objective of our work was to quantitate the sensitivity, selectivity, and response time for the detection of chemical warfare agent-type molecules. Our working definition of sensitivity is the concentration of a target molecule that gives a detectable signal. A detectable signal, in this case, is one that exceeds the fluctuation of the background signal. The detectable concentration C_0 is determined by recording the signal strength, S_{ref}, for a calibrated reference sample concentration, C_{ref}, and comparing it to the background fluctuation level S_0 (the detection limit is $C_0 = C_{ref}S_0/S_{ref}$).

A model was also developed to relate the experimentally measured detection levels and response time. Basically, there is the usual trade-off in which sensitivity improves the longer one collects signals. We define τ_e as the response time required for the signal to grow to within $1/e$ of its final value and τ_0 as the response time required for the detected signal to exceed the background fluctuation level S_0. We consider τ_0 to be the response time for detection and τ_e the response time for the measurement of concentration. In addition, τ_0 can be considerably smaller than τ_e for target molecule concentrations well above the detection limit (*6*).

The response of our detection system to a 60-ppb sample of dimethyl sulfide in water-saturated air (i.e., 100% relative humidity, 17,000 ppm) is presented in Figure 5. An enlargement of the baseline region and a sensitivity scale are included. The ratio of the reference sample signal to background signal, (S_{ref}/S_0), is > 200, corresponding to a detection limit for dimethyl sulfide of < 300 parts per trillion (ppt). The measurement response time τ_e is 8 s; however, the detection response time τ_0 at 60 ppb is much less than a second. Finally, by varying the time for collecting the ion signal and averaging the signals over the background fluctuation, a trade-off between τ_e and C_0 can be made to enhance one parameter at the expense of the other.

Summary

Molecular beam MPI is a powerful research tool that has contributed enormously to our fundamental understanding of the spectroscopy and dynamics of excited-state molecules. It is only natural that the benefits of high

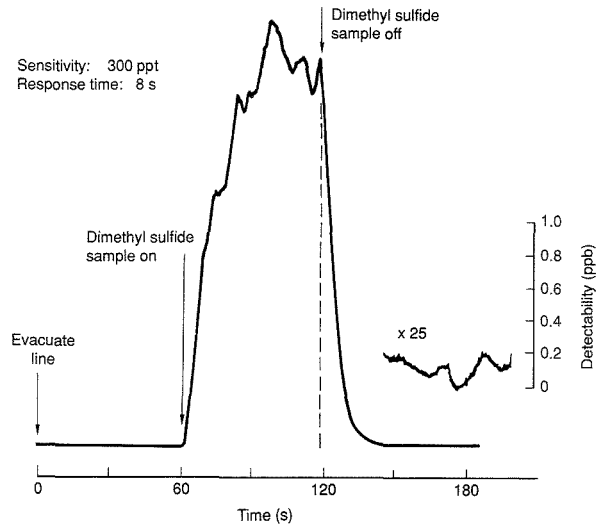

Figure 5. Sensitivity determination for a 60-ppb sample of dimethyl sulfide in water-saturated air.

resolution and sensitive detection would be recognized and applied toward molecular detection. The work reviewed here demonstrates the potential performance of molecular beam MPI-MS in terms of speed, sensitivity, and selectivity of detection. Many classes of compounds are favorable candidates for detection by REMPI. We have attempted to show that it is possible to overcome the challenges presented by complex molecules such as chemical warfare agents and pesticides. The maturing of molecular beam laser MS as a viable broad-based analytical tool depends only on the development of rugged, compact, and widely tunable sources of laser pulses.

I am indebted to my collaborators, James E. Pollard, Ronald B. Cohen, and John E. Wessel, who contributed substantially to various projects relating to laser molecular beam MS.

References

(1) *Lasers and Mass Spectrometry;* Lubman, D. M., Ed.; Oxford University Press: New York, 1990.
(2) a. Levy, D. H.; Wharton, L.; Smalley, R. E. In *Chemical and Biological Applications of Lasers;* Moore, C. B., Ed.; Academic Press: New York, 1977; Vol. 2, p. 1. b. Smalley, R. E.; Wharton, L.; Levy, D. H. *Acc. Chem. Res.* **1977,** *10,* 139.
(3) Lubman, D. M. *Anal. Chem.* **1987,** *59,* 31 A.
(4) Syage, J. A.; Wessel, J. E. *Appl. Spectrosc. Rev.* **1988,** *24,* 1.
(5) Syage, J. A. In *Lasers and Mass Spectrometry;* Lubman, D. M., Ed.; Oxford University Press: New York, 1990; p. 468.
(6) a. Syage, J. A.; Pollard, J. E.; Cohen, R. B. *Appl. Opt.* **1987,** *26,* 3516. b. Syage, J. A.; Pollard, J. E.; Cohen, R. B. Technical Report No. SD-TR-88-13, 1988; U.S. Air Force Systems Command (Space Division).
(7) Sin, C. H.; Tembreull, R.; Lubman, D. M. *Anal. Chem.* **1984,** *56,* 2776.
(8) Leutwyler, S.; Even, U. *Chem. Phys. Lett.* **1981,** *81,* 578.
(9) a. Long, S. R.; Christesen, S. D. *J. Phys. Chem.* **1989,** *93,* 6625. b. Sausa, R. C.; Miziolek, A. W.; Long, S. R. *J. Phys. Chem.* **1986,** *90,* 3994.
(10) a. Syage, J. A. *J. Chem. Phys.,* **1990,** *92,* 1804. b. Syage, J. A.; Steadman, *J. Chem. Phys. Lett.,* **1990,** *166,* 159. c. Steadman, J.; Syage, J. A. *J. Chem. Phys.,* in press.
(11) a. Syage, J. A.; Wessel, J. E. *J. Chem. Phys.* **1986,** *85,* 6806. b. Syage, J. A.; Wessel, J. E. *J. Chem. Phys.* **1987,** *87,* 3313. c. Syage, J. A.; Wessel, J. E. *J. Chem. Phys.* **1987,** *87,* 6207.
(12) Syage, J. A.; Wessel, J. E. *Appl. Opt.* **1987,** *26,* 3573.

Jack A. Syage received a B.A. degree from Hamilton College (1976) and a Ph.D. in physical chemistry from Brown University (1982). He accepted a postdoctoral position at Caltech under the guidance of Ahmed Zewail in 1982 and conducted studies in high-resolution and time-resolved picosecond molecular beam spectroscopy. He joined the Aerospace Corporation in 1984. His research interests, besides trace detection, include combustion kinetics, ultrafast phenomena, molecular cluster dynamics, transition-state spectroscopy, and reactions in intense laser fields.

LABORATORY SERVICE CENTER

DL-Asparagine • Basic Fuchsin • 2,3-Butylene Glycol • p-Chloranil
Cysteic Acid • 1,2-Diaminocyclohexanetetraacetic Acid • Dihydroxyacetone
3,3-Dimethylglutaric Acid • Dimethylglyoxime • 3,5-Dinitrobenzoic Acid
EDTA & Salts • Esculin • Hippuric Acid • 2-Hydroxy-iso-butyric Acid
Meldrum's Acid • 2-Mercaptobenzimidazole • Phenylhydrazine HCl
Potassium & Sodium m-Periodates • Sodium Diethyldithiocarbamate
Sodium Thioglycolate • Tetraiodoethylene • 3,4-Toluenedithiol & Zinc Salt
Toluidine Blue 0 • iso-Valeraldehyde • Vanillic Acid • Wright's Stain

Write for our Products List of over 3,000 chemicals

Tel: 516-273-0900 • TOLL FREE: 800-645-5566 Telefax: 516-273-0858 • Telex: 497-4275

EASTERN CHEMICAL
A Division of UNITED–GUARDIAN, INC.
P.O. Box 2500
DEPT. AC
SMITHTOWN, N.Y. 11787

Laboratory Service Center (Equipment, Materials, Services, Instruments for Leasing), Maximum space — 4 inches per advertisement. Column width, 2-3/16″; two column width, 4-9/16″. Artwork accepted. No combination of directory rates with ROP advertising. Rates based on number of inches used within **12** months from first date of first insertion. Per inch: **1″ — $165; 12″ — $160; 24″ — $155; 36″ — $150; 48″ — $145.**

CALL OR WRITE JANE GATENBY

ANALYTICAL CHEMISTRY
500 Post Road East
P.O. Box 231
Westport, CT 06880
203-226-7131/FAX: 203-454-9939

MICROELECTRODES
10μm Pt Au C
kosiow Scientific Co.
75 Gorge Rd. Edgewater, N.J. 07020
U.S.A 800-556-7569
201-941-4484 Fax: 201-941-4485

HELP WANTED ADS

ROP display at ROP rates. Rate based on number of insertions within contract year. Cannot be combined for frequency.

Unit	1-Ti	6-Ti	12-Ti
1″ (25 mm)	$190	$170	$160
	24-Ti	48-Ti	72-Ti
	$150	$140	$130

CALL OR WRITE JANE GATENBY

ANALYTICAL CHEMISTRY
500 Post Road East
P.O. Box 231
Westport, CT 06880
203-226-7131
FAX: 203-454-9939

INDUSTRIAL & ENGINEERING CHEMISTRY **RESEARCH**

Published monthly by the American Chemical Society

Editor: Donald R. Paul
Department of Chemical Engineering
University of Texas, Austin

Quality information that gives you the leading edge

Covering the broad, interdisciplinary field of chemical engineering and industrial chemistry, *Industrial & Engineering Chemistry Research* delivers peer-reviewed, monthly reports covering fundamental and theoretical aspects of chemical engineering. . . recent work on design methods and their applications. . . current and future products involving chemical engineering processes. . . process design and development. . . new technologies. . . and timely symposia.

Don't miss a single issue! Subscribe TODAY!

Volume 29 (1990)

	U.S.	Canada & Mexico	Europe Air Service Included	All Other Countries. Air Service Incl.
ACS Members				
1 Year	$ 55	$ 73	$ 84	$ 94
2 Years	$ 99	$135	$157	$177
Nonmembers	$372	$390	$401	$411

Member subscription rates are for personal use only.
Subscriptions are based on a calendar year.
Foreign payment must be made in U.S. currency by international money order, UNESCO coupons, or U.S. bank draft, or order through your subscription agency.
For nonmember rates in Japan, contact Maruzen Co., Ltd.
This publication is available on microfilm, microfiche, and the full text is available online on STN International.

Call Toll Free (U.S. and Canada): 1-800-227-5558
In D.C. and Outside the U.S. and Canada: 202-872-4363
Fax: 202-872-4615
Telex: 440159 ACSPUI or 892582 ACSPUBS
Cable Address: JEICHEM
Or Write: American Chemical Society, Marketing Communications Dept., 1155 Sixteenth Street, N.W., Washington, DC 20036

INDEX TO ADVERTISERS IN THIS ISSUE

CIRCLE INQUIRY NO.	ADVERTISERS	PAGE NO.
1	**Academic Press, Inc.** Academic Advertising	474A
24	***Camag Scientific, Inc.**	468A
35	**Eastman Kodak Company**	491A–492A
32, 33	***EG&G Princeton Applied Research** Market Force	481A
38	**Equipment Remarketing Company** Boston Financial & Equity Corporation	509A
60	***Hewlett-Packard Company** Brooks Communications	OBC
63	***Isotec, Inc.**	485A
90	***Matheson Gas Products** Kenyon Hoag Associates	473A
88	****E. Merck**	500B
92	**Merck & Company, Inc.** William Douglas McAdams, Inc.	495A
95, 96	***Nicolet Analytical Instruments**	471A
114, 115	***Sartorius Instruments** Techmarketing	482B–482E
125	**Shimadzu Scientific Instruments, Inc.**	503A
134–139	***SLM Instruments, Inc.**	IFC
130, 131	***Spectra-Physics**	467A
145	***Wheaton** The Wheaton Agency	474A

Directory section, see page 510A.

** See ad in ACS Laboratory Guide.*

*** Company so marked has advertisement in Foreign Regional edition only.*

Advertising Management for the American Chemical Society Publications

CENTCOM, LTD

President
James A. Byrne

Executive Vice President
Benjamin W. Jones

Clay S. Holden, *Vice President*
Robert L. Voepel, *Vice President*
Joseph P. Stenza, *Production Director*

500 Post Road East
P.O. Box 231
Westport, Connecticut 06880
(Area Code 203) 226-7131
Telex No.643310
FAX: 203-454-9939

ADVERTISING SALES MANAGER
Bruce E. Poorman

ADVERTISING PRODUCTION MANAGER
Jane F. Gatenby

SALES REPRESENTATIVES

Philadelphia, PA . . . CENTCOM, LTD., GSB Building, Suite 405, 1 Belmont Avenue, Bala Cynwyd, Pa. 19004. Telephone: 215-667-9666, FAX: 215-667-9353.

New York, NY . . . John F. Raftery, CENTCOM, LTD., 60 East 42nd St., New York, N.Y. 10165. Telephone: 212-972-9660

Westport, CT . . . Edward M. Black, CENTCOM, LTD., 500 Post Road East, P.O. Box 231, Westport, Ct. 06880. Telephone: 203-226-7131, Telex 643310, FAX: 203-454-9939

Cleveland, OH . . . Bruce E. Poorman, John C. Guyot, CENTCOM, LTD., 325 Front St., Suite 2, Berea, Ohio 44017. Telephone: 216-234-1333, FAX: 216-234-3425

Chicago, IL . . . Michael J. Pak, CENTCOM, LTD., 540 Frontage Rd., Northfield, Ill. 60093. Telephone: 708-441-6383, FAX: 708-441-6382

Houston, TX . . . Michael J. Pak, CENTCOM, LTD. Telephone: 708-441-6383

San Francisco, CA . . . Paul M. Butts, CENTCOM, LTD., Suite 1070, 2672 Bayshore Frontage Road, Mountain View, CA 94043. Telephone: 415-969-4604

Los Angeles, CA . . . Clay S. Holden, CENTCOM, LTD., Newton Pacific Center, 3142 Pacific Coast Highway, Suite 200, Torrance, CA 90505. Telephone: 213-325-1903

Boston, MA . . . Edward M. Black, CENTCOM, LTD. Telephone: 203-226-7131

Atlanta, GA . . . John C. Guyot, CENTCOM, LTD. Telephone: 212-972-9660

Denver, CO . . . Paul M. Butts, CENTCOM, LTD. Telephone: 415-969-4604

United Kingdom

Reading, England . . . Malcolm Thiele, Technomedia Ltd., Wood Cottage, Shurlock Row, Reading RG10 OQE, Berkshire, England. Telephone: 073-434-3302, Telex #848800, FAX: 073-434-3848

Lancashire, England . . . Technomedia Ltd., c/o Meconomics Ltd., Meconomics House, 31 Old Street, Ashton Under Lyne, Lancashire, England. Telephone: 061-308-3025

Continental Europe . . . Andre Jamar, International Communications, Inc., Rue Mallar 1, 4800 Verviers, Belgium. Telephone: (087) 22-53-85, FAX: (087) 23-03-29

Tokyo, Japan . . . Sumio Oka, International Media Representatives Ltd., 2-29 Toranomon, 1-Chome Minato-ku Tokyo 105 Japan. Telephone: 502-0656, Telex #22633, FAX: 591-2530

People who make the news, read the News.

When you're managing a chemical company these days, you need to get to the bottom of the news that affects your business. That's why executives throughout the industry read CHEMICAL & ENGINEERING NEWS each week.

It's the only weekly chemical magazine that covers the news from all three angles, business . . . science . . . technology. And with a full-time Washington bureau, C&EN covers the White House, Capitol Hill, the Supreme Court, and the federal regulatory agencies that affect science policy.

Read the weekly the newsmakers read.

Read CHEMICAL & ENGINEERING NEWS.

CHEMICAL & ENGINEERING NEWS

BUSINESS
SCIENCE
TECHNOLOGY

American Chemical Society, 1155 Sixteenth Street, NW, Washington, DC 20036, 800-227-5558
Telex: 440159 ACSP UI or 89 2582 ACSPUBS Telecopier: 202-872-4615

Analytical CHEMISTRY

EDITOR: **GEORGE H. MORRISON**

ASSOCIATE EDITORS: **Catherine C. Fenselau, Georges Guiochon, Walter C. Herlihy, Robert A. Osteryoung, Edward S. Yeung**

Editorial Headquarters
1155 Sixteenth St., N.W.
Washington, DC 20036
Phone: 202-872-4570
Telefax: 202-872-4574

Managing Editor: Sharon G. Boots

Assistant Managing Editor: Mary Warner

Associate Editor: Louise Voress

Assistant Editors: Grace K. Lee, Alan R. Newman

Editorial Assistant: Felicia Wach

Contributing Editor: Marcia Vogel

Director, Operational Support: C. Michael Phillippe

Head, Production Department: Leroy L. Corcoran

Art Director: Alan Kahan

Designers: Amy Meyer Phifer, Robert Sargent

Production Editor: Elizabeth E. Wood

Circulation: Claud Robinson

Editorial Assistant, LabGuide: Joanne Mullican

Journals Dept., Columbus, Ohio

Associate Head: Marianne Brogan

Journals Editing Manager: Joseph E. Yurvati

Senior Associate Editor: Rodney L. Temos

Published by the
AMERICAN CHEMICAL SOCIETY
1155 16th Street, N.W.
Washington, DC 20036

Publications Division

Director: Robert H. Marks

Journals: Charles R. Bertsch

Special Publications: Randall E. Wedin

Manuscript requirements are published in the January 1, 1990 issue, page 89. Manuscripts for publication (4 copies) should be submitted to ANALYTICAL CHEMISTRY at the ACS Washington address.

AUTHOR INDEX

Argentine, S. M., 853

Brondeau, J., 864
Brundrett, R. B., 868

Canet, D., 864
Christian, G. D., 849
Clark, G. D., 849
Clark, M. B., Jr., 870
Colvin, O. M., 868
Conboy, J. J., 800
Cotter, R. J., 793, 868

Davis, K. L., 846
Dose, E. V., 816
Dulik, D. M., 868

Elbayed, K., 864
Emary, W. B., 868

Fedkiw, P. S., 875
Fenselau, C., 868

Gardella, J. A., Jr., 870
Glish, G. L., 786
Guiochon, G., 816

Hanna, C. P., 849
Heithmar, E. M., 857
Henion, J. D., 800
Hinners, T. A., 857
Hunter, R. L., 878

Kabra, P. M., 807

Lebrilla, C. B., 878
Lin, W.-Y., 821
Lindberg, W., 849
Lu, Z., 826

Martin, M. W., 800
Martin, W., 868
McGlashen, M. L., 846
McIver, R. T., Jr., 878
McLuckey, S. A., 786
Miller, W. R., 810
Mishra, K. K., 821
Montigny, F., 864
Moore, A. W., Jr., 840
Mori, E., 821
Morris, M. D., 846

Olesik, J. W., 840
Orth, R. G., 796

Poiger, H., 796

Rajeshwar, K., 821
Rhoderick, G. C., 810
Rice, G. W., 853
Riviello, J. M., 857
Rowan, J. T., 857
Ruzicka, J., 849
Ryan, D. A., 853

Spengler, B., 793

Tran, C. D., 830, 835
Tuinman, A. A., 786

Van Berkel, G. J., 786

Wang, D. T.-S., 878
Wang, J., 826
Weidner, J. W., 875
Wendling, J. M., 796
Whitman, D. A., 849
Williams, D. E., 807

Yuan, Z.-m., 868

Zhang, W., 830, 835
Zweigenbaum, J. A., 800

Porphyrin Pyrrole Sequencing: Low-Energy Collision-Induced Dissociation of $(M + 7H)^+$ Generated in Situ during Ammonia Chemical Ionization

Gary J. Van Berkel,* Gary L. Glish, and Scott A. McLuckey

Analytical Chemistry Division, Oak Ridge National Laboratory, Oak Ridge, Tennessee 37831-6365

Albert A. Tuinman*

Department of Chemistry, University of Tennessee, Knoxville, Tennessee 37996

A method for pyrrole sequencing of porphyrins, based on high-pressure ammonia chemical ionization mass spectrometry/mass spectrometry (CI-MS/MS), is presented. High-pressure ammonia CI of porphyrins promotes formation of reduced molecular species and tri-, di-, and monopyrrolic fragment ions. The masses and pattern of the pyrrolic fragment ions can be used to determine the pyrrole sequence of the porphyrin. However, because of the complex ion source chemistry involved, these CI mass spectra are difficult to reproduce and are complicated by a plethora of structurally uninformative peaks. As such, pyrrole sequence elucidation based on the CI mass spectrum alone can be arduous, especially in the case of asymmetrically substituted porphyrins. In this paper, the MS/MS daughter ion spectrum of in situ formed $(M + 7H)^+$ (i.e., the protonated porphyrinogen) is used to determine the porphyrin pyrrole sequence. Low-energy (30–100 eV) collision-induced dissociation (CID) of $(M + 7H)^+$, using a hybrid mass spectrometer of BEqQ geometry, yields specific patterns of tri-, di-, and monopyrrolic daughter ions from which the pyrrole sequence of the porphyrin and combined mass of the substituents on the individual pyrroles can be determined. The daughter ion spectrum is more reproducible than the CI mass spectrum, and because of the reduction in chemical noise, the daughter ion spectrum is simpler to interpret. Several porphyrins of different pyrrole sequence are used to demonstrate the CI-MS/MS sequencing method. The capability of the CI-MS/MS method to sequence the pyrroles of porphyrins within a simple mixture of nonisobaric porphyrins is also demonstrated.

INTRODUCTION

Porphyrin structure determination by mass spectrometry (MS) was, until recently, limited due to the inability to fragment the stable porphyrin tetrapyrrole macrocycle (*1–3*). Macrocycle fragmentation is necessary if the pyrrole sequence of the porphyrin and the location of the substituent groups on the individual pyrrolic units are to be determined. High-pressure chemical ionization (CI) of porphyrins, using ammonia (*4–9*) or hydrogen (*10–13*) as the reagent gas, has been found to promote in situ reduction and decomposition of the porphyrin macrocycle. The end result is a relatively complex mass spectrum consisting of mono-, di-, and tripyrrolic fragment ions. These CI mass spectra have proven useful for porphyrin pyrrole sequencing and for confirming porphyrin structural assignments made by using other techniques (*4–13*). The CI-MS method is particularly useful when only a small amount of sample, insufficient for nuclear magnetic resonance of X-ray crystallography (i.e., less than several hundred micrograms), is available for analysis.

Unfortunately, the ammonia and hydrogen CI mass spectra obtained from any porphyrin are complicated by a plethora of peaks, most of which provide redundant structural information or are uninformative. Also, the appearance of the CI mass spectrum of a particular porphyrin is dependent on ion source conditions. In fact, spectra can vary greatly from scan to scan and from analysis to analysis. This spectral variability, coupled with the complexity of each spectrum, severely inhibits the analysis of unknowns, especially asymmetrically substituted porphyrins. Variability of the CI mass spectrum results from the complex ion source chemistry responsible for the porphyrin reduction/decomposition process. As demonstrated previously (*6, 9*), the ions observed in porphyrin ammonia CI mass spectra originate from both gas-phase and source-surface reactions. Surface-assisted reduction of the porphyrin within the ammonia CI plasma produces $(M + nH)$ species, which have a lower macrocycle stability than the porphyrin. These reduced species can desorb from the surfaces intact and be ionized and detected, or they can thermally decompose on the surfaces. Pyrrolic units formed on the surfaces by thermal decomposition eventually desorb, possibly undergoing additional reactions in the gas phase, and are then ionized and detected. Thermal decomposition of the reduced species on the source surfaces is the major source of the structurally informative pyrrolic ions and is also the source of the majority of the uninformative peaks in the spectrum.

One method of obtaining porphyrin structural information with increased spectrum reproducibility and less chemical noise is to study selectively the gas-phase chemistry of one particular reduced molecular species produced in situ using mass spectrometry/mass spectrometry (MS/MS) (*14*). Two reasons suggest that the most logical species to study is $(M + 7H)^+$, which experiments (*9*) have indicated is the protonated porphyrinogen (i.e., the protonated *meso*-hexahydroporphyrin, 1). The first reason stems from the fact that mass spectrometric analysis of in vitro prepared porphyrinogens has proven to be a useful means of obtaining information on the pyrrole sequence of the respective porphyrin. Budzikiewicz and co-workers (*15, 16*), for example, showed that electron ionization (EI) of a porphyrinogen produces a series of structurally significant tri-, di-, and monopyrrolic fragment ions that result from cleavage of the macrocycle at the meso positions (i.e., bridging carbons C-5, C-10, C-15, and C-20 in 1). In addition, Van Berkel et al. (*17*) found that collision-induced dissociation (CID) of a protonated porphyrinogen, using a quadrupole ion trap, produced a daughter ion spectrum similar to, but less complex than, the EI mass spectrum of the same porphyrinogen. The ability to produce the porphyrinogen in situ, using a conventional high-pressure CI

* Authors to whom correspondence should be addressed.

0003-2700/90/0362-0786$02.50/0

plasma, circumvents the problem of preparing and handling these air-sensitive compounds outside of the mass spectrometer. The second reason for choosing to study $(M + 7H)^+$ is that, under the appropriate experimental conditions, it is usually the most abundant of the reduced species formed. Maximum abundance of the ion of interest is desirable so as to facilitate the MS/MS experiment.

Previous studies (*6*, *9*), using a BE geometry (B, magnetic sector; E, electric sector) mass spectrometer, have shown that high-energy (5 keV) CID of in situ produced $(M + 7H)^+$ produces a daughter ion spectrum consisting of tri-, di-, and monopyrrolic fragments. In principle, the daughter ion spectrum of $(M + 7H)^+$ acquired on a BE instrument can be used to determine the pyrrole sequence of the porphyrin. In practice, however, the kinetic energy released upon macrocycle decomposition degrades daughter ion mass resolution when an electric sector is used for the second stage of mass analysis (*14*). This limits the amount of information that might otherwise be obtained since broad peaks from the major daughter ions can mask the presence of less abundant, but structurally informative, fragments. Also, the high-energy CID process results in fragmentation of substituent groups from the individual pyrrolic units, adding complexity to the daughter ion spectrum.

The problem of poor daughter ion mass resolution and substituent group fragmentation can be overcome, however, by using any one of several other MS/MS instruments (*14*). Use of the appropriate instrument allows the full benefit of the CI-MS/MS technique for pyrrole sequencing of porphyrins to be realized. In this paper, high-pressure ammonia CI is used to produce protonated prophyrinogens from porphyrins in situ. A hybrid mass spectrometer of BEqQ geometry (q, rf-only collision quadrupole; Q, analyzer quadrupole) is used to obtain low-energy (30–100 eV) CID spectra of $(M + 7H)^+$ with unit mass daughter ion resolution. Several porphyrins of different pyrrole sequence are analyzed to demonstrate the CI-MS/MS technique. Also demonstrated is the capability to pyrrole sequence the porphyrins within a simple mixture of nonisobaric porphyrins.

EXPERIMENTAL SECTION

Samples. Figure 1 shows the structures of the five porphyrins investigated in this study. 2,3,7,8,12,13,17,18-Octaethyl-21*H*,23*H*-porphine (octaethylporphyrin, **2**), dimethyl 3,7,12,17-tetramethyl-21*H*,23*H*-porphine-2,18-dipropionate (deuteroporphyrin IX dimethyl ester, **3**), and ethyl 13,17-diethyl-3,7,8,12,18-pentamethyl-21*H*,23*H*-porphine-2-propionate (methylpyrroporphyrin XXI ethyl ester, **5**) were obtained from Aldrich Chemical (Milwaukee, WI). Porphine (**4**) was obtained from Porphyrin Products (Logan, UT) and a sample of 15,17-butano-3,8-diethyl-2,7,12,18-tetramethyl-21*H*,23*H*-porphine (**6**) was obtained from P. S. Clezy (University of New South Wales). All samples were used as received from their respective supplier.

Mass Spectrometry. All spectra were obtained on a hybrid mass spectrometer of BEqQ geometry (B, magnetic sector; E, electric sector; q, rf-only collision quadrupole; and Q, analyzer quadrupole) located at the University of Tennessee: the ZAB-EQ from VG Analytical.

High-pressure ammonia CI mass spectra were acquired with an ion source temperature of 423 K, a reagent gas pressure (ammonia, National/Bower, Philadelphia, PA) of (1.3–2.0) × 10^{-4} Torr (measured in the vacuum source housing), an electron energy of 150 eV, an emission current of 1.0 mA, and an accelerating potential of 8 kV. Although the ion source thermostatic control was set to a temperature of 423 K, the ion source temperature observed during the course of extended experiments rose to as much as 438–443 K. This was due to heating from the electron ionization filament and the desorption chemical ionization (DCI) probe used to introduce the sample into the ion source. It was found that preconditioning the ion source by operating under these CI conditions for 10 min prior to sample introduction often enhanced the reduction process.

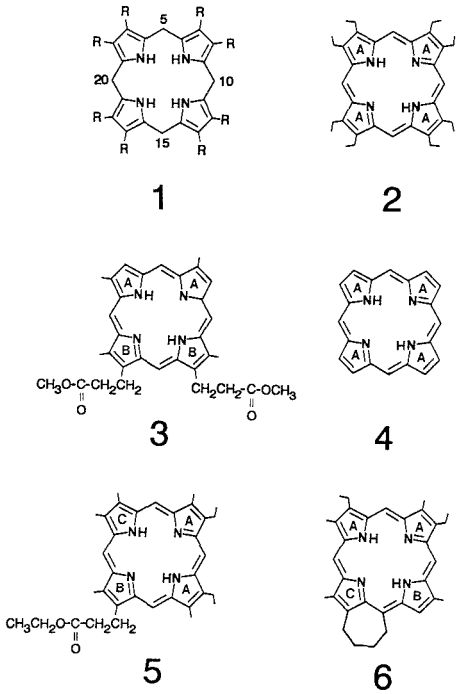

Figure 1. Structures of the compounds investigated in this study: (**1**) basic porphyrinogen structure, (**2**) octaethylporphyrin, (**3**) deuteroporphyrin IX dimethyl ester, (**4**) porphine, (**5**) methylpyrroporphyrin XXI ethyl ester, and (**6**) 15,17-butano-3,8-diethyl-2,7,12,18-tetramethyl-21*H*,23*H*-porphine.

Porphyrin was introduced into the ion source by using a DCI probe fitted with a platinum DCI coil. The DCI coil was fashioned from 0.127 mm diameter platinum wire by wrapping it four times around a pencil lead 0.89 mm in diameter. Total length of the platinum wire used to fashion the coils was approximately 13 mm, ±10%. The coils were welded to the ends of nickel posts on the DCI probe. Typically, 1–5 μg of prophyrin was dissolved in chloroform and then applied to the DCI coil in stages using a microsyringe. The DCI current was ramped from 0 to 1.4 A at 3.75 mA s^{-1} and then held at 1.4 A for several minutes, while acquiring mass spectra by scanning the magnetic sector from 700 to 70 u at a rate of 6 s/decade. With the structure of the porphyrin being analyzed known, the "best" CI mass spectrum with which to determine the pyrrole sequence was chosen from among the numerous acquired.

Daughter ion MS/MS spectra were acquired under ion source conditions similar to those used to obtain the CI mass spectra except that a larger sample of porphyrin (typically 20–50 μg) was used as well as a different DCI probe current ramp. The DCI current was manually controlled to maintain a steady $(M + 7H)^+$ peak for tuning of the instrument for MS/MS. The $(M + 7H)^+$ ions were selected with the sector portion of the instrument (BE) and then decelerated to 30, 70, or 100 eV (laboratory). CID was performed in the rf-only collision quadrupole (q) using argon as the collision gas. Argon pressure, measured with an ionization gauge outside the 254 mm long collision quadrupole, was 1.5 × 10^{-5} Torr, corresponding to an estimated pressure of 3 mTorr inside the quadrupole. For acquisition of the MS/MS spectrum, the DCI current was ramped quickly (35 mA s^{-1}) to 1.4 A and held there while the analyzer quadrupole (Q) was scanned from 30 to 600 u at 4 s/scan to analyze the daughter ions formed by CID. To enhance sensitivity, the MS/MS data were collected by using the VG Analytical multichannel acquisition (MCA) mode, which is a software simulation of true multichannel arrays. In a typical

Table I. Porphyrin Classification Scheme[a,b]

porphyrin structural type	pyrrole sequence	monopyrroles	dipyrroles	tripyrroles
A_4	AAAA	A	AA	AAA
A_3B	AAAB	A, B	AA, AB	AAB, AAB*, ABA*
A_2B_2	AABB	A, B	AA, AB, BB	AAB, ABB
	ABAB	A, B	AB	ABA, BAB
A_2BC	AABC	A, B, C	AA, AB, BC, CA	AAB, ABC*, BCA*, CAA
	ABAC	A, B, C	AB, AC	ABA, BAC, ACA
ABCD	ABCD	A, B, C, D	AB, BC, CD, DA	ABC, BCD, CDA, DAB
	ACBD	A, B, C, D	AC, CB, BD, DA	ACB, CBD, BDA, DAC
	ABDC	A, B, C, D	AB, BD, DC, CA	ABD, BDC, DCA, CAB

[a] Classification scheme ignores structural and positional isomers of the substituent groups on the individual pyrroles. [b] For a particular porphyrin pyrrole sequence tripyrroles marked with an asterisk have the same mass but a different pyrrole sequence.

experiment approximately 16 quadrupole scans were acquired.

RESULTS AND DISCUSSION

Porphyrin Reduction and Decomposition. The mechanisms responsible for reduction and decomposition of the porphyrin macrocycle in a high-pressure ammonia CI plasma have been discussed in detail elsewhere (*9*). In the context of this paper it is important to understand that the fragmentation observed is a reflection of the chemistry of the reduced species produced in situ, rather than the chemistry of the porphyrin. As a result, the appearance of a CI mass spectrum is highly dependent on those ion source parameters that affect the porphyrin reduction. The more important parameters appear to be the nature of the ion source surfaces, the composition of the CI plasma, and the ion source temperature.

Porphyrin reduction in the CI plasma has been shown to be a surface-assisted reaction (*9*). The reaction can be enhanced by "preconditioning" the source surfaces by operating under CI conditions for several minutes prior to sample introduction into the ion source and by operating at low ion source temperatures, thereby increasing the likelihood of porphyrin–surface interactions. Thermal decomposition of the surface-bound reduced species has been determined to produce the majority of the structurally significant pyrrolic fragments (*9*). However, this is also the major source of the uninformative peaks that appear in the spectrum. Adding further complexity to the spectrum are the pyrrolic fragments that originate from gas-phase decompositions of the reduced species.

As a result of the dependence of the reduction/decomposition process on ion source conditions, the appearance of the CI mass spectrum can vary considerably, even from scan to scan. Choosing a priori the spectrum that best represents the structure of an unknown porphyrin is usually not possible. Only by knowing the structure of the porphyrin being analyzed can a spectrum which best reflects that structure be chosen from the numerous spectra normally acquired during an experiment. Therefore, some subjective criteria, such as those used by Djerassi and co-workers (*4*, *5*), must be used to select a spectrum for an unknown. As demonstrated below, this consitutes a severe limitation of the CI-MS technique, especially when analyzing porphyrins with an asymmetrical pyrrole sequence.

Ammonia CI Mass Spectra. An ammonia CI mass spectrum of octaethylporphyrin (**2**) that accurately represents its pyrrole sequence is shown in Figure 2. The major ions observed in this spectrum are the pseudomolecular species, $(M + nH)^+$, where n = 1, 3, 5, and 7, and the tri-, di-, and monopyrrolic fragment ions. As an aid to interpreting the fragmentation pattern in this and other porphyrin CI mass spectra, porphyrins can be classified according to the number of pyrrole rings of different mass that they contain, as shown

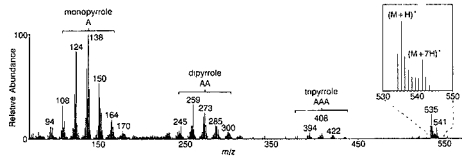

Figure 2. Ammonia CI mass spectrum of octaethylporphyrin (**2**).

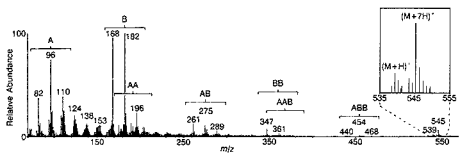

Figure 3. Ammonia CI mass spectrum of deuteroporphyrin IX dimethyl ester (**3**).

in Table I (*5*, *10*). (This same classification scheme is used in interpretation of the $(M + 7H)^+$ CID spectra as described below.) Denoting the pyrrole rings of different mass making up the macrocycle by the letters A, B, C, and D allows the porphyrins to be divided into five structural types A_4, A_3B, A_2B_2, A_2BC, and ABCD, ignoring structural and positional isomers of the substituent groups on each pyrrole. The pyrroles of these structural types can be arranged to give nine different pyrrole sequences, each of which is characterized by a unique set of mono-, di-, and tripyrrolic units. These tri-, di-, and monopyrrolic units are each manifest in the CI mass spectrum as a triad of peak clusters. For a particular mono-, di-, or tripyrrole triad, the peaks within each of the three respective peak clusters correspond to that pyrrolic unit containing either 0, 1, or 2 terminal meso carbons (*4*, *5*). Octaethylporphyrin is a totally symmetrical or A_4 type porphyrin, and therefore, only one monopyrrole (A, m/z 124, 138, and 150), one dipyrrole (AA, m/z 259, 273, and 287), and one tripyrrole (AAA, m/z 394, 408, and 422) triad peak cluster is observed in its CI mass spectrum (Figure 2).

The A_4 type prophyrins, like octaethylporphyrin, yield the simplest CI mass spectra, but even their interpretation is complicated by the numerous peaks associated with each triad. As the number of pyrroles of different mass in the porphyrin macrocycle increases, the CI mass spectrum of the porphyrin becomes increasingly complex and more difficult to interpret. This effect can be seen in the CI mass spectrum of deuteroporphyrin IX dimethyl ester (**3**) shown in Figure 3. Deuteroporphyrin IX dimethyl ester has an AABB pyrrole sequence. Therefore, two monopyrrole (A, m/z 82, 96, and 110; B, m/z 168, 182, and 196), three dipyrrole (AA, m/z 175, 189, and 203; AB, m/z 261, 275, and 289; BB, m/z 347, 361, and

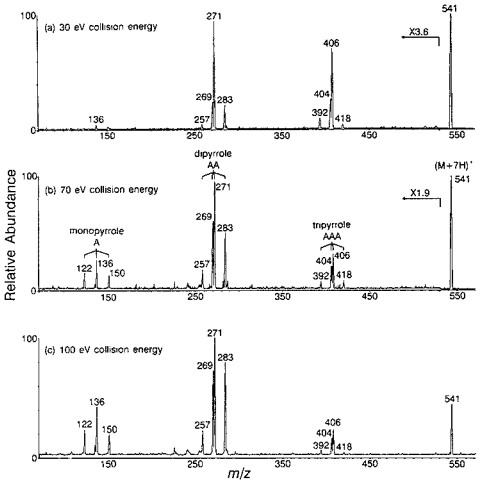

Figure 4. The CID spectra of $(M + 7H)^+$ from octaethylporphyrin (**2**) obtained at laboratory collision energies of (a) 30 eV, (b) 70 eV, and (c) 100 eV.

375), and two tripyrrole (AAB, m/z 354, 368, and 382; ABB, m/z 440, 454, and 468) triad peak clusters are to be expected in the CI mass spectrum (Table I). In the spectrum obtained, however, the monopyrroles are the only distinct peak clusters while the tri- and dipyrroles are of much lower relative abundance. This absence or poor representation of structurally informative peaks often limits the utility of a CI mass spectrum for pyrrole sequencing. Usually contributing to this problem is the abundant chemical noise, particularly at low mass, that makes it difficult to determine which peaks make up the structurally representative peak triads. Even when all of the peak clusters are apparent, the utility of the CI mass spectrum for pyrrole sequencing of a complex porphyrin can be severely limited due to the overlap in mass of many of the numerous triad peak clusters (e.g., B and AA in Figure 3). This overlap can effectively mask the presence of structurally diagnostic peaks.

Collision-Induced Dissociation (CID) of $(M + 7H)^+$. Our previous CID studies of the various reduced molecular species in porphyrin CI mass spectra (*8*, *9*) indicated that the daughter ion spectrum of $(M + 7H)^+$ was of potential use for pyrrole sequencing. That potential is realized in this study by using a BEqQ geometry instrument to obtain low-energy CID daughter ion spectra of $(M + 7H)^+$ with unit mass resolution of the daughter ions. By studying selectively the gas-phase decomposition of $(M + 7H)^+$, a simple, reproducible, and pyrrole sequence specific spectrum is acquired, even for complex porphyrins.

Interpretation of the CID Spectrum. Low-energy CID daughter ion spectra of $(M + 7H)^+$, generated in situ from octaethylporphyrin during ammonia CI, are shown in Figure 4. These spectra were acquired at laboratory collision energies of 30, 70, and 100 eV, respectively. Examination of these CID spectra reveals the occurrence of an even-mass peak "triplet" (m/z 122, 136, and 150), an odd-mass peak "quadruplet" (m/z 257, 269, 271, and 283), and an even-mass peak "quadruplet" (m/z 392, 404, 406, and 418). At a collision energy of 30 eV (Figure 4a), the peak quadruplets dominate the CID spectrum while the peak triplet can just be distinguished from background noise. As the collision energy is increased (Figure 4b, 70 eV), the abundance of the peaks in the even-mass quadruplet decreases while the abundance of the peaks in both the odd-mass quadruplet and the even-mass triplet increases. At a collision energy of 100 eV (Figure 4c), the abundance of the even-mass quadruplet peaks is greatly reduced. Additional daughter ions, probably arising from substituent group fragmentation, are also observed in this CID spectrum. Of the three CID spectra in Figure 4, the spectrum acquired at a collision energy of 70 eV offers the best compromise of reasonable abundance of what are shown below to be the structurally diagnostic peaks without significant interference from substituent group fragmentation. Therefore, the CID spectrum obtained at a collision energy of 70 eV is used to pyrrole sequence octaethylporphyrin and each of the other porphyrins investigated in this study.

Determining the pyrrole sequence of a porphyrin from the CID spectrum of $(M + 7H)^+$ requires assignment of the individual peak triplets and quadruplets as either tri-, di-, or monopyrroles. This pattern of pyrrolic units characterizes the porphyrin as having one of the nine possible pyrrole sequences shown in Table I. It is also useful to assign the sets of daughter ions to the portion of the porphyrin macrocycle to which they correspond. The peak triplets and quadruplets can be identified as mono-, di-, or tripyrroles based on the nitrogen rule. For example, $(M + 7H)^+$ from octaethylporphyrin is an even-electron ion with an even number of nitrogens, and therefore, an odd-mass (m/z 541). The daughter ions produced are even-electron species so that the pyrrolic fragments with an even number of nitrogens, i.e., the dipyrroles, have an odd-mass, and the species with an odd number of nitrogens, i.e., the tripyrroles and monopyrroles, have an even-mass. Since octaethylporphyrin has an AAAA pyrrole sequence, the three sets of daughter ion peaks observed in the CID spectrum should represent the monopyrrole, A, dipyrrole, AA, and tripyrrole, AAA portions of the macrocycle (see Table I). Therefore, the even-mass peak triplet (m/z 124, 136, and 150) is assigned as monopyrrole A, the odd-mass peak quadruplet (m/z 257, 269, 271, and 283) as dipyrrole AA, and the even-mass peak quadruplet (m/z 392, 404, 406, and 418) as tripyrrole AAA.

Assignment of the daughter ion peaks to specific portions of the macrocycle is trivial for octaethylporphyrin and other A_4 type porphyrins. This is not the case, however, for the more complex porphyrins analyzed in this study. For these porphyrins, the peaks can be assigned by assembling the expected di- and tripyrroles from their constituent monopyrroles. In order to do this it is necessary to define a "monopyrrole unit". Each of the monopyrrole peak triplets observed in the CID spectrum is assigned a different letter designation, either A, B, C, or D. The center peak in each triplet corresponds to that monopyrrole with one meso carbon attached. The respective "monopyrrole unit" for each triplet is defined as having a mass (M_X) one unit less than the mass of the center peak ($M_X + 1$) in the respective monopyrrole triplet (e.g., M_A = 135 u for octaethylporphyrin). The lower and higher mass peaks in each triplet, which occur at m/z values of $M_X - 13$ and $M_X + 15$, are the monopyrrole with no meso carbons and two meso carbons, respectively. (Note that the sum of the masses for the four monopyrrole units of which the porphyrin macrocycle is comprised equals the mass of the porphyrinogen, i.e., $(M + 6H)$.)

A "dipyrrole unit" can be viewed as being comprised of two monopyrrole units with a mass equal to the sum of the masses of its constituent monopyrrole units (e.g., M_{AA} = 270 u for octaethylporphyrin). The peaks of each dipyrrole quadruplet occur at m/z values of $M_{XY} - 13$, $M_{XY} - 1$, $M_{XY} + 1$, $M_{XY} + 13$. The peaks at m/z $M_{XY} - 1$ and $M_{XY} + 1$ are comprised of two monopyrrole units (i.e., two pyrrole rings and two meso carbons), while the peaks at m/z $M_{XY} - 13$ and $M_{XY} + 13$ contain one less and one more meso carbon, respectively, than

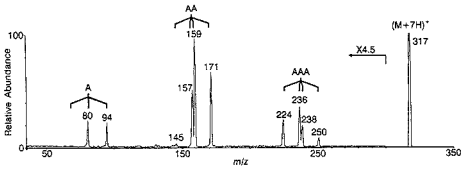

Figure 5. The CID spectrum of $(M + 7H)^+$ from porphine (**4**) obtained at a laboratory collision energy of 70 eV.

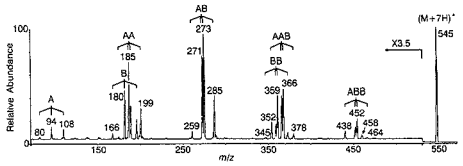

Figure 6. The CID spectrum of $(M + 7H)^+$ from deuteroporphyrin IX dimethyl ester (**3**) obtained at a laboratory collision energy of 70 eV.

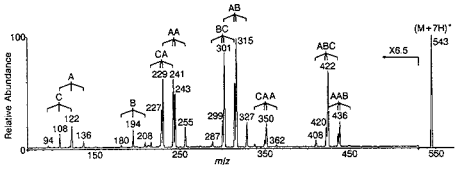

Figure 7. The CID spectrum of $(M + 7H)^+$ from methylpyrroporphyrin XXI ethyl ester (**5**) obtained at a laboratory collision energy of 70 eV.

the basic dipyrrole unit. In an analogous fashion, a "tripyrrole unit" can be defined as consisting of three monopyrrole units with a mass equal to the sum of the masses of those monopyrrole units (e.g., M_{AAA} = 405 u for octaethylporphyrin). The peaks of each tripyrrole quadruplet occur at m/z values of $M_{XYZ} - 13$, $M_{XYZ} - 1$, $M_{XYZ} + 1$, and $M_{XYZ} + 13$. The peaks at m/z $M_{XYZ} - 1$ and $M_{XYZ} + 1$ are comprised of three monopyrrole units (i.e., three pyrrole rings and three meso carbons), while the peaks at m/z $M_{XY} - 13$ and $M_{XY} + 13$ contain one less and one more meso carbon, respectively, than the basic tripyrrole unit.

Porphyrins with different substituent groups, but the same pyrrole sequence, have the same pattern of peaks in the CID spectrum (with the exception noted below). The masses at which the pyrrolic daughter ions are observed will be shifted, however, because of the difference in masses of the substituent groups. This is demonstrated in Figure 5, which shows the CID spectrum of $(M + 7H)^+$ from porphine (**4**), another A_4 type porphyrin. Since the pyrrole sequence of porphine is the same as that of octaethylporphyrin, the same pattern of pyrrolic daughter ions is expected in the CID spectrum. This is indeed the case for the tripyrrole AAA (M_{AAA} = 237 u, m/z 224, 236, 238, and 250), but the $M_{AA} - 13$ member (m/z 145) of the dipyrrole AA quadruplet (M_{AA} = 158 u, m/z 145, 157, 159, and 171) has an unusually low abundance and monopyrrole A (M_A = 79 u) appears as a doublet (m/z 80 and 94) rather than the expected peak triplet. Absence of the expected monopyrrole peak at m/z 66 can, however, be readily explained.

The species that corresponds to the missing monopyrrole peak ($C_4H_4N^+$) contains an insufficient number of carbon atoms to accommodate the four double bond equivalents necessary for a stable structure. Therefore, this particular monopyrrole unit is unlikely to form. It seems probable that the monopyrrole daughter ions that are observed in the CID spectra can form stable species of a pyridinium type structure via ring expansion. Either a meso carbon or a carbon in an alkyl substituent group might be involved in such a ring expansion. When neither is present (as is the case for the missing $C_4H_4N^+$ species), then the fragment is unstable and unlikely to form. Therefore, absence of the low mass peak in a monopyrrole triplet (i.e., the species containing no meso carbons) might be used as evidence that the substituent groups on that pyrrole do not afford the possibility of ring expansion. In the case of the dipyrrole, no explanation for the lower than expected abundance of the peak at m/z 145 is apparent.

The combined mass of the substituent groups on the individual monopyrroles can also be derived from the CID spectrum of $(M + 7H)^+$. A "monopyrrole unit" devoid of substituent groups has a mass of 77 u. Therefore, the mass of the monopyrrole unit minus 77 equals the combined mass of the substituent groups on that monopyrrole (i.e., $M_{SX} = M_X - 77$). For octaethylporphyrin this corresponds to 135 minus 77, or 58 u as expected for two ethyl groups. In the case of porphine, this corresponds to 79 minus 77, or 2 u, which is correct for the two hydrogen substituents present. Knowing the combined mass of the substituents on each pyrrole ring, along with information from the EI mass spectrum regarding the identity of the substituent groups on the porphyrin macrocycle, aids in identification of the substituent group pairs on each pyrrole.

Analysis of Complex Porphyrins. The advantages of the CI-MS/MS technique over CI-MS for pyrrole sequencing of porphyrins are best illustrated by the analysis of porphyrins made up of pyrroles of different masses. As shown above, the CI mass spectrum of these more complex porphyrins can be extremely difficult or nearly impossible to interpret. Figure 6 shows the CID spectrum of $(M + 7H)^+$ from deuteroporphyrin IX dimethyl ester (**3**). In contrast to the CI mass spectrum of this porphyrin (Figure 3), the CID spectrum of $(M + 7H)^+$ is relatively simple and straightforward to interpret. Two monopyrroles, three dipyrroles, and two tripyrroles can be identified in the CID spectrum by searching for peak triplets and quadruplets of odd- or even-mass. This pattern of pyrrolic units correctly characterizes this porphyrin as having an AABB pyrrole sequence (Table I). By use of the procedure described above, the portions of the porphyrin macrocycle represented by the various sets of peaks can be assigned. The peak triplet at m/z 80, 94, and 108 is assigned as monopyrrole A (M_A = 93 u) and the triplet at m/z 166, 180, and 194 as monopyrrole B (M_B = 179 u). Thus, the peak quadruplet at m/z 173, 185, 187, and 199 is dipyrrole AA (M_{AA} = 186 u), the quadruplet at m/z 259, 271, 273, and 285 is dipyrrole AB (M_{AB} = 272 u), and the peak quadruplet at m/z 345, 357, 359, and 371 is dipyrrole BB (M_{BB} = 358 u). The peak quadruplet at m/z 352, 364, 366, and 378 is assigned to tripyrrole AAB (M_{AAB} = 365 u) and the quadruplet at m/z 438, 450, 452, and 464 is tripyrrole ABB (M_{ABB} = 451 u).

As with octaethylporphyrin and porphine, the mass calculated for the substituent groups on the monopyrroles (M_{SA} = 16 u and M_{SB} = 102 u) is consistent with the methyl/hydrogen and methyl/methyl propionate substituent pairs on the respective monopyrroles. The one peak not accounted for by macrocycle fragmentation in Figure 6 is m/z 458, which lies within the ABB quadruplet. This peak is easily explained, however, by noting that it corresponds to the species resulting from α-cleavage of one of the ester-containing substituent groups from the macrocycle of the protonated porphyrinogen, i.e., $(M + 7H - 87)^+$.

The CID spectrum of $(M + 7H)^+$ from methylpyrroporphyrin XXI ethyl ester (**5**), a porphyrin with an AABC pyrrole sequence, is shown in Figure 7. The CI mass spectrum of this porphyrin (not shown) is extremely difficult to interpret because of the overlap in mass of the multiple triad peak clusters and poor representation of some of the expected

Table II. Expected Pyrrolic Daughter Ions in the CID Spectrum of $(M + 7H)^+$ from 15,17-Butano-3,8-diethyl-2,7,12,18-tetramethyl-21*H*,23*H*-porphine (6)

	pyrrolic unit	$M_X - 13$	$M_X + 1$	$M_X + 15$
monopyrroles	A (M_A = 121 u)	108	122	136
	B (M_B = 93 u)	80	94	108
	C (M_C = 147 u)	134	148	162

	pyrrolic unit	$M_{XY} - 13$	$M_{XY} - 1$	$M_{XY} + 1$	$M_{XY} + 13$
dipyrroles	AA (M_{AA} = 242 u)	229	241	243	255
	AB (M_{AB} = 214 u)	201	213	215	227
	BC (M_{BC} = 240 u)	227	239	241	253
	CA (M_{CA} = 268 u)	255	267	269	281

	pyrrolic unit	$M_{XYZ} - 13$	$M_{XYZ} - 1$	$M_{XYZ} + 1$	$M_{XY} + 13$
tripyrroles	AAB (M_{AAB} = 335 u)	322	334	336	348
	ABC (M_{ABC} = 361 u)	348	360	362	374
	CAA (M_{CAA} = 389 u)	376	388	390	402

pyrrolic fragments. Determination of the pyrrole sequence from the CID spectrum, however, is straightforward. The three monopyrrole peak triplets (A, M_A = 121 u; B, M_B = 193 u; C, M_C = 107 u), four dipyrrole peak quadruplets (AA, M_{AA} = 242 u; AB, M_{AB} = 314 u; BC, M_{BC} = 300 u; CA, M_{CA} = 228 u), and three tripyrrole peak quadruplets (AAB, M_{AAB} = 435 u; ABC, M_{ABC} = 421 u; CAA, M_{CAA} = 349 u) in the CID spectrum distinguish this porphyrin as having an AABC pyrrole sequence (Table I). The combined mass calculated for the substituent groups on monopyrroles A (M_{SA} = 44 u), B (M_{SB} = 116 u), and C (M_{SC} = 30 u) is consistent with the methyl/ethyl, methyl/ethyl propionate, and methyl/methyl substituent group pairs present on these monopyrroles, respectively.

The last porphyrin to be discussed is 15,17-butano-3,8-diethyl-2,7,12,18-tetramethyl-21*H*,23*H*-porphine (**6**). This porphyrin has the same pyrrole sequence (AABC) as porphyrin **5**, but, unlike the other porphyrins so far described, it contains a seven-membered exocyclic ring which bridges a pyrrole ring with a meso carbon. Porphyrins with exocyclic rings are of wide occurrence in nature and are especially prominent in certain fossil fuels and organic-rich sediments (*18*). Previous studies (*11*) have indicated that the presence of an exocyclic ring complicates the CI mass spectrum because of preferential retention of the substituted meso carbon on the pyrrole containing the exocyclic ring. Therefore, certain peaks are absent from the spectrum, or of reduced abundance, that would be expected in the spectrum of a similar porphyrin that did not contain an exocyclic ring. In order to determine the effect of the exocyclic ring on the CID spectrum of $(M + 7H)^+$ from porphyrin **6**, the spectrum predicted (using the procedure described above) for a porphyrin with the same pyrrole sequence and the same combined mass for the substituent groups, but without an exocyclic ring, was compared with the actual spectrum observed. Table II lists the masses predicted for the mono-, di-, and tripyrrolic peaks in the CID spectrum and Figure 8 shows the actual CID spectrum obtained.

Assuming that cleavage between pyrroles B and C proceeds with preferential retention of the ring-substituted meso carbon on C, distinct differences between the predicted and observed spectrum would be expected. For the monopyrroles this would include the absence of the $M_B + 15$ species (m/z 108; two terminal meso carbons on B) and absence of the $M_C - 13$ species (m/z 134; no terminal meso carbons on C). In the case of the dipyrroles, the $M_{CA} - 13$ species (m/z 255; no terminal meso carbons on CA) and the $M_{AB} + 13$ species (m/z 227; two terminal meso carbons on AB) should not be observed. For the tripyrroles, the $M_{AAB} + 13$ species (m/z 348; two terminal meso carbons on AAB) and the $M_{CCA} - 13$ species (m/z 376; no terminal meso carbons on CAA) would not be expected in the spectrum. The dashed lines in Figure 8 indicate those peaks that are not expected. Except for one case (the absence of a peak at m/z 376) these predictions cannot be verified or refuted since peaks from other pyrrolic ions fall at the same masses. Other porphyrins with exocyclic rings, for which the sets of pyrrolic peaks have minimum overlap of masses, must be studied to determine the extent of preferential retention of the substituted meso carbon on the pyrrole containing the exocyclic ring.

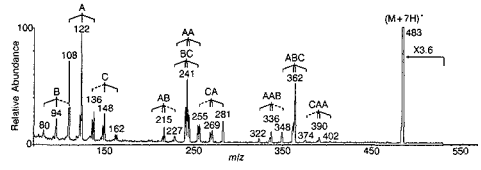

Figure 8. The CID spectrum of $(M + 7H)^+$ from 15,17-butano-3,8-diethyl-2,7,12,18-tetramethyl-21*H*,23*H*-porphine (**6**) obtained at a laboratory collision energy of 70 eV. Dashed lines indicated unexpected peaks as discussed in text.

In addition to the absence of the peak at m/z 376, the observed CID spectrum from **6** differs from the predicted CID spectrum by the presence of the peaks at m/z 120, 146, and 160. These peaks, as well as the peaks at m/z 134, 148, and 162, can be attributed to monopyrrole C, which contains the exocyclic ring. As discussed above, a peak at m/z 134, corresponding to $M_C - 13$, is not expected if there is preferential retention of the ring-substituted meso carbon on monopyrrole C. The abundant peak at m/z 134 does not, however, refute the possibility of preferential cleavage. For example, the species at m/z 120 and 134 might be products of exocyclic ring opening followed by losses of ethylene (i.e., $(M_C + 1 - 28)^+$ and $(M_C + 15 - 28)^+$, respectively). The other unexpected peaks at m/z 146 and 160 can be explained as resulting from dehydrogenation of the exocyclic ring (i.e., $(M_C + 1 - 2)^+$ and $(M_C + 15 - 2)^+$, respectively). Interestingly, however, analogous dehydrogenation peaks are not observed in the peak patterns of the di- or tripyrroles that incorporate the exocyclic ring. Although, dehydrogenation and fragmentation of the exocyclic ring appears to complicate the CID spectrum, the daughter ions resulting from these processes serve to indicate the presence of an exocyclic ring on the macrocycle and also serve to identify the pyrrole on which the ring is located. Thus, the CI-MS/MS method appears to be useful for pyrrole sequencing of porphyrins with an exocyclic ring, but these types of systems will require further study.

Analysis of Porphyrin Mixtures. An important advantage of CI-MS/MS over CI-MS lies in the capability of the former

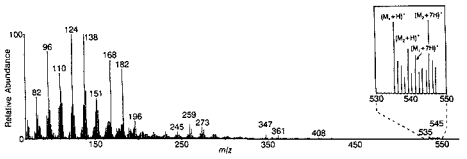

Figure 9. Ammonia CI mass spectrum of a mixture (approximately 1:1 (w/w)) of octaethylporphyrin (M_1, **2**) and deuteroporphyrin IX dimethyl ester (M_2, **3**).

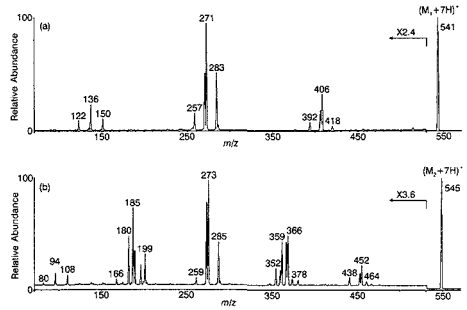

Figure 10. CID spectrum of $(M + 7H)^+$ from (a) octaethylporphyrin ($(M_1 + 7H)^+$), and (b) deuteroporphyrin IX dimethyl ester ($(M_2 + 7H)^+$) in a mixture of octaethylporphyrin (**2**) and deuteroporphyrin IX dimethyl ester (**3**). Both CID spectra were obtained at a laboratory collision energy of 70 eV.

technique to provide for pyrrole sequencing of porphyrins within a simple mixture of nonisobaric porphyrins. Such sequencing is not possible using the CI mass spectrum of the mixture, because the individual pyrrolic ions observed cannot be assigned to a specific porphyrin. However, by obtaining the CID spectrum of each $(M + 7H)^+$ species produced from the porphyrins in the mixture, it is possible to overcome this ambiguity.

To demonstrate this capability, a mixture of octaethylporphyrin (M_1, **2**) and deuteroporphyrin IX dimethyl ester (M_2, **3**) (approximately 1:1 (w/w)) was prepared and analyzed. An ammonia CI mass spectrum of this mixture is shown in Figure 9. This spectrum is quite complex since it is a convolution of the CI mass spectra obtained from the individual compounds (see Figures 4 and 6). Determining which peaks represent the structurally significant triad peak clusters is difficult and assignment of individual pyrrolic units to one particular porphyrin is not possible. However, the protonated porphyrinogen from both porphyrins (i.e., $(M_1 + 7H)^+$ and $(M_2 + 7H)^+$) is generated in sufficient abundance so that the CID spectrum of each can be obtained. The CID spectra of these $(M + 7H)^+$ species in the mixture, which are shown in Figure 10, are virtually identical with the CID spectra of the respective $(M + 7H)^+$ species that were obtained when analyzing the individual compounds (Figures 4 and 6).

A warning is in order, however, when attempting to use the CI-MS/MS sequencing method for mixture analysis when the porphyrins in the mixture differ in mass by less than 7 u. When faced with this situation, one must consider the possibility of contamination of one $(M + 7H)^+$ peak by lesser reduced species of a higher molecular weight porphyrin in the mixture. In the case above, for example, the porphyrins differ in mass by only 4 u. Therefore, the ions at m/z 541 could include $(M_2 + 3H)^+$ species as well as the expected $(M_1 + 7H)^+$. Fortunately, this was not a problem as the CID spectra obtained from the $(M + 7H)^+$ species in the mixture were the same as the CID spectra obtained from the pure compounds.

An assessment of the dangers inherent in analyzing mixtures of this type will require further investigation of the CID fragmentation patterns of the lesser reduced porphyrin species (i.e., $(M + nH)^+$, where $1 \leq n \leq 6$).

CONCLUSIONS

The pyrrole sequence of a porphyrin can readily be determined from the low-energy CID spectrum of $(M + 7H)^+$, a reduced porphyrin species produced in situ during high-pressure ammonia CI of that porphyrin. This CI-MS/MS sequencing method can be applied to sequencing of porphyrins that contain an exocyclic ring as well as to those porphyrins that do not contain such a ring. In addition, determination of the combined mass of the substituent groups present on the individual pyrroles and pyrrole sequencing of porphyrins within simple mixtures of nonisobaric porphyrins are possible with the CI-MS/MS method.

The major limitations of the CI-MS/MS sequencing method are the relatively large sample quantities required for the analysis (approximately 20–50 μg) and the fact that the sample is not recoverable after analysis. Little can be done to alter the destructive nature of the mass spectrometric analysis. Fortunately, however, the amount of material consumed is still well below that which would be needed to obtain reliable NMR data (approximately 300–500 μg). More efficient production of the protonated porphyrinogen within the ion source, as well as more efficient means of MS/MS, could reduce the amount sample required for CI-MS/MS analysis. Furthermore, a more detailed understanding of the mechanism by which $(M + 7H)^+$ fragments, especially when an exocyclic ring is present on the macrocycle, might provide clues as to how more structural information, such as the structure and position of the substituent groups on individual pyrroles, can be assessed via mass spectrometric methods.

ACKNOWLEDGMENT

The authors thank P. S. Clezy (University of New South Wales) for providing a sample of 15,17-butano-3,8-diethyl-2,7,12,18-tetramethyl-21*H*,23*H*-porphine.

LITERATURE CITED

(1) Jackson, A. H.; Kenner, G. W.; Smith, K. M.; Alpin, R. T.; Buzikiewicz, H.; Djerassi, C. *Tetrahedron* **1965**, *21*, 2913–2924.
(2) Smith, K. M. In *Porphyrins and Metalloporphyrins*, Smith, K. M., Ed.; Elsevier: Amsterdam, 1975; pp 381–398.
(3) Budzikiewicz, H. In *The Porphyrins*, *Vol. III*.; Dolphin, D., Ed.; Wiley: New York, 1982; pp 395–461.
(4) Jiang, X.; Wegmann-Szente, A.; Tolf, B.; Kehres, L. A.; Bunnenberg, E.; Djerassi, C. *Tetrahedron Lett.* **1984**, *25*, 4083–4086.
(5) Tolf, B.; Jiang, X.; Wegmann-Szente, A.; Kehres, L. A.; Bunnenberg, E.; Djerassi, C. *J. Am. Chem. Soc.* **1986**, *108*, 1363–1374.
(6) Van Berkel, G. J.; Glish, G. L.; McLuckey, S. A. *Proceedings of the 36th ASMS Conference on Mass Spectrometry and Allied Topics*, *San Francisco, CA*; American Society for Mass Spectrometry: East Lansing, MI, 1988, pp 302–303.
(7) Van Berkel, G. J.; Glish, G. L.; McLuckey, S. A., Tuinman, A. A. *Proceedings of the 37th ASMS Conference on Mass Spectrometry and Allied Topics*, *Miami Beach, FL*; American Society for Mass Spectrometry: East Lansing, MI, 1989, pp 796–797.
(8) Van Berkel, G. J.; Glish, G. L.; McLuckey, S. A. *Org. Geochem.* **1989**, *14*, 203–212.
(9) Van Berkel, G. J.; Glish, G. L.; McLuckey, S. A.; Tuinman, A. A. *J. Am. Chem. Soc.* **1989**, *111*, 6027–6035.
(10) Shaw, G. J.; Eglinton, G.; Quirke, J. M. E. *Anal. Chem.* **1981**, *53*, 2014–2020.
(11) Wolff, G. A.; Chicarelli, M. I.; Shaw, G. J.; Evershed, R. P.; Quirke, J. M. E.; Maxwell, J. R. *Tetrahedron* **1984**, *40*, 3777–3786.
(12) Sundararaman, P.; Gallegos, E. J.; Baker, E. W.; Slayback, J. R. B.; Johnston, M. R. *Anal. Chem.* **1984**, *56*, 2552–2556.
(13) Evershed, R. P.; Wolff, G. A.; Shaw, G. J.; Eglinton, G. *Org. Mass Spectrom.* **1985**, *20*, 455–453.
(14) Busch, K. L.; Glish, G. L.; McLuckey, S. A. *Mass Spectrometry/Mass Spectrometry*; VCH Publishers: New York, 1988.
(15) Budzikiewicz, H.; Pesch, R. *Org. Mass Spectrom.* **1976**, *11*, 821–830.
(16) Budzikiewicz, H.; Neuenhaus, W. *Heterocycles* **1977**, *7*, 251–257.
(17) Van Berkel, G. J.; Glish, G. L.; McLuckey, S. A. *Proceedings of the 36th ASMS Conference on Mass Spectrometry and Allied Topics*, *San Francisco, CA*; American Society for Mass Spectrometry: East Lansing, MI, 1988; pp 639–640.

(18) Filby, R. H.; Van Berkel, G. J. In *Metal Complexes in Fossil Fuels*, Filby, R. H., Branthaver, J. F., Eds.; American Chemical Society: Washington, DC, 1987; pp 2–39.

RECEIVED for review October 30, 1989. Accepted January 24, 1990. Research sponsored by the U.S. Department of Energy Office of Basic Energy Sciences under Contract DE-AC05-84OR21400 with Martin Marietta Energy Systems, Inc. The UTK Chemistry Mass Spectrometry Center is funded by the Science Alliance, a State of Tennessee Center of Excellence. The NSF Chemical Instrumentation Program also contributed to acquisition of the ZAB-EQ (Grant No. CHE-86-09251).

Ultraviolet Laser Desorption/Ionization Mass Spectrometry of Proteins above 100 000 Daltons by Pulsed Ion Extraction Time-of-Flight Analysis

Bernhard Spengler and Robert J. Cotter*

Department of Pharmacology and Molecular Sciences, Middle Atlantic Mass Spectrometry Facility, The Johns Hopkins University School of Medicine, Baltimore, Maryland 21205

UV laser desorption mass spectra of large proteins (up to 116 kDa) have been obtained on a Wiley-McLaren type time-of-flight instrument with pulsed ion extraction. Intense ion signals could be observed following delay times of several microseconds prior to ion acceleration and extraction. Initial kinetic energy distributions of ions could be determined from the drift time between the probe tip and the ion optical axis and were found to be about 1 eV, in contrast to measurements by retarding potential techniques at the detector site.

INTRODUCTION

The ultraviolet laser desorption of organic molecules has recently received a great deal of attention following the introduction of matrix techniques by Karas et al. (*1*), which have extended this ionization method to the field of protein analysis by mass spectrometry (*2*). Detailed studies by this group of the physicochemical mechanisms involved in the laser-induced desorption of ions (*3*, *4*) led to the development of a versatile technique for *matrix assisted* desorption/ionization of proteins with molecular masses up to 274 800 daltons (*5*, *6*). Their results were obtained by using the frequency quadrupled output (266 nm) from a Nd:YAG laser, a suitable UV-absorbing matrix (nicotinic acid), a commercial laser microprobe time-of-flight mass spectrometer equipped with a *reflectron* (*7*) mass focusing system, and an ion detection system capable of detecting low-velocity heavy ions. Following the initial work of Karas and Hillenkamp, two other groups have subsequently demonstrated the matrix-assisted laser desorption of large proteins, using a *linear* time-of-flight mass spectrometer with a two-stage ion extraction and acceleration geometry (*8*) and a modified commercial plasma desorption instrument (*9*), respectively. In addition, Tanaka et al. (*10*) have introduced a somewhat different technique for the analysis of high mass proteins, using a nitrogen laser and a matrix composed on a slurry of a finely divided metal powder in glycerol.

All of the instruments used thus far for high mass protein analysis have had a geometry in which ions are created in the time of flight axis with the sample deposited on a conducting, equipotential surface normal to the ion optical axis, a geometry which is intended to minimize the mass defocusing effects due to *spatial distribution* (*11*, *12*). The ions are accelerated and extracted promptly in these instruments, using a high electrical field to minimize the effects of the *initial kinetic energy distribution* (*11*, *12*). This geometry is commonly used for the time-of-flight mass analysis of ions produced by laser desorption (*13*), plasma desorption (*14*), and static SIMS (secondary ion mass spectrometry) techniques (*15*). Alternatively, Cotter et al. (*12*, *16*) have noted that *spatial* and *energy focusing* of ions produced by desorption techniques can be achieved by using the *time-lag* focusing scheme introduced by Wiley and McLaren (*17*) for electron impact ionization. This scheme, which has been incorporated into time-of-flight instruments employing CO_2 laser desorption (*16*) and liquid SIMS (*18*), does not require that ions be formed on an equipotential or conducting surface, and employs a relatively low, pulsed extraction voltage to remove ions from a grounded ion source. thus, this paper describes for the first time the detection of large proteins in an instrument with a pulsed extraction geometry in which the ions are created outside the time-of-flight axis from a surface parallel to the ion optical axis. In addition, while time-delayed ion extraction is employed for energy focusing, it also provides a convenient means for determining the initial kinetic energies of the ions desorbed by the UV laser as they drift from the sample surface to the ion optical axis.

EXPERIMENTAL SECTION

The instrument configuration used for the experiments reported here is much the same as that employed previously for IR laser desorption (*16*) and has been described in detail earlier (*19*). However, several modifications were made to enable desorption ionization of large proteins. A scheme of the instrument is shown in Figure 1. The laser used is a Quantel International (Santa Clara, CA) Model YG 660 frequency quadrupled Nd:YAG laser with output energies of 15 mJ/pulse at 266 nm and a pulse width of 5 ns. It can be operated between 10 Hz and single shot with an energy output stability better than ±10%. The laser beam can be attenuated by means of color filter glasses (Schott Glass Technologies, Inc., Duryea, PA). Focusing is accomplished with a 300 mm focal length quartz lens to a spot size diameter of approximately 150 μm. The mass spectrometer is a modified CVC Products (Rochester, NY) Model 2000 linear time-of-flight instrument with time-delayed, pulsed ion extraction and a three-stage acceleration region between the *source* and *drift* regions. The duration of the ion extraction (drawout) pulse was increased to 30 μs, the time needed for ions up to 200 000 daltons to leave the drawout region. Silver was used as the probe tip substrate material.

In order to increase the detection efficiency for low-velocity heavy ions, a postaccelerating detector was constructed, using a Thorn/EMI (Fairfield, NJ) venetian blind type electron multiplier.

0003-2700/90/0362-0793$02.50/0

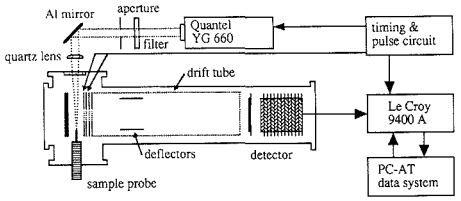

Figure 1. Block diagram of the UV laser desorption ionization instrument.

An additional dynode (also of the venetian blind type) was placed between the end of the drift region and the multiplier. The voltage on this dynode could be varied from −3 kV (the voltage on the drift tube) to −20 kV, so that ion/electron conversions could be made for positive ions with kinetic energies of up to 20 keV. Secondary electrons from this dynode were then accelerated toward the first dynode (−3 kV) of the multiplier, and the analog signal at the multiplier anode collected as a negative voltage at 50 Ω with respect to ground. This detection arrangement proved to be more satisfactory than the postacceleration detector described previously (*18*) which employed a dual channelplate detector.

Time of flight data are required and stored on a LeCroy (Chestnut Ridge, NY) Model 9400A digital oscilloscope/transient recorder, with a maximum time resolution of 10 ns and 32 000 data points. Further processing was done by PC-based software. Mass spectral data were averaged over various numbers of single-shot spectra.

Peptide samples were obtained from Sigma Chemical Co. (St. Louis, MO) and prepared as 10^{-5} M solutions in ultrapure water. Nicotinic acid was used as a matrix in a 50 mM aqueous solution. A 1 μL portion of peptide solution was mixed with 1 μL of matrix solution and dried on the probe tip prior to insertion into the mass spectrometer.

RESULTS AND DISCUSSION

The proteins tested so far include bovine insulin (MW 5733.5, dissolved in 0.1% of trifluoracetic acid), chicken egg white lysozyme (MW ca. 14 400), bovine trypsin (MW ca. 23 800), porcine pepsin (MW ca. 32 700), bovine albumin (MW ca. 66 000), phosphorylase b (MW ca. 97 400), and *E. coli* β-galactosidase (MW ca. 116 000). (Molecular weights are the values approximated by the manufacturer.) All peptides showed clearly detectable signals in their laser desorption mass spectra.

The most satisfactory results were obtained on this instrument when the sample probe tip was some distance from the ion optical axis; i.e. the ions were not formed in a direct line of sight to the detector. The optimal ion extraction delay time then depends upon the length of time needed for the ions to drift from the probe surface to the center of the source region. Therefore, in order to determine the proper settings of drawout delay time for a given probe tip position, it was necessary to determine the initial kinetic energies (velocities) of the desorbed ions. Knowledge of initial ion kinetic energies is of course of considerable interest for understanding the ionization mechanisms and for the development of better designs to improve ion focusing and mass resolution. The kinetic energy distributions of ions have been measured on a variety of time-of-flight instruments, most commonly by the *retarding potential technique* using a repeller grid in front of the detector. In this case the initial kinetic energy distributions are determined from the first derivative of the measured ion intensity vs repeller grid potential curves. The repeller grid potential is varied over a small voltage range near the accelerating voltage and, thus, enables the determination of relatively small differences in energy carried by ions accelerated to high final kinetics energies. It should be noted that, in addition to the kinetic energy at the time of ion formation, such measured energy distributions also reflect (among other things) the effects of Coulomb repulsion, space charging, and (in the case of ions desorbed from an equipotential surface in the presence of a high field) surface roughness and samples thickness.

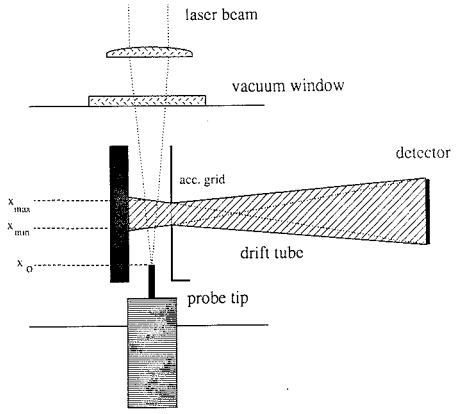

Figure 2. Diagram of the ion source, indicating the useful region in front of the drawout grid. Ions within x_{max} and x_{min} are transmitted to the detector.

In the pulsed extraction instrument described here, the initial kinetic energies of desorbed ions can be measured more easily and more precisely by varying the time delay between the laser pulse and ion drawout pulse and monitoring the intensity of the ion signal. Figure 2 provides a somewhat more detailed view of the geometry of the ion source in order to illustrate this method. In contrast to thermal desorption processes (*16*), the ions formed at near threshold irradiances by pulsed UV lasers are desorbed only for the duration (5 ns) of the laser pulse. Desorbed ions drift toward the center of the source with a velocity determined by their initial kinetic energies and are accelerated and transmitted to the detector only if they were located within the region bounded by x_{min} and x_{max} at the time of the imposition of the drawout pulse. A plot of the ion intensities versus delay time thus gives ion velocities within an uncertainty defined by $(x_{max} - x_{min})/t$, which can then be converted to an energy distribution. The distances used for the described measurement were

$$x_{min} - x_0 = 7.6 \text{ mm}$$

$$x_{max} - x_{min} = 6.4 \text{ mm}$$

Figure 3 shows the time intensity profile of tryptophan, that has been used as a test substance. Intensities of the molecular ion at mass 205 and the major fragment ion at mass 130 are shown. Due to their lower mass, the arrival time of the fragment ions is lower than that of the molecular ions. Conversion of the data to kinetic energies results in the plot shown in Figure 4. Since the kinetic energy interval, corresponding to the interval $x_{max} - x_{min}$, is itself a function of the delay time, a plot of ion intensity versus average kinetic energy would not represent the ion energy spectrum correctly. Thus a plot of intensity per unit energy interval versus average kinetic energy has been used in Figure 4. The mean kinetic energies of both fragment and molecular ions are shown to be about 1 eV. This is an interesting result, because repeller grid measurements for ions desorbed by both IR and UV lasers (*20–22*) have produced values of energy spreads (composites of initial kinetic energy, Coulomb repulsion, space charging, surface roughness in a high accelerating field, etc.) in the range of 10–100 eV. It should be noted that Coulomb repulsion and

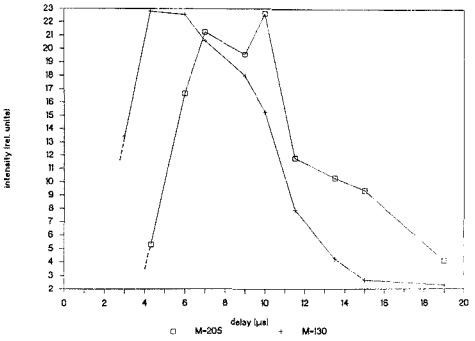

Figure 3. Relative intensities of tryptophan molecular ions and fragment ions versus the delay time between the laser desorption pulse and the ion drawout pulse.

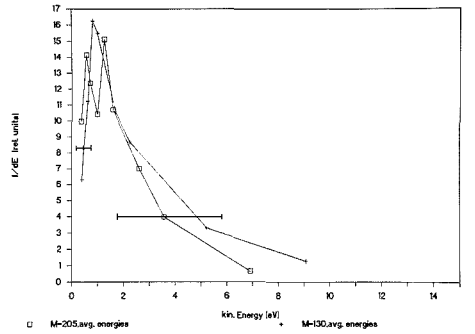

Figure 4. Initial kinetic energy distributions of the tryptophan molecular ions and fragment ions.

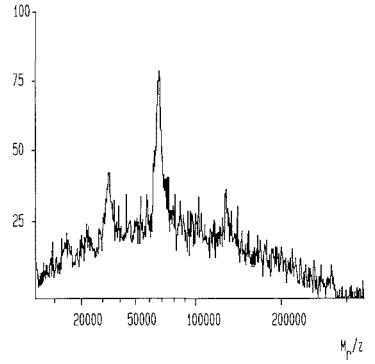

Figure 5. Matrix-assisted UV laser desorption mass spectrum of bovine albumin (MW ca. 66 000 amu), averaged over 214 single-shot spectra. A 10-pmol portion of analyte was used for preparation.

space charging can effect the measurements in our experiment as well. However, their effects on the kinetic energy distribution would be much higher in an accelerating system with a high electric field applied.

The measured kinetic energies of tryptophan were used to determine the appropriate delay times for the detection of large proteins which were then optimized from observations of their spectra.

Figure 5 shows a mass spectrum of bovine albumin (MW ca. 66 000), showing the singly charged molecular ion, the doubly charged molecular ion, and a dimer ion. Despite the

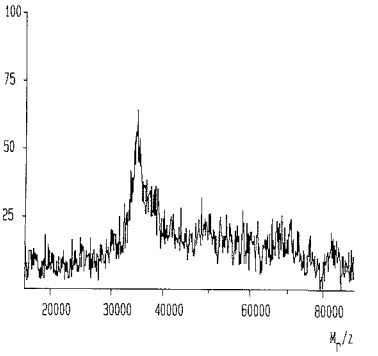

Figure 6. Matrix-assisted UV laser desorption mass spectrum of porcine pepsin (MW ca. 32 700 amu), averaged over 114 single-shot spectra. A 10-pmol portion of analyte were used for preparation.

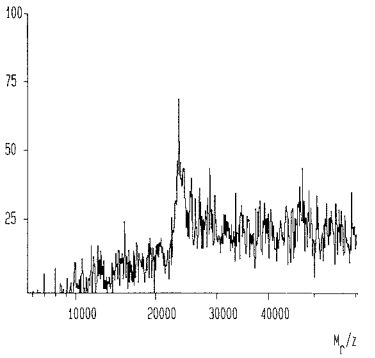

Figure 7. Matrix-assisted UV laser desorption mass spectrum of bovine trypsin (MW ca. 23 800 amu), averaged over 255 single-shot spectra. A 10-pmol portion of analyte was used for preparation.

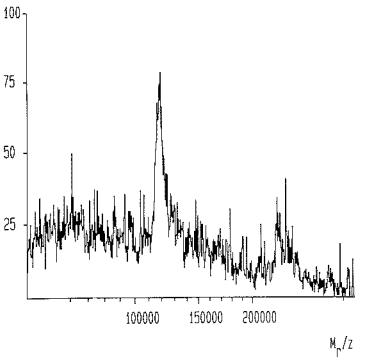

Figure 8. Matrix-assisted UV laser desorption mass spectrum of *E. coli* β-galactosidase (MW ca. 116 000 amu), averaged over 200 single-shot spectra. A 10-pmol portion of analyte was used for preparation.

relatively low initial kinetic energy distribution, mass resolution is somewhat poor. As described by Beavis and Chait (8), this is due in part to the formation of both protonated molecular ions and those carrying one or more matrix molecules. These could be distinguished in the fine structure of the molecular ion peak of insulin (data not shown) but cannot

be resolved in the time-of-flight mass spectra of much larger structures.

The UV laser desorption mass spectra of porcine pepsin (MW ca. 32 700) and bovine trypsin (MW ca. 23 800) are shown in Figures 6 and 7, respectively. The mass spectrum of β-galactosidase (MW ca. 116 000) is shown in Figure 8. In this spectrum the dimer at ca. 232 000 daltons is detected. The fact that the large molecular ions produced by UV laser desorption are stable over long periods has been demonstrated in the earliest reports (*1*, *5*) of this technique, since an ion reflection system was employed. Thus, observation of these ions following several microseconds of delay between ion formation and mass analysis is consistent with their high internal stability.

CONCLUSIONS

Detection of high-mass UV laser desorbed molecular ions could be achieved in a Wiley-McLaren type instrument with pulsed extraction geometry. Initial kinetic energies of these ions are shown to be much smaller than previously assumed, and their survival following ion extraction delay times of up to 30 μs attests to their low internal energy as well. Mass resolution is comparable to that observed by other investigators and appears to be affected primarily by the formation of a variety of molecular ion species including adduct ions with the matrix, rather than the initial kinetic energy distribution or the metastable decomposition of ions during acceleration. These measurements as well as future investigations using the special extraction geometry can help to overcome the actual problems of the method and hopefully will lead to further instrumental improvements. At the same time, the results suggest that relatively routine and reliable measurements may be obtained on a low-cost commercial time-of-flight mass spectrometer.

LITERATURE CITED

(1) Karas, M.; Bachmann, D.; Bahr, U.; Hillenkamp, F. *Int. J. Mass Spectrom. Ion Processes* **1987**, *78*, 53.
(2) Karas, M.; Hillenkamp, F. *Anal. Chem.* **1988**, *60*, 2299.
(3) Karas, M.; Bachmann, D.; Hillenkamp, F. *Anal. Chem.* **1985**, *57*, 2935.
(4) Spengler, B.; Karas, M.; Bahr, U.; Hillenkamp, F. *J. Phys. Chem.* **1987**, *91*, 6502.
(5) Karas, M.; Bahr, U.; Ingendoh, A.; Hillenkamp, F. *Angew. Chem., Int. Ed. Engl.* **1989**, *28*, 760.
(6) Hillenkamp, F.; Karas, M. *Proceedings of the 37th ASMS Conference on Mass Spectrometry and Allied Topics*; American Society for Mass Spectrometry: East Lansing, MI, 1989; p 1168.
(7) Mamyrin, B. A.; Karataev, V. I.; Shmikk, D. V.; Zagulin, V. A. *Sov. Phys.—JETP (Engl. Transl.)* **1973**, *37*, 45-48.
(8) Beavis, R. C.; Chait, B. T. *Rapid Commun. Mass Spectrum.* **1989**, *3*, 233.
(9) Salehpour, M.; Perera, I.; Kjellberg, J.; Hedin, A.; Islamian, M. A.; Hakansson, P.; Sundqvist, B. U. R. *Rapid Commun. Mass Spectrom.* **1989**, *3*, 259.
(10) Tanaka, K.; Waki, H.; Ido, Y.; Akita, S.; Yoshida, Y.; Yoshida, T. *Rapid Commun. Mass Spectrom.* **1988**, *2*, 151.
(11) Opsal, R. B.; Owens, K. G.; Reilly, J. P. *Anal. Chem.* **1985**, *57*, 1884-1889.
(12) Cotter, R. J. *Biomed. Environ. Mass Spectrom.* **1989**, *18*, 513-532.
(13) Hillenkamp, F.; Kaufmann, R.; Nitsche, R.; Unsold, E. *Appl. Phys.* **1975**, 341.
(14) Macfarlane, R. D.; Torgerson, D. F. *Science* **1976**, *191*, 920.
(15) Chait, B. T.; Standing, K. G. *Int. J. Mass Spectrom. Ion Phys.* **1981**, *40*, 185.
(16) Van Breemen, R. B.; Snow, M.; Cotter, R. J. *Int. J. Mass Spectrom. Ion Phys.* **1983**, *49*, 35-50.
(17) Wiley, W. C.; McLaren, I. H. *Rev. Sci. Instrum.* **1955**, *26*, 1150.
(18) Olthoff, J. K.; Honovich, J. P.; Cotter, R. J. *Anal. Chem.* **1987**, *59*, 999-1002.
(19) Olthoff, J. K.; Lys, I.; Demirev, P.; Cotter, R. J. *Anal. Instrum.* **1987**, *16*, 93-115.
(20) Spengler, B.; Bahr, U.; Hillenkamp, F. *Inst. Phys. Conf. Ser.* **1988**, *94*(2), 137.
(21) Mauney, T.; Adams, F. *Int. J. Mass Spectrom. Ion Processes* **1984**, *59*, 103.
(22) Van der Peyl, G. J. Q.; Van der Zande, W. J.; Bederski, K.; Boerboom, A. J. H.; Kistemaker, P. G. *Int. J. Mass Spectrom. Ion Phys.* **1983**, *47*, 7.

RECEIVED for review October 25, 1989. Accepted January 17, 1990. This work was supported by a grant, DIR 86-10589, from the National Science Foundation and carried out at the Middle Atlantic Mass Spectrometry Laboratory, an NSF Shared Instrumentation Facility. B. Spengler was supported by a Deutsche Forschungsgemeinschaft Fellowship.

Determination of [^{3}H]-2,3,7,8-Tetrachlorodibenzo-*p*-dioxin in Human Feces to Ascertain Its Relative Metabolism in Man

Jay M. Wendling* and Robert G. Orth

Monsanto Company, 800 North Lindbergh Boulevard, St. Louis, Missouri 63167

Hermann Poiger

Institute of Toxicology, Federal Institute of Technology and University of Zurich, Schorenstrasse 16, CH-8603 Schwerzenbach, Switzerland

Human feces samples from a self-dosing experiment were analyzed by gas chromatography/mass spectrometry (GC/MS) for [^{3}H]-2,3,7,8-tetrachlorodibenzo-*p*-dioxin (^{3}H-2378-TCDD) to determine that 36-44% of the radioactivity was attributable to the parent compound. This method, using isotope dilution analysis, proved to be difficult due to the unexpectedly higher native 2378-TCDD background which created abnormally large precision ranges around the calculated feces concentrations of 0.1-0.2 pg/g. These results were supported by additional analyses involving the GC/MS chemical cleanup method combined with liquid scintillation counting which showed that at most, 50% of the radioactivity was due to 2378-TCDD metabolites resulting in a minimum metabolism of 50% for these samples.

INTRODUCTION

At the Fifth International Symposium on Chlorinated Dioxins and Related Compounds (i.e., Dioxin '85) held in Bayreuth, Federal Republic of Germany, results were given of a self-dosing experiment performed by Dr. Poiger of the Federal Institute of Technology, Switzerland, which for the first time provided human data for the half-life of elimination of [^{3}H]-2,3,7,8-tetrachlorodibenzo-*p*-dioxin (TCDD) (*1*). The excretion half-life was observed to be 2120 days or 5.8 years. This number falls within an estimated half-life range of 3.5-6.9 years calculated from adipose tissue concentrations and estimated daily intake (*2*).

The self-dosing half-life value was determined based only on feces concentrations of radioactive equivalents of TCDD.

0003-2700/90/0362-0796$02.50/0

Any excretion in the urine is believed to be insignificant since the levels of radiolabeled equivalents in urine were not detectable. However, the feces results gave no insight as to what portion of the excreted radioactive "TCDD equivalents" are metabolites or the parent 2378-TCDD molecule. Studies that involved the fate of 2,3,7,8-TCDD in laboratory animals indicated that metabolism was of importance in the elimination process (*3–5*). Researchers have identified many mammalian metabolites in both urine and bile but found that the rates and routes of elimination are highly species dependent (*6–10*). In addition, other metabolites discovered in feces but not found in bile as well as unchanged TCDD may enter the intestinal lumen via pathways perhaps comparable to lipid metabolism (*6, 11, 12*). These data suggest a possibility that part of the TCDD equivalents in human feces could be due to metabolized TCDD.

To determine whether metabolism of TCDD has occurred in man, feces samples from the self-dosing experiment were analyzed to quantify the actual radiolabeled TCDD in the feces and the difference between the measured TCDD level and the value of "TCDD equivalents" as metabolites of TCDD. This was performed by combining chemical cleanup methods with high-resolution gas chromatography/mass spectrometry (GC/MS).

Based on calculations using the known total radiolabeled equivalents, the detection limit required was within the limits of the method. This calculation assumed that there would be an insignificant native TCDD background in the feces and that all of the radiolabeled TCDD contained two tritium atoms. These assumptions proved to be false and the analysis quite difficult due to the interference from the normal background level of native 2,3,7,8-TCDD present in human feces. The analysis was further complicated by the coposition of the ingested radiolabeled TCDD, which was found to be a mixture of untritiated (native), monotritiated, and ditritiated 2,3,7,8-TCDD. This made it necessary to use multiple approaches to obtain and verify results.

EXPERIMENTAL SECTION

The method used for the GC/MS analysis of nonlabeled TCDD in human feces is similar to those reported for other biological tissues (*13–15*) and has been reported (*16*). The modifications necessary for the GC/MS analysis of ^{3}H-TCDD are given below with a brief description of additional analytical methods used. Prior to beginning any work with chlorinated dioxins, one should become familiar with techniques for the safe handling of these potential toxicants as well as any local, state, or federal regulations concerning use, storage, and disposal of both dioxin and radioactive materials and contaminated wastes. An excellent article addressing laboratory setup and precautions has been published by Alexander et al. (*17*).

Sample Preparation. Approximately 20 g of feces, previously lyophilized and homogenized, was weighed into glass bottles and spiked with $^{13}C_{12}$-TCDD as a surrogate standard. The samples were digested overnight with concentrated sulfuric acid and then extracted with hexane. The extracts were then passed through three column chromatography steps using 20% (w/w) sulfuric acid/silica gel, Woelm Basic Alumina, and 18% (w/w) Carbopack C/Celite (*13, 18*). Reference 18 can be obtained through the U.S. EPA, CLP Sample Management Office, P.O. Box 818, Alexandria, VA 22313. Tribromobiphenyl, which is used as an internal standard to determine recovery, was added to the collected eluent from the last column. The eluent was then concentrated to 10 μL for subsequent GC/MS analysis.

GC/MS Analysis. Analysis was performed on a VG ZAB E mass spectrometer equipped with a Hewlett-Packard (HP) Model 5890 gas chromatograph. The HP 5890 was operated with helium carrier gas at 7 psi using splitless injection into a 30-m J&W DB5 capillary column programmed to hold at 180 °C for 1 min then ramped at 10 °C per minute to 250 °C. The double-focusing mass spectrometer was operated in the electron-impact ionization mode at 32 eV with a mass resolution of 5000. Selected ion monitoring was used to monitor the ions representing each isotope as follows:

m/z 316.9824 = perfluorophenanthrene (lockmass)

m/z 319.8965 = n(native)-TCDD

m/z 321.8936 = n-TCDD + $^3H_1$-TCDD

m/z 323.8906 = n-TCDD + $^3H_1$-TCDD + $^3H_2$-TCDD

m/z 325.8877 = n-TCDD + $^3H_1$-TCDD + $^3H_2$-TCDD

m/z 327.9070 = n-TCDD + $^3H_1$-TCDD + $^3H_2$-TCDD

m/z 329.9040 = $^3H_1$-TCDD + $^3H_2$-TCDD

m/z 331.9368 = $^3H_2$-TCDD + $^{13}C_{12}$-TCDD

m/z 333.9338 = $^{13}C_{12}$-TCDD

m/z 389.8077 = tribromobiphenyl (internal standard)

Positive identification of the desired analytes was made by comparing peak retention times to the surrogate ($^{13}C_{12}$-TCDD) standards added to the samples and to analytical standards which were analyzed along with the samples.

To calculate percent recoveries, representative peak areas for $^{13}C_{12}$-TCDD (m/z 333.9) were ratioed to the peak area of the internal standard, tribromobiphenyl (TBB, m/z 389.8). These ratios were compared to standards to determine the actual percent recovery of TCDD.

A standard of [1,6-$^3H_2$]-2,3,7,8-tetrachlorodibenzo-*p*-dioxin (dpm)/ng of TCDD) was received from Dr. Alan Poland, McArdle Laboratory for Cancer Research at the University of Wisconsin (*19*). The isotopic purity was determined by using isotope dilution techniques (*20*) and GC/MS analysis using the conditions described above. The standard activity was calculated by

$$A/A_0 = \exp(-kt_{1/2}) \quad (1)$$

where A is the activity as determined from liquid scintillation counting and the decay constant, k, of a tritium atom is 1.067×10^{-7} M^{-1}) as calculated from a half-life of 4510 days (*21*). The experimental activity was then converted to the concentration of the standard based on the relative contributions of each isotope using the following formulas:

$$\frac{\text{dpm } ^3H_1\text{-TCDD}}{1.067 \times 10^{-7}\ \text{M}^{-1}}\left(\frac{1\ \text{molecule}}{1\ \text{tritium}}\right)\left(\frac{1\ \text{mole}}{6.02 \times 10^{23}}\right)\left(\frac{324\ \text{g of TCDD}}{\text{mole}}\right) = \text{g of } ^3H_1\text{-TCDD} \quad (2)$$

$$\frac{\text{dpm } ^3H_2\text{-TCDD}}{1.067 \times 10^{-7}\ \text{M}^{-1}}\left(\frac{1\ \text{molecule}}{2\ \text{tritiums}}\right)\left(\frac{1\ \text{mole}}{6.02 \times 10^{23}}\right)\left(\frac{326\ \text{g of TCDD}}{\text{mole}}\right) = \text{g of } ^3H_2\text{-TCDD} \quad (3)$$

The concentration was also checked by GC/MS against the National Bureau of Standards (NBS) Standard Reference Material (SRM) 1614, which has a concentration of 67.8 ng/mL.

Oxidation/LSC Quantitative Analysis. Approximately 0.5 g of lyophilized and homogenized feces were weighed into a Combusto-cone (Packard), then 0.1 g of cellulose powder was added. The samples were then run through a Packard Model B 306 Tri-Carb sample oxidizer. Tritiated water was collected and diluted with Monophase 40 (Packard). Samples were counted for 60 min on a Beckman LS9800 liquid scintillation counter (LSC). Quenching was monitored by H# (*22*) so samples were corrected to determine the actual activity (i.e., disintegrations per minute, dpm).

Combined GC/MS and LSC Analysis. An additional amount of the self-dosing feces samples were run through the GC/MS workup method (including addition of the surrogate standard $^{13}C_{12}$-TCDD). At the final concentration step, TBB was added and the sample was diluted to the mark in a 1-mL class A volumetric flask. Twenty percent or 200 μL was removed and added to 15 mL of Instagel (Packard) cocktail for LSC analysis.

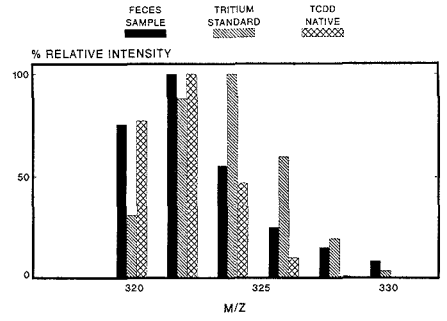

Figure 1. Measured isotopic ratios for the molecular ions of TCDD for feces sample, tritium standard, and nonlabeled 2,3,7,8-TCDD standard.

Table I. Validation and Determination of the Relative Contribution of Each TCDD Isotope in the ^{3}H-TCDD Analytical Standard

m/z[a]	peak areas	n-TCDD	$^3H_1$-TCDD	$^3H_2$-TCDD	residual
319.9	1311.02	1311.02	NA[b]	NA	NA
321.9	3759.34	1691.41	2067.93	NA	NA
323.9	4256.59	794.57	2667.94	794.08	NA
325.9	2550.52	167.16	1253.32	1024.4	105.56
327.9	829.63	18.74	263.67	481.27	65.95
329.9	148.28	NA	29.57	101.25	17.39
% contribution		31.4	49.6	19.0	

[a] m/z, mass to charge ratio. [b] NA, not applicable.

The remaining volume was analyzed by GC/MS to determine the percent recovery of TCDD.

Quality Assurance/Quality Control (QA/QC). To provide QA/QC samples, raw feces were collected from volunteers. These samples were pooled, lyophilized, and homogenized to simulate the self-dosing samples. Four pooled feces samples were prepared as above and analyzed by GC/MS. Two of these samples were spiked with different amounts of the ^{3}H-TCDD standard given above prior to acid digestion. Also, two samples containing no feces were run where one served as a solvent blank while the other was spiked with ^{3}H-TCDD. Feces from the volunteer pool were spiked with varying amounts of ^{3}H-TCDD and run on the oxidizer and analyzed by LSC as stated above. These results were used to determine a mean recovery of 85.7% for the oxidizer.

RESULTS AND DISCUSSION

The relative chlorine isotope abundances used for isotopic dilution calculations were experimentally determined by analyzing pure samples of n-2,3,7,8-TCDD and tritiated 2,3,7,8-TCDD. These isotopic distributions can be seen in Figure 1. The experimentally determined ratio for the four-chlorine system was 77.5:100:47:10:1, which compares favorably with calculated ratios of 77:100:49:11:1. The isotopic distribution of the analytical standard provided by Dr. Poland was calculated by using the experimentally determined isotopic ratios and is given in Table I. The residuals found at m/z 325.9, 327.9, and 329.9 represent the remaining area not accounted for in the individual calculations. These residuals are around 10% of the total area for that mass which, considering the propagation of error in the calculation, are within the limits of instrumental precision. This suggests that the calculations and the percent contribution of each isotope are correct.

The standard concentration was determined in two ways. The ratio of the radiolabeled standard to ^{13}C-TCDD was obtained by GC/MS and compared to the ratio obtained for NBS SRM 1614 relative to ^{13}C-TCDD. The value for the concentration of the radiolabeled standard was then calculated by using the experimentally determined radiolabeled distribution. The standard was found to have a total TCDD concentration of 299 ng/mL by this approach. The second method was to determine the number of dpm's for the labeled TCDD by LSC and calculate the concentration by using eqs 2 and 3, which yielded a total TCDD value of 325 ng/mL. These concentrations are certainly within the precision of the quantitation.

Table II. Oxidation/LSC Results of Tritium Analysis of Self-Dosing Feces Samples

sample	N	av dpm/g[a]	TCDD equivalents
J	3	144 ± 21	0.57 (0.60)[b]
X	2	62.3 ± 4.6	0.25 (0.34)[b]

[a] dpms corrected for background and recovery. [b] Results in parentheses were determined at Institute of Toxicology. TCDD equivalents are in picograms per gram.

The results of the tritium analysis of the self-dosing feces by oxidation/LSC analyses are shown in Table II for two different feces samples and are given in "TCDD equivalents". Since LSC is a nonspecific detector, these values include $^3H_1$-TCDD, $^3H_2$-TCDD, and metabolites. This analysis was also carried out independently at The Institute of Toxicology where the results were calculated directly from the listed activity and were not made available for comparison with the values determined by this laboratory until the completion of the analyses. For samples labeled J and X, this laboratory measured 0.57 and 0.25 pg/g respectively, as compared to the previously measured values of 0.60 and 0.34 pg/g. The fact that the two separate analyses result in similar numbers supports the accuracy of the isotopic distribution and subsequent calculations.

Figure 1 shows the isotopic distribution of a feces sample, tritium standard, and nonlabeled TCDD standard for the different ions monitored for this analysis. Ideally, the isotopic dilution method described above for determining the relative concentrations of the various forms of TCDD in the tritiated standard would also have been used on the feces. However, as can be seen in Figure 1 the feces sample distribution reflects mostly a native contribution. This background level was estimated at between 0.7 and 1.0 pg/g, which is an amount greater than 5 times the level of the tritiated species.

Since the isotopic dilution methods work best when each form of TCDD is at approximately the same or higher concentrations than interfering forms of TCDD, then an alternative approach was required. For m/z 321.9 and 323.9, the contribution to the observed peaks by $^3H_1$-TCDD and $^3H_2$-TCDD was very small. Subtracting the n-TCDD contribution from these peaks was possible but the estimated error in the residual was prohibitively large. As an alternative, peak areas at m/z 325.9, 327.9, and 329.9 were used where, as can be seen in Figure 1, the contribution from the n-TCDD is substantially smaller compared to $^3H_1$-TCDD and $^3H_2$-TCDD. This small contribution can also be seen in Figure 2 where the feces mass chromatograms for m/z 321.9 and 327.9 are shown. Figure 2 shows the decreased contribution of the native TCDD along with an increase in signal to noise due to less chemical noise for m/z 327.9. By use of these ions, the individual species cannot be accurately separated into two values, so the results have been reported as the sum of $^3H_1$-TCDD and $^3H_2$-TCDD or "total ^{3}H-TCDD". This method raises detection limits because 325.9 represents only 48% of the highest ^{37}Cl abundance of $^3H_1$-TCDD. In addition, a small contribution to these peaks occurred from trace levels (<1%) of incompletely labeled $^{13}C_{12}$-TCDD (i.e., $^{13}C_{10}$-TCDD, $^{13}C_8$-TCDD, and $^{13}C_6$-

Table III. GC/MS Results of Feces Analysis for ^{3}H-TCDD[a]

sample	pooled feces	pooled feces	solvent blank	feces LS	feces HS	feces J	feces X	solvent LS
weight, g	20.03	20.26	20.00	20.48	20.44	20.38	20.56	20.00
S, pg/g					0.07	0.06	0.06	
result, pg/g	ND (<0.10)	ND (<0.10)	ND (<0.09)	ND (<0.09)	0.31	0.21	0.13	ND (<0.08)
pg/g added				0.0502	0.252			0.0514
% recovery	59	59	68	63	67	82	71	77

[a] The results are given in picograms per gram of feces. ND, none detected (detection limit). S, estimated sample standard deviation. LS and HS are low and high spikes.

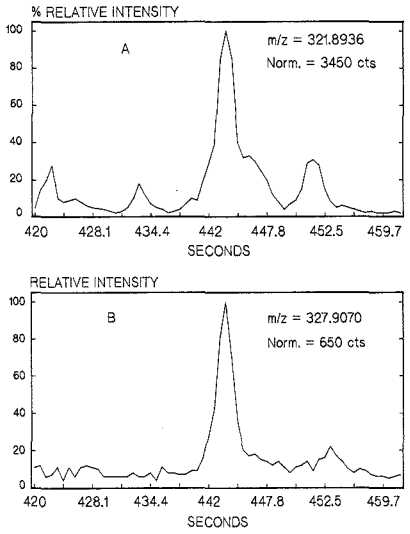

Figure 2. Feces mass chromatograms for selected ion monitoring of m/z 321.8936 (A) and m/z 327.9070 (B).

TCDD). This made it necessary to subtract these contributions.

The results of the GC/MS analysis of the feces samples are given in Table III showing that three samples had detectable levels of ^{3}H-TCDD representing both $^3H_1$-TCDD and $^3H_2$-TCDD. The result of the QA/QC sample labeled "feces HS" of 0.31 ± 0.07 pg/g is within one standard deviation of the expected value of 0.25 pg/g confirming the accuracy of the method. This result also proves that any tritium exchange with hydrogen that might have occurred due to the extreme conditions of the sample preparation was not observed, and this phenomenon is not believed to be significant. The low spikes were at levels which assumed that the self-dosing feces would have minimum contributions from background TCDD. Because of the increase in the detection limit caused by the use of the alternate isotope dilution approach presented above, the low spikes were below the limit of quantitation for the method. Comparing the GC/MS results of feces samples J and X to the average results of Table II, one may calculate that the ^{3}H-TCDD compounds represent 35.9% and 44.1%, respectively, of the total "TCDD equivalents". Conversely, this means that 64.1% and 55.9% of the TCDD are metabolized for the two samples.

As can be seen in Table III the sample standard deviation based on the standard calibration curve for J is 29% and for X is 46%. Given this imprecision, further work was done to support the GC/MS results by combining the GC/MS cleanup method with LSC. With the samples subjected to the chemical cleanup method for analysis by GC/MS, it was assumed that

Table IV. LSC Results of Feces Subjected to the Chemical Cleanup Method for GC/MS

sample	% recovery	dpm/g[a]
J	46.8	72.64
X	75.6	27.30

[a] Results given in disintegrations per minute (dpm). dpm corrected for background, recovery, and volume (0.2). g, gram of feces.

most, if not all, of the metabolites would be removed prior to the LSC and the activity found would represent only ^{3}H-TCDD. Metabolites found in animal studies have been identified as hydroxylated tri- and tetrachlorinated dibenzo-*p*-dioxins, diphenyl ethers, and dichlorocatechols (*6*, *8*, *9*, *23*). If the metabolites in humans are similar, then this assumption should be valid. The results of this analysis are found in Table IV. Given the previous assumptions made, one may calculate the amount of TCDD actually contributing to the original radioactivity of the feces found in Table II to be 50.4% and 43.8% for samples J and X, respectively. However, these measurements represent the most (within limits of precision) amount of the parent ^{3}H-TCDD possible. If metabolites are still present after the GC/MS cleanup procedure, then this value would be less. Conversely, this means that an absolute minimum (again, within limits of precision) of 49.6% and 56.2% of TCDD is metabolized for the two respective samples.

CONCLUSIONS

The results showed that the excreted radiolabeled TCDD represented, at most, approximately 50% of the amount of "TCDD equivalents". Although the precision leaves doubt as to the exact amount, certainly the results from the combined approaches show that a significant portion of 2,3,7,8-TCDD is metabolized by man. It should be noted that the effort described in this paper was conceived after the dosing had occurred. The results of this work certainly show that this type of analysis can be used in a carefully designed study to meet the objectives previously stated.

ACKNOWLEDGMENT

The authors thank Jeanne Sebaugh of Sebaugh's Information Services for her work in the statistical analysis of the data, Alan Poland of McArdle Laboratory for Cancer Research for generously providing the [1,6-$^3H_2$]-2,3,7,8-TCDD standard, and Fred Hileman for his valued advice in conducting the study.

Registry No. TCDD, 1746-01-6.

LITERATURE CITED

(1) Poiger, H.; Schlatter, C. *Chemosphere* **1986**, *15*(9–12), 1489–1494.
(2) Geyer, H. J.; Scheunert, I.; Filsher, J. G.; Korte, F. *Chemosphere* **1986**, *15*(9–12), 1495–1502.
(3) Olson, J. R.; Gasiewicz, T. A.; Neal, R. A. *Toxicol. Appl. Pharmacol.* **1980**, *56*, 78–85.
(4) Olson, J. R. *Toxicol. Appl. Pharmacol.* **1986**, *85*, 263–273.
(5) Gasiewicz, T. A.; Olson, J. R.; Geiger, L. H.; Neal, R. A. In *Human and Environmental Risks of Chlorinated Dioxins and Related Compounds*;

Tucker, Young, and Gray, Eds.; Plenum Press: New York, 1983; pp 495-525.
(6) Poiger, H.; Buser, H.-R.; Weber, H.; Zweifel, U.; Schlatter, C. *Experentia* **1982**, *38*, 484.
(7) Olson, J. R.; Gasiewicz, T. A.; Geiger, L. E.; Neal, R. A. In *Accidental Exposure to Dioxins, Human Health Aspects*; Coulston, F., Pocchiara, F., Eds.; Academic Press: New York, 1983; pp 81-100.
(8) Poiger, H.; Buser, H.-R. In *Biological Mechanisms of Dioxin Action*; Banbury Report 18; Poland, A., Kimbrough, R. D., Eds.; Cold Spring Harbor Laboratory: Cold Spring Harbor, NY, 1984; p 39.
(9) Neal, R. A.; Gasiewicz, T. A.; Geiger, L. H.; Olson, J. R.; Sawahata, T. *Biological Mechanisms of Dioxin Action*; Banbury Report 18; Poland, A., Kimbrough, R. D., Eds.; Cold Spring Harbor Laboratory: Cold Spring Harbor, NY, 1984; p 49.
(10) Gasiewicz, T. A.; Geiger, L. E.; Rucci, G.; Neal, R. A. *Drug Metabolism and Disposition* **1983**, *11*(5), 397-403.
(11) Patton, J. S. In *Physiology of the Gastrointestinal Tract*; Johnson, L. R., Ed.; Raven Press: New York, 1981; Vol. 2, pp 1123-1139.
(12) Patterson, D. G., Jr.; Lapeza, C. R., Jr.; Barnhart, E. R.; Groce, D. F.; Burse, V. W. *Chemosphere* **1989**, *19*(1-6), 127-134.
(13) Albro, P. W.; et al. *Anal. Chem.* **1985**, *57*, 2717-2725.
(14) Graham, M.; Hileman, F. D.; Orth, R. G.; Wendling, J. M.; Wilson, J. D. *Chemosphere* **1986**, *15*(9-12), 1595-1600.
(15) Wendling, J.; Hileman, F.; Orth, R.; Umbreit, T.; Hesse, E.; Gallo, M. *Chemosphere* **1989**, *18*(1-6), 925-932.
(16) Wendling, J.; Orth, R. G.; Poiger, H.; Hileman, F. D. *Chemosphere*, in press.
(17) Alexander, L. R.; Patterson, D. G.; Meyers, G. L.; Holler, J. S. *Environ. Sci. Technol.* **1986**, *20*(7), 725-730.
(18) U.S. EPA. 2,3,7,8-Tetrachlorodibenzo-*p*-dioxin in Soil and Sediment by High Resolution Gas Chromatography/Low Resolution Mass Spectrometry. Statement of Work—Dioxin Analysis; Solicitation IFB WA-84-A002, 1983.
(19) Poland, A.; Glover, E.; Kende, A. S. *J. Biol. Chem.* **1976**, *251*(16), 4936-4946.
(20) Tolgyessy, J.; Brown, T.; Kyrs, M. In *Isotope Dilution Analysis*; Pergamon Press: New York, 1972.
(21) In *CRC Handbook of Chemistry and Physics*, 66th ed.; Weast, R. R., Ed.; CRC Press, Inc.: Boca Raton, FL, 1986; p B-234.
(22) Horrocks, D. L. *J. Radioanal. Chem.* **1978**, *43*, 489-521.
(23) Mason, G.; Safe, S. *Toxicology* **1986**, *41*, 153-159.

RECEIVED for review September 14, 1989. Accepted January 3, 1990.

Ion Chromatography/Mass Spectrometry for the Determination of Organic Ammonium and Sulfate Compounds

J. J. Conboy and J. D. Henion*
Drug Testing and Toxicology, Cornell University, 925 Warren Drive, Ithaca, New York 14850
M. W. Martin* and J. A. Zweigenbaum
Analytical Technology Division, Eastman Kodak Company, Rochester, New York 14652-3712

The ion spray liquid chromatography/mass spectrometry (LC/MS) interface is coupled via a postsuppressor split with an ion chromatography (IC) system. The micromembrane suppressor selectively removes over 99.9% of the ion-pair agents required for ion chromatography from the eluent. The resulting solution consists of analyte, organic modifier, and water, which is compatible with ion evaporation mass spectrometry. A flow rate of 0.8 or 1.0 mL/min from the column was split after suppression such that approximately 10-20 μL/min was directed to the ion spray LC/MS interface, which was coupled to an atmospheric pressure ionization (API) mass spectrometer. This system provided a convenient way to effect isocratic and gradient separations of organic ions under chromatographic conditions incompatible with most forms of mass spectrometric ionization. This work describes the separation and positive ion detection of quaternary ammonium drugs and tetraalkylammonium compounds of industrial importance using both single and tandem mass spectrometric detection (e.g., IC/MS and IC/MS/MS). The former easily provided the molecular weights of these compounds while the latter gave some structural information. The limit of detection (LOD) of 40 pg injected on-column for tetrapropylammonium cation is a factor of 10 better than that obtained with the conventional IC conductivity detector. The separation, detection, and identification of some alkyl sulfates and sulfonates are also shown with negative ion detection. Again, IC/MS readily produced the molecular weights of these compounds while IC/MS/MS provided some structural information.

INTRODUCTION

Ion chromatography, an innovative technique for the separation and detection of non-UV-absorbing ionic compounds, was first reported by Small, Stevens, and Bauman in 1975 (*1*). Originally, this technique combined low-capacity pellicular ion-exchange resins with high-capacity eluent stripper (or suppressor) columns allowing the use of conductivity for universal and sensitive detection. Suppressor columns were designed to replace the eluent counterions (and later ion-pairing agents) with weakly conducting species. Because of the need to regenerate the suppressor and to minimize the additional dead volume it provided, the hollow-fiber (*2, 3*) and ion-exchange (*4*) membrane suppressors were developed. The introduction of micromembrane suppressors offered many advantages including gradient elution with conductivity detection and widespread use of mobile-phase ion chromatography (MPIC) (*5*). MPIC, similar to ion-pair reversed-phase high-performance liquid chromatography (HPLC), was developed to provide separation of organic cations or anions on a polystyrene-based resin column with subsequent eluent suppression and conductivity detection.

Suppressors for ion chromatography utilize an ion exchange membrane to replace analyte counterions in the eluent with either protons (anionic separations) or hydroxide ions (cationic separations). For example, when cationic species such as quaternary ammonium ions are separated by employing a strong organic acid (e.g., 5 mM methanesulfonic acid) as an ion-pair agent, a suppressor with an anion exchange membrane is required. The latter is a polymeric material with bonded quaternary ammonium groups. In MPIC with conductivity detection, an aqueous solution of tetrabutylammonium hydroxide (60 mM) serves as regenerant. The suppressor reaction is as follows:

$$H^+ + CH_3SO_3^- + OH^-\text{–}R = CH_3SO_3^-\text{–}R + H_2O$$

where R denotes the resin phase. Since the membrane in this example is selectively permeable toward anions, methylsulfonate in the eluent is exchanged for hydroxide ion from the regenerant. The hydroxide ions combine with protons from the methanesulfonic acid to produce water. Cations (i.e., protons and quaternary ammonium ions) are excluded from

0003-2700/90/0362-0800$02.50/0

the ion-exchange membrane by the positively charged bonded ionic groups. The suppressor serves two functions: it reduces the background conductivity of the eluent and converts the quaternary ammonium salt to a more highly conducting hydroxide. By analogy, separation with alkaline eluents using cation exchange membrane suppressors and acid regenerants are used for the separation of anions (e.g., alkyl sulfates and sulfonates).

The majority of IC separations utilize the nonselective conductivity detector. Its lack of selectivity had led to the pursuit of alternative detection schemes. Electrochemical detection has been successfully applied to the separation of electroactive species such as cyanide, sulfide, iodide, and bromide (*6*), while the pulsed amperometric detector, described by Johnson and co-workers, permits detection of aldehydes, alcohols, and carbohydrates (*7–10*). Element-selective detection such as atomic absorption (*11*), direct-current plasma (*12*), and inductively coupled plasma (ICP) spectroscopy (*13*) have also been used to attain selective and sensitive detection in ion chromatography.

The most selective, sensitive, and yet universal detector for organic ions is the mass spectrometer. The thermospray LC/MS interface was the first demonstration of coupling an ion chromatograph to a mass spectrometer (*14*). A recent report described the analysis of carbohydrate samples with a limit of detection of 1 μg and a linear response to 1000 μg (*15*). In addition, the direct interfacing of IC with continuous-flow fast-atom bombardment (FAB) MS has also been reported (*16*). None of these studies have examined the effects of a suppressor on analyte sensitivity or chemical noise from the eluent nor have they demonstrated practical analytical utility. The requirement for chemical noise reduction in the mass spectrometer is analogous to the importance of background conductivity suppression in IC. The coupling of MPIC to a mass spectrometer would allow the applicability of chemical suppression for the separation and detection of both organic cations and anions to be examined.

An alternative approach for coupling an ion chromatograph to a mass spectrometer could be via formation of gas-phase ions at atmospheric pressure. Since the analyte exiting the suppressor in aqueous solution is ionic, it is possible to "evaporate" ions directly from the condensed phase into the gas phase. This may be readily accomplished by the ion spray LC/MS interface (*17, 18*). In this system, microsized droplets formed from the effluent of the IC suppressor are subjected to field-assisted ion evaporation (*19*) by the application of a high potential field (3 kV) to an electrically conducting capillary carrying the effluent stream. If the flow of liquid through this capillary is maintained at a rate below 100 μL/min, gas-phase ions are readily generated which may then be sampled into the mass analyzer of a mass spectrometer designed for sampling ions formed at atmospheric pressure.

Although the mechanistic details of this field-assisted ion evaporation are not entirely clear, it is known that the process freely occurs provided certain criteria are met. The charge density of analyte ions in the evaporating microdroplet appears to reach a maximum whereupon the ejection of the ion takes place by, for example, Coulombic explosion (*20*). Factors that seem to favor this process include the presence of organic solvents such as methanol or acetonitrile, low ionic strength of buffers or modifiers, the absence of inorganic nonvolatile salts, and the presence of the analyte as an organic cation or anion in solution.

Because these conditions are easily met by IC with chemical suppression, organic ions may be characterized by coupling the ion spray LC/MS interface directly to the suppressor effluent. When the gas-phase ions are sampled through the orifice of an atmospheric pressure ionization (API) tandem quadrupole mass spectrometer, one can obtain both molecular weight and structural information for these analytes.

This work presents results for the IC/MS and IC/MS/MS determination of both organic cations and anions of several industrially important compounds. A comparison of results between on-line ion chromatography with single MS and tandem mass spectrometry highlights the advantages of mass spectrometric detection. The former readily provides molecular weight determination while the latter provides some structural characterization. This work will describe the potential utility of API IC/MS and IC/MS/MS.

EXPERIMENTAL SECTION

Reagents. All water used was 18 MΩ cm quality obtained from a Barnstead NANOpure II Cartridge System (Sybron/Barnstead, Boston, MA). All other reagents had a purity of 99% or better unless otherwise specified. Acetonitrile (Baker Analyzed HPLC reagent), lithium hydroxide monohydrate, and hydrochloric acid (Ultrex ultrapure reagent), were obtained from Baker (J. T. Baker, Phillipsburg, NJ). Eluents were prepared from methanesulfonic acid (Eastman Kodak Co., Rochester, NY) and 0.10 N tetrapropylammonium hydroxide (Dionex, Sunnyvale, CA). A 0.50 N working solution of methanesulfonic acid was used for convenient eluent preparation. Regenerants used for suppression of eluent ions in cation separations were prepared at 60 mM concentration from either lithium hydroxide monohydrate or a 55 wt % solution of tetrabutylammonium hydroxide (Southwestern Analytical Chemicals, Austin, TX). The regenerant used for suppression of eluents in separations of anions was prepared at 12.5 mM concentration from double-distilled, in Vycor, sulfuric acid (GFS Chemicals, Columbus, OH). The bromide salts of tetrapropylammonium, tetrabutylammonium, tetrapentylammonium, and tetrahexylammonium and the sodium salts of decyl sulfate, and *p*-toluenesulfonic acid were obtained from Eastman Kodak. Bardac LF is a trade name for a 50% aqueous solution of dioctyldimethylammonium chloride (Lonza, Inc., Fairlawn, NJ). Sodium salts of octyl sulfate, dodecyl sulfate (98%), tetradecyl sulfate (95%), and octadecyl sulfate (93%) were obtained from Aldrich (Aldrich Chemical Co., Milwaukee, WI). Solutions for analysis were prepared by volumetric dilution of 1 mg/mL stock standards in the solvent composition of the appropriate eluent.

Chromatography. A Wescan Model 266 ion analyzer (Alltech Associates, Deerfield, IL) was used at 1 μS full-scale with a Waters 590 pump (Millipore, Milford, MA), which maintained an eluent flow rate of 0.80 mL/min. Injection volumes of 100 μL were made via a Rheodyne 7125 injector valve (Rheodyne, Cotati, CA). A Polymer Laboratories PLRP-S 5 μm, 100-Å pore size, polystyrene column (Polymer Laboratories, Shropshire, UK) was used with either a CMMS-1 cation suppressor or an AMMS-MPIC anion suppressor (Dionex), for the separation of cations or anions, respectively. Gradient separations were performed on a Dionex MPIC-NS1 10 μm polystyrene/divinylbenzene column utilizing a Waters 600 MS pump at a flow of 1.0 mL/min. Regenerant flow was maintained with helium head pressure sufficient to provide a flow of 1–2 mL/min. Lithium measurements were made with a Perkin-Elmer Model 2380 flame atomic absorption spectrometer (Perkin-Elmer, Norwalk, CT).

Mass Spectrometry. The split effluent from the suppressor was connected to a Sciex, Inc., TAGA 6000E triple-quadrupole mass spectrometer (Sciex, Thornhill, Ontario, Canada) equipped with an ion spray liquid chromatography/mass spectrometer interface (*17*) and an atmospheric pressure ion source operated in the positive- or negative-ion mode (*18*). In this system, ions are sampled into the vacuum for mass analysis through a 100-μm orifice in the end of a skimmer cone extended toward atmosphere. The ion sampling cone is bathed in a dry nitrogen "curtain gas" (*18*). The flow (0.5 L/min) of dry nitrogen facilitates declustering sovent-ion adducts and desolvating the droplets. High vacuum in the analyzer region of the mass spectrometer is achieved by cryogenically cooled surfaces maintained at 16–20 K. During routine operation the indicated analyzer vacuum was (7–9) × 10^{-6} Torr and during collision-induced dissociation (CID) the analyzer vacuum was 1.5 × 10^{-5} Torr. Argon was used for CID in the collision chamber (second quadrupole) with 2 × 10^{14} atoms/cm^2

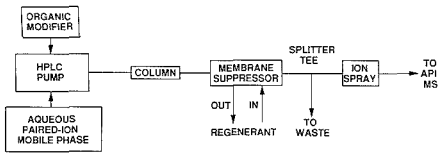

Figure 1. Block diagram of combined ion chromatography and mass spectrometry system.

target gas thickness. The parent ions transmitted to the second quadrupole for CID were the molecular ions of the quaternary ammonium compounds or the negative molecular ions of the sulfate compounds following their field-induced desorption from the condensed phase. The channel electron multiplier with floating power supply was used in the pulse counting mode. Ion abundances in counts per second (counts/s) were collected at 1.0 amu steps with measurement time limits (MTL) of 5–30 (typically 10) ms per step for full scan MS and MS/MS, and MTL of 0.1–1.0 (typically 0.5) s per step for selected ion monitored (SIM) scans.

A block diagram of the combined IC/MS system is shown in Figure 1. The gradient HPLC pumping system forms the appropriate organic solvent–aqueous paired-ion eluent to effect separation of the target analytes on the polymer-based columns. The column effluent was passed between two ion-exchange membranes in the suppressor with regenerant flowing in a counter direction outside the membranes. The suppressor dead volume was < 50 μL (5). The ion-pair agent in the eluent was efficiently exchanged in the suppressor with either protons or hydroxide ions to produce water. The suppressor outlet was connected to a splitter-tee, which consisted of a fine metering valve (Part No. MCVT-1-50, SGE, Austin, TX). By appropriate ajustments of this metering valve, a fraction (approximately 1–2%) of the suppressor effluent could be directed to the ion spray LC/MS interface, while the excess effluent was directed to waste. The split ratio was determined by comparing the flow rate of the waste effluent from the energized ion spray apparatus splitter to the calibrated flow rate of the HPLC pump. The ion spray LC/MS interface was maintained at a positive potential of 3 kV for formation of gas-phase cations and a negative potential of −3 kV to form gas-phase anions. All IC/MS results described in this work utilized this postsuppressor split so that an injection of 100 ng of material, for example, resulted in only about 1–2 ng of material going to the mass spectrometer. The greatest sensitivity for a given amount injected was obtained by optimizing the flow of effluent through the ion spray apparatus. The optimum split ratio was determined experimentally by repetitive injections.

Postsuppression Background Ion Measurements. The eluent used in the analysis of tetraalkylammonium ions, 5 mM methanesulfonic acid in 70% acetonitrile, was pumped directly through the CMMS-1 suppressor at 0.8 mL/min with the regenerant flow maintained at 1–2 mL/min. After suppression, 25 mL of effluent was collected for subsequent analysis. This volume was either concentrated 8-fold through evaporation, after adding two drops of hydrochloric acid, or analyzed neat to determine regenerant cation content. Tetrabutylammonium ion was determined by ion chromatography while lithium ion was measured by flame atomic absorption spectrometry (flame AA). Another 25-mL portion of effluent was collected, two drops of 1.0 N lithium hydroxide added, and the resulting solution concentrated 8-fold. From this solution, the remnant level of methanesulfonic acid was determined by ion chromatography.

RESULTS AND DISCUSSION

The purpose of this study was to explore the feasibility of coupling an ion chromatograph to the ion spray LC/MS interface (*17*) to obtain on-line mass spectra from organic ions dissolved in the chromatographic effluent. The first goal was to determine whether organic ions in the suppressor effluent such as quaternary ammonium compounds, alkyl sulfates, and alkylsulfonates could be desorbed as ions into the gas phase and sampled into the vacuum system of the mass spectrometer. Also, because many of the common eluent constituents for ion chromatography are not compatible with mass spectrometric ionization processes, it was important to learn whether the suppressor could adequately exchange the eluent ions for regenerant ions to form water. These preliminary experiments demonstrate that the ion spray LC/MS interface in combination with the suppressor provides a convenient and sensitive means of accomplishing IC/MS.

Following exchange of organic cations or anions in the IC eluent for protons or hydroxide, respectively, water is produced. Because of the higher flow required by 4-mm-i.d. IC columns, only a portion of this effluent is passed to the ion spray LC/MS interface. The ion spray LC/MS interface provides a combination of pneumatic nebulization and electrospray ionization (*21*) to produce a liquid spray of very small, highly charged droplets in close proximity to the ion sampling orifice of an atmospheric pressure ionization (API) mass spectrometer. The dissolved organic ions undergo a form of field-induced desorption/ionization from the condensed phase into the gas phase. Following this, the ions are sampled into the API ion entrance orifice and mass analyzed. Ionization occurs at ambient temperature and atmospheric pressure and is a very mild process that results in essentially no fragmentation of the molecular ion species.

Background Ion Measurements. Chemical noise originating from traces of IC eluent was monitored between 100 and 800 daltons with and without chemical suppression. A 1–2 order of magnitude reduction in ion current originating from ionized eluent constituents was observed with the suppressor in-line. However, a distinct molecular ion at 242 was evident at 10^5 counts/s (vs a background of ca. 10^3 counts/s) with tetrabutylammonium hydroxide as regenerant. The m/z 242 ion was still present but in a diminished capacity (10^4 counts/s) with lithium hydroxide regenerant.

The CMMS-1 suppressors are tested by the manufacturer with tetrabutylammonium hydroxide and the particular suppressor used in this work was initially employed with tetrabutylammonium hydroxide. The tetrabutylammonium background problem could be alleviated if the mass spectrometer scan range excluded this background ion. However, to detect the tetrapropyl- and tetrabutylammonium ions in this work at m/z 186 and 242, respectively, scans through the lower mass range was required.

The invasion of 5 mM methanesulfonic acid in 70% acetonitrile eluent by regenerant co-ions was measured after suppression by the cation micromembrane suppressor. Tetrabutylammonium ion was measured at 3.7 μg/mL (15 μM) by conventional ion chromatography while lithium at 2.1 μg/mL (300 μM) was determined by flame AA. Interestingly, the cation suppressor that was subjected to extensive use with lithium hydroxide regenerant still showed tetrabutylammonium ion at 0.12 μg/mL (0.50 μM), corroborating the MS data.

The cation micromembrane suppressor contains fixed cation sites. These sites will repel the cationic co-ions from either the regenerant or eluent side of the membrane (Donnan exclusion). Of course, a small amount of co-ion can penetrate into the membrane. The amount of invading co-ion is dependent on size, number of charges, and concentration of the electrolyte. Dasgupta (*22*) has reported ion penetration rates for several anions and cations through various cation and anion exchange membrane materials. He found that penetration of cations through a PTFE-based anion exchange tubular membrane in aqueous media followed the order $Li^+ \gg NMe_4^+ > NEt_4^+ > NPr_4^+$. This trend is confirmed by the difference in breakthrough concentration between lithium and tetrabutylammonium regenerants found in this study.

After suppression with lithium hydroxide, the concentration of remnant eluent (i.e., methanesulfonic acid) was found to be <0.04 μM by ion chromatography. A remnant concen-

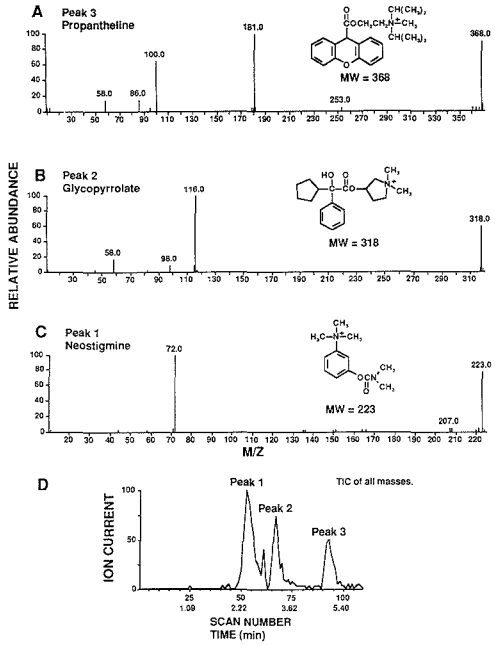

Figure 2. Full-scan IC/MS/MS analysis of 100 ng each of a synthetic mixture of quaternary ammonium drugs under positive ion detection. The lower panel (D) shows the total ion current profile for sequential scanning of the product ion spectra obtained from the corresponding chromatographic peaks 1–3, and the upper three panels (A–C) show the individual MS/MS product ion spectra resulting from each molecular ion. Collision energy used was 50 eV laboratory frame; data were acquired from 10 amu to the m/z of the parent ion at 1.0 amu steps for 10 ms per step.

tration of 0.49 μM methanesulfonic acid was found when tetrabutylammonium hydroxide was used as regenerant. This corresponds to a conversion efficiency of >99.9% for both regenerant cations with the CMMS-1. In this context, conversion efficiency refers to the percent of methanesulfonic acid that is converted to water by the suppressor exchange reaction.

IC/MS of Organic Cations. Figure 2 shows the on-line IC/MS/MS analysis of a synthetic mixture of quaternary ammonium drugs (100 ng each). This separation was accomplished on a Polymer Laboratories PLRP-S 5 μm column using an eluent of 5 mM methanesulfonic acid in 40% acetonitrile at a flow of 0.80 mL/min. The suppressor was a Dionex CMMS-1 with 60 mM lithium hydroxide as regenerant. The total effluent was split such that a flow of approximately 10–20 μL/min passed through the ion spray LC/MS interface. This split ratio was used throughout this work. Full-scan IC/MS of these compounds performed in a separate experiment showed little fragmentation, so the molecular ion was ideal for subsequent CID. The lower panel (D) in Figure 2 shows the total ion-current (TIC) chromatogram for the IC/MS/MS determination of the three drugs. The full-scan CID product ion mass spectrum for each component in this mixture is shown in the corresponding upper panels (A–C). Note that these data result from 1 to 2 ng of each drug going into the mass spectrometer. These data were obtained with a collision energy of 50 eV laboratory frame and a collision gas thickness of 2×10^{14} atoms/cm^2. The parent ion for each drug was sequentially focused (according to retention time) into the collision cell while the third quadrupole mass analyzer was scanned from 10 amu to the parent m/z at 1.0 amu steps with

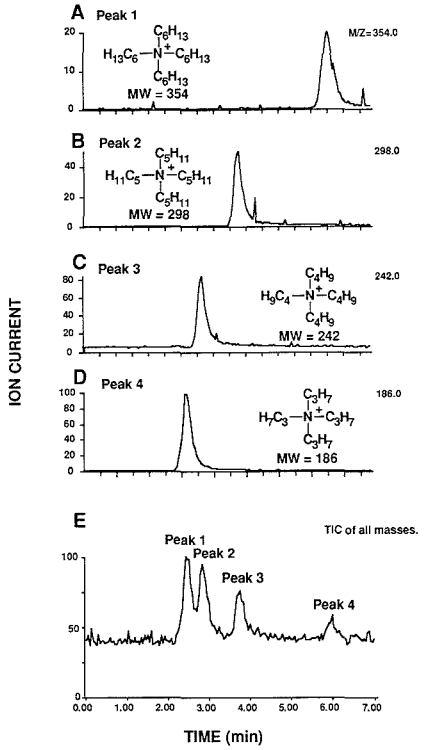

Figure 3. Full-scan IC/MS analysis of a synthetic mixture of industrially important quaternary ammonium compounds under positive ion MS detection. The lower panel (E) shows the total ion current profile for the four components following injection of a solution containing 100-ng levels of each compound. The postsuppressor split delivered 1–2 ng per component to the mass spectrometer. The upper four traces (A–D) show the extracted ion-current profiles for each of the four quaternary ammonium parent ions. Data were acquired from 180 to 400 amu at 1.0 amu steps for 10 ms per step.

MTL of 10 ms per step. The product ion spectra are relatively simple, but contain structurally significant fragment ions, which could facilitate the characterization of these compounds. Selected reaction monitoring (SRM) experiments should provide improved detection limits allowing trace analysis capabilities for these compounds.

Figure 3E shows the full-scan TIC and Figure 3A–D the extracted ion-current profiles (EICP) for the molecular ion species of four industrially important quaternary ammonium compounds. This synthetic mixture contained four symmetrical tetraalkylammonium compounds where the alkyl groups varied from n-propyl through n-hexyl. The data for 100 ng of each compound injected on-column reveal the chromatographic integrity and signal response provided by the IC/MS system. The signal-to-noise level of the TIC is reduced due to chemical noise in the base line (note once again that only 1–2 ng/component is going to the mass spectrometer due to the postsuppressor split). Inspection of the base-line mass spectra indicates that low levels of tetrabutylammonium ions from the IC suppressor system are present in the effluent.

The on-line separation of four tetraalkylammonium ions shown in Figure 3 was carried out using the PLRP-S 5-μm column with 5 mM methanesulfonic acid in 70% acetonitrile at 0.80 mL/min. The suppressor, regenerant, and flow conditions were as reported for the quaternary ammonium drugs.

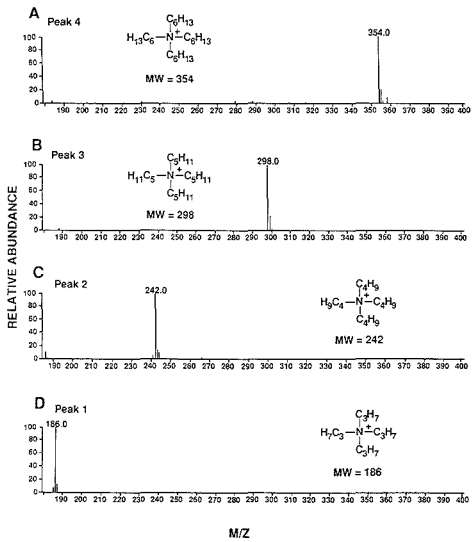

Figure 4. Full-scan IC/MS background subtracted mass spectra from the total ion chromatogram in Figure 3E. Panels D–A show the full-scan IC/MS spectra obtained from the corresponding chromatographic peaks 1–4, respectively.

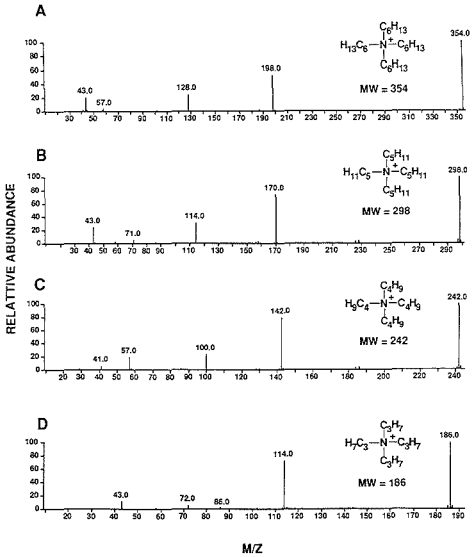

Figure 5. Full-scan IC/MS/MS analysis of the same mixture of 100 ng each of the quaternary ammonium compounds shown in Figures 3 and 4. These CID product ion spectra were obtained with a collision energy of 50 eV laboratory frame while sequentially focusing each parent ion into the collision cell. Data were acquired from 10 amu to the m/z of the parent ion at 1.0 amu steps for 10 ms per step.

The mass spectral data shown in Figure 4 reveal the simplicity of ion spray mass spectra for compounds of this type which are desorbed from aqueous solution. This approach virtually guarantees molecular weight determination but provides no structural information. However, full-scan IC/MS/MS analysis of this same mixture was carried out using injected levels of 100 ng on-column of each component to give the CID mass spectra shown in Figure 5. Again, the parent ion was focused by the first quadrupole into the collision cell whereupon a collision energy of 50-eV laboratory frame (collision gas thickness was 2×10^{14} atoms/cm^2) yielded product ions which were then mass analyzed by the third quadrupole.

Although the members of this series of tetraalkylammonium compounds are very similar, their CID mass spectra differ significantly, allowing their structural characterization. For example, the highest mass, most abundant fragment observed for each compound is increased by 28 daltons as the series goes from tetrapropyl- through tetrahexylammonium ion. Although the molecular weight is incremented 56 daltons due to the four additional methylenes for each higher analogue, the predominant fragmentation process apparently favors losing one intact alkyl group following β-cleavage of the alkyl chain of the ion. The resulting methylenedialkylammonium ion could explain the most abundant fragment observed in each CID spectrum shown in Figure 5. In addition, another series of fragments are seen at m/z 128, 114, 100, and 86 in parts A–D of Figure 5 respectively, which appear consistent with another loss of the corresponding alkyl group less its methylene. Further experiments would be required to document these speculations, but the fragments are structurally informative for their characterization. The appearance of alkyl ions including m/z 43, 57, and 71 (presumably C_3H_7, C_4H_9, and C_5H_{11}) in Figure 5 is also consistent with the structures of the tetraalkylamines.

The isocratic separation of tetrapropyl-, tetrabutyl-, tetrapentyl-, and tetrahexylammonium ions with 5 mM methanesulfonic acid in 70% acetonitrile eluent with lithium hydroxide as regenerant and conductivity detection was performed to determine limits of detection (LOD). Based on the method of Knoll (*23*), the LOD for IC calculated for tetrapentylammonium ion is 8 ng injected on-column. The relative conductivity response of tetrapropylammonium ion indicates a LOD of 2 ng. Better detection limits would be expected with tetrabutylammonium hydroxide as regenerant because the measured background conductivity is approximately 1 order of magnitude lower (2.5 μS vs 23–25 μS).

To explore the ultimate limit of detection for these tetraalkylammonium compounds using ion spray API/MS, successive dilutions were made of tetrapropylammonium bromide followed by selected ion monitoring (SIM) IC/MS using the same chromatographic conditions as presented above. Figure 6 shows the SIM chromatographic signal for m/z 186 obtained for the on-column injection of 40 pg of the tetrapropylammonium compound following a blank injection. Although this detection limit could perhaps be improved further, even with the 1–2% postcolumn split it is at least a factor of 10 better than routinely provided by conductometric detection after suppression.

An application of industrial interest utilized the IC/MS/MS to study the surfactant Bardac LF. This material, a trade name for dioctyldimethylammonium chloride, is present in a commonly employed polymerization initiator. The concentration of surfactant in the initiator is a critical factor in determining the performance of synthesized polymers. The eluent was 5 mM methanesulfonic acid in 70% acetonitrile pumped at 0.8 mL/min. The column was a PLRP-S 5 μm with the CMMS-1 suppressor and 60 mM lithium hydroxide as regenerant. Following ion chromatography, this mixture gave two peaks with a major peak at 3.27 min that has approximately 6-fold the area of the minor peak at 4.00 min. The major chromatographic peak showed an ion at m/z 270 which is consistent with dioctyldimethylammonium ion. The IC/MS technique demonstrated that the minor peak is not an isomer

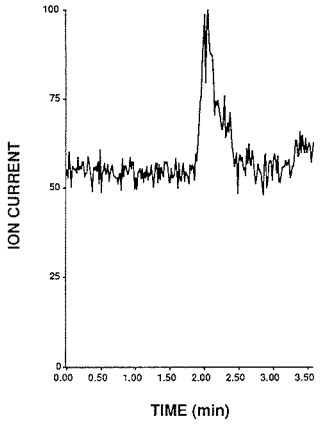

Figure 6. SIM IC/MS analysis of an injected solution containing 40 pg of tetrapropylammonium bromide following a blank injection of eluent. The parent ion at m/z 186 was monitored with a MTL of 100 ms following a postsuppressor split which directed 1–2% of the IC effluent to the mass spectrometer. The tip of the ion spray apparatus was directed more toward the orifice and the split ratio was adjusted to increase the flow toward the mass spectrometer to optimize sensitivity for this compound in the SIM mode. Since the residence time in the transfer line between splitter and ion spray was reduced due to a higher flow rate, the retention time of this compound is less than that in Figures 3 and 4.

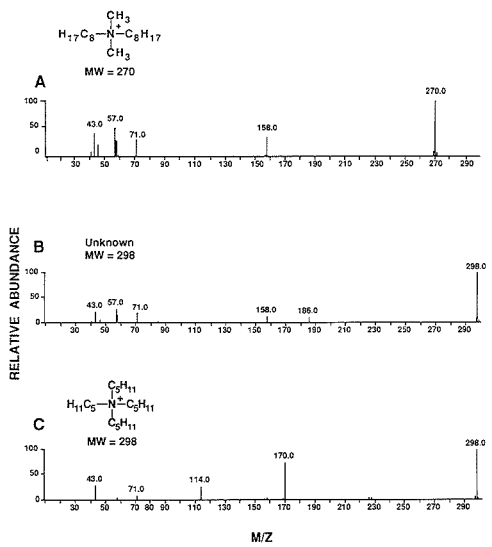

Figure 7. Full-scan product ion spectra obtained from the IC/MS/MS analysis of a 100-μL injection of a 10 μL/mL Bardac LF solution which contained two IC chromatographic peaks. These spectra were obtained by using a collision energy of 50 eV laboratory frame while focusing the corresponding parent ions into the collision cell with positive ion detection. The panels A–C in this figure represent the product ion spectra from (A) m/z 270 parent ion of dioctyldimethylammonium ion, (B) unknown molecular weight 298, and (C) tetrapentylammonium ion from the corresponding bromide. Data were acquired from 10 amu to the m/z of the parent ion at 1.0 amu steps for 10 ms per step.

but rather a component with an apparent molecular weight of 298. The IC/MS/MS of these peaks are shown in Figure 7A,B. For comparison, the IC/MS/MS of tetrapentylammonium ion (M^+ = 298) is shown in Figure 8C.

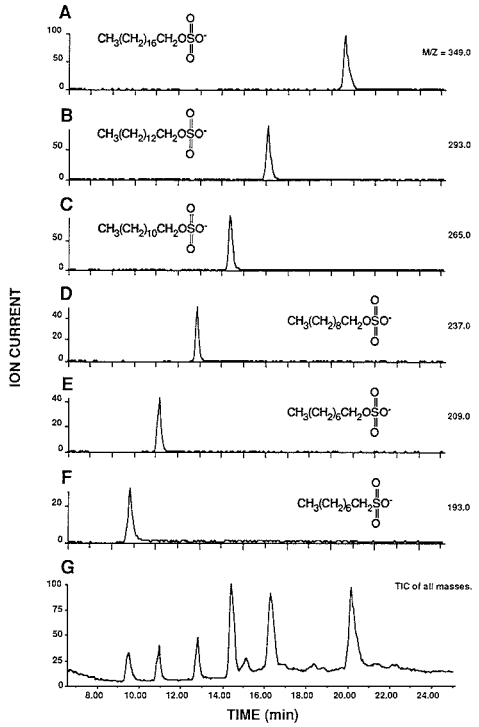

Figure 8. SIM IC/MS analysis of a synthetic mixture of alkyl sulfate and sulfonate compounds where the alkyl group ranged from C-8 to C-18 (G). Injected levels of 1 μg were made under negative-ion conditions while the postsuppressor split directed 1–2% of this mixture to the mass spectrometer. The selected ions represented the singly charged parent anions for each compound (A–F). Data were acquired at the m/z of each molecular ion with a MTL of 500 ms.

The CID mass spectrum in Figure 7A is consistent with the structure of the dioctyldimethylammonium cation. The low mass ion series appearing at m/z 43, 57, and 71 is compatible with the alkyl groups in this compound. The loss of 112 atomic mass units from this molecular ion at m/z 270 to give the m/z 158 product ion is congruous with the loss of C_8H_{16} or one of the octyl groups less a proton. This is analogous to the well-known Hofmann elimination of quaternary ammonium salts that can occur in alkaline solution. The molecular ion reflects two additional methylene groups and the same loss of 112 to give m/z 186. Another product ion at m/z 158 appears to support this point by the loss of 140 atomic mass units. The same low mass ion series is also observed in Figure 7B. These experimental results suggest not an isomeric quaternary ammonium compound but rather a related higher alkyl analogue. Although it does not appear obvious what the unknown compound is in Figure 7B, logical possibilities can be suggested which would require additional IC/MS/MS studies on selected standards allowing the identification of this unknown contaminant. This example illustrates the potential of combining IC with MS and MS/MS for separation and characterization of unknown components from a difficult matrix.

IC/MS on Organic Anions. A final example of the utility of IC/MS using the ion spray LC/MS interface coupled to the suppressor is shown with the separation and detection of a mixture of alkyl sulfates and sulfonates. Because these

compounds are anionic, the polarity of the ion spray electrode and all other potentials of the mass spectrometer and detection system were reversed from what they were for the quaternary amines. Thus, negative ions were desorbed from the microdroplets formed in the ion spray process, sampled into the vacuum system, and mass analyzed.

A synthetic mixture of alkyl sulfates and sulfonates ranging from C-8 to C-18 was separated and passed via the ion spray interface to the mass spectrometer. The compounds in the mixture, at a level of 1 μg each, were separated by gradient elution on a Dionex MPIC-NS1 column at a flow rate of 1.0 mL/min. The A solvent was 5% acetonitrile and 2 mM tetrapropylammonium hydroxide while the B solvent was 75% acetonitrile and 2 mM tetrapropylammonium hydroxide. A linear gradient profile from 10 to 99% B in 15 min was generated to separate the components in the mixture. Sulfuric acid at 12.5 mM concentration was used as regenerant with a Dionex AMMS-MPIC suppressor. The effluent from the suppressor was transferred to the mass spectrometer via the ion spray LC/MS interface maintained at −3 kV.

Figure 8A–F shows the SIM ion current profiles for the negatively charged parent ions for each of the alkyl sulfate or sulfonate compounds as they eluted from the system. SIM was performed in this case because the mass spectra of these compounds are very simple, showing only the negatively charged parent ion with no fragmentation, as is typical of ion spray (*17*). The sensitivity of these compounds was reduced by IC/MS with suppression compared with that found by reversed-phase HPLC with acetonitrile/water and ammonium acetate buffers (*24*). This is probably due to the nature of the quaternary ammonium ion used as a pairing agent, which appears to suppress the desorption of the anion from the condensed phase into the gas phase. This creates some chemical background even at low concentrations. When the suppressor was removed, the chemical noise increased by 2 orders of magnitude within the mass range of the analytes of interest (m/z 150–400).

Although single MS analysis of these compounds readily determines their molecular weights, additional structural information is needed for their characterization. Tandem mass spectrometry on-line with the chromatographic separation is an efficient means of getting this structural information. Figure 9A–C shows the CID mass spectra of three of the sulfates from Figure 8 plus *p*-toluenesulfonate (Figure 9D) from a separate isocratic run. The molecular weights are 209, 237, 265, and 171. With a collision energy of 50 eV laboratory frame, there is only limited fragmentation resulting from the collision-induced processes. However, m/z 80 readily appears which is consistent with the presence of the negatively charged SO_3^- moiety while the m/z 97 ion is present in the CID mass spectra of Figure 9A–C supporting the presence of negatively charged HSO_4^-. Because very little additional evidence is available in these CID mass spectra, it is not obvious how to determine the details of the alkyl moiety. However, the mass difference between the parent ion and the abundant sulfur-containing ion is a helpful indication of the size of the alkyl group. For example, the m/z 209 ion in Figure 9C appears to lose 112 daltons to produce the abundant m/z 97 ion. This is consistent with the mass of the C-8 alkyl fragment, C_8H_{17}, in this octyl sulfate. It is possible that branched hydrocarbons may give additional structural information with well-known fragmentation occurring at branched sites.

A rather interesting consequence of the IC/MS TIC of the synthetic mixture of alkyl sulfates (Figure 8C) was the appearance of an extra peak at m/z 193 eluting before octyl sulfate. In routine work at our laboratory the magnitude of this peak was observed to vary from lot to lot of tetrapropylammonium hydroxide. When an IC/MS/MS run was

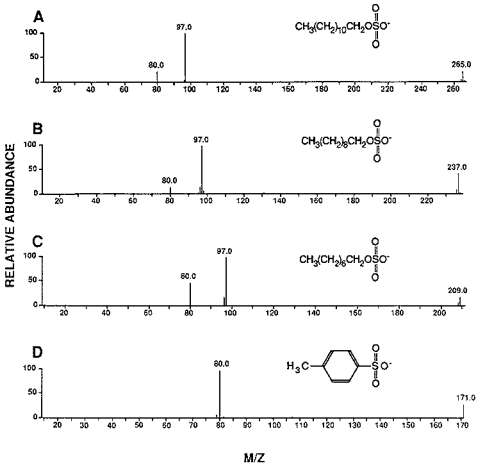

Figure 9. Full-scan IC/MS/MS product ion spectra of three alkyl sulfates from Figure 9 plus *p*-toluenesulfonate from a separate analysis. The collision energy used in this experiment was 50 eV laboratory frame and the corresponding anionic parent ions were sequentially focused into the collision cell. The compounds characterized were (A) dodecyl sulfate, (B) decyl sulfate , (C) octyl sulfate, and (D) *p*-toluenesulfonate. Data were acquired from 10 amu to the m/z of each parent ion at 1.0 amu steps for 50 ms per step.

made, a negatively charged fragment at m/z 80 indicated the impurity was a sulfonate. Since octanesulfonic acid (M^- at m/z 193) and hexanesulfonic acid (M^- at m/z 165) are also packaged by the vendor, it is probable that there is contamination. A retention time and mass spectra match between the impurity and octanesulfonate was confirmed on a separate injection.

SUMMARY AND CONCLUSIONS

Chromatography of ionic or ionizable compounds requires ionic or buffered eluents to achieve satisfactory separations. When unknown components appear, it is desirable to maintain chromatographic integrity while providing on-line LC/MS. Buffers and ion-pair agents, although useful in the separation process, are detrimental to the desorption process into the mass spectrometer by increasing chemical noise, reducing sensitivity, and creating an additional maintenance burden. Chemical suppression of ionic eluent components supplies an ideal solution to this problem. The ionic constituents of the eluent are removed, leaving analyte ions. The technique would not be suitable for ions having the same sign as the ion-pair agent species or neutral species which could ion-exchange or partition, respectively, into the membrane.

This work demonstrates that chemically suppressed IC (where ion-pair agents are removed from eluent by a suppressor) is well-suited for coupling to an ion spray LC/APIMS interface for IC/MS. Although the chromatographic flow rate is too high for total effluent introduction into the interface, a postsuppressor split easily provided a stable, reduced flow. The advantages of this approach are the avoidance of elevated temperatures and high back pressures obtained with the thermospray LC/MS interface and ease of coupling IC to MS. Even with the unfavorable postsuppressor split, at least 10-fold improvement in sensitivity over conventional IC detection was obtained. Refinements in the system should improve the sensitivity further. In addition, the valuable molecular weight information of IC/MS coupled with the option of IC/MS/MS for structural information gives this technique considerable

analytical utility. Its application to polar, ionic, and zwitterionic compounds suggests its potential value to pharmaceutical, biochemical, and environmental problems.

ACKNOWLEDGMENT

We thank Dr. Paul Milazzo and Mr. Edward McClean of Eastman Kodak Company for the flame AA measurements of lithium.

LITERATURE CITED

(1) Small, H.; Stevens, T. S.; Bauman, W. C. *Anal. Chem.* **1975**, *47*, 1801-1809.
(2) Stevens, T. S.; Davis, J. C.; Small, H. *Anal. Chem.* **1981**, *53*, 1488-1492.
(3) Bouyoucos, S. A. *J. Chromatogr.* **1982**, *242*, 170-176.
(4) Hanaoka, Y.; Marayama, T.; Muramoto, S.; Matsuura, T.; Nanba, A. *J. Chromatogr.* **1982**, *239*, 537-548.
(5) Smith, R. E. *Ion Chromatography Applications*; CRC Press, Inc.: Boca Ratan, FL, 1988; pp 12-13.
(6) Rocklin, R. D.; Johnson, E. L. *Anal. Chem.* **1983**, *55*, 4-7.
(7) Hughes, S.; Johnson, D. C. *Anal. Chim. Acta* **1981**, *132*, 11-22.
(8) Hughes, S.; Johnson, D. C. *J. Agric. Food Chem.* **1982**, *30*, 712-714.
(9) Hughes, S.; Meschi, P. L.; Johnson, D. C. *Anal. Chim. Acta* **1981**, *132*, 1-10.
(10) Welch, L. E.; LaCourse, W. Z.; Mead, D. A., Jr.; Johnson, D. C. *Anal. Chem.* **1989**, *61*, 555-559.
(11) Ricci, G. R.; Shepard, L. S.; Colovos, G.; Hester, N. E. *Anal. Chem.* **1981**, *53*, 610-613.
(12) Urasa, I. T.; Fernus, F. *Anal. Chem.* **1987**, *59*, 1563-1568.
(13) LaFreniere, K. E.; Fassel, V. A.; Eckels, D. E. *Anal. Chem.* **1987**, *59*, 879-887.
(14) Pacholec, F.; Eaton, D. R.; Rossi, D. T. *Anal. Chem.* **1986**, *58*, 2581-2583.
(15) Simpson, R. C.; Fenselau, C. C.; Lee, Y. C.; Townsend, R. R; Cotter, R. J. Presented at the 37th ASMS Conference on Mass Spectrometry and Allied Topics, Miami Beach, FL, May 21-26, 1989.
(16) Al-Omair, A. S.; Todd, J. F. J. Presented at the 36th ASMS Conference on Mass Spectrometry and Allied Topics, San Francisco, CA, June 1988.
(17) Bruins, A. P.; Covey, T. P.; Henion, J. D. *Anal. Chem.* **1987**, *59*, 2642-2646.
(18) Covey, T. R.; Lee, E. D.; Bruins, A. P.; Henion, J. D. *Anal. Chem.* **1986**, *58*, 1451A-1461A.
(19) Iribarne, J. V.; Dziedzic, P. J.; Thomson, B. A. *Int. J. Mass Spectrom. Ion Phys.* **1983**, *50*, 331-347.
(20) Schmelzeisen-Redeken, G.; Rollgen, F. W.; Writz, H.; Vogtle, F. *Org. Mass Spectrom.* **1985**, *20*, 752-756.
(21) Whitehouse, C. M.; Dreyer, R. N.; Yamashita, M.; Fenn, J. B. *Anal. Chem.* **1985**, *57*, 675-679.
(22) Dasgupta, P. K.; Bligh, R. Q.; Lee, J.; D'Agostino, V. *Anal. Chem.* **1985**, *57*, 253-257.
(23) Knoll, J. E. *J. Chromatogr. Sci.* **1985**, *23*, 422-425.
(24) Weidolf, L. O. G.; Lee, E. D.; Henion, J. D. *Biomed. Environ. Mass Spectrom.* **1988**, *15*, 283-289.

RECEIVED for review September 12, 1989. Accepted January 16, 1990. We gratefully acknowledge Sciex, Inc., for partial financial support.

Extended Life for Blood Serum Analysis Columns Using Dual Zone Chromatographic Materials

Dwight E. Williams*

Dow Corning Corporation, Midland, Michigan 48640

Pokar M. Kabra

Department of Laboratory Medicine, University of California, San Francisco, California 94143

Column lifetimes of novel dual zone material (DZM) adsorbents were evaluated by direct serum injection analysis for drugs by high-performance liquid chromatography. Porous silica was converted to DZMs in which the outer zone was enriched in an immobilized lipophobic moiety, the perfluorobutylethylenesilyl group, and the internal zone was enriched in a lipophilic octadecylsilyl group. Performance during repetitive serum analyses for phenobarbital and carbamezepine by reverse phase HPLC was compared to that of control adsorbents of the same composition but without the dual zone distribution. The DZM columns had lifetimes up to 4 times longer than the controls. Furthermore, under these conditions, even the control columns had considerably longer lifetimes than conventional but more retentive reverse phase columns. The DZM column lifetimes also appeared to be comparable to or better than those of the recently introduced Pinkerton packings and have much better adsorbent design flexibility and pH operating latitute.

INTRODUCTION

It is recognized that liquid chromatographic (LC) columns are fouled by exposures to large amounts of proteinaceous samples. Such exposures can be encountered during process-scale LC separations as well as during high-performance LC (HPLC) analysis for small molecules and proteins in biological fluids or fermentation broths. The manifestation of this fouling depends upon whether the proteins are themselves being determined or whether proteins are simply part of the sample matrix.

In the first case, the initial stage of fouling is often manifested by a transient gain in efficiency (resolution) and protein recovery (*1*). This initial stage is thought to represent the elimination of trace amounts of overly avid adsorption sites by covering them with small amounts of tenaciously adsorbed protein. However, efficiency and even retentivity are eventually severly degraded by much greater protein exposure in both cases (*2*, *3*).

Most types of columns and adsorbents, regardless of the separation mode or of the pore diameter, must be periodically renewed after large protein exposures. The cause of performance degradation in wide-pore adsorbents is not understood, but it appears to involve poisoning of a large fraction of the adsorption sites by permanently retained sample components. When exposure of the adsorbent is limited to filtered protein solutions (*3*), such poisoning may reflect the gradual accumulation of a film of denatured protein. Renewal is achieved either by a cleaning procedure or by column replacement. Column renewal procedures are often difficult or provide incomplete restoration of performance.

0003-2700/90/0362-0807$02.50/0

The injection of clarified plasma or serum samples into reverse phase HPLC columns for drug analysis is especially problematic. Rapid efficiency loss occurs because the high organic content of the mobile phase that is usually required during reverse phase chromatography also causes the highly concentrated serum protein to coagulate and plug the column. Furthermore, even when such coagulation can be avoided by lowering the organic content of the mobile phase, the serum protein rapidly builds up as an adsorbed layer on the reverse phase adsorbent.

The particular vulnerability of wide-pore adsorbents to performance loss induced by high exposure to proteins is avoided since typical adsorbents for serum analysis have pore sizes that exclude protein from the interior, where the vast majority of the reverse phase surfaces reside. Unfortunately, a marked efficiency loss still occurs, probably due to retarded diffusion of small solutes into occluded pore mouths (*2*). To prevent premature failure of columns, serum protein is usually removed prior to HPLC analysis (*4*), a step that is both costly and time-consuming.

It is possible to reduce the strength of adsorption of the protein to the particle exterior and, hence, to reduce the extent of pore-mouth plugging. This may be done by choosing an adsorbent that bears a weakly retentive immobilized group combined with a complementary mobile phase that mutes the adsorptivity of that particular surface. However, surfaces weakly adsorptive to protein are also likely to be weakly adsorptive to small solutes. Accordingly, surface-mediated separation would not occur to any great extent.

This dilemma can be resolved by placing the nonadsorptive groups on the exterior of the porous adsorbent and the adsorptive groups on the internal surfaces. Recently, novel column packings have been developed that permit direct serum injection in this way. However, one such approach suffers from intrinsically poor column efficiency since the external treatment appears to partially block the pores (*5*). Another approach, that of externally selective enzyme cleavage (*6*), suffers from a limited scope of immobilized groups and a strong sensitivity to the pH of the mobile phase. A recent extension of this approach (*7*) has ameliorated these limitations.

The limitations can be avoided in a third approach, by the use of dual zone materials (DZMs), in which one type of organosilyl group is attached to the external zone and another to the internal zone. Such materials can be made by silylating porous silica under conditions where the reaction is so fast that its rate is controlled by the rate of diffusion into the pores (*8, 9*). This first ultrafast reagent is used in a substoichiometric amount to attach a first residue primarily in the external zone.

This step may be followed by reaction with a second silylating agent, which finds few unreacted silanols at the exterior and hence reacts preferentially with the internal silanols. The range of first (external) and second (internal) groups is broad in scope.

Candidates for the weakly adsorptive external group include those nonionic, hydrophilic groups used for gel filtration (*1, 10*) and hydrophobic interaction (*11, 12*) chromatography. Additional candidates include ionic groups (*6*), immobilized protein (*5*), or lipophobic fluorocarbon groups (*13*). In each case, however, inertness to protein adsorption requires the proper choice of mobile phase to match the packing (*14*).

It has been shown that the perfluorobutylethylenedimethylsilyl (PFB) group on silica displays reduced adsorption of lipophilic solutes, including that of blood serum protein (*9*). This is in accordance with previously published data showing that immobilized perfluoroalkyl groups on silica display much less retention both for small molecules and for proteins than does the comparable alkyl group (*9, 13, 15*). Furthermore, it has been shown that a DZM with external PFB groups displays less serum protein adsorption than the mixed phase composition (MPC) with comparable group densities but with no spatially separated structure (*9*). Therefore, we postulate that similar DZMs optimized for direct serum analysis for drugs by HPLC would show extended column lifetimes.

To test the idea that extended column lifetime would be conferred by the unique DZM structure, we prepared a number of DZM columns and comparable MPC controls. Accelerated determinations of column lifetime were obtained by using direct serum injection under conditions chosen to induce rapid degradation of column performance. We expected that even the MPC columns would show improved lifetimes, since we designed them to be less strongly retentive than conventional octadecylsilyl (ODS) columns.

EXPERIMENTAL SECTION

Adsorbents were made by using the general procedures described earlier (*8, 9*). Dual zone structure was attained by using an ultrareactive leaving group (*N*-methylacetamidyl) to attach the PFB group to the external zone. The mixed phase compositions were made by using a mixture of PFB and ODS silanes bearing the rather sluggishly reactive, chloride-leaving group. The same reverse-phase ODS group was present as described earlier (*9*), but in amounts adjusted to provide reduced retentivity, so that therapeutic drugs could be readily eluted at 20% organic mobile phase.

Four adsorbents were made, two DZMs and two MPCs. DZM-2 had a greater amount of PFB than DZM-1 but was otherwise very similar in averge composition. Each control, MPC-1 and MPC-2, had the same average composition as its corresponding DZM. The extent of dual zone structure (DZE) was assayed by procedures similar to those described previously (*9*). In the present study, the equation used was as follows:

$$\mathrm{DZE} = \Gamma_e(\mathrm{PFB})/\Gamma_a(\mathrm{PFB}) - 1 \qquad (1)$$

where Γ_e(PFB) and Γ_a(PFB) are the surface densities in molecular residues/nm^2 for the PFB group on the external and on the average surface (throughout the porous adsorbent), respectively.

Values for Γ_a(PFB) were determined from bulk %F via a conventional combustion-based method and from the specific surface area of the silica. Compensation for the weight increase due to the immobilized residue was done in the usual manner (*16*).

Values for Γ_e(PFB) were determined from the linear dependence upon the F/Si ratio, as measured by electron spectroscopy for chemical analysis (ESCA) using a Physical Electronics Model 550 spectrometer (*8*). We have found this relationship to be approximately linear for PFB-treated silicas that had varying Γ_a(PFB) values and in which the dual zone structure was avoided by using a slugglishly reactive, chloride leaving group. The linear calibration factor was found to be 1.25 (residues/nm^2) × (Si/F). The linearity is expected for submonolayer coverage of porous materials (*17*) such as ours, although the presence of one substrate-specific atom (Si) in the immobilized residue leads to a slight deviation from linearity.

The silica used was a nominal 60A chromatographic silica obtained from ICN/Woelm. The surface area was 424 m^2/g as measured by bulk analysis for fluorine in a sample that had been saturatively treated at room temperature under conditions known to result in a coverage of 1.66 molecules/nm^2 of PFB. This method for measuring the reactive surface area (18) is convenient to apply. However, an error in this measurement does not affect the above DZE value since both Γ_e(PFB) and Γ_a(PFB) contain the surface area in their denominators. The average particle size was 10μm, as measured by laser light scattering.

The treated silica was packed by procedures similar to those described earlier (*9*) in 10-cm stainless steel columns that were tested for their capacity and efficiency for the separation of anticonvulsant drugs (phenobarbital and carbamazepine). Initially, the columns were tested with aqueous standards for these two drugs, with the mobile phase containing 2-propanol/0.1 M phosphate buffer (pH 6.8) at a ratio of 1:4 by volume at a flow rate of 2.0 mL/min. The detector wavelength was set at 254 nm. Initial retentivity was assayed from the capacity factor of the

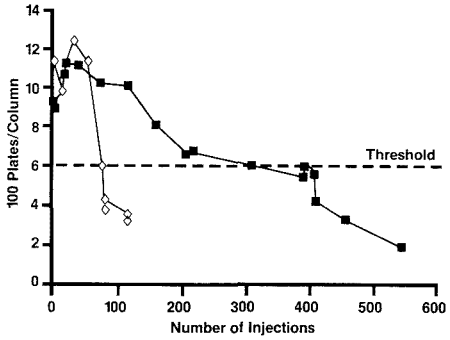

Figure 1. Column efficiency versus number of 10-μL serum injections on DZM-1 column (■) and MPC-1 column (◇).

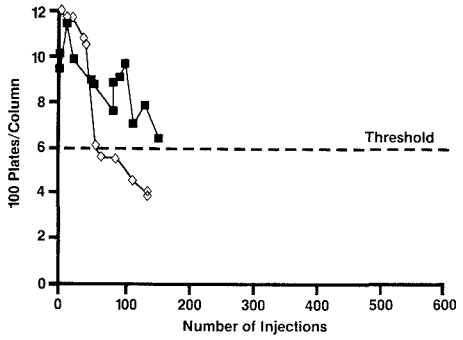

Figure 2. Column efficiency versus number of 10-μL serum injections on DZM-2 column (■) and MPC-2 column (◇).

column for naphthalene at 40% MeCN/60% water.

The columns were protected by a 0.5-μm prefilter and by centrifugation of all samples. The four columns were tested by repetitive 10-μL injections of pooled clinical samples of human serum. The pooled serum was spiked with two anticonvulsant drugs, phenobarbital and carbamazepine, at levels of 100 and 25 μg/mL, respectively. Column efficiencies in theoretical plates per column were assessed from the serum carbamazepine peak using the band half-width method (*19*) of measurement.

RESULTS AND DISCUSSION

The test assay chosen was not atypical. However, the conditions were chosen to be atypical in order to induce rapid column degradation in these comparative tests. Such conditions would probably not be practiced in routine use: no protective precolumn was used, and the amount of organic modifier in the mobile phase was chosen to be just below that level which would cause column plug-up by serum protein precipitation. Such relatively high levels of organic solvent are thought to promote the denaturation of adsorbed protein and, hence, to accelerate column degradation. 2-Propanol at 20% by volume was chosen as the modifier because it has the strongest elution power and thus would reveal whether or not the column packing was too retentive for direct serum analysis.

Column back pressure did not rise systematically during any of these experiments. The occasional rises that did occur were eliminated by changing the prefilter.

Figure 1 shows data for columns DZM-1 and its control MPC-1. Column efficiency drops much faster for the control than for the dual zone column. The column is still useful at a cutoff of about 600 plates for this particular clinical analysis. We define *column lifetime* as the amount of serum exposure that reduces column efficiency to 600 plates. The DZM-1 column tolerates 400 injections (4 mL) of serum before failure; the comparable control fails after only 70 injections (0.7 mL).

Another way of comparing the two types of columns is by measuring efficiency after 150 injections; we define this measurement as *column durability*. Again, the DZM-1 column is much more durable by this measurement than its control.

Figure 2 shows lifetime data for column DZM-2 and its control, MPC-2. This figure shows more data scatter than the previous one. However, again, the control column showed a steep decline in efficiency with increasing serum dosage, whereas the dual zone column showed a considerably longer column lifetime as well as greater durability. Note that DZM-2 was also better than MPC-1. However, neither DZM-2 nor MPC-2 performed as well as the corresponding DZM-1 and MPC-1.

Figure 3 illustrates overall column performance. Both DZM columns provide substantially greater column life and durability than either control. DZM-1 is substantially better than

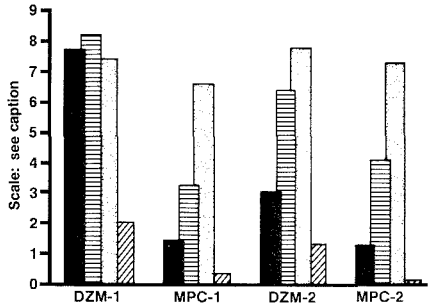

Figure 3. Column data for two DZM columns and two MPC control columns: ordinate scale for lifetime (solid area) as defined in text and divided by 50; for durability (horizontal lines) as defined in text and divided by 100; for initial retentivity (dotted area) as defined in text for the capacity factor of naphthalene; for dual zone extent (slanted lines) as defined in eq 1.

DZM-2, which has somewhat greater PFB content, but is otherwise similar. All four columns have approximately the same initial retentivity for small solutes. In fact, the MPC controls are slightly less retentive, which thus excludes the possibility that they adsorbed more protein and failed more quickly simply due to greater overall retentivity. Column lifetime is strongly correlated with the extent of DZM character, which substantiates our initial hypothesis that such materials provide advantages as fouling-resistant adsorbents.

To put these results into context, we note that the DZM approach gives access to a very large variety of immobilized groups through use of readily available or easily synthesizable silylating agents. This variety includes silane-immobilized peptides and proteins. It is straightforward to incorporate the major portion of this variety into DZM structures. The primary constraint is that the external residue must not be self-reactive with the ultrafast leaving group, e.g., with the *N*-methylacetamidyl group. In practice, this is not a major constraint.

In contrast, other approaches for making layered porous materials have rather severe limitations, in our opinion. For example, the size-excluded enzyme approach (*6*) relies upon obtaining an enzyme that modifies an immobilized residue by solvolysis or oxidation. There are many residues and modifications of residues that are known to be chromatographically useful, but for which no suitable enzyme has yet been found. It is clear that a sufficiently intense effort can select or even design such enzymes if there is sufficient motivation and resources to support such efforts. However, it also seems clear that the DZM approach can generate a large

variety of structures more rapidly.

CONCLUSIONS

DZMs in which the outer zone was enriched with the PFB group displayed much longer column lifetime than MPC controls with comparable overall composition. The best column material, DZM-1, had 4 times longer life than its control. PFB-rich adsorbents display a markedly lesser degree of serum protein adsorption than ODS-rich ones (*9*), suggesting that the mechanism by which the DZM provided longer life is by minimizing deposits of adsorbed protein that can plug the outer pore structure of the packing. Such plugging is known to cause loss of column efficiency. Comparison to the literature indicates the DZM-1 had comparable or longer lifetime under these challenging conditions than the recently introduced Pinkerton packings (*6*) and provides greater adsorbent design and pH operational latitude than the latter. Even our control columns displayed markedly longer lifetimes than conventional reverse phase columns.

DEDICATION

This article is dedicated to the memory of my coauthor, Professor Pokar M. Kabra, deceased February 1990.

ACKNOWLEDGMENT

We thank Peter Lo, Elizabeth Norton, and Eric Cosens of Dow Corning for providing silanes and for preparing treated silica and HPLC columns. We thank Jeff Wall of the UCSF school of medicine for obtaning the clinical HPLC data.

LITERATURE CITED

(1) Unger, K. *TrAC, Trends Anal. Chem.* **1983**, *2*, 271.
(2) Arvidson, T.; Wahlund, K. G.; Daoud, N. *J. Chromatogr.* **1984**, *317*, 213.
(3) Tice, P. A.; Mazaroff, I.; Li, N. T.; Regnier, F. E. *J. Chromatogr.* **1987**, *410*, 43.
(4) Kabra, P. M.; Stafford, B. E.; Marton, L. J. *Clin. Chem.* **1977**, *23*, 1284.
(5) Yoshida, H.; Morita, I.; Tamai, G.; Masujima, T.; Tsura, T.; Takai, N.; Imai, H. *Chromatographia* **1985**, *19*, 466.
(6) Hagestam, I. H.; Pinkerton, T. C. *Anal. Chem.* **1985**, *57*, 1757.
(7) Haginaka, J.; Yasud, N.; Wakai, J.; Matsunaga, H.; Yasuda, H.; Kimura, Y. *Anal. Chem.* **1989**, *61*, 2445.
(8) Williams, D. E.; Tangney, T. J. *Silanes, Surfaces and Interfaces*; Leyden, D., Ed.; Gordon and Breach: New York, 1986; p 471.
(9) Williams, D. E. *Chemically Modified Surfaces*; Leyden, D., Collins, W., Eds.; Gordon and Breach: New York, 1988; p 515.
(10) Engelhardt, H.; Mathes, D. *J. Chromatogr.* **1979**, *305*, 185.
(11) Fausnaugh, J. L.; Kennedy, L. A.; Regnier, F. E. *J. Chromatogr.* **1984**, *317*, 141.
(12) Miller, N.; Freibush, B.; Karger, B. L. *J. Chromatogr.* **1985**, *316*, 519.
(13) Xindu, G.; Carr, P. W. *J. Chromatogr.* **1983**, *269*, 96.
(14) Rivier, J. E. *J. Chromatogr.* **1980**, *202*, 211.
(15) Billiet, H. A.; Schoenmakers, P. J.; de Galan, L. *J. Chromatogr.* **1981**, *218*, 443.
(16) Berendsen, G. E.; de Galan, L. *J. Liq. Chromatogr.* **1978**, *1*, 561.
(17) Fung, S. C. *J. Catal.* **1979**, *58*, 454.
(18) Gilpin, R. K.; Burke, M. F. *Anal. Chem.* **1973**, *45*, 1383.
(19) Snyder, L. R.; Kirkland, J. J. *Introduction to Modern Liquid Chromatography*, 2nd ed.; Wiley-Interscience: New York, 1979; Chapter 5.

RECEIVED for review October 24, 1989. Accepted January 11, 1990.

Multipoint Calibration of a Gas Chromatograph Using Cryogenic Preconcentration of a Single Gas Standard Containing Volatile Organic Compounds

George C. Rhoderick* and Walter R. Miller

National Institute of Standards and Technology, Center for Analytical Chemistry, Gas and Particulate Science Division, Gaithersburg, Maryland 20899

Methodology is described for the use of a cryogenic preconcentration technique to increase the sample amount of trace volatile toxic organic compounds in a gas matrix for analysis by gas chromatography. A gas chromatograph equipped with a flame-ionization detector was set up for the analysis of such gas mixtures in a nitrogen balance gas. A system was assembled to preconcentrate cryogenically the gas sample and then inject it onto the chromatographic column. The system was evaluated for analytical precision and to determine if it could be used to construct a calibration curve for the instrument using a single calibration gas standard. An experiment was also performed to determine the trapping efficiency for the organic compounds using the system as constructed. The operating procedure evaluated for cryogenically preconcentrating the sample involved trapping the sample for different time intervals at a set sample flow rate. The analytical data from this procedure were plotted for each compound in the gas standard using linear forced zero regression. Results indicate that the method is very linear over the concentration range of 1–13 nmol/mol (parts per billion) for the operating conditions studied. This determination of linearity now allows the use of one calibration gas standard to develop a calibration range for an instrument.

INTRODUCTION

The need to measure low levels of volatile toxic organic compounds has increased over the last several years as a result of federal and state environmental programs aimed at monitoring compounds from industrial emissions, hazardous waste dumpsites, and hazardous waste incineration. These programs have been implemented due to the documentation of several of these organics as potential carcinogens (*1*, *2*). The U.S. Environmental Protection Agency (EPA) has identified many volatile organic compounds, both halogenated and nonhalogenated, that represent public health risk (*3*). Regulatory standards are being drawn up to reduce the level of these compounds released into the environment and, at the same time, the human exposure to these species.

The National Institute of Standards and Technology (NIST) has been involved for many years in the preparation, analysis, and certification of gas standards containing volatile toxic organic compounds at levels of 1–15 ppb. Reliable measurements of these hazardous organic compounds can be difficult to make at these low concentration levels. Detection and quantification of these organic compounds at such levels are difficult using a gas chromatograph equipped with a flame-ionization detector (GC–FID). Instrument response can be increased by sampling larger volumes; however, chroma-

tographic peak shapes and analytical precision are compromised when more than 10 mL of sample is injected. Because of the low concentration levels of the organics, the response is very poor and some compounds cannot be detected. The electron capture detector (ECD) is much more sensitive for certain compounds and much less sensitive for others. The relative response of the ECD from compound to compound can vary by as much as 10^6, while the relative response of the FID only varies by about 10^2 for certain C_1 to C_8 halogenated and nonhalogenated species in the same mixture and at the same concentrations. This characteristic of the ECD would result in overloading the detector with certain species while trying to detect others. Therefore the use of the FID is more desirable, but it is also necessary to increase the amount of organic material injected onto the chromatographic column without increasing the gas sample volume.

In the past, analytical techniques involving sorbents or cryogenic temperature have been used to preconcentrate air samples and cylinder-contained gas standards containing parts-per-billion levels of volatile organic compounds. These enriched samples have been analyzed by capillary column GC–ECD and GC–FID (*4, 5*) or mass spectrometry (GC–MS) (*6, 7*). Others have used a method involving the use of an automated cryogenic system to determine volatile organic compounds in air by pulling the sample, contained in polymeric bags, canisters, or on solid adsorbents, through a trap immersed in a cryogenic fluid such as liquid nitrogen (*8*). Badings et al. reported the use of cryogenic trapping system that uses different types of fused silica and glass traps with several calibration standards of organic compounds in water (*9*) with good linear results. Others have reported the use of similar types of systems as well as fully automated systems for cryogenic preconcentration (*10, 11*).

The authors utilized a method of preconcentration that did not require the use of sorbents, and their associated uncertainties due to their adsorption/desorption efficiencies. This method was evaluated for use as a calibration system that utilized a single standard contained in a compressed gas cylinder. The gas standards used were previously prepared by a microgravimetric technique developed at the National Institute of Standards and Technology (NIST) (*12–14*). This paper describes the cryogenic preconcentration method and the use of the procedure to calibrate an analytical system with a single calibration gas standard. The use of a low concentration standard, having the same nominal concentration as the unknown(s) being measured, and cryogenic preconcentration allow the standard to be treated in the same manner as the unknown and is considered good experimental technique. This method also allows a laboratory with only a single standard to perform a multipoint calibration, as opposed to a single-point calibration.

EXPERIMENTAL SECTION

Apparatus. A gas chromatograph (GC) equipped with an FID and a 2.3 m by 1.6 mm i.d. stainless steel column packed with a 1% loading of poly(ethylene glycol) modified with nitroterephthalic acid on 60/80 mesh graphitized carbon black was used for the analyses. The column oven was held at 45 °C for 8 min, then raised to 180 °C at 8 °C/min and then to 220 °C at 20 °C/min. A wide bore capillary column of borosilicate glass, 60 m by 0.75 mm i.d., with a 1 μm thick film of dimethylpolysiloxane was also tried. The column oven temperature for this capillary column was held at 32 °C for 7 min, then raised to 170 °C at 4 °C/min and held until the last peak eluted. A six-port gas sampling valve, constructed of stainless steel with a carbon-filled Teflon rotor, was mounted on the frame of the instrument so that it was accessible from almost any direction. A sample loop, of 200 mm open tubular 0.8 mm i.d. stainless steel with no packing material, was connected to the appropriate ports on the sampling valve. A stainless steel, single stage, low dead volume regulator was connected to the cylinder containing the gas standard. Since

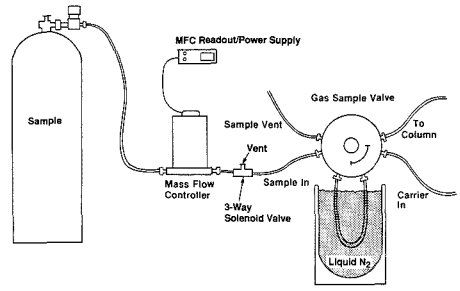

Figure 1. Diagram of the cryogenic trapping system from sample to column.

the accuracy and reproducibility of the sample flow are crucial to the method, the 1.6 mm i.d. stainless steel sample line from the regulator on the gas standard was connected to the inlet of a 0–100 mL/min mass flow controller (MFC). The MFC used is constructed of 316 stainless steel with Teflon O-ring seals. The outlet from the MFC went to a three-way stainless steel solenoid valve and then to the gas sampling valve using 0.8 mm i.d. stainless steel tubing (Figure 1). The solenoid valve was used to stop the sample flow prior to injection, thereby ensuring that all samples were injected at the same pressure.

Materials. The organic gas standards used were prepared by NIST in aluminum cylinders equipped with CGA-350 brass valves. The cylinders were treated by a specialty gas manufacturer to deactivate the cylinder walls and the valves were cleaned to eliminate possible contaminants such as degreasing compounds. The matrix gas in the standards was dry, pure nitrogen. A standard containing 18 organic compounds was used so that many different organic species could be studied.

Flow Calibration. The flow out of the MFC was measured with a soap-bubble flow meter. The bubble flow meter volume was calibrated by repeated measurements (6–10) of the mass of water contained between the volume marks used for the flow determinations. This volume was calculated by using the formula $V = m/d$, where V is the volume (mL), m is the mass of water (g), and d is the density of water (g/mL) at the observed temperature. The percent relative standard deviation (%RSD) [calculated from the equation (sd/mean) × 100, where sd is the standard deviation of the mean], of the mass of water is a measure of the precision of the volume determination and was found to be ±0.2%.

Once the volume of the bubble flow meter was determined, the flow through the MFC was measured several times (6–10) whenever a new setting was made. The %RSD of the observed timing measurements is a measure of the precision of the MFC and was found to have an average value of ±0.3%. Since the flow was measured for each control setting, the reproducibility of the MFC (i.e., the ability to reset a particular flow) does not enter into the overall error assessment for the flow. The uncertainty of the flow, and therefore the effective trapping volume, is calculated by combining, in quadrature, the uncertainties of the volume calibration and the precision of the controller. This yields an estimated total uncertainty at 1 standard deviation of ±0.33% for the flow measurements.

Procedure. The sample pressure at the single-stage regulator of the gas standard cylinder was set at 200 kPa. The sample flow through the MFC was set at 51.0 mL/min as determined by using the soap-bubble flow meter. The GC was programmed, using the run table of the integrator/control module, to do the following: (1) 5.0 min, stop sample flow (by way of the solenoid valve); (2) 5.1 min, inject sample onto the column, which was accomplished by using a 90° air actuator to turn the valve. When the integrator/control module of the GC was prompted to start an analysis, the sample loop was submerged in a Dewar of liquid nitrogen. The sample, which was flowing at a constant 51 mL/min, was collected cryogenically in the sample loop for 5 min for an effective volume of 255 mL of sample. No problems, such as plugs, with the possible trapping of some of the nitrogen from the sample were observed during the analysis. When the gas

Table I. Imprecision of Replicate Injections for a Single Sample Using a Packed Column

compound	GC area response			average	std dev	%RSD
	inject 1	inject 2	inject 3			
bromomethane	25.31	24.86	24.72	24.96	0.31	1.2
vinyl chloride	45.62	44.92	44.91	45.15	0.41	0.9
methylene chloride	26.11	25.56	25.71	25.79	0.28	1.1
1,3-butadiene	67.17	66.69	66.37	66.74	0.40	0.6
trichlorofluoromethane	3.84	4.12	3.76	3.91	0.19	4.8
chloroform	22.07	21.97	21.77	21.94	0.15	0.7
1,2-dichloroethane	49.46	48.95	49.73	49.38	0.40	0.8
1,1,1-trichloroethane	55.31	55.51	55.03	55.28	0.24	0.4
carbon tetrachloride	11.86	12.42	12.24	12.17	0.29	2.4
1,2-dichloropropane	77.05	77.14	77.99	77.39	0.52	0.7
trichloroethylene	51.23	50.73	51.16	51.04	0.27	0.5
benzene	135.32	134.63	135.70	135.22	0.54	0.4
1,2-dibromoethane	44.09	44.29	44.77	44.38	0.35	0.8
tetrachloroethylene	64.42	65.93	65.63	65.33	0.80	1.2
toluene	158.72	160.73	160.43	159.96	1.08	0.7
chlorobenzene	137.80	138.68	139.84	138.77	1.02	0.7
ethylbenzene	180.33	180.38	181.86	180.86	0.87	0.5
o-xylene	170.02	170.53	171.37	170.64	0.68	0.4
average						1.1

sample valve was automatically switched to inject the trapped sample onto the column, the Dewar of liquid nitrogen was replaced with a beaker of hot water at 95 °C to vaporize the organic compounds. Hot oil at 170 °C was also tried to see if a higher temperature had any effect on peak sharpness and precision.

Once the system was set up, experiments were performed to determine: (1) if there were any sorption/desorption effects within the sampling system, (2) the reproducibility (analytical precision) of replicate injections of a single sample, (3) the effect on the trapping efficiency by precooling the traps or no precooling before flowing sample through them, (4) the trapping efficiencies of different trapping times and the same flow rate, and (5) the effect on the trapping efficiency using different flow rates.

To determine the efficiency of the trap, the first sample loop trap (main trap) was followed by a second (breakthrough collection) trap of the same size and material. The sample flow rate was set at 51.0 mL/min. At the start of the run, both traps were simultaneously immersed in liquid nitrogen for 5 min. When the sample valve was actuated into the inject mode, the cryogen from the breakthrough trap was removed and replaced with the beaker of hot water. After the run was completed, another run was started, but this time only the main trap was immersed in cryogen for 5 min. When the sample valve was automatically actuated to the inject mode, the cryogen on this main trap was replaced with the beaker of hot water.

To determine if precooling the traps before flowing the sample through them had any effect on the efficiency, the sample flow was diverted. The traps were immersed in the cryogen for 1.5 min and then the sample was directed through the traps for 5 min. Once the gas sample valve was actuated to the inject mode, the cryogen was removed from the breakthrough trap and heated with the hot water. Once it was determined that precooling the traps made no difference in the results, precooling was discontinued. The procedure, using the main and breakthrough collection traps without precooling, was repeated using different trapping times at the same sample flow rate. Several different flow rates were then tried, using the same procedure described above.

After the trapping efficiency experiments were concluded, the main experiments of the system began. These experiments involved the trapping of the standard sample at different trap times using the same flow rate. The results of these experiments would tell us if one standard and cryogenic concentration could be used to linearly calibrate an instrument. The run table program was set for a cryogenic preconcentration trapping time of 5 min. The gas standard was set for a flow of 51.0 mL/min through the mass flow controller. A trapping sequence was made and the sample injected onto the GC column. After the run was completed, another run was started using a different trapping time which was programmed into the run table. Subsequent sampling and injections of the same standard were made using different trapping times for each analysis. After this study was completed, the same procedure was applied using different flow rates.

RESULTS AND DISCUSSION

The objective of this research was to determine if a single gas standard and a cryogenic trapping method could be used to linearly calibrate a GC. However, the cryogenic trapping system had to be checked out for performance and behavior before the linearity could be determined. Experiments were conducted to determine what problems may occur and how they may affect the results of the research.

The first experiment in this study was to determine if there would be any adsorption and subsequent desorption of organic compounds within the sampling system. A cylinder of dry, ultrahigh-purity nitrogen was purged through the system overnight. The next morning, flowing at 51 mL/min through the trap for 5 min for an effective volume of 255 mL, the nitrogen was passed through the cryogenic trap. The resulting analysis showed no compounds were detected. We then passed 1 L of the pure nitrogen through the trap and injected onto the column. Still, no compounds were detected. The 10 ppb organic gas standard was connected to the sampling system and 255 mL of the gas standard was passed through the trapping system followed by injection of the trapped sample onto the chromatographic column. After several trap and inject sequences, the nitrogen cylinder was reconnected to the sampling system and again 1 L of nitrogen was passed through the trap. The subsequent injection and chromatographic analysis detected no organic compounds. This result assured us that there were no apparent adsorption–desorption processes occurring within the trapping system, which would contaminate successive trappings and injections.

The second experiment was to determine how well we could reproduce this manual method of cryogenic preconcentration. Three injections of cryogenically trapped samples from the standard were made. The responses from the three injections were averaged for each compound and the standard deviation of that average was calculated. The percent relative standard deviation was then computed, which represented the imprecision of the method. The method proved to be very precise, with the imprecision ranging from 0.2% to 4.8% for the various compounds, with an average value of 1.1% (see Table I). The packed and capillary columns both gave excellent results; however, the data in Table I is from the packed column. There was no visible difference in peak sharpness between the two columns and the imprecision was about the

Table II. Comparison of Trapping Efficiencies for 1.5 min Precooling of Traps before Start of Run versus Straight Cooling from Start of Run[a]

compound	% trapping efficiencies: precooling	straight cooling	% difference[b]
bromomethane	84.4	83.9	0.5
vinyl chloride	81.2	80.6	0.6
methylene chloride	87.9	87.9	0.0
1,3-butadiene	81.2	82.6	−1.4
trichlorofluoromethane	*c*	*c*	*c*
chloroform	87.7	87.1	0.6
1,2-dichloroethane	87.4	85.6	1.8
1,1,1-trichloroethane	80.6	81.6	−1.0
carbon tetrachloride	*c*	*c*	*c*
1,2-dichloropropane	85.2	84.4	0.8
trichloroethylene	85.2	82.6	2.6
benzene	84.2	83.1	1.1
1,2-dibromoethane	83.6	82.5	1.1
tetrachloroethylene	83.2	80.9	2.3
toluene	81.4	81.3	0.1
chlorobenzene	81.1	79.3	1.8
ethylbenzene	82.0	80.7	1.3
o-xylene	80.3	79.7	0.6
average	83.5	82.7	0.8

[a] Flow rate of 51 mL/min for 5 min. Packed column. [b] Difference equals precooling minus straight cooling. [c] The response for these compounds is weak under normal cryogenic trapping conditions so when analyzing only the breakthrough, or second trap, one could visibly see a peak but it was not integrated. Therefore no efficiency could be calculated.

same for both. The difference between the two columns was that under the conditions described, the 18 organic compounds were separated much better on the packed column. It should be noted that if one can start at subambient oven temperatures, then the separations on the capillary column are very good. However, at the time of this investigation, the authors did not have the cryogenic oven capability on the GC. Therefore, the packed column was used throughout the study. There also was no observable difference in peak shape or imprecision using hot water or hot oil to facilitate vaporization of the trapped sample. The hot water was used exclusively since it represented less of a health and flammability hazard than the hot oil.

The third experiment was to determine the efficiency of the trap and to determine if there would be any difference in the trapping efficiencies between precooling the traps before flowing sample through them and trapping the sample without precooling the traps. Table II lists the organic compounds and the corresponding trapping efficiencies for each method. The efficiency of the trap was calculated by adding the GC area response for the breakthrough trap to the GC area response for the main trap yielding the total response at one flow rate and trap time. The response of the main trap was then divided by the total response and multiplied by 100 to obtain the precent trapping efficiency. The average difference in the trapping efficiency between the precooling and the straight cooling is 1.1%. This is the same value as the average imprecision of replicate injections, previously discussed and shown in Table I. Although a few of the compounds show a slightly higher difference in the efficiencies when compared to their corresponding imprecision (e.g., trichloroethylene with a difference of 2.6% between the trapping efficiencies has only a 0.5% RSD in its analytical imprecision), we believe there is no real difference between precooling and no precooling based on the imprecision measured at specific flow rates.

The fourth and fifth experiments were developed to determine the trapping efficiencies at one particular flow setting but using different trapping times and then using different flow rates. Table III lists the trapping efficiencies for the 18 organic compounds in the gas standard used. The flow rate was a constant 55.0 mL/min and the trapping time was varied. Basically, the efficiency is the same no matter what the trapping time, with averages of 82.9–84.0%. There are no efficiency data for trichlorofluoromethane and carbon tetrachloride because the response of the breakthrough trap, even though observable on the chromatogram, was very small and was not integrated. Similar results were obtained at different flow rates. Table IV shows the efficiencies at different flow rates for the same trapping time. The average efficiency at

Table III. Trapping Efficiencies Using Different Trapping Times at the Same Sample Flow Rate of 55.0 mL/min Using Packed Column

compound	% trapping efficiencies: 2 min trap	5 min trap	8 min trap
bromomethane	84.6	84.5	85.3
vinyl chloride	83.9	83.7	84.8
methylene chloride	86.1	85.1	85.0
1,3-butadiene	86.0	85.2	85.1
trichlorofluoromethane	*a*	*a*	*a*
chloroform	87.1	84.9	84.4
1,2-dichloroethane	85.9	84.8	84.6
1,1,1-trichloroethane	83.9	83.7	84.3
carbon tetrachloride	*a*	*a*	*a*
1,2-dichloropropane	86.3	84.6	84.0
trichloroethylene	82.7	82.5	83.7
benzene	84.1	83.4	83.8
1,2-dibromoethane	79.1	84.9	84.9
tetrachloroethylene	82.3	81.8	85.5
toluene	82.2	83.1	82.6
chlorobenzene	77.3	81.3	81.3
ethylbenzene	78.2	82.8	82.3
o-xylene	76.8	82.4	82.5
average	82.9	83.7	84.0

[a] The response for these compounds is weak under normal cryogenic trapping conditions, so when analyzing only the breakthrough, or second trap, one could visibly see a peak but it was not integrated. Therefore no efficiency could be calculated.

Table IV. Trapping Efficiencies at Different Flow Rates Using the Same Trapping Time of 5 min Using Packed Column

compound	% trapping efficiencies: 20.5 mL/min	55.0 mL/min	86.0 mL/min
bromomethane	83.9	84.5	84.0
vinyl chloride	80.9	83.7	83.4
methylene chloride	85.1	85.1	83.2
1,3-butadiene	82.6	85.2	84.9
trichlorofluoromethane	*a*	*a*	*a*
chloroform	84.6	84.9	81.8
1,2-dichloroethane	85.6	84.8	82.5
1,1,1-trichloroethane	81.5	83.7	82.6
carbon tetrachloride	*a*	*a*	*a*
1,2-dichloropropane	83.7	84.6	81.4
trichloroethylene	82.0	82.5	81.6
benzene	82.6	83.4	81.8
1,2-dibromoethane	83.0	84.9	81.7
tetrachloroethylene	80.6	81.8	81.1
toluene	81.3	83.1	81.1
chlorobenzene	80.2	81.3	79.5
ethylbenzene	81.3	82.8	81.3
o-xylene	80.0	82.4	79.0
average	82.4	83.7	81.9

[a] The response for these compounds is weak under normal cryogenic trapping conditions, so when analyzing only the breakthrough, or second trap, one could visibly see a peak but it was not integrated. Therefore no efficiency could be calculated.

Table V. Linear Forced Zero Regression of Data for 1,1,1-Trichloroethane for Constant Flow Rate and Varied Trap Time Using Packed Column

GC area response	calibrated trap time, min	predicted trap time, min	residual (pred − cali)	% relative residual
11.64	1.00	0.98	−0.02	−2.0
24.09	2.00	2.02	+0.02	+1.0
36.12	3.00	3.04	+0.04	+1.3
46.87	4.00	3.94	−0.06	−1.5
60.48	5.00	5.08	+0.08	+1.6
71.11	6.00	5.98	−0.01	−0.2
84.60	7.00	7.11	+0.11	+1.6
93.88	8.00	7.89	−0.11	−1.4
			absolute mean =	1.3

Table VI. Linear Forced Zero Regression of Data for 1,2-Dibromoethane for Constant Flow Rate and Varied Trap Times Using Packed Column

GC area response	calibrated trap time, min	predicted trap time, min	residual (pred − cali)	% relative residual
7.38	1.00	0.94	−0.06	−5.5
15.78	2.00	2.02	+0.02	+0.9
23.03	3.00	2.95	−0.05	−1.8
30.68	4.00	3.93	−0.07	−1.9
39.67	5.00	5.08	+0.08	+1.5
47.16	6.00	6.03	+0.03	+0.6
55.29	7.00	7.07	+0.07	+1.0
61.92	8.00	7.92	−0.08	−1.0
			absolute mean =	1.8

a particular flow rate for 16 of the 18 compounds ranges from 81.9% to 83.7%, with efficiencies for the remaining two compounds estimated to be within that range. These results show that the trapping efficiency is not affected by flow rate or trapping time and, therefore, it is not necessary to have two traps in the system. One trap can be relied upon to give consistent results even though 100% of the material is not retained.

The findings from the efficiency experiments would lead one to conclude that a linear calibration line could be constructed by using varying trapping times at a constant flow rate. Therefore, more rigorous experiments were performed for a number of different trapping times at a constant flow rate of 51.0 mL/min. The data for each individual organic compound were plotted using a forced zero linear regression of trapping time verses GC area response. Table V shows the regression for 1,1,1-trichloroethane while Table VI gives results for 1,2-dibromoethane. The predicted trap time (t_p) was determined from the regression plot for each of the calibrated

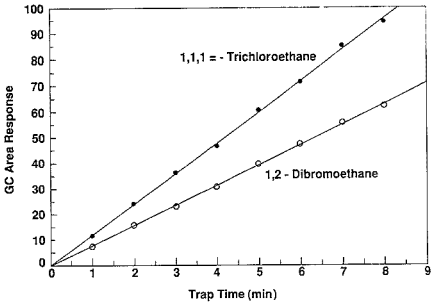

Figure 2. Forced zero linear regression of trap time versus GC area response at a constant flow rate of 51 mL/min for 1,1,1-trichloroethane and 1,2-dibromoethane.

trap times (t_c). The residuals were calculated by subtracting the t_c from the respective t_p. The percent relative residual (%R) was then calculated for each trap time using the equation $[(t_p - t_c)/t_c] \times 100$. The mean of the residuals was then calculated using the absolute values of %R. The mean represents one way to determine the imprecision in the set of calibrated trap times. The %R's are randomly dispersed negative and positive, which is a typical pattern for good linear data. Figure 2 illustrates the linearity of the data for 1,1,1-trichloroethane and 1,2-dibromoethane. This was consistent for all 18 of the organic compounds in the mixture and shows that this method of cryogenic preconcentration is a viable one for producing a linear calibration range using just one gas standard. The uncertainty in the calibration was determined by using the mean %R. Calibration uncertainties, expressed at 1 standard deviation, ranged from ±1% for some compounds to as high as ±5% for other compounds. The average uncertainty for the 18 compounds was ±2%. The regressions show that this procedure is indeed linear.

This method of varying the trapping time at a constant sample flow rate was checked for linearity at different flow rates, but the testing was not as rigorous. Five different trapping times were used at each of the flow rates. The data were plotted by using a forced zero linear regression of calibrated trapping time verses GC area response. Figure 3 shows these regressions for 1,1,1-trichloroethane and illustrates that they are indeed linear. It should be noted that one cannot compare the area response at one particular trap time between the different flow rates. This is due to the fact that the experiments for these plots were accomplished on different days and the sensitivity of the detector varies somewhat from day to day.

Discussion of Applications. The cryogenic preconcentration technique has two useful applications. First, it is a

Table VII. Linear Forced Zero Calibration Curve for 1,1,1-Trichloroethane Using a Single Gas Standard and Packed Column

trap time, min	volume, mL	ratio	calcd concn, ppb	peak area	predicted concn, ppb	% relative residual
1.00	51	0.20	1.56	11.64	1.53	−2.0
2.00	102	0.40	3.3	24.09	3.16	1.1
3.00	153	0.60	4.69	36.12	4.75	1.2
4.00	204	0.80	6.25	46.87	6.16	−1.5
5.00	255	1.00	7.82	60.48	7.95	1.6
6.00	306	1.20	9.38	71.11	9.34	−0.4
7.00	357	1.40	10.95	84.60	11.11	1.5
8.00	408	1.60	12.51	93.88	12.33	−1.4
					absolute mean =	1.3
5.00	255	1.00	unknown 1	77.83	10.23 (10.17)[a]	
5.00	255	1.00	unknown 2	38.62	5.06 (5.10)[a]	

[a] Actual concentration of unknown given to authors after analysis and predicted concentrations had been calculated.

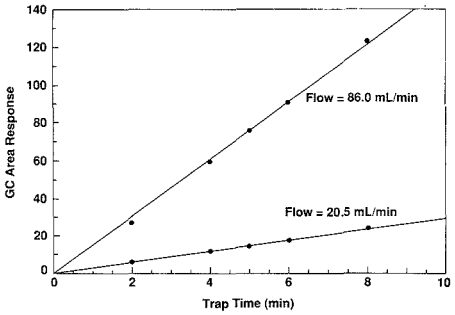

Figure 3. Forced zero linear regression of trapping time versus GC area response at two different flow rates for 1,1,1-trichloroethane.

viable technique for increasing the amount of organic sample for analysis by GC-FID, which in turn allows better measurement precision. The second application is the use of a single gas standard to produce a calibration curve by trapping for different times at a constant flow rate. For example, the flow rate for the standard would be set at 51 mL/min, which would remain constant throughout the calibration. The standard would then be trapped cryogenically for say 5 min. The volume of the sample trapped is then calculated ($f_c \times$ time; where f_c is the calibrated flow rate) and set equal to unity. This volume is then assigned the certified concentration of the standard for the compound of interest. All other calculated volumes for different trap times are ratioed to that volume designated as unity and the concentrations (C_c) at each calibration point are calculated by multiplying the certified concentration of the standard by the respective ratio. A plot of C_c verses GC area response is then applied and regression analysis performed on the data. The predicted concentration at each point is determined by the regression analysis used and the %R is calculated from the equation $[(C_p - C_c)/C_c] \times 100$. The mean of the %R's is calculated and this value represents the measure of the precision of the method. The concentration of the unknown, which is trapped cryogenically for the same amount of time as unity (5 min), is then predicted from the generated line based upon its GC area response. As an example, the data for 1,1,1-trichloroethane treated in this manner is shown in Table VII. To test the actual procedure and to demonstrate this application, the concentration of 1,1,1-trichloroethane in two different gas mixtures was determined by using the sampling conditions for unity described above. The calibration line predicted a concentration of 10.23 ppb for unknown 1 and 5.06 ppb for unknown 2. The actual gravimetric concentration for unknown 1 was 10.17 ppb and 5.10 ppb for unknown 2. This was indeed excellent agreement and solidified the validity of this method.

The results of this research show that a very linear multipoint calibration range from at least 1 to 15 ppb can be obtained by using a single standard, cryogenic trapping, a constant flow rate, and varied trapping times. This method is viable at least over the flow ranges studied in this paper.

ACKNOWLEDGMENT

The authors wish to acknowledge William D. Dorko, leader of the Gas Metrology Research Group of the Gas and Particulate Science Division, for his valued input and discussion of this research and Rance A. Velapoldi, chief of the Gas and Particulate Science Division, for input on certain experiments.

LITERATURE CITED

(1) *IARC Monographs on the Evaluation of Carcinogenic Risk of Chemicals to Man*: International Agency for Research on Cancer, World Health Organization: Geneva, Switzerland, 1972, Vol. 1, pp 53–65, and 1974, Vol. 7, pp 203–216, 291–305.
(2) Trane, R. E. *Science* **1977**, *195*, 443.
(3) von Lehmden, D. J. Conference on Recent Developments in Monitoring Methods for Toxics in the Atmosphere, Boulder, CO, July 1987.
(4) Termonia, M.; Alaerts, G. *J. Chromatogr.* **1985**, *328*, 367–371.
(5) Rhoderick, G. C. In Proceedings, *EPA/APCA International Symposium on Measurement of Toxic and Related Air Pollutants*; U.S. EPA/APCA eds.; APCA: Pittsburgh, PA, 1988; VIP-10; pp 259–264.
(6) Arnts, R. R. *J. Chromatogr.* **1985**, *329*, 399–405.
(7) Scott, D. R. *Anal. Chem.* **1986**, *58*, 881–890.
(8) McClenny, W. A.; Pleil, J. D.; Holdren, M. W.; Smith, R. N. *Anal. Chem.* **1984**, *56*, 2947–2951.
(9) Badings, H. T.; de Jong, C.; Dooper, R. P. M. *HRC CC, J. High Resolut. Chromatogr. Chromatogr. Commun.* **1985**, *8*, 755–763.
(10) Howe, G. B. In *Proceedings, EPA/APCA Interantional Symposium on Measurement of Toxic and Related Air Pollutants*; APCA: Pittsburgh, PA, 1988; VIP-10, pp 265–276.
(11) Melcher, R. G.; Caldecourt, V. J. *Anal. Chem.* **1980**, *52*, 875–881.
(12) Schmidt, W. P.; Rook, H. L. *Anal. Chem.* **1983**, *55*, 290–294.
(13) Rhoderick, G. C.; Cuthrell, W. F.; Zielinski, W. L., Jr. In *Transactions, APCA/ASQC Speciality Conference on Quality Assurance in Air Pollution Measurements*; Johnson, T. R., Penkala, S. J., Eds.; APCA: Pittsburgh, PA, 1985; pp 239–246.
(14) Rhoderick, G. C.; Zielinski, W. L., Jr. *Anal. Chem.* **1988**, *60*, 2454–2460.

RECEIVED for review August 31, 1989. Accepted January 9, 1990. Partial support of this research was funded by the U.S. Environmental Agency's Atmospheric Research and Exposure Assessment Laboratory under IAG DW-139322187-01-0.

Anal. Chem. 1990, 62, 816–820

Calibrating Detector Responses Using Chromatographic Peak Shapes

Eric V. Dose and Georges Guiochon*

Department of Chemistry, University of Tennessee, Knoxville, Tennessee 37996-1600, and Analytical Chemistry Division, Oak Ridge National Laboratory, Oak Ridge, Tennessee 37831

A new method for calibrating time-independent detector responses using only a series of chromatographic peak shapes is presented. The method provides an alternative to steady-state detector calibration which may be difficult experimentally, as in gas chromatography, or too expensive or material-intensive, as in preparative chromatography. In the new method a calibration-curve model function is adopted, and model parameter values are determined. The values used are those that minimize the difference between the analyte amounts injected into the chromatography and the analyte amounts computed from applying the calibration curve to the experimental peak shapes. Examples of applications to linear and nonlinear calibration curves are given.

Chromatographs do not directly measure concentrations of eluting analytes. Instead they measure responses such as changes in ultraviolet (UV) absorption, conductivity, or refractive index of the eluent which are related to analyte concentration. When measured response depends solely and monotonically upon analyte concentration, a calibration curve relating the two can be constructed.

There are two classes of calibration curves used in chromatography. The first and most common relates an integrated amount eluted (i.e., an amount injected) to the height, area, or width (in flow-injection analysis, or FIA) of a response peak caused by a sample zone flowing through the detector. This type of calibration curve is most useful in analytical chromatography and requires either that the sample zone shape be reproducible and independent of the amount eluted or that the detector response be strictly proportional to the concentration (herein "linear" response).

In this article we consider a second class of calibration, absolute calibration, which directly relates the concentration in the detector at a given moment to the response at that moment. In preparative chromatography the shape of the eluted zone depends on the amount injected. Thus calibration by the first method above is impractical since the practice of preparative chromatography requires knowledge of the temporal characteristics of the eluting bands, not just of the total amount of material contained therein. Absolute calibration is also needed for physical methods such as frontal analysis and correlation chromatography, which require that one convert measured detector responses to concentrations. Such calibration curves are commonly measured simply by filling the detector with several solutions of known analyte concentrations, measuring the steady-state response, and interpolating between the measured points (*1*, *2*) to construct a smooth working curve. This operation is best done dynamically, that is under the same flow conditions as those under which the curves will be used. At a minimum, steady-state measurements require enough time and solution to completely flush any previous solution out of the pumps, tubing, and detector before each measurement. Such steady-state conditions are difficult to achieve in many important cases such as preparative chromatography, where large amounts of expensive materials may be needed. Further, in gas chromatography (GC), steady-state concentrations are generated only with difficulty (*3*, *4*), particularly when the detector is to be calibrated for multiple analytes.

If a detector's response is always proportional to the analyte concentration in the detector, calibration and a measure of confidence in the proportionality factor may be accomplished in very few measurements (*5*, *6*). However, nonlinear relationships often exist (*7–9*), and it is important in these cases to know the shape of the calibration curve over the entire response range of interest since falsely assuming linearity strongly affects moments (*10*), detection limits (*11*), and other quantities (*12*, *13*) derived from chromatographic peak shapes.

We present a method for constructing absolute calibration curves from the shapes of several response peaks caused by elution of zones of known amounts of analyte, that is, a method for constructing steady-state calibration curves without making steady-state measurements. In the new method, an appropriate calibration-curve model equation is selected and an initial estimate of the model's parameters are made. The observed detector responses are transformed to concentrations, and these concentrations are integrated in time to give an estimated amount injected for each peak. The parameter values are then adjusted repeatedly to give the closest agreement between the estimated and known amounts injected *for all the chromatograms*. On convergence the last set of parameters is taken to be the best calibration curve conforming to the model equation. This new method eliminates altogether the need for steady-state measurements even when absolute calibration is needed. We expect that it will prove most useful in GC, in preparative-scale LC, and in some physical studies like chromatography-based isotherm determinations.

EXPERIMENTAL SECTION

4-Nitrotoluene (Aldrich) was reagent grade. Acetonitrile (Burdick and Jackson) was HPLC grade. Each material was from a single manufacturer's lot in order to minimize spectral and base-line inconsistencies.

UV measurements were made using a Hewlett-Packard Model 1090 liquid chromatograph equipped with a Hewlett-Packard Model 1040A diode-array UV detector. For steady-state measurements, solutions of 4-nitrotoluene in acetonitrile were mixed with pure acetonitrile at the low-pressure pumps and then were passed directly into the detector. Peak shapes were measured by injecting the same 4-nitrotoluene solutions into the flow stream and passing the stream directly into the detector. These injections were accomplished by increasing the proportion of the total flow delivered from the higher-concentration solution by a known percentage for a known length of time. Flow rates at the column were 1 mL/min, and all steady-state absorbances are averages over 2 min. Peak shapes were measured at time intervals of 0.640 s, yielding 40–100 nonzero samples per peak. In no case was a steady-state absorbance less than 0.003 AU or greater than 3.0 AU used. Since the detector reported high-concentration absorbances to 4.0 AU, no stray light problems were indicated.

Numerical computation was performed to double precision (16 decimal digits) using VAX FORTRAN on Model 8800 computers (Digital Equipment Corp.). Routines computing the Akima spline

0003-2700/90/0362-0816$02.50/0

function (*14*) are from the IMSL Mathematical Library (Houston, TX).

RESULTS AND DISCUSSION

Method Description. This calibration method consists of three steps: collection of peak shape data, selection of an appropriate calibration-curve model equation, and adjustment of the model equation's parameter values to give the best agreement between the computed amount eluted and the known amount injected for each chromatogram.

As in analytical calibration, accurately known amounts of target analyte are injected sequentially. Rather than only recording some summary statistic of the peak profile like peak height or area, one must record the entire peak shape as a table of detector responses vs time readings. Each response reading should be corrected for base-line drift, etc., although this requirement is no more stringent than is true for accurate peak-area determination. The raw data set is thus a series of several corrected response vs time tables, one table for each amount injected. Since changes in the model parameter values will change the relative contributions of different response levels even in a single peak, this data set cannot be reduced to summary statistics. The raw data must be accessible and must be transferred from the chromatograph to an adequate computer.

One could conceivably adopt as a calibration-curve model any mathematical expression whose value is determined by a finite set of parameters. However, useful choices are restricted to nonoscillating functions at the least. At best a model expression will describe physically meaningful relations between concentration and detector response. High-order polynomials are particularly poor choices due to their tendency to oscillate in an attempt to account for data scatter and for truncation of the series expansion represented by the finite order of feasible polynomials. Oscillation-damping splines are much better choices if a large number of adjustable parameters are desired, though they too may oscillate in attempts to interpolate very noisy data. We find that given an appropriate model expression, four adjustable parameters are quite sufficient to fit real data over 3 orders of magnitude of concentration (see Results and Discussion).

Before parameter values can be refined, initial values must be estimated. For this purpose it is very helpful if parameter values exist for which the model expression is reduced to linearity. For example, for an N-order polynomial model with coefficients a_i, $i = 0, 1, 2, ..., N$, one may start with $a_1 = dC/dA$ and $a_i = 0$ for all other a_i. In the general case, one may begin with initial parameter values yielding a calibration curve representing the average concentration/absorbance ratio for the N peak shapes used, that is with

$$\frac{dC}{dA} = \frac{1}{N}\sum_{i=1}^{N}\frac{M_i/F}{\int_{\tau_i} A(t)\,dt} \qquad (1)$$

where C is the concentration, A is the detector response (absorbance), M_i is the mass or number of moles injected, F is the flow rate, t is time, and τ_i is the finite time interval over which peak shape i has measurably nonzero concentration. Such parameter starting values are satisfactory for all but the most extremely nonlinear calibration cases. Analytical expressions of the calibration curve may generally be cast into linear form by setting all but one parameter equal to zero. Spline and other interpolative expressions generally are best cast into linear form by explicitly setting each concentration equal to the product of dC/dA and the corresponding absorbance.

The parameter-refinement step may then be accomplished with any abstract search method that is sufficiently robust to find the minimum of the error function

$$E(P) = \frac{1}{N - N_P}\sum_{i=1}^{N}\frac{\left[M_i - \int_{\tau_i} C(A(t),P)\,dt\right]^2}{M_i^2} \qquad (2)$$

where P is the parameter set, N_P is the number of adjustable parameters, and $C(A(t))$ is the concentration computed from the model expressions (with the current parameter values) and the response $A(t)$. This function simply expresses the mean square relative difference between the known amounts injected and the amounts estimated from the chromatogram shapes and the trial calibration curve defined by the model equation and the values of the parameters P. We find that $E(P)$ is very well behaved; that is, it is smooth with respect to small changes in the values of the parameters.

For one- and two-parameter models, both Newton and gradient-search methods will generally yield best parameter values very rapidly. Where more parameters are used, the error surface described by plotting $E(P)$ as a function of the independent parameters P becomes more complex and may exhibit local minima and other features difficult to search. In such cases, knowledge of the shape of the surface is strictly local to a given point, and gradient-search methods become very inefficient. Thus for more than two or three parameters, a method capable of searching complex error surfaces is needed. For consistency we have in all the present work used modified simplex methods (*15*, *16*) with boundary-handling improvements (*17*). Since the error function $E(P)$ is very rapidly evaluated, the cost of the somewhat larger number of evaluations that simplex methods often require is outweighed by the methods' robust nature and stability.

The simplex search method generates a sequence of trial parameter sets P. Each parameter set should be tested and confirmed to be legal before $E(P)$ is evaluated. For example, in the linear case, the slope $P_1 = dC/dA$ must be positive. This restriction is not likely to be violated since $E(P)$ varies nearly quadratically with the single parameter P_1. Since the simplex method searches for lower $E(P)$, it can generate a negative trial P_1 only by beginning at a very bad starting guess far above the optimum P_1 and projecting past the optimum. Similar situations occur more often with more parameters, and it is important to verify that each parameter set tested is legal. At a minimum this means ensuring that the calibration model is defined for each trial P. For splines we further reject each trial P that yields spline oscillation in a plot of C vs A. Our means of recovery from illegal trial sets have been given earlier (*17*). As in the linear case mentioned above, good initial estimates of P are valuable since they minimize both the computational time and the number of illegal trial parameter sets.

HPLC Test Results. Two independent sets of calibration data were collected for the 4-nitrotoluene/acetonitrile system: steady-state responses (UV absorbances) at various concentrations, and chromatograms containing peaks corresponding to various amounts injected. Both sets of data were collected at two wavelengths, 274 and 304 nm, corresponding to the spectral maximum and spectral inflection point, respectively. At each wavelength, data were taken at two spectral bandwidths, 4 and 40 nm. The 40 nm bandwidth data were included in order to exaggerate calibration-curve nonlinearity at the spectral inflection point. The spectrum has been used previously in testing of models for UV chromatographic detector nonlinearity (*18*).

The present calibration method was applied to the chromatogram data. An example chromatogram is given in Figure 1. In all such chromatograms, the six broad peaks from 20 through 40 min retention time were used (the other peaks in each chromatogram were used to verify the stability of the flow system and detector during the chromatograms). Each such set of six peaks covers 1 order of magnitude in amount

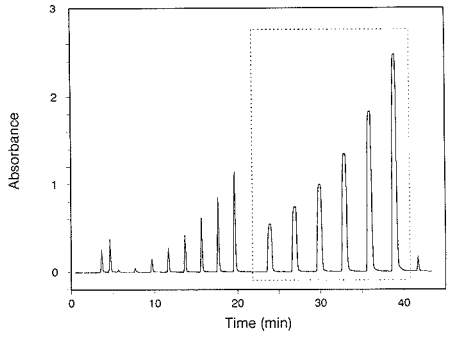

Figure 1. Example chromatogram used in calibration method described in this article. The peaks between 22 and 40 min retention time were used. This chromatogram was measured by using UV detection at 304-nm wavelength and 40-nm rectangular band-pass.

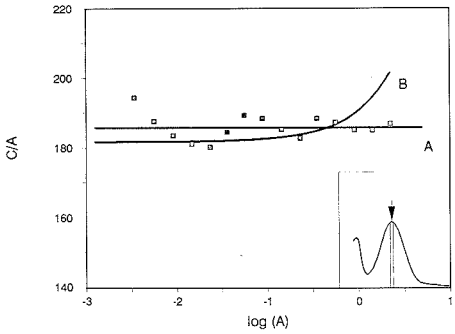

Figure 2. Comparison of steady-state UV calibration data (points) and calibration curves from chromatographic data using linear (curve A) and hyperbolic-sine (curve B, see text) models for 4-nitrotoluene in acetonitrile at a wavelength (274 nm) and band-pass (4 nm) yielding nearly linear UV response: concentrations in 10^{-6} M; insert, arrow and vertical lines indicate band-pass.

injected. At each wavelength–concentration range combination were taken four chromatograms, each covering a decade of amount injected. From the resulting 24 peaks we used only those whose maximum absorbance was within the absorbance limits given in the Experimental Section.

From the nearly perfectly linear data at the spectral maximum (274 nm) and narrow bandwidth (4 nm), the method yields an excellent estimate of the mean molar absorptivity. In Figure 2, the plotted points represent the steady-state calibration points measured as plateaus in a frontal-analysis calibration experiment, and the curves represent the calibration-curve functions with the best parameter values, that is, those yielding a minimum in $E(P)$ for the given model. (In Figures 2–5, C/A is plotted vs log A to suppress the general correlation of C with A and to emphasize the nonlinearity of the calibration curve (*19*). The curves were actually fitted as log C vs log A.)

From the chromatograms was determined a linear calibration curve (Figure 2, curve A). The constant C/A level of this curve is in excellent agreement with values from the steady-state data. Note that the curves in Figures 2–5 are in no way fits to the points, but the points and curves represent calibration data obtained through two completely different methods from two different raw data sets.

This linear-model calibration case is not a trivial one. While there are certainly easier ways to measure linear calibration curves in analytical HPLC, the same is not true in GC or in preparative LC systems where the introduction of constant, known analyte concentrations is difficult or expensive. By contrast, both of the latter systems are well suited to measuring chromatograms from pulse injections of known amounts of analyte. By use of the computing system named in the Experimental Section, the absolute linear calibration curve was extracted from the pulse chromatograms in less than 1 s of CPU time. In this simple example is demonstrated the essence of this calibration method: computational effort replaces experimental difficulty.

From the same chromatograms used to determine the linear curve A in Figure 2, curve B was determined by using the two-parameter hyperbolic sine calibration curve expression

$$A = \epsilon_0 bC - \log\left(\frac{\sinh\,(K\epsilon_1 bC\Delta/2)}{K\epsilon_1 bC\Delta/2}\right) \qquad (3)$$

where ϵ_0 is the zero-concentration-limit molar absorptivity, b is the light path length through the sample, C is the analyte concentration, K is the natural logarithm of 10, a_1 is the derivative of molar absorptivity with respect to wavelength, and Δ is the (rectangular) spectral bandwidth. In this expression, derived in previous work (*18*), spectral descriptors ϵ_0 and ϵ_1 are the adjustable parameters. In order to apply eq 2 to this model, eq 3 must be inverted to solve for C as a function of A; this is most easily accomplished numerically by Newton approximation. It appears from curve B that this model has overestimated the nonlinearity at high absorbances. Since the error estimate of the two-parameter model is actually higher than that of the linear model ($E(P)$ = 0.006 74 vs 0.006 60), the simpler linear model should be adopted in this case.

Spline functions are convenient for specifying calibration-curve models with four or more adjustable parameters. Though there are many different splines available for interpolation between specified points, many splines tend to oscillate when interpolating between noncollinear points. Most useful are so-called nonoscillating spline types, which minimize some measure of oscillation, for example the integral of the squared second derivative. We have used such an interpolating function, the Akima spline (*14*), as our third model, placing log A on the abcissa and log C on the ordinate. The adjustable parameters specifying a particular calibration curve are the log C values at specific, constant values of the log A. Since the Akima spline does not extrapolate well to absorbances outside the span of specified points' abcissas, at least one log A value should be larger than the logarithm of the highest absorbance to which the curve will be applied. Extrapolation to lower absorbance values than the lowest abcissa is performed by using the unique quadratic function satisfying these conditions:

$$\begin{cases} C(0) = 0, \\ \left(\dfrac{\partial C}{\partial A}\right)_{A=A_1} = \dfrac{C_1}{A_1}\delta_S, \\ \dfrac{\partial^2 C}{\partial A^2} = \dfrac{2C_1}{A_1^2}(\delta_S - 1) \end{cases} \qquad (4)$$

where A_1 is the leftmost abcissa on the spline and where $\delta_S = (\partial \log (C)/\partial \log (A))_{A=A_1}$, that is, the slope of the spline at A_1. These conditions ensure that the extrapolated calibration curve passes through the origin and is continuous in the first and second derivatives with the spline (at the lowest absorbance point).

In Figure 3 are given the best spline-model calibration curve (center curve) and the same experimental steady-state points as in Figure 2. For reference, the higher and lower curves are

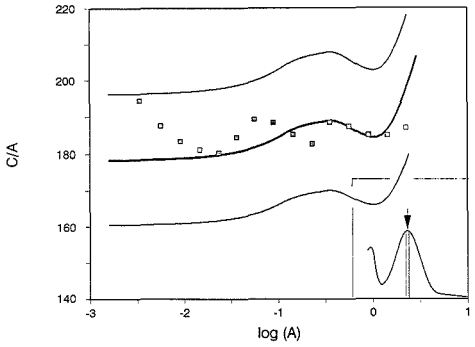

Figure 3. Comparison of steady-state calibration data (points) and calibration curve from chromatographic data using Akima spline model (center curve) for 4-nitrotoluene in acetonitrile at a wavelength (274 nm) and band-pass (4 nm) yielding nearly linear UV response. Outer curves enclose a 10% error envelope about the best (center) curve. Concentrations were 10^{-6} M. Insert: Arrow and vertical lines indicate band-pass.

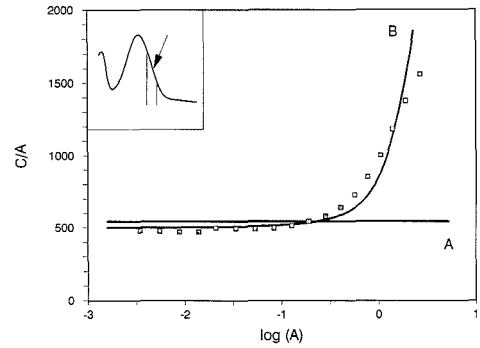

Figure 4. Comparison of steady-state UV calibration data (points) and calibration curves from chromatographic data using linear (curve A) and hyperbolic-sine (curve B, see text) models for 4-nitrotoluene in acetonitrile at a wavelength (304 nm) and band-pass (40 nm) yielding strongly nonlinear UV response: concentrations in 10^{-6} M; insert: arrow and vertical lines indicate band-pass.

10% higher and lower in absorbance than the center curve. The spline oscillates slightly in C/A (but not in C) to accommodate noise in the peak-shape data. Note that because the peak-shape curve and steady-state points in Figure 3 are determined from independent data sets, the spline shape does not correlate well with the steady-state calibration noise. The spline-model curve actually has larger error $E(P)$ than does the linear-model curve (0.007 20 vs 0.006 60), indicating that the model offers no improvement over the linear model for this analyte-wavelength-bandwidth combination.

The data set taken at 274-nm wavelength and 40-nm bandwidth as well as that taken at 304-nm wavelength and 4-nm bandwidth yield essentially linear calibration curves and thus behave very much like the above linear case. However, chromatographic peaks measured at the spectral inflection point (304 nm) and wide bandwidth (40 nm, rectangular) yield a best linear calibration curve (Figure 4, curve A) which does not match the steady-state points. The two-parameter hyperbolic-sine function fares much better (Figure 4, curve B), and the best such calibration curve matches the independently measured steady-state points within about 10% everywhere. The Akima-spline curve (Figure 5, center curve) matches the steady-state data even more closely, within a 10% error en-

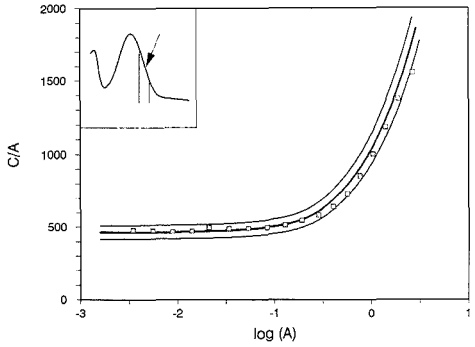

Figure 5. Comparison of steady-state calibration data (points) and calibration curve from chromatographic data using Akima spline model (center curve) for 4-nitrotoluene in acetonitrile at a wavelength (304 nm) and band-pass (40 nm) yielding strongly nonlinear UV response. Outer curves enclose a 10% error envelope about the best (center) curve. Concentrations were 10^{-6} M. Insert: Arrow and vertical lines indicate band-pass.

velope (outer curves) for all but one data point. The error function values $E(P)$ for the linear, hyperbolic-sine, and Akima-spline model curves are 0.0848, 0.0120, and 0.000 937, respectively.

While the spline model function may oscillate due to unavoidable errors in the peak shape data, the extent of this oscillation has been small in our experience and should not cause serious problems unless the curve's derivatives are themselves important to the analyst. Thus, since the spline model generally performs at least as well as the linear and hyperbolic-sine models and since the minor oscillations and computational time have not caused us problems, we recommend the spline model's use. Though selection of abcissa values for the adjustable ordinates defining a spline is somewhat arbitrary, use of a geometric progression of abcissa values covering the likely range of detector responses has performed well in our hands. One spline point per decade of response (four points for three decades) has been sufficient.

The simplex method gave the best model parameter values, which were independent of the initial parameter estimates, a reasonable indication of robustness. In test cases using the hyperbolic-sine (two-parameter) and spline-model (four-parameter) models, initial parameter values giving a linear curve always converged to known best parameter values within a reasonable number of iterations. However, the search path of the spline model can be tortuous, and the current error function value $E(P)$ may not decrease smoothly. For example in Figure 6, if the search progress were judged only on the basis of unchanging $E(P)$, the parameter set at iteration 50 might have been taken as the best set. However, even though $E(P)$ is nearly constant within a contracting phase (e.g., Figure 6, cycles 35–70), it is also true that the parameter-space simplex contracts preferentially in certain directions; that is, it is preparing to project into a different (and hopefully better) region of parameter space. It is clear that the best set has clearly not been found by cycle 50 in Figure 6 since $E(P)$ eventually decreases by two-thirds, after which it does not decrease further. This illustrates the danger of stopping the search prematurely. While it is common practice to limit simplex searches to no more than, say $100N_P$ to $200N_P$ iterations in order to prevent waste of computer time, it may also be wise not to accept apparent convergence before another lower limit, say $30N_P$ to $50N_P$ iterations. Nearly all simplex searches performed in this work achieved final convergence after $50N_P$ to $100N_P$ iterations.

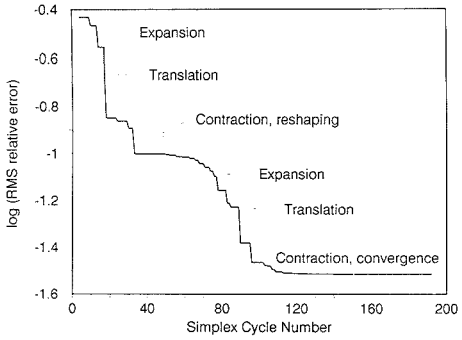

Figure 6. Logarithm of the error function $E(P)$ value (eq 2, text) during refinement of the parameter set P defining a spline-model calibration curve for 4-nitrotoluene in acetonitrile at a wavelength (304 nm) and band-pass (40 nm) yielding strongly nonlinear UV response. Labels within the figure specify the behavior of the simplex during the refinement.

In summary, the HPLC test results indicate that the present method can extract linear or nonlinear absolute calibration curves from peak shape data with an accuracy of no worse than 5–10%. Indeed, a substantial part of the difference between the peak-shape-derived calibration curves and the steady-state data points may be attributable to error in the steady-state data. It it quite possible that the errors of direct, steady-state calibration and of the present method may be similar or even greater in the steady-state case.

Comparison with Steady-State Calibration Methods. The calibration approach presented here is most useful for studies where concentration vs detector response calibration is important and where steady-state methods are difficult. Because of the utterly different types of data taken in the two methods, one must attend to their accuracies in different ways.

In GC, accurate pulse injections are very much easier to achieve than are accurate steady-state concentrations delivered to the detector. Calibration using the steady-state approach must refer to an independently known quantity; for example the rate at which analyte mass evaporates from a reservoir. Since gas chromatographs are already designed to inject accurately a known volume of solution of known concentration, the present method is experimentally more natural even though computationally more demanding.

However, even in other flow methods like HPLC determination of nonlinear isotherms, the present approach will be useful for reasons other than convenience. Less solvent and far less analyte will be used in the present method than in the steady-state methods. This advantage of the present method is most important when the analyte is expensive or in limited supply, when solvents are expensive or are used in large volume, as in preparative-scale chromatography, or when instrument-use or labor costs are high enough to offset the computational costs. Balances between the costs of experiment- and computation-intensive methods will likely increasingly favor computation over the next few years.

Minor amounts of linear base-line drift are easily corrected for in the present methods. In steady-state methods, drift affects the data very much more because drift's contribution to the measured response is cumulative. By contrast, in the present method it is possible (and advisable) to check that base-line levels are equal before and after each peak used.

The present method is in some ways more demanding than steady-state calibration. The computational demands are obviously larger than steady-state methods even when interpolation is included in the latter. Since the flow rate is critical to the estimates of the amounts injected (eq 1), its magnitude must be well-known at least within each peak. Also, transient noise like voltage spikes may be more critical in the present method, depending on where it falls within the chromatogram, than it is in the steady-state method. Spikes in the steady-state case can generally be eliminated either by inspection, by using Winsorized estimates of the mean response at each concentration (*20*), or by eliminating the highest and lowest data points before averaging responses at a given concentration. Finally, to achieve an unambiguous solution using the present method, the number of chromatographic peaks N used must be larger than the number of parameters N_P in the calibration curve model expression. This last restriction is not difficult to achieve since even in the spline model N_P is only 4.

The present method may be further adapted to specific calibration requirements. For example, one could use Bayesian methods (*21*) during data collection to help select the next injection amount so that the most information about the curve can be obtained in the fewest injections. In another example, if the analyte is expensive or limited in availability, one could adapt reversed-flow calibration techniques (*22*) to the present methods. As the analyte zone is passed repeatedly through the detector, it will become broader and less concentrated. In principle a single injection could yield a whole range of peak shapes and thus an absolute calibration curve.

ACKNOWLEDGMENT

We thank ADA, Inc., for the gift of software permitting the fast transfer of raw data from the chromatograph to the VAX computers. We acknowledge the University of Tennessee Computing Center's support of the computational effort.

LITERATURE CITED

(1) Janssens, G. *Anal. Chim. Acta* **1979**, 449–453.
(2) Wegschneider, W. Trace Residue Analysis. *ACS Symp. Ser.* **1985**, *No. 284*, 167–181.
(3) Dondi, F.; Gonnord, M.-F.; Guiochon, G. *J. Colloid Interface Sci.* **1977**, *62*, 303–315.
(4) Muniak, W.; Witkiewicz, Z.; Woryna, E.; Kusinska, E.; Twardowski, A.; Goca, B. *J. Chromatogr.* **1988**, *436*, 323–327.
(5) Kurtz, D. A.; Rosenberger, J. L.; Tamayo, G. J. Trace Residue Analysis. *ACS Symp. Ser.* **1985**, *No. 284*, 133–165.
(6) Dorschel, C. A.; Ekmanis, J. L.; Oberholtzer, J. E.; Warren, F. V. W., Jr.; Bidlingmeyer, B. A. *Anal. Chem.* **1989**, *61*, 951A–968A.
(7) Grimsrud, E. P. *J. Chromatogr.* **1980**, 117–125.
(8) Pfeiffer, C. D.; Larson, J. R.; Ryder, J. F. *Anal. Chem.* **1983**, *55*, 1622–1624.
(9) Mitchell, D. A. Trace Residue Analysis. *ACS Symp. Ser.* **1985**, *No. 284*, 115–131.
(10) Carr, P. W. *Anal. Chem.* **1980**, *52*, 1746–1750.
(11) Schwartz, L. M. *Anal. Chem.* **1983**, *55*, 1424–1426.
(12) Foley, J.; Dorsey, J. *Anal. Chem.* **1983**, *55*, 730–737.
(13) Schudel, J. V. H.; Guiochon, G. *J. Chromatogr.* **1988**, *457*, 1–12.
(14) Akima, H. *J. Assoc. Computing Mach.* **1970**, *17*, 589–602.
(15) Nelder, J. A.; Mead, R. *Computer J.* **1964**, 308–313.
(16) Aberg, E. R.; Gustavsson, A. G. T. *Anal. Chim. Acta* **1982**, 39–53.
(17) Dose, E. *Anal. Chem.* **1987**, *59*, 2420–2423.
(18) Dose, E. V.; Guiochon, G. *Anal. Chem.* **1989**, *61*, 2571–2579.
(19) Colin, H.; Guiochon, G.; Martin, M. In *Practice of High Performance Liquid Chromatography*; Engelhardt, H., Ed.; Springer-Verlag: Berlin, 1988; esp. pp 30–31.
(20) Dixon, W. J.; Massey, F. J., Jr. *Introduction to Statistical Analysis*, 3rd ed.; McGraw-Hill: New York, 1969; sect. 16-4.
(21) Unadkat, J. D.; Beal, S. L.; Sheiner, L. B. *Anal. Chim. Acta* **1986**, *181*, 27–36.
(22) Katsanos, N. A.; Karaiskakis, G. *Analyst* **1987**, 809–813.

RECEIVED for review November 2, 1989. Accepted January 17, 1990. This work has been supported in part by grant DE-FG05-86ER13487 from the U.S. Department of Energy, Office of Energy Research, and by the cooperative agreement between the University of Tennessee and Oak Ridge National Laboratory.

Thermal Analyses of Compound Semiconductors Using Differential Scanning Calorimetry. Application to Compositional Analyses of Cathodically Electrosynthesized Cadmium Telluride

Wen-Yuan Lin, Kamal K. Mishra, Erik Mori, and Krishnan Rajeshwar*

Department of Chemistry, The University of Texas at Arlington, Arlington, Texas 76019-0065

Differential scanning calorimetry (DSC) was used, we believe for the first time, for compositional analyses of a compound semiconductor. The Cd–Te system electrosynthesized by a cathodic route was used as a model to define the limits and power of this analytical tool. Thus changes in the composition of the electrodeposited material were monitored as a function of deposition potential. Samples deposited at potentials ≥−600 mV (vs SCE) contained excess Te in addition to CdTe and those synthesized at −696 and −698 mV contained both excess Cd and Te. The composition switched abruptly to a large excess of Cd near 700 mV. The excess Cd and Te were detected and quantitated by their characteristic DSC signals at 318 and 447 °C, respectively. Changes in compositional profiles as a function of solution hydrodynamics and TeO_2 concentration as well as chemical reactions between the excess Cd and Te are described.

INTRODUCTION

Compositional variability and nonstoichiometry are frequent problems associated with the growth of compound semiconductors. For example, formation of Te precipitates has been observed in thin films and single crystals of CdTe and $Hg_{1-x}Cd_xTe$ grown by a variety of techniques including vacuum evaporation (*1*), Bridgman (*2, 3*), and electrodeposition (*4, 7*). Tellurium precipitation is deleterious to many optical and optoelectronic device applications of these materials (*2*). Thus the development of analytical techniques for the compositional analyses of compound semiconductors has technological implications. Table I presents a summary of the state-of-the-science. Many candidates among the techniques listed (e.g. atomic spectroscopies, polarography) yield only the *total* amount of a given species, e.g. Te in CdTe. On the other hand, techniques such as XRD, TEM, and XPS which are sensitive to the *chemical* state of the semiconductor component (i.e., free Te vs Te in CdTe) are semiquantitative in nature and are severely limited by analysis and sample factors such as crystallinity (XRD, TEM) and peak resolution (XPS). The Raman microprobe has been effective for the detection of Te precipitates in CdTe crystals (*2*) and appears to be a technique of much promise, although its quantitative capabilities remain to be established.

There is clearly a need for identifying and evaluating new techniques for the compositional analyses of compound semiconductors. This paper explores the applicability in this regard of thermal analysis techniques such as differential scanning calorimetry (DSC). Since its discovery in 1964, DSC has been successfully applied to the analysis of a wide variety of materials; reviews of these applications are available (*18–20*). The predecessor of this technique, namely differential thermal analysis (DTA), has also played a pivotal role in the elucidation of phase diagrams (including many involving components of importance to semiconductor technology, cf. refs 21 and 22). Reisman has described how DTA could be used to study the thermal synthesis of CdSe and other group II–VI counterparts from the component elements (*23*). To our knowledge, the utility of thermal analysis techniques such as DSC for semiconductor compositional analyses has not been previously explored. In this paper, we will describe the use of DSC as a semiconductor analysis tool with electrosynthesized CdTe as a model system. The electrosynthesis of CdTe was carried out via a cathodic route (*24, 25*).

* Author for Correspondence.

EXPERIMENTAL SECTION

Differential scanning calorimetry was performed on a Du Pont 9900 thermal analysis system fitted with the Model 910 accessory module. The software supplied by the manufacturer was used for the analyses of DSC thermograms. Commercial samples of In and Zn (99.999% purity) were used as calibration standards. The melting transitions of In and Zn at 156.6 and 419.5 °C have enthalpies of 28.4 and 109 J/g, respectively (*26*). The melting endotherms were usually recorded after one or two initial "conditioning" heat–cool cycles through the transition. Nitrogen was flushed through the DSC cell at the rate of ca. 80 mL/min. Sealed Al sample pans were used in all the cases. Nominal sample mass was ca. 1 mg. A heating rate of 15 °C/min was employed.

A standard three-electrode configuration was employed for both stationary and hydrodynamic deposition of the CdTe thin films. The voltammetric data were displayed on a Houston Instrument Model 2000 X-Y recorder. The rotating disk electrode (RDE) assembly consisted of a Model RDE-4 Pine Instrument bipotentiostat and an AFMSRX rotator spun at a rate of 400 rpm. An EG&G Princeton Applied Research Model 273 potentiostat was used for the stationary deposition mode. A Pt disk electrode (1.1 cm diameter) was used as the substrate for hydrodynamic deposition experiments. Its surface was pretreated using literature procedures (*27*). Titanium foil (Alfa) was used as the substrate for the stationary deposition experiments. Its surface was initially sanded on a 320-grit Carbimet disk (Buehler), subsequently polished with Al_2O_3 and finally rinsed with distilled deionized water. The immersed foil area was ca. 6 cm^2, and the amount of electrodeposited material on the foil was measured coulometrially (10–25 C). The electrodeposited material was scraped off from the substrate and then dried in an air oven at ca. 90 °C for 8 h to remove moisture.

Electrodeposition of CdTe, unless otherwise noted, was carried out at 25 °C from a 0.5 M H_2SO_4 matrix containing 0.5 M of $CdSO_4$ (Alfa) and 5.0×10^{-4} M of TeO_2 (Alfa, Puratronic Grade). All potentials herein are quoted with respect to a saturated calomel electrode (SCE) reference.

RESULTS AND DISCUSSION

Electrodeposition Chemistry. As discussed elsewhere (*28*), Pourbaix diagrams identify the major Te species at pH ≤ ~2 to be $HTeO_2^+$. The important electrochemical and chemical reactions pertinent to this study are

$$Cd^{2+} + 2e^- = Cd^0;\ E_1^\circ = -0.64\ V \quad (1)$$

$$HTeO_2^+ + 3H^+ + 4e^- = Te^0 + 2H_2O;\ E_2^\circ = 0.31\ V \quad (2)$$

$$Cd^0 + Te^0 = CdTe;\ \Delta G^\circ = -9.97 \times 10^4\ J/mol \quad (3)$$

As discussed by Kröger (*25*), the negative free energy of compound formation effectively shifts the reduction of Cd^{2+}

0003-2700/90/0362-0821$02.50/0

Table I. A Summary of Analytical Techniques Available for Compositional Analyses of Compound Semiconductors

technique	comments	refs[a]
Auger electron spectroscopy (AES)	suffers from matrix effects; elemental oxidation state not readily available	5–8
X-ray photoelectron spectroscopy (XPS, ESCA)	spectral resolution poor	34
electron probe for microanalysis (EPMA)	requires rather thick (1 μm) samples to avoid substrate interference; yields only total assays	6, 9, 10
energy dispersive analysis of X-rays (EDAX)	matrix effects rather severe; yields only total species content	11, 12
low-energy electron-induced X-ray spectrometry (LEEIXS)	elemental oxidation state not available	13
X-ray diffraction (XRD)	films must be crystalline	4, 5, 7
transmission electron microscopy (TEM)	similar problems as above	–
neutron activation analysis	yields only total species content	8
atomic spectroscopics	same handicap as above	8
particle-induced X-ray emission	yields only total species content; matrix effects	8
polarography	yields only total species content	14–17
Raman microprobe	able to discriminate species chemical state; quantitation capabilities as yet undefined	2

[a] These example studies have largely been drawn from literature on the CdTe system.

ions to potential regimes positive of the "free" $Cd^{2+} \rightarrow Cd^0$ reduction (reaction 1). Thus the underpotential deposition of Cd^{2+} as CdTe may be represented by reaction 4.

$$Cd^{2+} + Te^0 + 2e^- = CdTe;\ E_4° = -0.10\ V \qquad (4)$$

The above thermodynamic expectations have been verified by experiment both by us (*6*, *10*, *12*, *28*, *29*) and by other authors (*24*, *25*), and CdTe formation has been detected by XRD (*4*, *5*, *7*), electron spectroscopies (*5–8*), X-ray fluorescence (EDAX) (*11*, *12*), (EPMA) (*6*, *9*, *10*), and cyclic photovoltammetry (*30*). Panicker et al. (*24*) characterized the film composition in terms of their rest potentials, E_{rest}, in the deposition bath. Thus films with $E_{rest} \leq -0.66$ V contained almost exclusively Cd^0, those with $E_{rest} = \sim -0.11$ V were pure Te^0, samples wtih $E_{rest} \leq \sim -0.30$ V consisted of n-type CdTe (Cd rich), and those with $E_{rest} \geq \sim -0.30$ V were comprised of p-type CdTe (Te rich). Such gradation of composition through the deposition potential range (see below) has subsequently been verified by other authors (*4*, *31*).

Figure 1 contains a representative cyclic voltammogram for a Ti electrode in contact with the electrodeposition bath containing Cd^{2+} and $HTeO_2^+$ ions. On the basis of our previous work (*28*, *29*), we assign the initial wave at –0.30 V (which culminates in a plateau) to reaction 2. The discontinuity in this wave at ~–0.50 V is attributable to the underpotential assimilation of Cd^{2+} ions into the preformed Te layer as CdTe (reaction 4). Finally, the sharp cathodic feature, the nucleation loop, and the anodic stripping wave on the return scan ~–0.70 V originate from reaction 1. Note that reactions 2 and 4 are observed at potentials negative to the thermodynamically predicted values underlining the kinetics limitations associated with them. On the other hand, reaction 1 appears to be facile and occurs closer to equilibrium. Similar arguments may be advanced to account for the discrepancy between our observations from scanning experiments and the data from the rest potential measurements of Panicker et al. (*24*).

To evaluate the utility of DSC as a compositional analysis tool, a series of samples were electrodeposited at potentials ranging from –0.20 to ~–0.75 V, and then analyzed by DSC. To define the limiting situations and for quantitative analyses, these data were also compared with those obtained for pure Te, Cd, and CdTe as reference standards. While the first two samples were electrodeposited from baths wherein Cd^{2+} and TeO_2 were omitted respectively, an authentic commercial sample of CdTe (in powder form) was used as the standard for DSC runs which are discussed next.

DSC Thermograms of Cd, Te, and CdTe. In order that DSC proves to be efficacious for the detection and quantitation

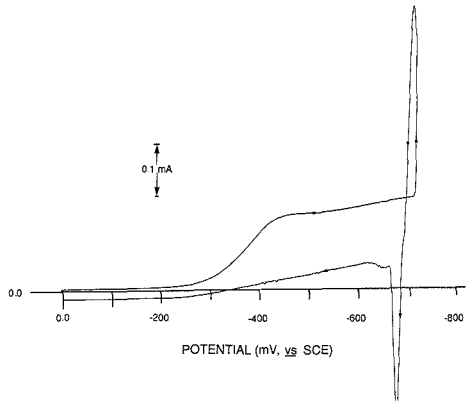

Figure 1. Cyclic voltammogram (potential scan rate, 0.01 V s^{-1}) at a Ti foil electrode in 0.5 M H_2SO_4 containing 5 × 10^{-4} M TeO_2 and 0.5 M $CdSO_4$.

of these three species, the analytical signals (i.e. endotherms) originating from them must be preferably located at distinctly different temperature regimes. A rough analogy here is the analytical situation involving the spectroscopic analysis of a mixture using analytical peaks of the components at characteristic wavelengths. Parts a and b of Figure 2 contain DSC traces for Cd and Te, respectively. The melting transitions of Cd and Te are clearly well separated. The transition temperatures of 318 and 447 °C for Cd and Te (with an associated estimation uncertainty of ±1 °C) are in reasonable agreement with previously published (*23*) DTA values of 321 and 450 °C, respectively. By use of Zn as calibration standard, fusion enthalpies of 59 and 140 J/g were determined for Cd and Te, respectively. These may be compared with previously quoted values of 58.4 and 137.4 J/g (*32*).

A DSC scan of pure CdTe revealed no features up to 500 °C—an expected behavior since this compound melts at 1041 °C (*32*), and no solid-state (crystallographic) transformations are known in the range from 25 to ~500 °C. Thus, in the Cd–Te system, the expectation is that excess Cd and Te may be detected by the presence of characteristic DSC features at 318 and 447 °C. A quantitative estimate of these components is available from the areas encompassed by the observed DSC peaks, and the (known) fusion enthalpy of the pure component (cf. Figure 2a,b).

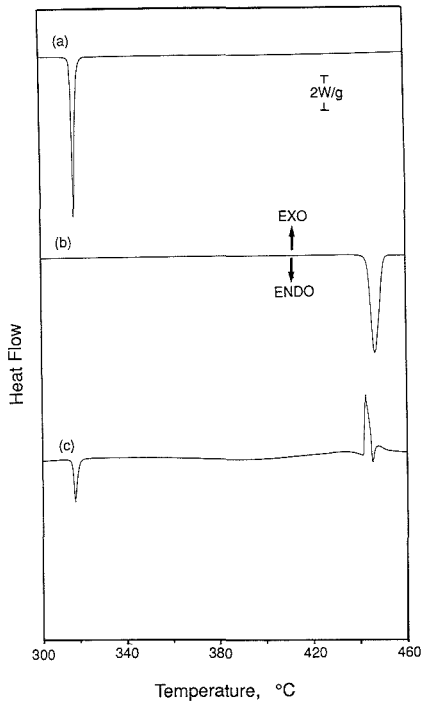

Figure 2. DSC thermograms (heating rate, 15 °C/min) for electrodeposited samples of (a) Te, (b) Cd, and (c) a mixture of Cd and Te in 50:50 weight ratio.

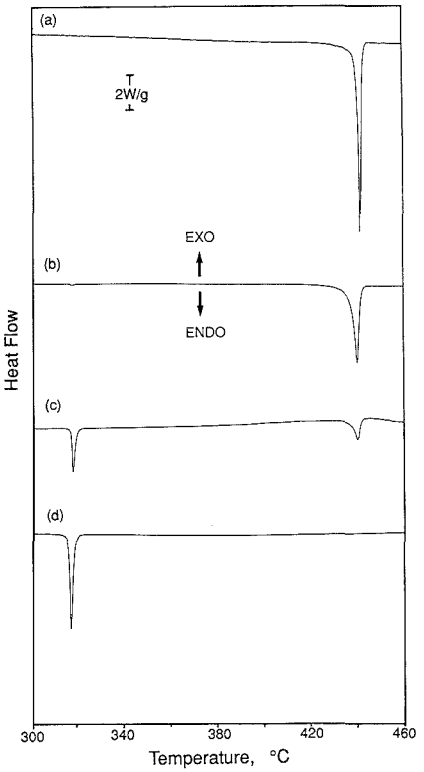

Figure 3. DSC thermograms (heating rate, 15 °C/min) for electrodeposited films on Ti substrate containing Te, Cd, and CdTe. The deposition potential (in mV) was (a) −600, (b) −696, (c) −698, and (d) −700.

To assess the quantitative efficacy of DSC for excess Te and Cd determinations, a series of authentic mixtures of CdTe with Te and Cd were respectively prepared and then analyzed by this technique. From these tests, we estimate that 5% excess (by weight) of Te may be quantitated with a nominal error of ±5%, 2% excess of this species at ±7% and 1% detected with an uncertainty of ±11%. Similar performance levels were observed for Cd. The fact that the detection uncertainties are comparable in the two cases in spite of the rather large difference in the magnitude of the transition enthalpies (see above) suggests that a major portion of the analytical error resides with weighing and sample preparation. At this stage of the work we have not further optimized the variables in the quantitation procedure (e.g. sample mass) such that the sensitivity quoted above should be regarded as conservative; i.e. further improvements ought to be possible.

The data in Figure 2 on the Cd–Te system underline the sensitivity of DSC to the chemical state of a particular species, i.e. both Cd and Te manifest *distinctly different* signals depending on whether they are present in the elemental state or as a compound (CdTe). This is a feature that only four (XRD, TEM, XPS, Raman microprobe) of the many techniques listed in Table I share. (Auger electron spectra are sensitive in many instances to the chemical bonding situation, for e.g. Si vs SiO_2; cf. ref 33. However, the consequent alterations in the line shape profiles are subtle and not readily amenable to quantitative analyses.) Techniques such as XRD and TEM will not work if the samples are highly amorphous. In XPS, the shifts in the binding energies with oxidation state are certainly not very large (for example, 572.7 eV for Te in the elemental state and 572.1 eV for the −2 oxidation state, cf. ref 34), and quantitation requires peak deconvolution procedures. Methods based on optical spectroscopies (such as Raman scattering) do have the required molecular specificity for qualitative identification. As mentioned before, however, the quantitative capabilities of the Raman microprobe remain to be established.

It must also be recognized that while complete resolution of the analytical signals due to component species (the case with the model Cd–Te system here, cf. Figure 2) does prove to be an analytical convenience, it is conceivable that thermal signals could be overlapped in other systems. Even in these cases, DSC could be effectively used for compositional analyses, for example by appropriate control of variables such as purge gas composition, temperature scan rate, etc. (*35*). A further analogy may be drawn here with the matrix solution techniques employed for the analysis of multicomponent mixtures by optical spectroscopics. Again, at this (relatively infant) stage of development of the semiconductor analysis protocol by DSC, we have chosen not to consider such complications.

DSC Analyses of Electrodeposited Samples. Figure 3 contains DSC thermograms for samples electrodeposited at four (increasingly negative) potentials starting at −600 mV. Comparison with Figure 2 reveals that the sample electrodeposited at −600 mV contains excess Te (in addition to CdTe), those electrosynthesized at −696 and −698 mV contain both Cd and Te in the (free) elemental state, and the sample formed at −700 mV contains a large excess of Cd. Further quantitative estimates by DSC are contained in Figure 4 which

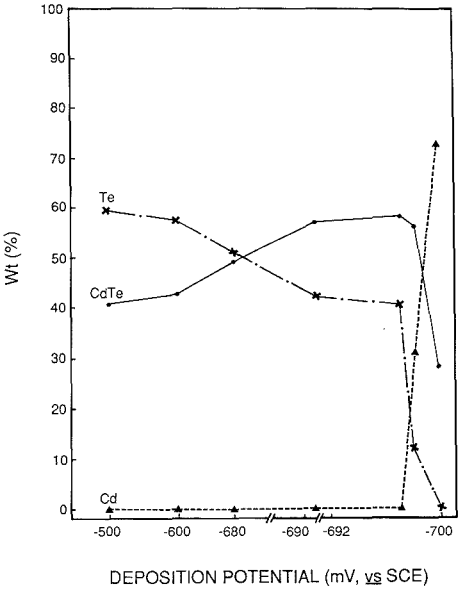

Figure 4. Effect of deposition potential on the electrodeosit composition. The material was electrodeposited on Ti substrate from a stationary bath. The CdTe content was determined by difference.

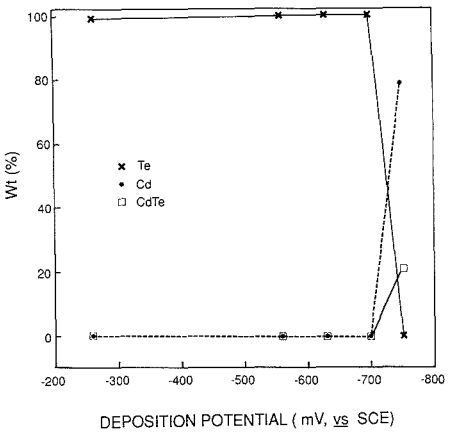

Figure 5. Same as Figure 4 but on a Pt rotating disk cathode.

also includes data on other specimens not shown in Figure 3. It is quite remarkable how the composition of the electrodeposited material switches dramatically over a potential range of 4–5 mV near −700 mV! While models had previously been advanced which predicted such abrupt changes in composition for CdTe (*36*), experimental verification was hitherto not available.

Influence of Te Concentration and Solution Hydrodynamics on Electrodeposit Composition. The Kröger model (*24, 25*) emphasizes the need to maintain a low ($\leq\sim10^{-4}$ M) concentration of the Te species and a high concentration of Cd^{2+} ions in the electrolyte in order to deposit equal amounts of Cd and Te. The interfacial concentration of $HTeO_2^+$ thus is maintained close to zero during the deposition process. The influence of stirring rate on the current density was briefly studied by Panicker et al. (*24*), although no corresponding film analyses were made. We thought it would be of interest to examine the sensitivity of the electrodeposit composition to solution hydrodynamics and TeO_2 concentration. To do this, the data described in the preceding section were compared with the results from experiments employing a 2-fold increase in the TeO_2 concentration and a rotating Pt cathode. The results from DSC analyses of such samples are contained in Figure 5.

Contrary to the previous case (cf. Figure 4), the electrodeposit composition changes from 100% Te to 80% excess Cd within a range of ~50 mV near −700 mV. In other words, there is negligible formation of CdTe when the solution is stirred and a relatively high concentration of TeO_2 is employed! The electrodeposition of Te^0 is enhanced by 1–2 orders magnitude by a combination of solution stirring and the high TeO_2 concentration. However, the underpotential deposition of Cd as CdTe (reaction 4) is kinetically sluggish and cannot effectively compete under these conditions. When potentials close to where free Cd^0 deposition is thermodynamically possible (reaction 1) are accessed, this kinetically facile reaction (see above) takes over and the composition abruptly switches to a large excess of Cd.

The dramatic difference in the compositional profiles in Figures 4 and 5 provides rather conclusive experimental verification for the essential correctness of the Kröger model (*24, 25*). While substrate differences (Ti in the stationary deposition case vs Pt in the experiment described in the preceding paragraphs) could possibly also play a role, we certainly do not believe it to be the overriding factor.

Chemical Reaction between Free Cd and Te. A possible complication that must be considered is chemical reaction between the *excess* component species in the free (elemental) state; i.e. in the model system considered here, it is conceivable that excess Cd could react with excess Te to yield CdTe in situ.

The DSC thermogram in Figure 2c presents such a situation wherein a mixture of Cd and Te was utilized as the starting material. A chemical reaction between Cd and Te is signaled by an exothermic signal in the vicinity of the Te fusion. The heat released in the chemical reaction (reaction 3) swamps the endothermic effect from Te fusion. Thus a closer examination of the Te DSC signal reveals a complex shape with an endothermic tendency preceding the exothermic peak and a further endothermic deflection at the trailing edge of the exotherm. Apparently the chemical reaction between Cd and Te is promoted by Te fusion. A similar exotherm at 429 °C (heating rate, 2.5 °C/min) was noted by Reisman and Berkenblit in their DTA study (*23*). Reheat cycles of DSC scans similar to those contained in Figure 2c reveal attenuation of the signals from the free Cd and Te resulting from their conversion to CdTe. In fact, quantitative analyses of such trends permit elucidation of the chemical reaction kinetics between Cd and Te as a function of time and temperature. Such experiments are in progress and will be described in a future report.

It is interesting to note the absence of exothermic effects (due to CdTe formation) under the experimental conditions pertaining to Figure 3b,c. Particularly noteworthy is the situation in Figure 3c, wherein although both Cd and Te are present in noticeable amounts in the elemental state, the topochemistry is presumably such that in situ formation of CdTe is hindered. We believe that the CdTe, which is also present as the third component in this case, precludes effective contact of the Cd and Te phases.

Finally, many chalcogens such as Te are known to undergo amorphous to cyrstalline transitions. For example, Okuyama

and Kumagai (*37*) noted a "rapid and drastic" decrease in electrical resistivity of vacuum-evaporated Te thin films on a glass substrate at temperatures ranging from 10 to 40 °C—an effect that these authors attributed to crystallization of the amorphous samples. Amorphous-to-glass and glass-to-crystalline transitions have been observed by DTA at ~50 and ~110 °C for Se prior to melting at ca. 220 °C (*38–40*). Exothermic effects from crystallization of Te were not noted in the DSC scans for any of our Te samples. It is thus likely that crystallization occurred in our samples close to ambient temperatures. By the same token, the occurrence of crystallization concomitant with fusion (an effect that would introduce significant error into the quantitation of Te, see above) is also considered extremely unlikely. Even for electrodeposited CdTe, annealing at 200 °C appears to be sufficient to induce crystallinity as monitored by XRD (*41*).

ACKNOWLEDGMENT

Preliminary experiments were conducted by Ranjana Segal. We also thank the Du Pont Co. for the donation of some of the thermal analysis equipment used in this work.

LITERATURE CITED

(1) Fujii, M.; Kawai, T. *Sol. Energy Mater.* **1988**, *18*, 23–35.
(2) Shin, S. H.; Bajaj, J.; Moudy, L. A.; Cheung, D. T. *Appl. Phys. Lett.* **1983**, *43*, 68–70.
(3) Wada, M.; Suzuki, J. *Jpn. J. Appl. Phys.* **1988**, *27*, L972–975.
(4) Takahashi, M.; Uosaki, K.; Kita, H. *J. Appl. Phys.* **1984**, *55*, 3879–3881.
(5) Takahashi, M.; Uosaki, K.; Kita, H.; Suzuki, Y. *J. Appl. Phys.* **1985**, *58*, 4292–4295.
(6) Bhattacharya, R. N.; Rajeshwar, K. *J. Appl. Phys.* **1985**, *58*, 3590–3593.
(7) Llabrés, J.; Delmas, V. *J. Electrochem. Soc.* **1986**, *133*, 2580–2585.
(8) Lyons, L. E.; Morris, G. C.; Horton, D. H.; Keyes, J. G. *J. Electroanal. Chem. Interfacial Electrochem.* **1984**, *168*, 101–116.
(9) Shih, I.; Qui, C.-X. *Mater. Lett.* **1985**, *3*, 446–448.
(10) Bhattacharya, R. N.; Rajeshwar, K.; Noufi, R. N. *J. Electrochem. Soc.* **1985**, *132*, 732–734.
(11) Fatas, E.; Herrasti, P.; Arjona, F.; Camarero, E. G.; Medina, J. A. *Electrochim. Acta* **1987**, *32*, 139–148.
(12) Bhattacharya, R. N.; Rajeshwar, K.; Noufi, R. N. *J. Electrochem. Soc.* **1984**, *131*, 939–941.
(13) Rocke, A.; Montes, H.; Brissot, J.; Romand, M.; Josseaux, P.; Kirsch, de Mesmaeker *Appl. Surf. Sci.* **1985**, *21*, 12–28.
(14) Whitnack, G. C.; Donovan, T. M.; Ritchie, M. H. *J. Electroanal. Chem. Interfacial Electrochem.* **1967**, *14*, 197–204.
(15) Rao, G. S. R.; Reddy, S. J. *J. Indian Chem. Soc.* **1984**, *27*, 306–311.
(16) Rao, G. S. R.; Reddy, S. J. *Thin Solid Films* **1984**, *120*, 205–213.
(17) Darkowski, A.; Cocivera, M. *Talanta* **1986**, *33*, 187–189.
(18) Dollimore, D. *Anal. Chem.* **1988**, *60*, 274R–279R.
(19) McNaughton, J. L.; Mortimer, C. T. *MTP International Review of Science: Physical Chemistry Series 2*; Butterworths: London, 1975, Vol. 10.
(20) Wendlandt, W. W. *Anal. Chem.* **1984**, *56*, 250R–261R.
(21) Reisman, A.; Berkenblit, M.; Witzen, M. *J. Phys. Chem.* **1962**, *66*, 2210–2214.
(22) Sharma, R. C.; Chang, Y. A. *J. Cryst. Growth* **1988**, *88*, 193–204.
(23) Reisman, A.; Berkenblit, M. *J. Phys. Chem.* **1963**, *67*, 22–26.
(24) Panicker, M. P. R.; Knaster, M.; Kröger, F. A. *J. Electrochem. Soc.* **1978**, *125*, 566–572.
(25) Kröger, F. A. *J. Electrochem. Soc.* **1978**, *125*, 2028–2034.
(26) Kubaschewski, O.; Alcock, C. B. *Metallurgical Thermochemistry*, 5th ed.; Pergamon Press: Elmsford, NY, 1979.
(27) Adams, R. N. *Electrochemistry at Solid Electrodes*; Dekker: New York, 1969.
(28) Mori, E.; Baker, C. K.; Reynolds, J. R.; Rajeshwar, K. *J. Electroanal. Chem. Interfacial Electrochem.* **1988**, *252*, 441–451.
(29) Mori, E.; Rajeshwar, K. *J. Electroanal. Chem. Interfacial Electrochem.* **1989**, *258*, 415–429.
(30) Mishra, K. K.; Rajeshwar, K. *J. Electroanal. Chem. Interfacial Electrochem.* **1989**, *273*, 169–182.
(31) Takahashi, M.; Uosaki, K.; Kita, H.; Yamaguchi, S. *J. Appl. Phys.* **1984**, *60*, 2046–2049.
(32) *CRC Handbook of Chemistry and Physics*, 63rd ed.; CRC Press: Boca Raton, FL, 1982.
(33) Czanderna, A. W. *Methods of Surface Analysis*; Elsevier: Amsterdam, 1975.
(34) Kibel, M. H.; Kelly, C. G. *Mater. Austr.* **1987**, *11/12*, 15–17.
(35) Jang, G.-W.; Segal, R.; Rajeshwar, K. *Anal. Chem.* **1987**, *59*, 684–687.
(36) Engelken, R. D.; Van Doren, T. P. *J. Electrochem. Soc.* **1985**, *132*, 2910–2919.
(37) Okuyama, K.; Kumagai, Y. *Thin Solid Films* **1988**, *156*, 345–350.
(38) Kasap, S. O.; Juhasz, C.; Harwick, J. R. *Proceedings of the 3rd International Symposium of Industrial Uses of Se and Te*; Selenium-Tellurium Development Association: Darien, CT, 1984; pp 307–322.
(39) Bosnell, J. R.; Sounge, J. A. *J Mater. Sci.* **1972**, *7*, 1235–1243.
(40) Ludwig, W. *Proceedings of the 6th International Conference on Thermal Analysis*; Mackenzie, R. C., Ed.; Academic: New York, 1980; Vol. 1, pp 293–298.
(41) Valvoda, V.; Tousková, J.; Kindl, D. *Cryst. Res. Technol.* **1986**, *21*, 975–981.

RECEIVED for review November 17, 1989. Accepted January 16, 1990. This work was supported in part by the National Science Foundation (Grant MSM-86-17850).

Highly Stable Phospholipid/Cholesterol Electrode Coatings for Amperometric Monitoring of Hydrophobic Substances in Flowing Streams

Joseph Wang* and Ziling Lu

Department of Chemistry, New Mexico State University, Las Cruces, New Mexico 88003

Composite electrode coatings based on a mixture of phosphatidylcholine and cholesterol offer remarkable mechanical stability under vigorous hydrodynamic conditions. The greatly improved stability (over single-domain phospholipid layers) is attained without compromising the attractive permselective response of lipid electrodes. The enhanced stability is attributed to changes in the fluidity/packing associated with the presence of cholesterol. Due to its high stability, simplicity, and fast and permselective response, the coated electrode seems well-suited for flow measurements of hydrophobic compounds. Parameters affecting the film permeability and the amperometric response are explored in the presence of numerous solutes of biological and phamaceutical significance. Prevention of surface fouling (in the presence of surfactants) and applicability to selective assays of urine samples are illustrated. Such controlled access to the surface, based on solute polarity, greatly enhances the power of electrochemical flow detectors.

INTRODUCTION

Amperometric detection for flowing streams has proven to be a viable technique in many analytical problems demanding high sensitivity and selectivity (*1*, *2*). Further improvement in the performance of electrochemical detectors is highly desired to meet new challenges posed by clinical and environmental samples. One promising avenue to achieve such improvements is to design surface microstructures that meet specific detection needs (*3*, *4*).

Permselective coatings represent one direction by which modified electrodes can benefit flow analysis. This is accomplished by rejection from the surface of undesired, interfering species while allowing the transport of the analyte. The size or charge exclusion discriminative properties of polymeric coatings such as cellulose acetate (*5*, *6*), perfluorinated (*7*, *8*) or polyester (*9*) ionomers, or poly(vinylpyridine) (*10*) have been exploited successfully for flow measurements. Hence, high specificity toward small solutes or oppositely charged ones has been achieved in both flow injection and liquid chromatography operations. The prevention of surface fouling has been documented in the presence of various surfactants. New membrane barriers, based on different discrimination mechanisms, should provide new levels of selectivity to amperometric detectors.

This paper describes the properties, advantages, and utility of a glassy carbon thin-layer detector coated with a mixed lipid layer. Much research effort has been devoted recently to the development of electrode surfaces derivatized with hydrophobic materials (*11-14*). It has been shown that lipid coatings can prevent polar electroactive compounds from reaching the electrode surface but remain highly permeable to hydrophobic substances. Substantial improvements in the selectivity toward hydrophobic compounds have thus been demonstrated. Enhanced sensitivity has also been reported in connection with the hydrophobic accumulation into the lipid layer. Such properties, that are very attractive for flow analysis, have been illustrated by using cast films of palmitic or stearic acids (*13*, *14*) and particularly phosphatidylcholine (*11*, *12*), for voltammetry under batch (static) conditions.

A major obstacle to the development of lipid-based flow detectors has been the poor mechanical stability of the lipid layer. Such films rapidly lose their integrity under vigorous hydrodynamic conditions, which characterize amperometric detection. Several studies reported on difficulties in keeping lipid layers intact even under static conditions (*11*, *12*). Unlike short-term batch experiments, the long-term stability of the attached layer is a key factor for the performance of flow detectors. We have observed that a composite coating material, consisting of a mixture of phosphatidylcholine (PC) and cholesterol (CH), offers significantly higher mechanical stability than films of PC alone. It is well-known that doping of phospholipid membranes with steroids offers a useful means for internal modification of membrane parameters such as molecular packing or fluidity (*15-18*). In particular, the reduced water penetration and condensed packing thus obtained greatly enhance the mechanical strength. The present study illustrates that cast PC/CH coatings exhibits remarkable stability, while maintaining attractive permselective properties based on polarity. We wish to report on these observations, as well as on the features and analytical utility of PC/CH-coated amperometric detectors, in the following sections.

EXPERIMENTAL SECTION

Apparatus. The flow injection system consisted of the carrier reservoir, a Rheodyne Model 7010 injection valve (10-μL sample loop), interconnecting Teflon tubings, and a glassy carbon thin-layer detector (Model TL-5, Bioanalytical Systems (BAS)). All potentials are reported vs a Ag/AgCl reference electrode (Model RE-1, BAS). Flow of the carrier solutions was maintained by gravity. Some experiments used a rotating disk electrode (Model DDI 15, Pine Instruments). Experiments were conducted with an EG&G PAR Model 364 polarographic analyzer in connection with a Houston Omniscribe chart recorder.

Reagents. All solutions were prepared with double-distilled water. Ascorbic acid (Baker), cholesterol, L-α-phosphatidylcholine (Type XI-E), acetaminophen, cysteine, promethazine, uric acid, chlorpromazine, trimipramine, tyrosine, desipramine, and perphenazine (Sigma) were used without further purification. The supporting electrolyte/carrier solution was a 0.05 M phosphate buffer (pH 7.4). The urine sample was obtained from a healthy volunteer and diluted with the supporting electrolyte solution.

Procedure. Before its modification the glassy carbon surface was hand-polished with a 0.05-μm alumina slurry, rinsed with double-distilled water and sonicated in a water bath for 2 min. The "mixed" PC/CH solution was prepared by adding the desired amount of CH (usually 12 or 18 mg) to 1 mL of chloroform solution containing 10 mg of PC. The electrode was coated by placing (with a micropipet) 5 μL of the mixed PC/CH solution (to cover the active disk and its surroundings) on the electrode and allowing the solvent to evaporate. The resulting coating had thickness of about 2 μm. Ten microliters was employed for coverage of the rotating disk electrode. The solvent was allowed to evaporate in air for 5 min. Analogous experiments were peformed with

0003-2700/90/0362-0826$02.50/0

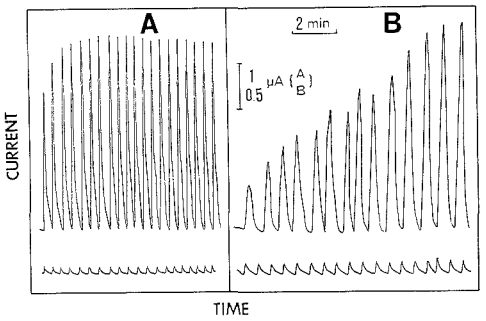

Figure 1. Detection peaks for repetitive injections of 5×10^{-4} M uric acid (A) and acetaminophen (B) solutions at the PC/CH- and PC-coated electrodes (bottom and top, respectively): applied potential, +0.8 V; flow rate, 0.4 mL/min; electrolyte (sample and carrier), 0.05 M phosphate buffer (pH 7.4). The composite layer contained 12 (A) and 18 (B) mg/mL CH.

single-domain PC or CH films, prepared by coating the glassy carbon surface with similar volumes of 10 mg/mL PC or 12 mg/mL CH solutions, respectively.

RESULTS AND DISCUSSION

The ability of hydrophobic layers, particularly phosphatidylcholine (PC) films, to hinder the transport and electron-transfer reactions of polar compounds is well-documented under static (quiescent) conditions (*11–14*). However, the dynamic situation prevailing in flow systems results in a rapid loss of the mechanical stability of PC coatings and hence in their ability to exclude polar substances. For example, Figure 1 shows typical anodic peaks for uric acid (A) and acetaminophen (B) at PC/CH- and PC-coated electrodes (bottom and top, respectively), obtained in a long run of repetitive flow measurements (20 successive injections within 10 min). A rapid increase of the flow injection peaks is observed at the single-domain phospholipid-coated electrode, reflecting the fast deterioration of the film integrity upon exposure to the flowing solution. The peak currents observed at the end of the experiment correspond to values obtained at the bare electrode (not shown), indicating complete removal of the film (as was supported also by visual observation of the surface). In contrast, the PC/CH-coated electrode gives very small and stable anodic peaks throughout this operation, indicating continuous discrimination against polar compounds. The peaks of Figure 1b are a part of 120 repetitive injections over a 60-min period. The rejection of uric acid and acetaminophen was retained throughout this operation. Visual observation of the surface at the end of the experiment indicated an intact PC/CH layer.

The high mechanical stability of PC/CH coatings was further tested under the vigorous hydrodynamic situation of the rotating disk electrode. Figure 2 shows current–time data for acetaminophen (A) and uric acid (B), recorded during an unbroken 3-h period while rotating the electrode at 1600 rpm. Also shown is the corresponding response of the bare electrode (dotted line). It is clear that the exclusion of polar compounds by the PC/CH film is retained over long periods of time despite the vigorous convective condition prevailing in the cell. The data of Figures 1 and 2 clearly demonstrate that stability problems characterizing lipid-coated electrodes are eliminated with PC/CH composite layers.

While polar compounds are effectively rejected by the PC/CH coating, hydrophobic ones are readily partitioned into the composite layer and detected at the glassy carbon substrate. For example, Figure 3 illustrates characteristic flow injection peaks for ascorbic acid (a), tyrosine (b), promethazine

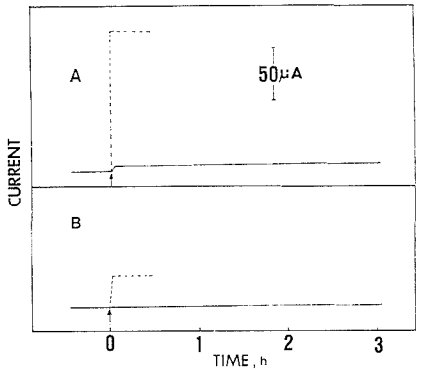

Figure 2. Current–time response for 2.5×10^{-4} M acetaminophen (A) and 5×10^{-4} M uric acid (B) at the lipid-coated and bare electrodes (solid and dotted lines, respectively): rotation speed, 1600 rpm. The composite layer contained 18 mg/mL CH. Other conditions are given in Figure 1.

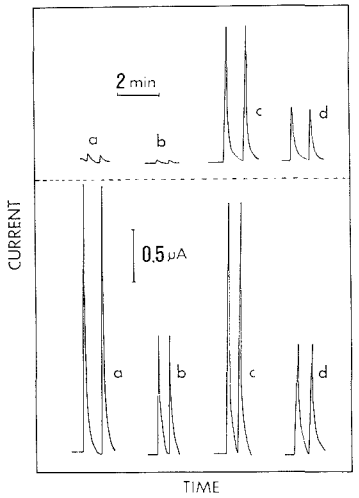

Figure 3. Detection peaks for ascorbic acid (a), tyrosine (b), promethazine (c), and trimipramine (d) at bare and PC/CH-coated electrodes (bottom and top, respectively). Conditions, are given in Figure 1B.

(c), and trimipramine (d) at bare and PC/CH-coated electrodes (bottom and top, respectively). Unlike the nearly complete elimination of the ascorbic acid and tyrosine signals, large peaks are observed, at the coated electrode, for the hydrophobic drugs. A fast response to dynamic changes in the concentration of such substances is also observed. For example, the peak width (at $0.6C_{max}$) of trimipramine is 5.1 s, as compared to 4.6 s at the bare electrode. This rapid response indicates effective "wash out" of hydrophobic compounds from the lipid layer, as desired for use in flow systems.

Figure 4 shows the dependence of the film permeability for 10 solutes of biological and pharmaceutical significance. The ratio between the current at the film-coated electrode over that at the bare one, i_m/i_b, is used as a measure of the permeability. The permeability profile of the PC/CH film (A) is in excellent agreement with changes of the solute polarity. For example, effective discrimination ($i_m/i_b < 0.05$) is observed against the polar species tyrosine, uric and ascorbic

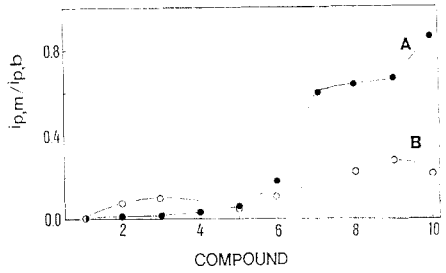

Figure 4. Permeability of PC/CH (A) and CH (B) films for different solutes: ascorbic acid (1), tyrosine (2), uric acid (3), acetaminophen (4), cysteine (5), desipramine (6), perphenazine (7), trimipramine (8), promethazine (9), and chlorpromazine (10). Conditions are as in Figure 1B, except that an applied potential of +0.9 V was used for 1, 5, 6, and 8.

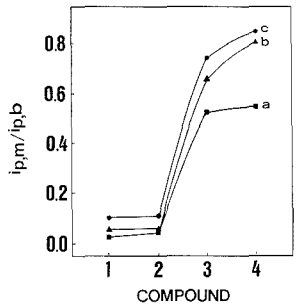

Figure 5. Permeability of PC/CH film containing different levels of CH: 18 (a), 12 (b), and 6 (c) mg/mL. Solutes used were ascorbic acid (1), tyrosine (2), promethazine (3), and trimipramine (4). Conditions are given in Figure 1B.

acids, cysteine, and acetaminophen. In contrast, the composite film permits passage of the hydrophobic antidepressant and phenothiazine drugs ($i_m/i_b > 0.2$). For most of these compounds the film coverage results with only modest attenuations of the response. The ability to measure selectively such drugs in the presence of polar interferences, indicated from this profile, will be illustrated in the following section. In addition to hydrophobicity, the permeability may be affected by electrostatic interactions (associated with the charge of the lipid layer). Also shown in Figure 4 is the corresponding permeability profile at the CH-coated electrode (B). This single-domain coating blocks access of all 10 solutes ($i_m/i_b < 0.3$), exhibiting only a slight preference toward hydrophobic substances. An analogous profile for the single-domain PC film is not shown because of the poor mechanical stability. This coating, however, exhibited higher permeability for all 10 compounds, with i_m/i_b ranging from 0.4 to 0.95 (as was indicated also from analogous cyclic voltammetric experiments).

The quantity of cholesterol present in the composite film can affect its permselective response and mechanical properties. Figure 5 shows the dependence of the film permeability on the composition of the mixed PC/CH coating. The three compositions tested exhibit the desired permselective properties. Increased permeability is observed for the four solutes upon decreasing the CH content. As a result, only 92% rejection of the polar tyrosine and ascorbic acid species is observed by using the 6 mg/mL CH coating. Such behavior is attributed, in part, to changes in the film thickness. The 12 mg/mL CH film offers the best compromise between effective

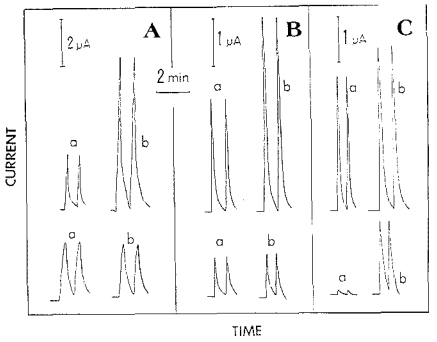

Figure 6. Injection peaks at bare (top) and PC/CH-coated (bottom) electrodes: (A) (a) 5×10^{-4} M chlorpromazine, (b) same as part a but after addition of 5×10^{-4} M uric acid; (B) (a) 1×10^{-4} M promethazine, (b) same as part a but after addition of 1×10^{-4} M cysteine; (C) (a) diluted (1:40) urine, (b) same as part a but after addition of 1×10^{-4} M trimipramine. Applied potential (B, C) was +0.9 V. Other conditions are given in Figure 1B.

exclusion of polar compounds, sensitive detection of hydrophobic ones, and good mechanical stability.

Similar to polymer-coated detectors (*6*, *10*), the response of the lipid electrode yielded a negligible dependence on the flow rate. For example, the limiting current for 5×10^{-4} M promethazine remained stable over the 0.7–5.0 mL/min range. Analogous rotating disk experiments (at rotating speeds ranging from 400 to 2500 rpm) exhibited a similar independence upon the convection rate. Such attractive behavior indicates that transport through the film becomes the major contributor to the total diffusional transport.

The permeability profiles of Figures 4 and 5 and the different mechanical stabilities indicate that the composite PC/CH coating exhibits properties superior to those of the two components alone. Such improvements are attributed to changes in fluidity/packing associated with the incorporation of sterols into phospholipid membranes. Such effects have been widely reported in the literature (*15–18*). For example, nuclear magnetic resonance studies with mixed phospholipid/CH systems indicated a strong interaction between the fatty acid chains of the phospholipid and CH (*18*). X-ray diffraction and capacitance measurements illustrated that the presence of CH decreases the depth of water penetration into phospholipid layers (*15*). Others reported on the condensation of a PC monolayer upon addition of CH (*16*). Such effects may account for the remarkable stabilization of the lipid layer observed in the present work.

The additional separation step, performed in situ, at the electrode surface, can benefit flow measurements in many practical situations. For example, Figure 6 illustrates the potential of the permselective transport characteristics of PC/CH-coated glassy carbon detectors for selective amperometric detection in flow injection systems. With the bare electrode (top) it is not feasible to detect chlorpromazine (A) or promethazine (B) selectivity in the presence of uric acid or cysteine, respectively, because of the additive (oxidation) response. In contrast, the PC/CH-coated electrode (bottom) effectively excludes the polar uric acid and cysteine from reaching the surface; as a result, the phenothiazine drugs are selectively detected (compare peaks a and b). The analytical advantage and practical utility that accrue from such rejection of polar compounds are best illustrated in Figure 6C for the selective detection of trimipramine in a diluted urine sample. A nearly complete elimination of the contribution of endogeneous oxidizable constituents is observed at the coated electrode (a). As a result, quantitation of the hydrophobic

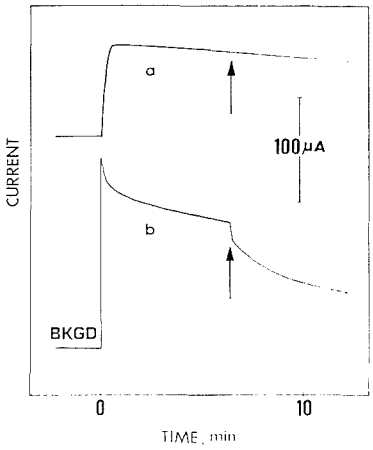

Figure 7. Current–time response for 2.5×10^{-4} M promethazine at the lipid-coated (a) and bare (b) electrodes. Arrows indicate addition of 50 ppm gelatin. Other conditions are given in Figure 2.

drug in urine is possible (with no sample treatment) under flow-injection conditions (b).

These flow injection data indicate that lipid coatings can add a new dimension of selectivity to amperometric detectors based on solute polarity. In addition to flow injection measurements, such discriminative properties may offer significant improvements for liquid chromatography detectors. Coverage of such detectors with a permeable lipid layer would permit "isolation" of hydrophobic solutes from coeluting ones. Complex chromatograms may thus be simplified without lowering the operating potential. Obviously the scope of such applications will be limited by the compatibility of the film integrity with the chromatographic mobile phase.

We investigated also the utility of the PC/CH film as a protective layer, aimed at minimizing electrode poisoning effects. Figure 7 shows current–time rotating disk data for promethzaine at PC/CH coated (a) and bare (b) electrodes. A rapid and significant loss of the activity of the bare electrode is observed in the presence of the analyte (t = 0 to 6.5 min) or organic surfactant (t = 6.5 to 12 min). The lipid electrode, in contrast, offers excellent resistance to surface fouling due to accumulation of reaction products (e.g. of oxidation of phenothiazine compounds) or adsorption of gelatin. Notice also the rapid response to the addition of the hydrophobic drug (t = 0).

The PC/CH-coated amperometric detector exhibits a well-defined concentration dependence and reproducible data. For example, a calibration plot constructed from repetitive injections of promethazine solutions of increasing concentration (2–14) $\times 10^{-5}$ M exhibited a linear response over the entire range (slope, 9.9 nA/μM; intercept, 4.4 nA; correlation coefficient, 0.998; conditions as in Figure 1B). A detection limit of 1.4×10^{-6} M promethazine (i.e. 4.4 ng in the 10-μL injected volume) was estimated based on the signal-to-noise characteristics (S/N = 3) of the 2×10^{-5} M promethazine peak. Analogous measurements of 2×10^{-5} M chlorpromazine and trimipramine yielded detection limits of 1.7×10^{-6} and 2.7×10^{-6} M, respectively. Hence, the inherent sensitivity of amperometric detectors is not compromised by coverage with lipid layers (when hydrophobic substances are concerned). A series of 24 successive injections of a 2.5×10^{-4} M promethazine solution was used to evaluate the precision of the response (conditions as in Figure 1B). The mean peak current found was 3.9 μA, with a range of 3.7–4.1 μA and a relative standard deviation of 3%. Such precision compares favorably with that obtained for phenothiazine compounds at bare electrodes.

In conclusion, the experiments described above illustrate that doping of PC film with CH imparts remarkable mechanical stability into phospholipid coatings. The high stability, under vigorous hydrodynamic conditions, allows use of lipid-coated electrodes for monitoring flowing streams. Such coverage of amperometric detectors with hydrophobic materials offers a new avenue for controlling the access to the surface, and hence greatly benefits flow measurements. The additional separation step, performed in situ at the detector surface, reduces further the attention necessary for sample pretreatment. Changes in packing/fluidity, associated with the incorporation of CH, particularly the decreased water penetration, appear to be responsible for the improved stability. Other steroids or lipid mixtrures may be suitable for this task. Additional advantages may be achieved by coupling the hydrophobic layer with other permselective films. These and related coatings may benefit other electrochemical and nonelectrochemical sensing schemes. Studies in these directions are in progress.

Registry No. Carbon, 7440-44-0; cholesterol, 57-88-5; L-α-phosphatidylcholine, 60-87-7; chlorpromazine, 50-53-3; trimipramine, 739-71-9; desipramine, 50-47-5; perphenazine, 58-39-9; ascrobic acid, 50-81-7; acetaminophen, 103-90-2; cysteine, 52-90-4; uric acid, 69-93-2; tyrosine, 60-18-4.

LITERATURE CITED

(1) Stulik, K.; Pacáková, V. *Electroanalytical Measurements in Flowing Liquids*; Ellis Horwood: Chichester, England, 1987.
(2) Kissinger, P. T. *Anal. Chem.* **1977**, *49*, 447A.
(3) Dong, S.; Wang, Y. *Electroanalysis* **1989**, *1*, 97.
(4) Zak, J.; Kuwana, T. *J. Electroanal. Chem.* **1983**, *150*, 645.
(5) Sittampalam, G.; Wilson, G. S. *Anal. Chem.* **1983**, *55*, 1608.
(6) Wang, J.; Hutchins, L. D. *Anal. Chem.* **1985**, *57*, 1536.
(7) Wang, J.; Tuzhi, P.; Golden, T. *Anal. Chim. Acta* **1987**, *197*, 129.
(8) Kaaret, T. W.; Evans, D. H. *Anal. Chem.* **1988**, *60*, 657.
(9) Wang, J.; Golden, T. *Anal. Chem.* **1989**, *61*, 1397.
(10) Wang, J.; Golden, T.; Tuzhi, P. *Anal. Chem.* **1987**, *59*, 740.
(11) Garcia, O. J.; Quintela, P. A.; Kaifer, A. E. *Anal. Chem.* **1989**, *61*, 979.
(12) Chastel, O.; Kauffmann, J. M.; Patriarche, G. J.; Christian, G. D. *Anal. Chem.* **1989**, *61*, 171.
(13) Tanaka, K.; Tamamushi, R. *J. Electroanal. Chem. Interfacial Electrochem.* **1987**, *236*, 305.
(14) Uchida, I.; Ishino, A.; Matsue, T.; Itaya, K. *J. Electroanal. Chem. Interfacial Electrochem.* **1989**, *266*, 455.
(15) Simon, S. A.; McIntosh, T. J.; Latorre, R. *Science* **1982**, *216*, 65.
(16) Benz, R.; Cros, D. *Biochim. Biophys. Acta* **1978**, *506*, 265.
(17) Yeagle, P. L.; Hutton, W. C.; Huang, C.; Martin, R. B. *Biochemistry* **1977**, *16*, 4344.
(18) Darke, A.; Finer, E. G.; Flook, A. G.; Phillips, M. C. *J. Mol. Biol.* **1972**, *63*, 265.

RECEIVED for review November 2, 1989. Accepted January 16, 1990. This work was supported by the donors of the Petroleum Research Fund, administered by the American Chemical Society, and by the National Institutes of Health (Grant No. GM 30913-06).

Thermal Lensing Detection of Lanthanide Ions by Solvent Extraction Using Crown Ethers

Chieu D. Tran* and Weifeng Zhang

Department of Chemistry, Marquette University, Milwaukee, Wisconsin 53233

A novel method has been developed to enhance the sensitivity and selectivity of the thermal lens detection of lanthanide ions. In this method, the rare-earth ions were selectively extracted from water to organic solvent with the use of crown ether, e.g., 18-crown-6, 15-crown-5 as synergistic extractant. The thermal lens signal intensity of the extracted ions in the organic phase can be enhanced up to 24-fold. This enhancement is due to the fact that the thermal lens signal is dependent on the thermooptical properties of the solvent, and water is a poor thermooptical solvent (low dn/dT and high thermal conductivity, k, values), whereas organic solvents are good themooptical media (high dn/dT and low k values). The well-defined cavities of the crown ethers restrict their complex formation (and hence solvent extraction) only with the rare-earth ions whose sizes are comparable to their cavities, and this is the origin for the improvement in the selectivity. For instance, with the use of 18-crown-6, up to 41% of the Er^{3+} ion can be extracted from water to chloroform, whereas the extraction yield for the Pr^{3+} ion, under the same experimental conditions, was only 28%. The thermal lens technique was used to determine the stoichiometry of the extracted ion pair complexes.

Trace characterization of lanthanide ions, i.e., La^{3+}, Ce^{3+}, Pr^{3+}, ..., Yb^{3+}, and Lu^{3+}, is considered to be one of the more difficult problems in spectrochemical analysis. Conventional radiochemical and atomic spectroscopic techniques such as neutron activation analysis and atomic absorption and atomic emission have achieved some degrees of success in the identification of these rare-earth ions (*1–9*). However, the use of these techniques in the area of general trace analysis is somewhat limited since the former technique requires radioisotopes and the latter suffers from low sensitivity and matrix interferences. Molecular spectroscopic methods have, in general, higher sensitivity and less interference. However, they have not been widely used for the trace detection of the rare-earth ions as compared to the atomic spectroscopic techniques. The limited application is due to the unique properties of these ions. For instance, conventional absorption techniques are not suitable for the trace characterization of these ions at very low concentration because the absorption of these ions, which is due to the forbidden f-f transitions, is too low to be detected. While the fluorescence method can provide higher sensitivity, it can only be used to detect four ions, namely Sm^{3+}, Eu^{3+}, Tb^{3+}, and Dy^{3+}, as these are the only lanthanide ions that fluoresce (*10–13*). Furthermore, in addition to the very low absorptivities, the luminescence quantum yields of these ions are very low (usually on order of 10^{-2} to 10^{-3}). As a consequence, sophisticated fluorescence apparatus utilizing a high-power pulsed laser and time-resolved detection is needed for the determination of these four ions at low concentrations (*10–13*). It is, therefore, particularly important that a novel technique that has higher sensitivity and selectivity be developed for the determination of these rare-earth ions at trace levels.

Thermooptical techniques, i.e., thermal lens, photothermal deflection, and photothermal refraction, have been demonstrated to be a sensitive method for low absorbance measurements (*14–16*). These techniques are based on the measurement of the temperature rise that is produced in an illuminated sample by nonradiative relaxation of the energy absorbed from a laser. In the thermal lens effect, the radially symmetric, Gaussian intensity distribution of the excitation laser beam generates heat that is strongest at the center of the beam because that is where the beam intensity is strongest. Consequently, a lenslike optical element is formed in the sample owing to the temperature gradient between the center of the beam and the bulk material. Under continuous illumination, the thermal lens reaches a steady-state strength S, which is given by

$$S = 1.205P(dn/dT)A/\lambda k \quad (1)$$

where P is the excitation laser power, A is the absorbance of the sample, λ is the excitation wavelength, and dn/dT and k are the temperature coefficient of the refractive index and thermal conductivity of the solvent, respectively. It is thus clear from eq 1 that the sensitivity of the thermal lens techniques not only is directly proportional to the excitation laser power P but also depends on the thermooptical properties of the solvent used. The former property enables the techniques to be used as an ultrasensitive method for the determination of trace chemical species at very low concentrations. In fact, trace chemical species in the form of gas, liquid, or solid whose absorptivities are of the order of 10^{-7} have been determined by using these techniques (*14–16*).

The second feature predicts the dependency of the signal intensity on the thermooptical characteristics of the solvent employed. A higher signal is expected to be achieved if the measurements are performed in solvents having high dn/dT and low thermal conductivity k values. Water is expected to be the worst solvent for thermooptical techniques as its dn/dT value is low while its k value is high. Generally, organic solvents, particularly, nonpolar solvents, are good thermooptical solvents because they have high dn/dT and low k values. In fact, it has been demonstrated that for the same analyte concentration and excitation laser power, thermal lens measurements in n-pentane and CCl_4 are 40 and 38 times more sensitive than those in water (*16*). It is thus possible to exploit this solvent dependency to enhance the sensitivity and to introduce the selectivity into the thermal lens techniques. One possibility is to form an inclusion complex between the analyte (guest) and macrocycle (host), which has a defined cavity size. It is anticipated that the inclusion complex formation will introduce hydrophobicity into the analyte, thereby enabling it to be extracted into a nonpolar solvent that has better thermooptical properties. As a consequence, the thermal lens signal will be greatly improved. Selectivity enhancement in this case would depend on the size selectivity of the macrocyclic host. Macrocyclic compounds such as crown ethers seem to fulfill this expectation (*17–20*).

Crown ethers are a group of macrocyclic ligands whose chemistry is of particular interest because of their ability to form complexes with a variety of metal ions (*1–9, 17–20*). This

0003-2700/90/0362-0830$02.50/0

complex formation is of extreme importance in analytical chemistry, particularly separation science, because it enables the selective extraction of metal ions from aqueous solution into organic phase (*1–9*). In fact, selective complex formation between the crown ethers such as 18-crown-6 and 15-crown-5 and lanthanide ions can be achieved by matching the metal ion size with the well-defined cavity size of the crown ether. This complex formation has been used to selectively extract the lanthanide ions from the aqueous solution to the organic phase for determination (*1–9*).

The information presented is indeed provocative and clearly indicates that it should be feasible to use the thermal lens technique for the sensitive determination of lanthanide ions and to employ the crown ether for the selective extraction of the metal ions from the thermooptically poor water phase to the thermooptically good organic phase in order to further improve the sensitivity and selectivity of the thermal lens technique. These possibilities have been investigated and the preliminary results are presented for the first time in this communication.

EXPERIMENTAL SECTION

Thermal lens signals were measured on a pump/probe thermal lens spectrometer. Detailed information on this apparatus has been described previously (*15, 16*). Unless otherwise stated, the 351.1-nm UV line or one of the visible lines, i.e., 454.5, 457.9, 465.8, 472,7, 476.6, 488.0, 496.5, 501.7, and 514.5 nm from a Coherent Innova 100-10 argon ion laser, was used as the excitation beam. Its intensity was kept at 20 mW and modulated at 20 Hz. Absorption spectra were taken on a Perkin-Elmer 320 spectrophotometer.

Lanthanide trications (Ln^{3+}) obtained as chloride salt (purity of 99.9% or better) were from Alfa Chemicals (Danvers, MA) or Aldrich Chemicals (Milwaukee, WI). Crown ethers, e.g., 18-crown-6, 15-crown-5, or 12-crown-4, were purchased from Parish Chemical Co. (Orem, UT) and used as received. Other chemicals were obtained from Aldrich Chemicals and used as received. Stock solutions of Ln^{3+} (1.0×10^{-1} or 1.0×10^{-2}) and of crown ethers (1.0 M) were prepared by dissolving the appropriate amount of $LnCl_3$ or crown ether in methanol.

Solvent Extractions. A 10-mL aliquot of an aqueous solution containing lithium benzoate (0.1 M), benzoic acid (0.03 M), lanthanide chloride (1.0×10^{-3} M), and the crown ether (0.1 M) was placed in a separatory funnel and vigorously shaken with 10 mL of organic solvent for about 10 min until equilibrium distribution was reached. The funnel was then settled for an hour until the two phases completely separated. Blank extraction was performed under the same conditions without the rare-earth ion. The thermal lens signals of both phases of the blank were taken as background signals. After the extraction, the concentrations of the lanthanide cation (Ln^{3+}) in water and organic phase were determined by the following procedures.

Determination of Concentration of Lanthanide Ion in the Aqueous Phases. A calibration curve for the aqueous phase was made for each lanthanide ion. This was accomplished by shaking 100 mL of water that contained lithium benzoate (0.1 M), benzoic acid (0.03 M), and the crown ether (0.1 M) with 100 mL of organic solvent. After the two phases separated, the water phase was divided into 10 equal portions into which different amounts of $LnCl_3$ were dissolved to make up 10 different standard solutions for the aqueous phase. The thermal lens signals of these solutions were then taken ($S_{(aq)std}$) and a calibration curve was constructed by plotting $S_{(aq)std}$ against the corresponding concentrations of the Ln^{3+} used. This calibration curve and the measured thermal lens signal of the unextracted ions in the water phase of the extracted solutions enabled the determination of the concentrations of the ions in the aqueous phase.

Determination of Concentration of the Lanthanide Ion (Ln^{3+}) in the Organic Phase. The concentration of lanthanide ion in the organic phase is the difference between the total ion concentration and the aqueous phase concentration. These values were calculated for each ion and verified by the back extraction method. In this back extraction procedure, the extracted lanthanide ion in the organic phase was stripped back to the pure water with the use of 1.0 M HCl solution. The thermal lens signal of the ion in this aqueous acid solution was then measured and its concentration was obtained with the calibration curve prepared from a set of standard solutions of Ln^{3+} in 1.0 M HCl aqueous solution. This back extraction process was necessary because the Ln^{3+} ions are not soluble in the organic solvent to enable the standard solutions and the calibration curve to be made. In all cases, the values obtained by subtraction agreed very well with the values determined by the back extraction method.

RESULTS AND DISCUSSION

Counteranions such as picric acid, 2,5-dinitrophenol, perchloric acid, bromocresol green, and dipicrylamine have been used previously in the solvent extraction of alkali, alkaline-earth metal, and lanthanide ions (*1–8*). It was possible to use these compounds because in these studies the extracted ions were either directly determined by atomic spectroscopic techniques or radiochemical methods or indirectly determined by measuring the absorption of the extracted counterions (*1–9*). However, in the present study, these compounds cannot be used because they absorb very strongly in the visible and near-UV region and their absorption spectra overlap with those of the lanthanide ions. As a consequence, the small thermal lens signals of the lanthanide ions were overshadowed by the large signals of the counteranions. A novel counteranion is, therefore, needed for the present extraction study. In selection of the new counteranion, the following factors need to be considered:

1. The absorption of the counteranion should not overlap with those of the lanthanide ions.
2. If an acid is selected, its pK_a value should be relatively low to provide a sufficient amount of its dissociated anion.
3. The counteranion should have not only adequate solubility in water but also the hydrophobicity to enable the complexes formed to be extracted into the organic phase.

Several different acids, which include perchloric, sulfonic, acetic, propionic, cyclohexane carbocyclic and benzoic acid, have been investigated. No observable extraction was found for perchloric, sulfonic, and cyclohexanecarboxylic acids. This is because the former two acids are not soluble in the organic phase and the reverse is true for the carbocyclic acid. Extraction yields of 1% and 2% were found when acetic and propionic acid were used to extract the Nd^{3+} ions from the aqueous phase into the chloroform with 15-crown-5. These low extraction yields can be explained in terms of the low hydrophobicity of these two acids. Benzoic acid gave relatively satisfactory results. Under the same conditions, the extraction yield obtained by using this acid was 13%. This acid is capable of providing a relatively high extraction yield because it satisfies all three conditions described above; i.e., it does not absorb any light at wavelengths longer than 300 nm where most lanthanide ions absorb, its benzene ring provides the required hydrophobicity, and its low pK_a value ($pK_a = 4.19$) (*21*) enables presentation in the dissociated form at a sufficient amount to render adequate solubility in water. The benzoate was, therefore, selected as a counteranion for the extractions. By use of this anion, the effect of pH on the extraction yield was then investigated. It was found that at low pH (i.e., pH values <4) the extraction yields were relatively poor because at these pHs, the benzoate existed mostly in the form of benzoic acid (HA), which cannot form ion pair with the crown ether–lanthanide cation complexes. The extraction yields fell again at pH > 5, presumably because at these pHs, the lanthanide ions formed complexes with OH^-, i.e., $Ln(OH)_3$, and precipitated down. The optimal pH was found to be 4.85 and this was the pH value used for all subsequent extraction experiments. Due to the fact that the optimal pH is only 0.66 pH unit from the pK_a of the benzoic acid, no additional buffer was used since lithium benzoate (0.1 M) and benzoic acid (0.03 M) can serve as the buffer. The pH of the aqueous phase

Table I. Effect of Solvent on the Extractions of Nd^{3+} with 15-Crown-5

solvent[a]	donor no.[b]	extraction yield,[a,c] %
heptanol	31	43
octanol	32	40
ethyl acetate	17	29
methylene chloride	2	24
chloroform	4	13
1,2-dichloroethane	0	9

[a] Extraction conditions: 0.1 M lithium benzoate; 1.0×10^{-3} M $NdCl_3$; 0.03 M benzoic acid, and 0.1 M 15-crown-5. [b] Data taken from ref 22. [c] Estimated errors, ±5%.

containing these two compounds was adjusted to the optimal pH of 4.85 with the use of LiOH and HNO_3.

The effect of solvent on the extraction yield has been investigated for Nd^{3+} by using 15-crown-5. Lithium benzoate (0.1 M) and benzoic acid (0.03 M) were used to provide the needed concentration of benzoate at the optimal pH; i.e., pH = 4.85. Lithium salt of benzoic acid instead of sodium or potassium salt was used to avoid the complication which may arise from the competing complex formation between the Na^+ or the K^+ and the Ln^{3+} with the crown ethers. Results obtained, shown in Table I, demonstrate that up to 43% and 40% extraction yields can be achieved with the use of heptanol and octanol. Relatively lower extraction yields were found for chlorinated solvents: 24%, 13%, and 9% for methylene chloride, chloroform, and 1,2-dichloroethane, respectively. No observable extraction was found when nonpolar solvents such as CCl_4, benzene, or cyclohexane were used. The results obtained can be explained in terms of the ability of the solvent to serve as a donor. The Gutmann's donor numbers (DN) for the solvents used are listed in Table I (*22*). As listed, solvents such as heptanol or octanol, which have high donor ability (DN = 31 and 32) can solubilize the ion pair formed between the crown ether–lanthanide ion and benzoate and therefore can provide higher extraction yield. Lower extraction yields were found for chlorinated solvents because they have relatively poor donor ability i.e., DN values for chloroform, methylene chloride, and 1,2-dichloroethane are 4, 2, and 0, respectively (*22*). It should be added that other effects such as the amount of water solubilized in the solvent might affect the extraction yields because the solubilized water might alter the physical properties of the solvent.

The effect of solvent extraction on the thermal lens signal of the Nd^{3+} was investigated by measuring the signal intensity of the same concentration of the lanthanide ion in water and in the extracted solvent phase using the same measurement conditions. The results are shown in Table II as the signal intensity relative to that in water, i.e., $(S_{solvent}/S_{water})_{expt}$, where $S_{solvent}$ and S_{water} are the thermal lens signals of the equal concentrations of the lanthanide ion in the extracted solvent and in the water, respectively. As listed in the table, for the same concentration of lanthanide ion, the thermal lens signal intensity can be enhanced up to 18, 20, or 24 times when the ion was extracted from water into methylene chloride, chloroform, or 1,2-dichloroethane, respectively. Enhancement can also be achieved but with lesser magnitude when the ion was extracted into such organic solvents as ethyl acetate, heptanol, and octanol. For comparison, the calculated enhancement values based on the dn/dT and thermal conductivity, k, values of water and organic solvents (*23*) are also listed in the Table II. In all cases, the experimental values are relatively lower than the calculated values. A variety of reasons might account for this discrepancy but the most likely one is probably due to the effect of the solubilized water in the organic solvents

Table II. Relative Thermal Lens Signal Intensity of Nd^{3+} in Different Media

solvent	$10^4(dn/dT)$,[b] K^{-1}	k,[b] mW cm^{-1} K^{-1}	$S_{solvent}/S_{water}$ calcd[c,d]	$S_{solvent}/S_{water}$ exptl[c]
water	−0.8	6.110	1	1
ethyl acetate[a]	−4.9	1.485	25	11
heptanol[a]	−4.0	1.600	25	13
octanol[a]	−4.0	1.600	25	14
1,2-dichloroethane[a]	−5.1	1.342	29	24
methylene chloride[a]	−5.5	1.213	34	18
chloroform[a]	−5.9	1.030	37	20

[a] Extraction conditions: 0.1 M lithium benzoate; 0.03 M benzoic acid; 1.0×10^3 M $NdCl_3$, and 0.1 M 15-crown-5. [b] Data taken from ref 23. [c] $S_{solvent}$ and S_{water} are the thermal lens signals of equal concentration of Nd^{3+} in the solvent and in water, respectively. [d] $(S_{solvent}/S_{water})_{calc}$ values are calculated based on the dn/dT and k values of solvents and water.

Table III. Size Effect on the Extractions of Lanthanide Ions by Crown Ethers[a-c]

metal ion	extraction yield, % 12-crown-4	15-crown-5	18-crown-6
Er^{3+}	12	39	41
Ho^{3+}	11	31	38
Dy^{3+}	d	33	37
Tb^{3+}	d	30	35
Eu^{3+}	d	25	31
Sm^{3+}	8	20	30
Nd^{3+}	6	14	29
Pr^{3+}	6	10	28

[a] Extractions conditions: 0.1 M lithium benzoate; 0.03 M benzoic acid; 1.0×10^{-3} M $LnCl_3$ and 0.1 M crown ether. [b] Measurements were performed at 351.1 nm for Dy^{3+}, Tb^{3+}, and Eu^{3+}; 476.9 nm for Sm^{3+} and Pr^{3+}; 488.0 nm for Er^{3+} and Ho^{3+}; and 514.5 nm for Nd^{3+}. [c] Estimated errors, ±5%. [d] Signals were too small to be measured accurately.

which results in lowering their dn/dT and heightening their k values.

The size effect on the extraction yield was investigated by extracting a series of lanthanide ions ranging from Pr^{3+} to Er^{3+} from the aqueous phase into the organic phase using different ethers, namely 12-crown-4 (12-C-4), 15-crown-5 (15-C-5), and 18-crown-6 (18-C-6). Chloroform was used as the organic phase in spite of the fact that the extraction yield in this solvent is relatively lower than those obtained by using other solvents such as heptanol and octanol (Table I). This is because the thermal lens signal enhancement in chloroform is relatively higher than those in other solvents (Table II) and the use of the alcohols for extraction often resulted in emulsions and usually required a relatively long time to separate into two phases. Table III lists the results obtained for 12-C-4, 15-C-5, and 18-C-6. As listed in the table, only small amounts of lanthanide ions (between 8% and 12%) were extracted into the chloroform phase when 12-C-4 was used as the extracting agent. This observation is in agreement with the results obtained by other workers who also found relatively poor extraction yields with 12-C-4 (*2*, *7*). The low extraction yields can be explained in terms of the mismatching in sizes of the crown ether and the lanthanide ions; i.e., the cavity of 12-C-4, which is between 1.2 and 1.5 Å, is too small to accommodate the lanthanide ions whose ionic diameters are between 1.76 and 2.02 Å (*24*). Substantial improvement in the extraction yield can be accomplished when 15-C-5 or

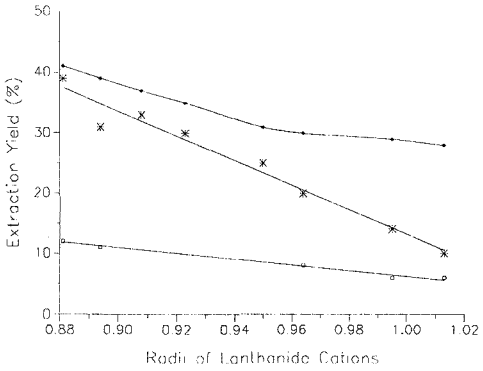

Figure 1. Extraction of lanthanide ions with 18-crown-6 (◆), 15-crown-5 (*), and 12-crown-4 (□).

18-C-6 was used as the extracting agent. For instance, up to 39% and 41% of Er^{3+} ions can be extracted from the aqueous phase into the chloroform phase with the use of 15-C-5 and 18-C-6, respectively (Table III). The enhancement in the extraction yield is probably due to the fact that the cavities of these crown ethers are sufficiently large (the cavities of 15-C-5 and 18-C-6 are 1.7–2.2 and 2.6–3.2 Å, respectively) (*25*) to accommodate the lanthanide ions and thus enable them to be extracted into the organic phase. Interestingly, these two crown ethers also offer noticeable selectivity in the extraction processes: At the same extraction conditions as those for the Er^{3+} ions, only 10% and 28% of the Pr^{3+} ions were extracted into the organic phase by 15-C-5 and 18-C-6, respectively. Clearer evidence of selectivity can be seen in Figure 1, which plots the extraction yields against the radii of the lanthanide ions. As depicted in the figure, the extraction yield decreases as the size of the ion increases. The size selection provided by the 15-C-5 is relatively better than that by the 18-C-6 even though, for the same ion, the extraction yields obtained by using the latter are higher than the former. This is probably because the cavity of the 18-C-6 is larger and hence more flexible than that of 15-C-5. It can, therefore, adopt a variety of conformations to accommodate the lanthanide ions having different sizes. Consequently, a rather low selectivity is obtained. The larger size of 18-C-6 also makes it more lipophilic than 15-C-5 and hence enables it to extract more metal ion from the aqueous phase into the organic phase.

Detailed information on the structure of the extracted ion-pair complexes can be obtained by determining the stoichiometry of the complexes.

The distribution coefficient (D) of the extraction

$$Ln^{3+} + nCE + mA^- \rightleftarrows (Ln(CE)_nA_m)^{(3-m)+}$$

is given by the following equation

$$D = \frac{\sum[Ln^{3+}]_{org}}{\sum[Ln^{3+}]_{aq}} \quad (2)$$

$$= \frac{[Ln(CE)_nA_m^{(3-m)+}]_{org}}{[Ln^{3+}]_{aq} + [Ln(CE)_n^{3+}]_{aq}} \quad (3)$$

where Ln^{3+}, CE, and A^- are the rare earth, crown ether, and benzoate anion, respectively. Because A^- is present in excess amounts, most of the $Ln(CE)^{3+}_n$ will form the ion-pair $Ln(CE)_nA_m^{(3-m)+}$ complexes and be extracted into the organic phase. Therefore, the $[Ln(CE)^{3+}_n]_{aq}$ is much smaller than $[Ln^{3+}]_{aq}$. Equation 3 will thus become

$$D = [Ln(CE)_nA_m^{(3-m)+}]_{org}/[Ln^{3+}]_{aq} \quad (4)$$

The complex formation between Ln^{3+} and CE in the aqueous solution is given by

$$Ln^{3+} + nCE_{aq} \rightleftarrows Ln(CE)_n^{3+}$$

$$K_f = [Ln(CE)_n^{3+}]_{aq}/[Ln^{3+}][CE]^n_{aq} \quad (5)$$

The complex $Ln(CE)^{3+}_n$ formed will be extracted into the organic phase by

$$[Ln(CE)_n^{3+}]_{aq} + mA^-_{aq} \rightleftarrows [Ln(CE)_nA_m^{(3-m)+}]_{org}$$

$$K_{ex} = [Ln(CE)_nA_m^{(3-m)+}]_{org}/[Ln(CE)_n^{3+}]_{aq}[A^-]^m_{aq} \quad (6)$$

From eqs 4–6

$$D = K_{ex}K_f[CE]^n_{org}[A^-]^m_{aq}/K_d^n \quad (7)$$

where K_d is the partition constant of the crown ether between the organic phase and aqueous phase, i.e.

$$K_d = [CE]_{org}/[CE]_{aq}$$

The initial concentration of crown ether, $[CE_0]$, can be expressed as

$$[CE_0] = [CE]_{org} + [CE]_{aq}$$

Therefore

$$\frac{[CE]_{org}}{[CE_0]} = \frac{K_d}{1 + K_d} \quad (8)$$

When eq 8 is substituted in eq 7

$$D = \frac{K_{ex}K_f[CE_0]^n[A^-]^m}{(1 + K_d)^n} \quad (9)$$

In the extraction, benzoic acid dissociates as

$$HA \rightleftarrows H^+ + A^-$$

with $$K_a = [H^+][A^-]/[HA]$$

because $[H^+] = [A^-]$

$$[A^-] = (K_a[HA])^{1/2} \quad (10)$$

When eq 10 is substituted into eq 9

$$D = \frac{K_a^{m/2}K_{ex}K_f[CE_0]^n[HA]^{m/2}}{(1 + K_d)^n}$$

and

$$\log D = \log \frac{K_{ex}K_fK_a^{m/2}}{(1 + K_d)^n} + \frac{m}{2}\log [HA] + n \log [CE_0] \quad (11)$$

The distribution coefficient D can be determined by measuring the concentrations of the lanthanide ion in the organic and in the water phases. The stoichiometry coefficient of the crown ether, n, can then be calculated from the slope of the plot of log D vs log $[CE_0]$ at constant concentration of HA and the coefficient of the counteranion, m, equals twice the slope of the plot of log D vs log [HA] at constant crown ether concentration. With this method, the stoichiometric values n and m for the extraction of lanthanide ions by 18-C-6 and 15-C-5 have been determined and the results are shown in Table IV. It is interesting to note that regardless of the size, all lanthanide ions form 1:1 complexes with 18-C-6 as well as with 15-C-5, and in all cases, there are three benzoate counterions to one lanthanide ion:crown ether trication complex. The fact that lanthanide ions form 1:1 rather than 1:2 complexes with the 15-C-5 or the 18-C-6 further supports the high selectivity observed for the extraction yields (Table III

Table IV. Stoichiometry of the Extracted Ion Pair Complexes $(Ln(CE)_nA_m)^{(3-m)+}$

lanthanide ion	crown ether	n	m
Er^{3+}	18-crown-6	0.98	2.8
Sm^{3+}	18-crown-6	0.94	2.9
Pr^{3+}	18-crown-6	0.92	3.1
Er^{3+}	15-crown-5	0.97	2.8
Tb^{3+}	15-crown-5	0.95	2.9

and Figure 1). This is because only a tight fit between one lanthanide ion and one crown ether is expected to render the high selectivity into the extraction processes. Similar stoichiometry coefficients have also been found by other workers (*2*, *24*, *26*). Complexes having different stoichiometry, e.g., 1:2:3 lanthanide ion:crown ether:counteranion, have also been reported (*3*, *6*, *7*), but in these studies, experimental conditions which are known to have a strong effect on the extraction processes, i.e., the type of the counterion, organic solvent, the pH, and ionic strength of the aqueous phase, ... are different from the present work.

Taken together, the results presented clearly demonstrate that crown ethers can facilitate the selective solvent extraction of the lanthanide ions, and this extraction process provides substantial enhancement in sensitivity as well as selectivity for the thermal lens detection of rare-earth ions. The sensitivity is enhanced because the ions are extracted from water, which is a poor thermooptical solvent (i.e., low dn/dT and high thermal conductivity), to a thermooptically good organic solvent. The well-defined cavity sizes of crown ethers restrict their complex formation (and hence solvent extraction) only to the rare-earth ions having appropriate sizes, and this is the origin for the improvement in selectivity. Experiments are now in progress to expand the application of this method to the analysis of multicomponent mixtures.

LITERATURE CITED

(1) Mohite, B. S.; Khopkar, S. M. *Anal. Chem.* **1987**, *59*, 1200.
(2) Tsay, L. M.; Shih, J. S.; Wu, SC. *Analyst* **1983**, *108*, 1108.
(3) Wenji, W.; Bozhong, C.; Zhong-Kao, J.; Ailing, W. *J. Radioanal. Chem.* **1983**, *76*, 49.
(4) Manchanda, V. K.; Chang, C. A. *Anal. Chem.* **1987**, *59*, 813.
(5) Hasegawa, Y.; Haruna, S. *Solvent Extr. Ion Exch.* **1984**, *2*, 451.
(6) Hasegawa, Y.; Masuda, M.; Hirose, K.; Fukuhara, Y. *Solvent Extr. Ion Exch.* **1987**, *5*, 255.
(7) Aly, H. F.; Khalifa, S. M.; Navratil, J. D.; Saba, M. T. *Solvent Extr. Ion Exch.* **1985**, *3*, 623.
(8) Ensor, D. D.; McDonald, G. R.; Pippin, C. G. *Anal. Chem.* **1986**, *58*, 1814.
(9) Tang, J.; Wai, C. M. *Anal. Chem.* **1986**, *58*, 3235.
(10) Fisher, R. P.; Winefordner, J. *Anal. Chem.* **1971**, *43*, 454.
(11) Guiyun, Z.; Jinghe, Y.; Zhikun, S. *Anal. Chim. Acta* **1988**, *215*, 331.
(12) Soini, E.; Lovgren, T. *CRC Crit. Rev. Anal. Chem.* **1987**, *18*, 105.
(13) Morin, M.; Bador, R.; Dechaud, H. *Anal. Chim. Acta* **1989**, *219*, 67.
(14) Tran, C. D. *Anal. Chem.* **1988**, *60*, 182.
(15) Franko, M.; Tran, C. D. *Anal. Chem.* **1988**, *60*, 1925.
(16) Tran, C. D.; Van Fleet, T. A. *Anal. Chem.* **1988**, *60*, 2478.
(17) Fendler, J. H. *Membrane Mimetic Chemistry*; John Wiley: New York, 1982.
(18) Armstrong, D. W. *Sep. Purif. Methods* **1985**, *14*, 212.
(19) Armstrong, D. W. *Anal. Chem.* **1987**, *59*, 84A.
(20) *Ordered Media in Chemical Separations*; Hinze, W. L., Armstrong, D. W., Eds.; American Chemical Society: Washington, DC, 1987.
(21) *CRC Hankbook of Chemistry and Physics*; Weast, R. C., Ed.; CRC Press, Inc.: Boca Raton, FL, 1985.
(22) Marcus, Y. *J. Solution Chem.* **1984**, *13*, 599.
(23) *Organic Solvents, Physical Properties and Methods of Purification*; Riddick, J. A., Bunger, W. B., Sakano, T. K., Eds.; John Wiley: New York, 1986.
(24) Bunzli, J.-C. G. In *Handbook on the Physics and Chemistry of Rare Earths*; Gschneidner, K. A., Eyring, L., Eds.; North-Holland: Amsterdam, 1987; Vol. 9, Chapter 60.
(25) Cheng, K. L.; Ueno, K.; Imamura, T. *Handbook of Organic Analytical Reagents*; CRC Press: Boca Raton, FL, 1982.
(26) Nakagawa, K.; Okada, S.; Inoue, Y.; Tai, A.; Hakushi, T. *Anal. Chem.* **1988**, *60*, 2527.

RECEIVED for review October 16, 1989. Accepted December 21, 1989. Acknowledgment is made to the donors of the Petroleum Research Fund, administered by the American Chemical Society, for financial support of this research.

Luminescence Detection of Rare-Earth Ions by Energy Transfer from Counteranion to Crown Ether–Lanthanide Ion Complexes

Chieu D. Tran* and Weifeng Zhang

Department of Chemistry, Marquette University, Milwaukee, Wisconsin 53233

A novel method has been developed to enhance the sensitivity and selectivity of the luminescence detection for lanthanide ions. In this method, the lanthanide ion, crown ether, and benzoate were compartmentalized into an ion pair complex in order to eliminate the quenching and to induce the energy transfer so that the luminescence detection for the lanthanide ions can be selectively enhanced. The molecular organization is achieved by using a crown ether such as 18-crown-6 or 15-crown-5 as the synergistic extracting agent and benzoate as the counterion to selectively extract the rare-earth ions from water into an organic solvent where they are subsequently determined by luminescence technique. Compared to lanthanide ions in aqueous solutions, the luminescence intensity of the extracted ion pair complexes is substantially enhanced. The luminescence intensities of the Tb^{3+}, Eu^{3+}, and Dy^{3+} ions were enhanced up to 4 times when they were extracted into ethyl acetate or into chloroform. This is because in water, the metal ions are quenched by the high-frequency vibrations of the OH group and this quenching is eliminated when they are extracted into the organic solvent. In addition, the measured luminescence intensity can be further enhanced up to 17 times by performing the measurement at the excitation wavelength where the lanthanide ions were not excited directly but indirectly through the energy transfer from the counterion (i.e., benzoate). The total enhancement by the extraction and energy transfer processes can, therefore, be up to 67 times. The mechanism of energy transfer and the use of this technique to measure the selective extractions of Tb^{3+}, Eu^{3+}, and Dy^{3+} ions are discussed.

Traditionally, trace determination of lanthanide ions has been considered to be one of the more difficult problems in chemical analysis. The difficulty stems from the similarity in the chemicall properties and the low absorptivities of these ions (*1*, *2*). As a consequence, it is very difficult to use conventional chemical methods for the separation and/or characterization of the ions as well as to employ such molecular spectroscopic techniques as absorption for their trace characterization. A highly sensitive and selective method that is capable of determining the lanthanide ions at very low concentrations is, therefore, particularly needed. The needs are even more pronounced as the industrial applications of these rare-earth ions increase.

Considerable advances have been made in the last few years, among them the method based on the use of crown ethers for selective solvent extraction of lanthanide ions seems to be the most effective (*1*, *3–5*). In this method, the crown ether is used as a synergistic extracting agent to selectively extract the lanthanide ions from the aqueous phase into the organic phase where they are subsequently determined by atomic spectroscopic methods, e.g., atomic absorption, emission, or radiochemical methods (*6–16*). Unfortunately, in spite of the fact that there are a large number of reports of this extraction technique during the last few years (*6–16*), the method is still relatively underutilized. A variety of reasons might account for this limited use, but the most likely one is probably due to the low sensitivity and high interference of the atomic spectroscopic methods used for the determination. Indirect detection by use of a highly absorbing fluorescent counterion (*6–21*) increases sensitivity but loses the specificity of direct detection. It is, therefore, of particular importance that a novel method that is based on the use of the fluorescence or absorption techniques to directly determine the lanthanide ions be developed.

Four of the lanthanide ions, namely Sm^{3+}, Eu^{3+}, Tb^{3+}, and Dy^{3+}, are known to luminesce in solution (*17–21*). Their low luminescence quantum yields (ϕ), however, necessitated the use of special techniques and/or apparatus such as high-power pulsed laser, time-resolved luminescence for their trace characterization (*18*, *19*). In principle, however, the ϕ value can be substantially improved by using a highly absorbing compound as a energy donor to absorb the excitation light and to subsequently transfer the energy to the lanthanide ion (acceptor). The ϕ value is enhanced by selecting a highly absorbing donor so that even in the case of very low energy transfer efficiency, the amount of the excited lanthanide ions produced is still substantially higher as compared to the case where the ions are excited directly. In fact, it has been known for some time that energy transfer occurs between aromatic hydrocarbons (donor) and lanthanide ions (acceptor); i.e., when the excitation is performed at the wavelengths where only the organic compounds absorb, the luminescence is observed as intense, narrow emission lines, which are characteristic of the lanthanide ions (*18–25*). Furthermore, the energy transfer in this case is the Förster type resonance energy transfer between the triplet state of the donor and the D states of the ion. The distance between the donor and acceptor can, therefore, be as large as 100 Å (*26*, *27*). As a consequence, the donor need not be directly chelated to the metal ion but only has to be in close proximity as in the case of a counteranion.

In the solvent extraction process, the lanthanide ions initially form complexes with the crown ether and the ion–crown ether cation complexes are then extracted into the organic phase by ion pair formation with the counteranion. Aromatic counteranions such as picrate have been generally used because they provide the needed lipophilicity (and hence solubility in organic phase) for the complexes ion pair formed (*6*, *14*). Therefore, it may be possible to use the counteranion to transfer the excitation energy to the lanthanide ion in order to enhance the emitted luminescence intensity. Unfortunately, in spite of its great potential, the use of a counterion to transfer energy has not been exploited. Such considerations prompted this study, which aims to investigate the possibility of improving the luminescence detection of lanthanide ions by energy transfer from the counterion to the metal ions. It will be reported, for the first time, in this communication that benzoate, when used as a counteranion, can transfer energy to the lanthanide ions such as Eu^{3+}, Tb^{3+}, and Dy^{3+}, and the enhancement in the luminescence intensity facilitates the use

0003-2700/90/0362-0835$02.50/0

of this technique for the direct determination of the extracted ions.

EXPERIMENTAL SECTION

Absorption spectra were taken on a Perkin-Elmer 320 spectrophotometer. A Perkin-Elmer LS-5 spectrofluorometer interfaced with a Perkin-Elmer 3600 data station was used to measure luminescence. Luminescence spectra were obtained by subtracting the corresponding blank signal from that of the analyte. The reported luminescence intensity values were obtained by integration of each luminescence spectrum for the entire peak under the peak.

Lanthanide ions, i.e., Sm^{3+}, Eu^{3+}, Tb^{3+}, and Dy^{3+}, obtained as chloride salt (purity of 99.999% or greater) were purchased from Aldrich Chemicals (Milwaukee, WI) or Alfa Chemicals (Danvers, MA) and used as received. Benzoic acid (Aldrich) was recrystallized from water. Crown ethers, e.g., 18-crown-6, 15-crown-5, and 12-crown-4 were purchased and used as received from Aldrich. Organic solvents were obtained from Burdick & Jackson (Muskegon, MI); water was distilled from an all-glass distillation apparatus. **Cautions:** crown ethers might cause some neurological effects if absorbed through the skin and chloroform is an suspected cancer agent.

Solvent Extraction. The lanthanide cations, Ln^{3+}, were extracted from the water phase into the organic phase with the use of crown ether, e.g., 18-crown-6, 15-crown-5, or 12-crown-4, as synergistic extracting agent and benzoate as the counteranion. Typically 10 mL of an aqueous solution containing lithium benzoate (0.1 M), benzoic acid (0.02 M) lanthanum chloride (1.0×10^{-3} M), and crown ether (0.1 M) was placed in a separatory funnel and vigorously shaken with 10 mL of ethyl acetate or chloroform for about 10 min until they attained distribution equlibrium. The funnel was then settled for an hour until two phases completely separated and the luminescence of the lanthanide ion in the organic phase was measured.

Knowledge on the concentrations of the lanthanide ions in the water before and after the extraction is needed in order to calculate the extraction yield. However, due to the quenching by the high-frequency vibrations of the OH group (*20*), the luminescence intensity of the ions in the water phase was too low to be determined accurately. Conversely, accurate measurement of the luminescence signal of the ions in the organic phase can be accomplished. This is because their luminescence intensities were substantially enhanced when they were extracted from the aqueous phase into the organic phase. Lack of the quenching by OH group in the organic phase is responsible for this enhancement. Luminescence calibration curves for organic solvents are needed for the determination of the concentrations of the lanthanide ions in these media. However, standard solutions cannot be prepared by simply dissolving the lanthanum chloride ($LnCl_3$) in the organic solvent because the chloride salts are insoluble in the organic solvents used. A series of lanthanum benzoate (LnB_3) compounds were therefore synthesized and used to prepare the standard solutions for the organic phase because these compounds have sufficient solubility in organic solvents.

Lanthanoid(III) benzoates (LnB_3) were prepared from lanthanide chloride and lithium benzoate according to procedures previously described (*28*). Typically, 1 g of lanthanide chloride (2.7 mM) was made into a paste by mixing with 2 mL of H_2O. The paste was dissolved by adding 3.0 mL of 6 N HCl. The solution was neutralized to incipient precipitation with 1 N NH_4OH and adjusted to pH 2 with HCl. The solution was then diluted to 100 mL, warmed nearly to boiling, and treated with 20 mL of 1.0 M lithium benzoate over a period of about 1 h. The mixture was digested for about 4 h, cooled to room temperature, filtered, washed to remove Cl^-, and dried. The sample was then recrystallized from a DMSO–water mixture and dried under vacuum for 1 day.

To prepare the standard solutions for the calibration curve, 100 mL of an aqueous solution containing lithium benzoate (0.1 M) or benzoic acid (0.02 M) and crown ether (0.1 M) was shaken with 100 mL of ethyl acetate or chloroform. After the two phases separated, the organic phase was divided into 10 equal portions into which different amounts of LnB_3 were dissolved to make up 10 different standard solutions. Luminescence spectra of these standard solutions were then measured, and the calibration curve

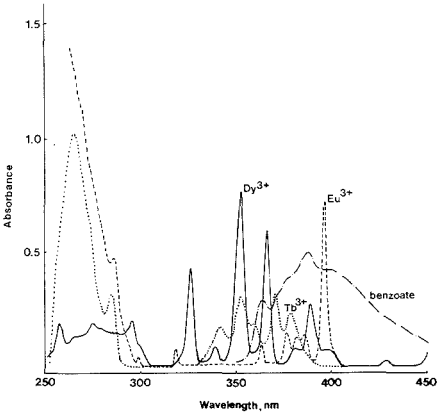

Figure 1. Absorption spectra of aqueous solutions of 1.0 M $TbCl_3$ (···), 0.5 M $EuCl_3$ (- - -), and 0.5 M $DyCl_3$ (——) and phosphorescence of lead benzoate (– · –).

was prepared by plotting the luminescence intensity against the concentration of the LnB_3. These calibration curves facilitate the determination of the concentrations of the Ln^{3+} concentrations in the organic phase from the measured luminescence signal intensities. The extraction yields were then calculated by dividing the concentration of the Ln^{3+} by the total concentration of the Ln^{3+} used.

RESULTS AND DISCUSSION

Figure 1 shows the absorption spectra of aqueous solutions of $TbCl_3$ (1.0 M), $EuCl_3$ (0.5 M), and $DyCl_3$ (0.5 M). As depicted in the figure, the lanthanide ions absorb very little at 290 nm. In all cases, the molar absorptivities for these ions at 290 nm are less than 1; i.e., $\epsilon_{290} = 0.185$, 0.670, and 0.330 M^{-1} cm^{-1}, for Tb^{3+}, Eu^{3+}, and Dy^{3+}, respectively. They have, however, relatively higher absorbances at 352 and 395 nm. The molar absorptivities for Tb^{3+} and Dy^{3+} at 352 nm and for Eu^{3+} at 395 nm are 0.207, 1.430, and 1.188 M^{-1} cm^{-1}, respectively. Conversely, the ethyl acetate solution of benzoate (this solution was prepared by mixing 5.0×10^{-4} M benzoic acid and 1.0×10^{-3} M sodium ethoxide in ethyl acetate) has a substantially higher absorbance at 290 nm ($\epsilon_{290} = 28$ M^{-1} cm^{-1}) but no absorption at 352 or 395 nm (spectrum is not shown). It is therefore, evident that for a mixture containing lanthanide ions and benzoate, 352- or 395-nm excitation produces only excited rare-earth ions, whereas 290-nm excitation will generate a large amount of excited-state benzoate.

The lanthanide ions were extracted from the aqueous phase into the organic phase with the use of crown ether such as 18-crown-6 or 15-crown-5 as synergistic extracting agent and benzoate as counteranion. Benzoate was selected from a series of widely used counteranions, which include picrate, 2,5-dinitrophenolate, perchlorate, bromocresol green, and dipicrylamine (*6–16*). This selection was based on the fact that the benzoate absorption spectrum does not overlap with that of the lanthanide ions, the triplet energy level of benzoate, 27 000 cm^{-1} (*29*), is much higher than the excited-state energy levels of the lanthanide ions, and, finally, the anion has adequate solubility in water as well as in organic solvents. The latter characteristics are due to the properties of the benzoic acid; i.e., its pK_a value is low enough (4.19) to enable it to present sufficiently in the water-soluble dissociated form and the presence of the benzene ring enables it to have the required lipophilicity.

The luminescence of the lanthanide ions was substantially enhanced when they were extracted into the organic phase.

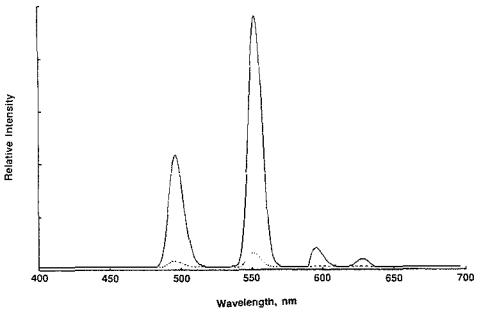

Figure 2. Luminescence spectra of extracted Tb^{3+}–15-crown-5–benzoate ion pair complexes in ethyl acetate: (---) excited at 352 nm; (——) excited at 290 nm.

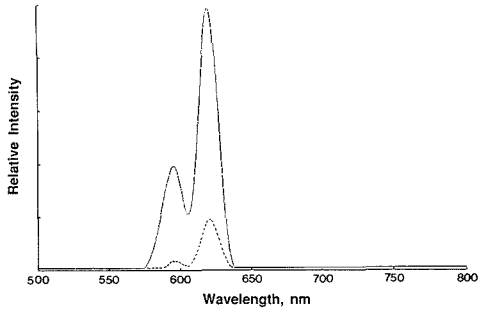

Figure 3. Luminescence spectra of extracted Dy^{3+}–15-crown-5–benzoate ion pair complexes in ethyl acetate: (---) excited at 352 nm; (——) excited at 290 nm.

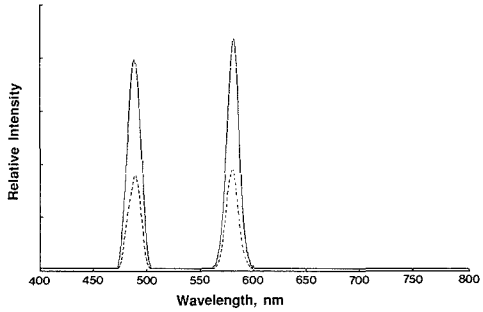

Figure 4. Luminescence spectra of extracted Eu^{3+}–15-crown-5–benzoate ion pair complexes in ethyl acetate: (---) excited at 395 nm; (——) excited at 290 nm.

The luminescence spectra of the extracted Tb^{3+}–crown ether–benzoate ion pair complexes in ethyl acetate are shown in Figure 2. The dashed line spectrum shown in this figure was obtained by exciting the complexes at 352 nm whereas the solid line spectrum was measured with 290-nm excitation wavelength. As described above, the Tb^{3+} ion has observable absorbance at 352 nm whereas the benzoate does not absorb at all this wavelength. Therefore, 352-nm excitation produced direct excitation of the lanthanide ion and the emission spectrum is, in fact, in agreement with the published fluorescence spectrum of Tb^{3+}; i.e., it comprises four narrow luminescence lines centered at 494, 550, 597, and 625 nm (*18–24, 30–31*). These peaks have been attributed to the $^7F_6 \leftarrow {}^5D_4$, $^7F_5 \leftarrow {}^5D_4$, $^7F_4 \leftarrow {}^5D_4$ and $^7F_3 \leftarrow {}^5D_4$ transitions, respectively (*30*). Due to the low luminescence quantum yield, the emission intensity is, as expected, very low. Excitation of the extracted ion pair complexes at 290 nm produced a spectrum whose shape is the same as that obtained by 352-nm excitation but whose intensity is substantially higher than that of the 352-nm excitation (Figure 2). As described above, the absorbance of the Tb^{3+} ion at 290 nm is much lower than that at 352 nm. Therefore, the observed emission spectrum is not due solely to the direct excitation of the ion, because if it were, it would have had lower intensity than the one taken by 352-nm excitation. Taken together with the facts that include the similar but substantially high intensity of the spectrum obtained at 290-nm excitation as compared to that measured by 352-nm excitation, the extracted ion pair complex contains one rare-earth ion and three benzoate anions whose absorbance at 290 nm is about 151 times more than that of the ion, it is clear that the enhancement in the observed emission intensity is due to the energy transfer from the benzoate counterion to the lanthanide ion. Similarly, benzoate counteranion can also transfer energy to the Eu^{3+} as well as to the Dy^{3+} ion in the ion pair complexes, which were extracted into the organic phase. The evidence for these energy transfer processes is shown in Figure 3 and 4, which illustrate that because of the energy transfer, the spectra obtained with 290-nm excitation have a similar band shape as those obtained by using the 352-nm (Dy^{3+}) and 395-nm (Eu^{3+}) excitation wavelengths but with substantially higher intensities.

As mentioned above, energy transfer from aromatic hydrocarbons such as naphthalene, 1-naphthaldehyde, benzil, benzophenone, benzaldehyde, tryptophane, and tyrosine to lanthanide ions such as Tb^{3+} or to Eu^{3+} has been reported (*22–24*). However, in all cases, the lanthanide ions are either directly chelated to the aromatic compounds or presented in much higher concentrations. The present study demonstrates for the first time that by using the (donor) aromatic compound as a counteranion of the extracted lanthanide–crown ether trivalent cation, energy transfer from the donor to the rare-earth ion acceptor can be achieved efficiently at much lower concentration.

The determination of the luminescence enhancement by energy transfer is not simple but rather requires special consideration. This is due to the fact that even though the absorbances of the lanthanide ions at 290 nm are very small, they cannot be ignored. As a consequence, the luminescence observed when exciting the lanthanum–crown ether–benzoate ion pair complexes at 290 nm is due to the emission of the excited lanthanide ions produced by the energy transfer as well as by the direct excitation of the rare-earth ions. Therefore, the contribution to the observed luminescence by the direct excitation of the lanthanide ions needs to be known in order to calculate the enhancement by the energy transfer. This information could be obtained by measuring the luminescence, excited at 290 nm, of the lanthanide ions in the organic solvents without the benzoate. Unfortunately, such solutions cannot be prepared because the lanthanide ions are not soluble in the organic solvents. Even though the lanthanide ions can be dissolved in water without the benzoate, their luminescence intensities in water are much lower than those in organic solvents. As a consequence, the luminescence of the aqueous solution of the lanthanide ions cannot be used to correct for the calculation of the enhancement by the energy transfer in the organic solvents.

The calculation of the luminescence intensity of the extracted lanthanide ion complexes in the organic solvent produced not by energy transfer but by direct absorption of the ions was performed based on the fact that luminescence intensity is directly proportional to the absorbance at the excitation wavelength (*20, 30*). Typically, the luminescence intensity of the extracted lanthanide ion–crown ether–ben-

Table I. Luminescence Enhancement of Lanthanide Ion Complexes by Extracting Into Organic Solvent and by Energy Transfer

ion	solvent	organic solvent enhancement (F_{sol}/F_{H_2O})	energy transfer enhancement ($(F_{sol})_{pres}/(F_{sol})_{abs}$)	total enhancement
Tb^{3+}	ethyl acetate	3.5	12.5	43.8
Tb^{3+}	chloroform	3.6	6.5	23.4
Dy^{3+}	ethyl acetate	4.0	15.0	60.0
Dy^{3+}	chloroform	4.0	5.3	21.2
Eu^{3+}	ethyl acetate	4.0	16.9	67.6
Eu^{3+}	chloroform	3.9	3.2	12.5

zoate ion pair complexes was measured by using two different wavelengths: 290 and 352 nm (for Tb^{3+} and Dy^{3+}) and 290 and 395 nm (for Eu^{3+}). The former (290 nm) is the wavelength at which energy transfer occurs, whereas at the latter wavelengths (352 or 395 nm), only the lanthanide ions were excited as the benzoate does not absorb at these wavelengths. Because the luminescence intensity of the lanthanide ion in the absence of energy transfer, F_{352}, is directly proportional to the absorbance of the ion at this wavelength, A_{352}, the luminescence intensity of the ion in the organic phase, excited at 290 nm and in the absence of the energy transfer, $F_{(290)abs}$ can be calculated from the F_{352}, A_{352}, and the A_{290} values. The A_{352} (or A_{395}) and A_{290} values were obtained from the absorption spectra of the lanthanide ions in water (without the benzoate). The calculated $F_{(290)abs}$ values enable the determination of the enhancement in the luminescence intensity of the lanthanide ion by energy transfer, EN. This EN value is defined as

$$EN = F_{(290)pres}/F_{(290)abs}$$

where $F_{(290)pres}$ and $F_{(290)abs}$ are the luminescence intensity of the extracted lanthanide ion complexes in the organic phase in the presence and absence of energy transfer, respectively. The EN values obtained are shown in Table I. As shown in the table, the luminescence of the Tb^{3+} ion in ethyl acetate was found to be enhanced 12.5 times when the benzoate counteranion was used to absorb the light and to subsequently transfer the energy to the metal ions. Compared to the Tb^{3+} ion, the luminescence enhancement by energy transfer is relatively higher when the Dy^{3+} or Eu^{3+} ion is used as acceptor. For instance, up to 15 and 17 times enhancement was achieved for Dy^{3+} and Eu^{3+}, respectively. The enhancement was also found to depend on the type of organic solvent used. Higher enhancement was found for ethyl acetate as compared to chloroform: for the same experimental conditions, the luminescence enhancement by energy transfer for Tb^{3+} ion in ethyl acetate was 12.5 times, whereas only 6.5 times enhancement was achieved in chloroform.

It should be added that in addition to the enhancement by energy transfer, the luminescence of the lanthanide ions is also increased when they are extracted from the water into the organic solvent. This is due to the quenching by the high-frequency vibrations (overtones) of the OH groups of water (*20*, *23*, *32*). To determine this enhancement, we used the lanthanoid(III) benzoate instead of the $TbCl_3$, $EuCl_3$, or $DyCl_3$ because the synthesized lanthanoid benzoate complexes are soluble in water as well as in organic solvents, whereas the chloride salt can only be dissolved in water. In this experiment, equal amounts of the lanthanoid(III) benzoate (i.e., TbB_3, EuB_3, and DyB_3) were dissolved in water and in organic

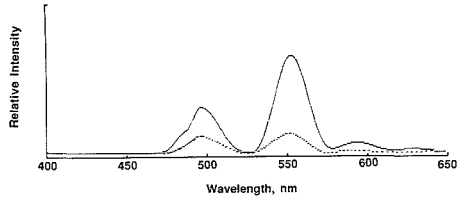

Figure 5. Luminescence spectra of equal concentration of Tb(benzoate)$_3^{3+}$ complexes in ethyl acetate (——) and in water (- - -).

Table II. Energy Transfer Parameters

ion	solvent	energy transfer efficiencies, %	overlap integral,[a] $cm^6\ mol^{-1}$	lifetime,[a] μs
Eu^{3+}	ethyl acetate	12.6	9.7×10^{-16}	110
Eu^{3+}	chloroform	1.8		
Dy^{3+}	ethyl acetate	5.5	6.5×10^{-16}	7
Dy^{3+}	chloroform	1.7		
Tb^{3+}	ethyl acetate	2.5	1.1×10^{-16}	425
Tb^{3+}	chloroform	1.2		

[a] Taken from ref 30.

solvents (ethyl acetate and chloroform), and the luminescence spectra were obtained by exciting the solutions at 352 nm (for TbB_3 and DyB_3) or 395 nm (for EuB_3). It should be added that the benzoate does not absorb at these wavelengths, so that the enhancement by energy transfer is absent in these cases. These results obtained for TbB_3 are shown in Figure 5. As expected, substantial enhancement in the luminescence was observed when the ion was dissolved in ethyl acetate as compared to that in water. The relative enhancement values, calculated by comparing the area under the luminescence spectra are listed in Table I. Up to 4-fold enhancement in the luminescence was achieved when the ions were extracted from the water phase to the ethyl acetate as well as to the chloroform. It is anticipated that the absolute enhancement by the organic solvents is probably higher than the 4-fold enhancement observed here, because no effort was made to dry the organic solvents.

Taken together, the results presented clearly demonstrate that up to 67 times enhancement in the luminescence intensity of the lanthanide ions can be achieved by simply extracting the ions from water into organic solvent and measuring the luminescence by using the excitation that facilitates the energy transfer from the counteranion to the ions.

The overlap integrals, J, were calculated in order to elucidate the mechanism for the energy transfer process. These J values are defined as (*26*, *27*)

$$J = \int F_D(\lambda)\ \epsilon_A(\lambda)\ \lambda^4\ d\lambda$$

where $F_D(\lambda)$ is the phosphorescence of the donor (benzoate) and $\epsilon_A(\lambda)$ is the molar extinction of the acceptor (lanthanide ions). The J value is thus the measurement of the overlap between the emission of the donor and the absorption of the acceptor. The phosphorescence spectrum of the lead benzoate taken from ref 31 is shown in Figure 1 and was used to calculate the J values. The calculated values are listed in Table II together with the lifetimes of the lanthanide ions. The luminescence enhancement seems to be in agreement with the overlap integral; i.e., a higher enhancement value is obtained when the overlap between the donor emission and the acceptor absorption is large. For instance, the luminescence enhancement is highest for Eu^{3+} and benzoate. This is in agreement with the highest degree of overlap between the

of the benzoate (Figure 1) and the highest J value (Table II).

transfer. Thus, the energy transfer seems to be governed by

$^4F_{9/2}$ (Dy^{3+}) states of the lanthanide ions. The observation that the magnitude of the luminescence enhancement by

lanthanide ions further confirms the fact that the energy transfer is by the resonance mechanism rather than the dif-

transfer efficiency would have been observed for ion having

whose lifetimes are about 3.8 (Eu^{3+}) and 60 (Dy^{3+}) times lower.

where A_{acc} and A_{don} are the absorbances of the acceptor

of the lanthanide ions, excited at 290 nm, in the presence and

complex is generally found to contain three counteranions per

transfer efficiencies are listed in Table II. As expected, the ET values are in good agreement with the overlap integral J

compared to those for chloroform. This observation can be explained in terms of the solvation effect and the relative

which has a Guttmann's donor number of 17, can solubilize the ion pair formed between the crown ether–lanthanide ion

a consequence of this good solubilization, the distance between

ergy transfer is known to be inversely proportional to R^6 (R is the distance between the donor and the acceptor), it is,

in ethyl acetate are much higher than those in chloroform.

By use of this energy transfer enhancement effect, the yields

into ethyl acetate and chloroform were determined (Table III). For example, as shown in the table, for Dy^{3+} ion a higher

by ethyl acetate is consistent with its better donor properties of the solvent as mentioned above.

in the extraction process. For the same crown ether, higher extraction yields were found for the Dy^{3+} ion, which has a

thus can fit better into the cavity of the macrocyclic crown. For the same ion, the 18-crown-6 can extract more than the

lanthanide ions can be accomplished by using crown ether to extract the ions from water into organic solvent where they

Lanthanide Trivalent Ions from the Aqueous Phase into the Organic Phase

ion	solvent	crown ether	anion	extraction yield, %
Dy^{3+}	chloroform	15-crown-5	benzoate	33
Tb^{3+}	chloroform	15-crown-5	benzoate	30
Dy^{3+}	chloroform	18-crown-6	benzoate	37
Tb^{3+}	chloroform	18-crown-6	benzoate	35
Dy^{3+}	ethyl acetate	15-crown-5	benzoate	58
Tb^{3+}	ethyl acetate	15-crown-5	benzoate	57
Dy^{3+}	ethyl acetate	18-crown-6	benzoate	57
Tb^{3+}	ethyl acetate	18-crown-6	benzoate	56

acid; 1.0×10^{-3} M $LnCl_3$; and 0.1 M crown ether. See text for de-

sensitivity of this technique is relatively higher than other methods because the luminescence intensity of the rare-earth

the organic solvent. In this preliminary study and with the use of benzoate as counteranion, only 67-fold enhancement

and the method can be further expanded to other ions such

closely matched to the excited-state energy levels of the lanthanide ions. This is the object of our current intense scrutiny.

LITERATURE CITED

(2) Beaudry, B. J.; Gschneidner, K. A., Jr. In Handbook on the Physics
Eds.; North-Holland Publishing: Amsterdam, 1979; Vol. 3, p 173.
bridge University Press: Cambridge, 1989.
Reagents; CRC Press: Boca Raton, FL, 1982.
W., Eds.; American Chemical Society: Washington, DC, 1987.
(7) Tsay, L. M.; Shih, J. S.; Wu, S. C. *Analyst* **1983**, *108*, 1108.
Chem. **1983**, *76*, 49.
(10) Hasegawa, Y.; Haruna, S. *Solvent Extr. Ion Exch.* **1984**, *2*, 451.
Exch. **1987**, *5*, 255.
Exch. **1985**, *3*, 623.
1814.
(15) Bunzil, J.-C. G. In *Handbook on the Physics and Chemistry of Rare*
dam, 1987; Vol. 9, Chapter 60.
1988, *60*, 2527.
(18) Soini, E.; Lovgren, T. *CRC, Crit. Rev. Anal. Chem.* **1987**, *18*, 105.
(20) Sinha, A. P. B. In *Spectroscopy in Inorganic Chemistry*; Rao, C. N.
(21) Fisher, R. P., Winefordner, J. D. *Anal. Chem.* **1971**, *43*, 454.
(23) Heller, A.; Wasserman, E. *J. Chem. Phys.* **1965**, *42*, 949.
1977, *99*, 7749.
Soc. **1978**, *100*, 1254.
Edelhoch, H., Eds.; Marcel Dekker: New York, 1975; Vol. 1, Chapter
(27) Forster, T. *Modern Quantum Chemistry*; Sinanoglu, O., Eds., Academ-

(28) Taylor, M. D.; Carter, C. P.; Wynter, C. I. *J. Inorg. Nucl. Chem.* **1968**, *30*, 1503.
(29) Baba, H.; Kitamura, M. *J. Mol. Spectrosc.* **1972**, *41*, 302.
(30) Sinha, S. P. In *Systematics and Properties of the Lanthanides*; D. Reidel Publishing: Dordrecht, 1983; p 451.
(31) Tran, C. D. *Anal. Chem.* **1988**, *60*, 182.
(32) Horrocks, W. D.; Albin, M. *Progress in Inorganic Chemistry*; Lippard, S. J., Ed.; Wiley: New York, 1984; Vol 31, p 1.
(33) Marcus, Y. *J. Solution Chem.* **1984**, *13*, 599.

RECEIVED for review October 12, 1989. Accepted January 19, 1990.

Influence of Small Amounts of Organic Solvents in Aqueous Samples on Argon Inductively Coupled Plasma Spectrometry

John W. Olesik* and Alvin W. Moore, Jr.

Department of Chemistry, Venable and Kenan Laboratories, CB 3290, University of North Carolina, Chapel Hill, North Carolina 27599-3290

The presence of organic solvents in aqueous samples in concentrations as low as 0.1% by volume had a large effect on emission and fluorescence signals. Both atom and ion emission signals were depressed when organic solvents were present. In contrast, Sr II fluorescence intensities were enhanced by up to a factor of 3.5 when the sample contained 2% (v/v) organic solvent. More ions were produced when the sample contained organic solvent. However, the fractions of atoms and ions that were excited and emitted light decreased. Ar and H emission intensities can be used as diagnostic signals to warn the operator when plasma conditions have changed due to the presence of organic solvents.

The introduction of organic solvents into an argon inductively coupled plasma is known to affect excitation conditions and maximum aspiration rates for a stable plasma (*1–5*). If the sample contains mixtures of organic solvents, matrix matching of the samples and calibration standards or internal standardization is necessary (*6*).

Organic solvents mixed with water appear to have less effect on plasma stability than pure organic solvents. For example, 75% methanol/25% water mixtures can be introduced into the plasma with uptake rates of up to 3 mL/min while the maximum pure methanol uptake rate was 0.1 mL/min (*2, 7*).

However, variations in the concentration of organic solvents as low as 0.08% by volume can have a significant effect on emission intensities (*8, 9*). Therefore, errors may occur if samples that contain organic solvents are analyzed by using aqueous calibration standards.

The presence of organic solvents can affect the nebulization process (*10*), the aerosol mass transport rate (*1, 2, 10, 11*), and the vapor mass loading (*2, 12–14*). Nebulization of organic solvents generally produces a droplet distribution with a smaller mean droplet diameter than for water (*10*). Many organic solvents have high evaporation rates (*1, 3*). As a result of either or both of these factors, sample mass transport efficiency is enhanced in comparison to aqueous samples.

The introduction of organics into the argon plasma generally causes a reduction in both excitation temperatures and electron number densities. Blades and Caughlin (*3*) and Boumans and Lux-Steiner reported (*4*) that a 500-W increase in power was necessary to match excitation conditions with organic solvent introduction to those when aqueous samples were introduced. The extra power required for organic species has been suggested to be due to changes in the enthalpy of the carrier gas (*4*), energy consumed for atomization of the organic species, or variations in the thermal (*4*) or electrical conductivity (*15*). The plasma impedance has been reported to increase when organic solvent is introduced (*16*).

Table I. Instrumentation and Experimental Parameters

power supply	Plasma Therm 2500W, 27.12 MHz (HFP-2500D)
impedance matcher	Plasma Therm (AMNPS-1)
incident power	1.0 kW
gas	Ar
outer gas flow rate	10.0 L/min
intermediate gas flow rate	0.9 L/min
central gas flow rate	0.9 L/min
torch	Plasma Therm Low Flow (Precision Glass Blowing of Colorado)
nebulizer	Meinhard concentric, TR-30-A3
spray chamber	Scott type double barrel
sample pump	Peristaltic (Gilson Minipuls 3)
sample uptake rate	1.1 mL/min
sample Concentration	50 ppm Sr as $SrCO_3$ in distilled deionized water or mixtures of water and acetone, acetonitrile, or ethanol, 0.1%, 0.4%, 1.0%, or 2.0% by volume
spectrometer	McPherson Model 2016B with 3600 g/mm holographic grating
entrance slit width	100 μm for emission 500 μm for fluorescence
detector	EG& G Princeton Applied Research Corp. OMA III with Model 1420 intensified diode array and Model 1211 high voltage pulser
laser	Molectron UV-400 nitrogen laser, Molectron DL-300 dye laser
laser dyes	bis-MSB (Sr II), Coumarin 460 (Sr I)
spectral lines	Sr I, 460.73 nm Sr II, 421.55 nm

Here we report investigation of the effect of organic solvents present in concentrations less than 2% by volume. A combination of emission and fluorescence measurements was used to separate changes in emission intensity due to excitation effects from those caused by changes in atom or ion number densities.

EXPERIMENTAL SECTION

Experimental parameters and instrumentation for measurement of Sr II and Sr I emission and fluorescence signals are listed in Table I.

The optical system used to acquire lateral emission and fluorescence images was described previously (*17*). Abel inversion was performed on laterally resolved emission data using the al-

0003-2700/90/0362-0840$02.50/0

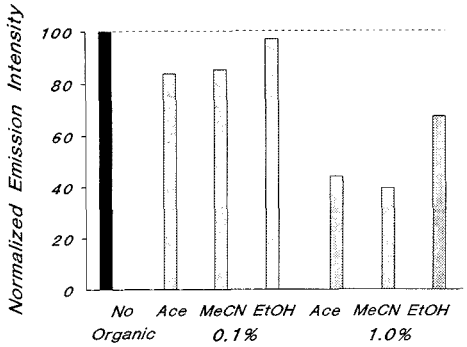

Figure 1. Change in Sr II emission intensity 14 mm above the load coil when organic solvents are present at a concentration of 0.1% or 1.0% by volume: Ace, acetone; MeCN, acetonitrile; EtOH, ethanol.

gorithm of Cremers and Birkebak (*18*).

Vertical emission profiles were acquired by using a single 2 in. diameter, 25 cm focal length, fused silica lens to form an image near the entrance slit of the spectrometer with a magnification of 0.38. A 1 in. diameter aperture was used for Sr II measurements. Exposure times of 16.6 and 64 ms were used for Sr II and Sr I measurements, respectively. Signals from 100 exposures were added.

RESULTS AND DISCUSSION

The presence of 0.1% (v/v) acetone or acetonitrile produced a 15% decrease in Sr II emission intensity in the normal analytical zone of the plasma (Figure 1). In contrast, the presence of 0.1% ethanol in water decreases the Sr II emission intensity by only 3%. When the concentration of each of the three organic solvents is increased to 1%, large decreases in Sr II emission intensity are observed (Figure 1). Of the three solvents ethanol produces the least severe depression in emission intensities.

Organic solvents generally have higher mass transport rates than water (*1, 2, 10, 11*). Increases in aqueous aerosol mass transport rate in inductively coupled plasma emission spectrometry decrease the emission intensity per mass of analyte aerosol entering the plasma (responsivity) (*19, 20*). The responsivity decreases most dramatically low in the plasma. It is likely that this is due to an increase in the number of desolvating droplets low in the plasma (*20, 21*). The peak emission intensity also moved higher in the plasma when the aerosol mass transport rate was increased.

When the concentration of acetonitrile in the aqueous sample was increased, the peak Sr II and Sr I emission intensity moved downward in the plasma (Figure 2). The presence of ethanol or acetone caused similar downward shifts. The shift was more pronounced for atom emission than ion emission. Depressions in the Sr II emission intensity in the presence of acetonitrile or acetone were more severe as the observation zone is moved higher in the plasma (Figure 3). In contrast, increased mass transport of aqueous aerosol produced larger depressions in emission responsivity low in the plasma (*20*).

The effect of equal volume fractions of ethanol was different from that of acetonitrile and acetone. The Sr II emission intensity was depressed by 38% at 9 mm above the load coil (ALC), 56% at 14 mm ALC, and 68% at 19 mm ALC in the presence 1.0% acetone. The magnitude of the Sr II emission intensity depression due to acetone was similar at 9 mm ALC, 14 mm ALC, and 19 mm ALC. One percent ethanol by volume depressed the Sr II emission intensity by 30% to 33% between 9 mm ALC and 19 mm ALC. The severity of the decrease in Sr I emission in the presence of each of the organic

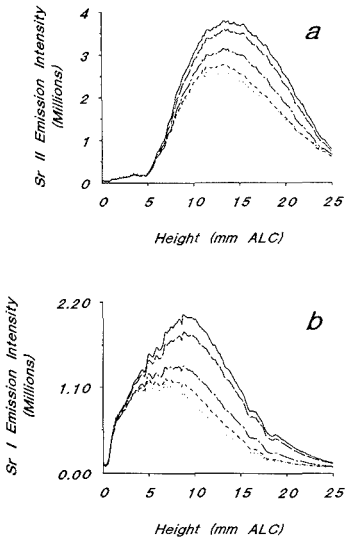

Figure 2. Intensity versus height in the plasma: (a) Sr II emission, (b) Sr I emission; concentration of acetonitrile by volume, 0% (——), 0.1% (– –), 0.4% (– – –), 1.0% (– –) and 2.0% (• • •).

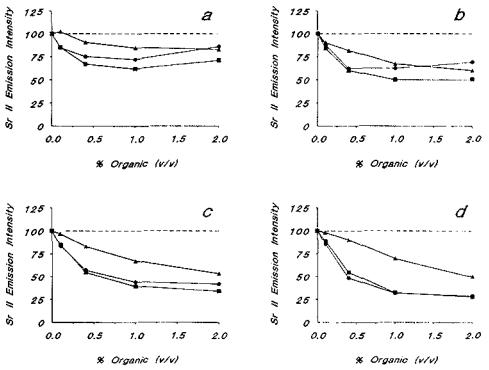

Figure 3. Changes in Sr II emission intensity as the concentration of organic solvent in the sample was changed: (a) 6 mm above the load coil, (b) 9 mm above the load coil, (c) 14 mm above the load coil, (d) 19 mm above the load coil; (■) acetonitrile, (●) acetone, (▲) ethanol.

solvents was greater at 14 mm ALC than at 9 mm ALC (Figure 4).

Long and Browner (*22*) observed that the peak analyte intensity occurred higher in the plasma when sample was introduced as an aqueous aerosol than when dry, electrothermally vaporized sample was used. The authors concluded that the location of the peak intensity depended on the distance droplets must travel before desolvation is complete. The results of Bates and Olesik (*20*) supported this conclusion.

We observed a downward shift in the location of the peak intensity when organic solvent was added. If the location of peak emission intensity is related to the point where desolvation is complete, either the droplets entering the plasma are smaller in the presence of organics or the desolvation rate is higher.

Changes in emission intensity can result from variations in the ion (atom) number density or changes in the fraction of ions (atoms) that emit. Therefore, we measured both

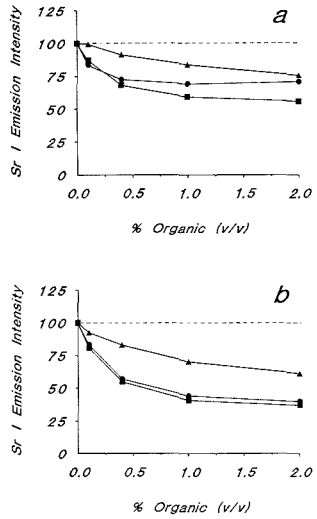

Figure 4. Changes in Sr I emission intensity as the concentration of organic solvent in the sample was changed: (a) 9 mm above the load coil, (b) 14 mm above the load coil; (■) acetonitrile, (●) acetone, (▲) ethanol.

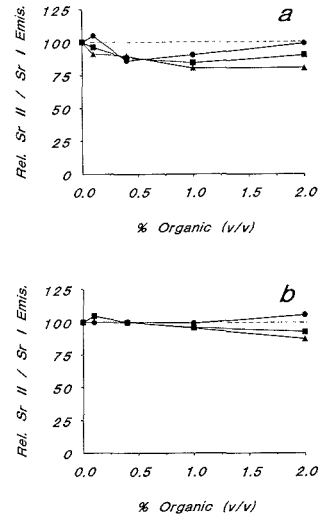

Figure 5. Changes in relative Sr II/Sr I emission intensity ratio. The intensity values for Sr II and Sr I emission without organic solvent were normalized to 100: (a) 9 mm above the load coil, (b) 14 mm above the load coil; (■) acetonitrile, (●) acetone, (▲) ethanol.

emission and fluorescence intensities. Fluorescence was saturated so that prefilter and quenching effects were minimized. The fluorescence intensity should be proportional to the ground-state number density. If the fraction of ions (atoms) in the ground state does not change due to the presence of organics, the fluorescence intensity should be proportional to the total ion (atom) number density.

The ion number density could change because of shifts in the ion–atom equilibrium or variations in the total analyte number density. If the presence of organic solvent affected the nebulization and aerosol modification processes, the amount of analyte entering the plasma per second could change. If the point where droplet desolvation and particle vaporization are complete moves down, the analyte number density at points above this could decrease as a result of diffusion.

Ion–atom emission intensities are often used to assess plasma conditions (*23–26*). At both 9 mm ALC and 14 mm ALC the Sr II/Sr I emission intensity ratio changed by less than 20% when the concentration of organic solvent was varied from 0 to 2.0% (Figure 5). Therefore, based only on the Sr I and Sr II emission data, it appeared the plasma conditions did not change drastically. The observed depressions in emission intensity might be attributed to decreases in the amount of sample reaching the plasma.

The fluorescence data show that the analyte ion number density increased as organic solvent was added (Figure 6). Enhancements were as large as 50%. The enhancement of the fluorescence intensities was larger higher in the plasma. In contrast, the Sr I fluorescence intensities decreased dramatically when organic solvent was added (Figure 7).

The fluorescence data suggest that there was a shift in the relative number of ions and atoms. It appears that there were more ions and fewer atoms. The ion-to-atom fluorescence intensity ratio increases by up to a factor of 3.5 (Figure 8). However, there is an offsetting decrease in the fraction of ions that emit light. The Sr II emission intensity fell when organic solvent was present. Sr II emission-to-fluorescence intensity ratio (E/F) fell by as much as a factor of 5 (Figure 9a,b). At

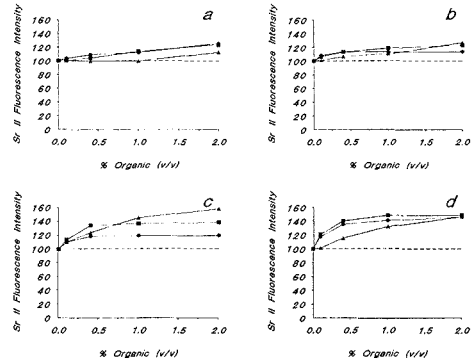

Figure 6. Sr II fluorescence (radially integrated) as the concentration of organic solvent in the sample was changed: (a) 6 mm above the load coil, (b) 9 mm above the load coil, (c) 14 mm above the load coil, (d) 19 mm above the load coil; (■) acetonitrile, (●) acetone, (▲) ethanol.

14 mm ALC each organic solvent caused a 50% or larger decrease in the Sr II E/F when present at a concentration of 2% by volume. Among the three organic solvents used, ethanol had the least severe effect on the Sr II E/F. The Sr I E/F decreased less in the presence of the organic solvents than the Sr II E/F (Figure 9c). At 14 mm ALC the Sr I E/F intensity ratio changed by less than 20% in the presence of ethanol.

The radially integrated data show that the Sr atom number density decreases in the presence of organics. The fraction of Sr atoms that is excited also falls. More Sr ions are produced when organic solvents are present. However, the fraction of Sr ions that is excited falls dramatically.

The observed behavior may be due to a combination of changes in droplet size or desolvation rate, ion to atom number densities, and the number of photons produced per atom or ion. If droplets entering the plasma are smaller, desolvation

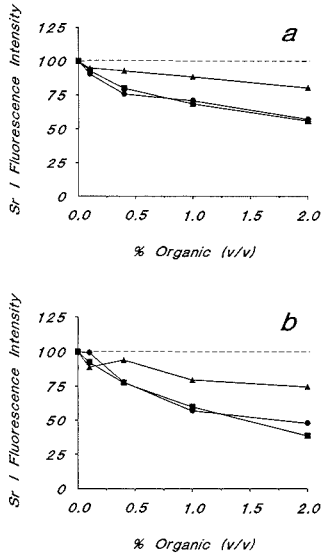

Figure 7. Sr I fluorescence (radially integrated) as the concentration of organic solvent in the sample was changed: (a) 9 mm above the load coil, (b) 14 mm above the load coil.

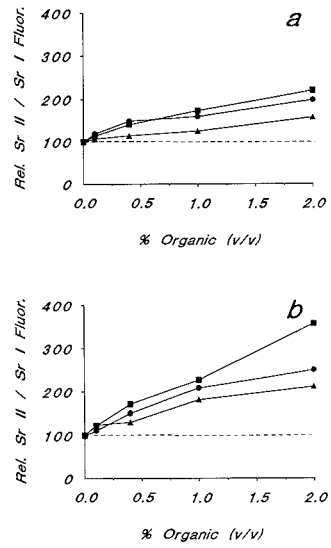

Figure 8. Relative Sr II/Sr I fluorescence intensity ratio as the concentration of organic solvent in the sample was changed: (a) 9 mm above the load coil, (b) 14 mm above the load coil; (■) acetonitrile, (●) acetone, (▲) ethanol. The intensity values for Sr II and Sr I fluorescence without organic solvent were normalized to 100.

should be complete lower in the plasma. Olesik et al. (*21*) showed that ion emission intensities are depressed near a desolvating water droplet while atom emission intensities increased. This observation can only be explained by a change in the relative number of ions and atoms toward more atoms. Therefore, if fewer droplets exist in the observation zone, the ion/atom number density ratio should increase. This is consistent with the observed fluorescence behavior. Further, we have made initial laser light scattering measurements. The

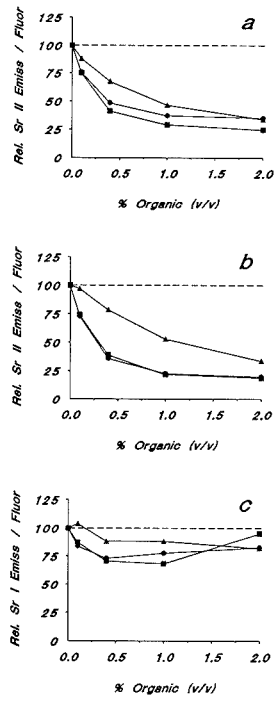

Figure 9. Relative emission/fluorescence intensity ratio as the concentration of organic solvent in the sample was changed: (a) Sr II 9 mm above the load coil, (b) Sr II 14 mm above the load coil, (c) Sr I 14 mm above the load coil. The intensity values for Sr II and Sr I emission and fluorescence without organic solvent were normalized to 100.

scattering intensity generally decreased when organic solvent was added to the aqueous sample. Therefore, fewer large droplets appeared to be present in the observation zone as the organic solvent concentration was increased.

The decrease in the fraction of excited, emitting atoms and ions could be due to changes in thermal transport properties, quenching of excited states via collisions with molecular species, or consumption of energy to atomize the organic species. The decrease in ion emission intensity was due to less efficient production of light rather than fewer ions. The addition of pure organic solvents to the plasma is known to reduce excitation temperatures and electron number densities significantly (*3*, *4*). Caughlin and Blades (*3*) observed a factor of 2 decrease in electron number density 15 mm above the load coil when xylene rather than water was introduced into the plasma. The severity of the plasma cooling can be reduced by reducing the amount of organic vapor entering the plasma (*13*, *14*).

The effect of the presence of organic solvents in the sample was both vertically and radially dependent. At 14 mm ALC Sr II fluorescence intensities were enhanced off-axis by the presence of each of the organic solvents (Figure 10). On axis, the changes in Sr II fluorescence intensity were different for each of the three organic solvents (Figures 10 and 11). Ethanol produced an enhancement of Sr II fluorescence intensities. As the fraction of acetonitrile in the sample was increased, the fluorescence intensity first increased (0.1%, 0.4% acetonitrile) and then decreased (1.0%, 2.0% acetonitrile). Concentrations of acetone that were 0.4% or greater depressed the fluorescence intensities.

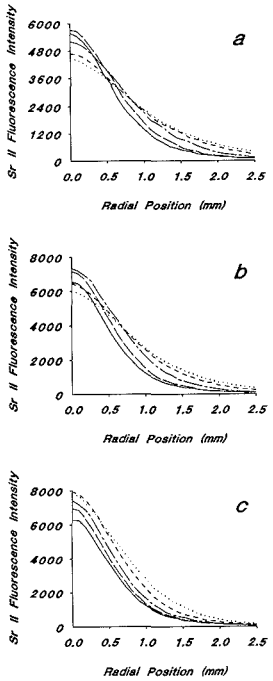

Figure 10. Sr II radially resolved fluorescence profiles at 14 mm above the load coil: (a) effect of acetone, (b) effect of acetonitrile, (c) effect of ethanol; concentration of organic solvent by volume, 0% (——), 0.1% (– –), 0.4% (– – –), 1.0% (– · –) and 2.0% (· · ·).

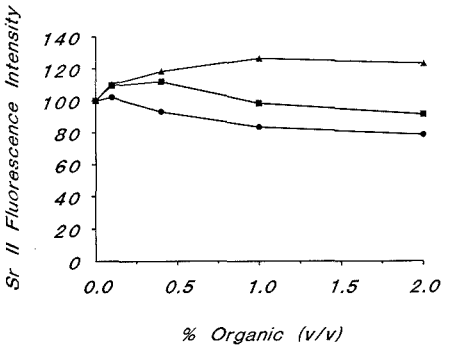

Figure 11. Sr II fluorescence in the radial center of the plasma at 14 mm above the load coil: (■) acetonitrile, (●) acetone, (▲) ethanol.

The Sr II emission intensities fell dramatically on-axis (Figure 12). Ethanol produced the smallest depression at least partially because it caused an increase in the ion number density, as shown by the rise in fluorescence intensity. Off-axis the depression in emission intensity was smaller. Increases in ion number density (as shown by fluorescence measurements) offset the decrease in the fraction of ions that were excited and emitted light.

Because small amounts of organic solvent can cause large depressions in emission signals, it would be useful to have diagnostic signals to inform the instrument operator when excitation conditions in the plasma are affected. Both Ar and

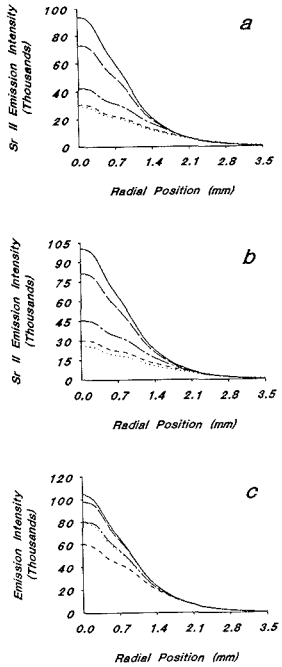

Figure 12. Sr II radially resolved emission profiles at 14 mm above the load coil: (a) effect of acetone, (b) effect of acetonitrile, (c) effect of ethanol; concentration of organic solvent by volume, 0% (——), 0.1% (– –), 0.4% (– – –), 1.0% (– · –) and 2.0% (· · ·).

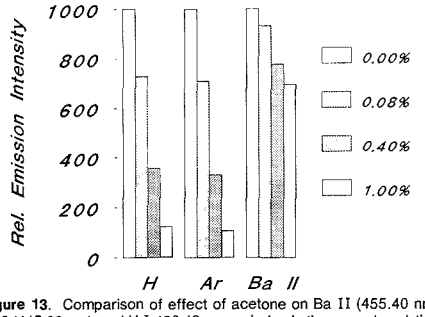

Figure 13. Comparison of effect of acetone on Ba II (455.40 nm), Ar I (415.86 nm), and H I 486.13-nm emission in the normal analytical zone.

H emission intensities were also severely affected by the presence of organic solvent (Figure 13). Therefore, each would be an effective diagnostic signal. C or C_2 emission, which increases with increasing amounts of organic solvent, could also be used as a diagnostic signal.

The large depression in Ar and H intensities shows that fewer atoms were excited when organic solvents were introduced into the plasma. The Ar and H emission depressions were more severe than those observed for Sr II or Ba II emission. This is most likely because Ar and H have large excitation energies in comparison to the Sr II or Ba II lines observed. Further, the Sr and Ba ion number densities increase with the addition of organic solvent. Analyte species with high excitation energies, such as Zn I or Zn II, will

probably be more severely affected than Sr II or Ba II emission as well.

CONCLUSIONS

The presence of small amounts of an organic solvent in an aqueous sample severely depressed emission intensities. This can produce large errors in analysis if concentration of the organic solvents in the calibration standards are not closely matched to the sample. Ar and H emission intensities are useful as diagnostic signals to warn the operator that plasma excitation conditions have been affected.

The depression of emission intensities when organic solvents are present in the sample suggests that excitation temperatures are lower. However, ion to atom emission intensity ratios change little in the normal analytical zone (14 mm ALC). Further, the ion-to-atom fluorescence intensity ratio increases dramatically when organic solvent is present in the sample. Increases in ion-to-atom intensity ratios are generally associated with increases in temperature.

The observed behavior is consistent with a combination of a cooler excitation temperature or quenching, a shift in the relative numbers of ions and atoms, and desolvation of droplets lower in the plasma. Desolvation of droplets appears to be complete lower in the plasma when organic solvents are present in the sample.

Further experiments are needed to understand the observed behavior. Experiments with a wider range of organic solvents are necessary to identify the physical or chemical properties leading to depression of emission intensities. Measurement of aerosol mass transport rates and tertiary droplet size distributions of pure aqueous solutions and solutions containing small fractions of organic solvents is also needed. The relative importance of aerosol versus vapor loading must be assessed. Changes in the effect of the presence of organic solvent as a function of applied power and central gas flow rate must be studied. The effect of the presence of organic solvent on species with a wide range of excitation and ionization energies must be investigated. Each of these studies is now underway in our laboratories.

ACKNOWLEDGMENT

Princeton Applied Research Corporation is thanked for loan of the intensified diode array. The Perkin-Elmer Corporation is acknowledged for donation of the ICP power supply and impedance matcher. The nitrogen laser pumped dye laser was on loan from the UNC Department of Chemistry Laser Laboratory. The important contributions of Don Brewer, Don Tice, Ken Vickers, Ralph Carney, Jules Kelley, and Harlan Mangum of the UNC Department of Chemistry Instrument Shop are recognized.

Registry No. acetone, 67-64-1; acetonitrile, 75-05-8; ethanol, 64-17-5.

LITERATURE CITED

(1) Boorn, A. W.; Browner, R. F. In *Inductively Coupled Plasma Emission Spectroscopy, Part II*; Boumans, P. W. J. M., Ed.; Wiley-Interscience: New York, 1987; Chapter 6.
(2) Boorn, A. W.; Browner, R. F. *Anal. Chem.* **1982**, *54*, 1402.
(3) Blades, M. W.; Caughlin, B. L. *Spectrochim. Acta* **1985**, *40B*, 579.
(4) Boumans, P. W. J. M.; Lux-Steiner, M. Ch. *Spectrochim. Acta* **1982**, *37B*, 97.
(5) Miyazaki, A.; Kimuira, A.; Bansho, K.; Umezaki, Y. *Anal. Chim. Acta* **1982**, *144*, 213.
(6) Botto, R. I. *Spectrochim. Acta* **1987**, *42B*, 181.
(7) Nisamaneepong, W.; Haas, D. L.; Caruso, J. A. *Spectrochim. Acta* **1985**, *40B*, 3.
(8) Olesik, J. W.; Williamsen, E. J.; Hadnagy, M. Pittsburgh Conference on Analytical Chemistry and Applied Spectroscopy, New Orleans, LA, February 1988; paper 1323.
(9) Olesik, J. W.; Alam, A.; Denker, M. S., unpublished research.
(10) Boorn, A. W.; Cresser, M. S.; Browner, R. F. *Spectrochim. Acta* **1980**, *35B*, 823.
(11) Greenfield, S.; McGeachin, H. McD.; Smith, P. B. *Anal. Chim. Acta* **1976**, *84*, 67.
(12) Maessen, F. J. M. J.; Seeverens, P. J. H.; Kreuning, G. *Spectrochim. Acta* **1984**, *39B*, 1171.
(13) Kreuning, G.; Maessen, F. J. M. J. *Spectrochim. Acta* **1987**, *42B*, 677.
(14) Kreuning, G.; Maessen, F. J. M. J. *Spectrochim. Acta* **1989**, *44B*, 367.
(15) Goldfarb, V. M.; Goldfarb, H. V. *Spectrochim. Acta* **1985**, *40B*, 177.
(16) Ito, T.; Kawaguchi, K.; Mizuike, A. *Bunseki Kagaku* **1979**, *28*, 648.
(17) Olesik, J. W.; Williamsen, E. J. *Appl. Spectrosc.* **1989**, *43*, 933.
(18) Cremers, C. R.; Birkebak, *Appl. Opt.* **1966**, *5*, 1037.
(19) Farino, J.; Miller, J. R.; Smith, D. D.; Browner, R. F. *Anal. Chem.* **1987**, *59*, 2303.
(20) Bates, L. C.; Olesik, J. W. The Effect of Sample Aerosol Transport Rate on Inductively Coupled Plasma Emission and Fluorescence, *J. Anal. At. Spectrosc.*, in press.
(21) Olesik, J. W.; Smith, L. J.; Williamsen, E. J. *Anal. Chem.* **1989**, *61*, 2002.
(22) Long, S. E.; Browner, R. F. *Spectrochim. Acta* **1986**, *41B*, 639.
(23) Caughlin, B. L.; Blades, M. W. *Spectrochim. Acta* **1984**, *39B*, 1583.
(24) Blades, M. W.; Caughlin, B. L.; Walker, Z. H.; Burton, L. L. *Prog. Anal. At. Spectrosc.* **1987**, *10*, 57.
(25) Boumans, P. W. J. M.; deBoer, F. *Spectrochim. Acta* **1977**, *32B*, 365.
(26) Furuta, F.; Nojiri, Y.; Fuwa, F. *Spectrochim. Acta* **1985**, *40B*, 423.

RECEIVED for review September 29, 1989. Accepted January 8, 1990. This work was supported by the UNC Department of Chemistry, a Du Pont Young Faculty Grant, and the Biomedical Research Support Grant Program of the Division of Research Resources from the National Institutes of Health (BRSGS07 RR07072).

Surface-Enhanced Raman Scattering of Dopamine at Polymer-Coated Silver Electrodes

Michael L. McGlashen, Kevin L. Davis, and Michael D. Morris*

Department of Chemistry, University of Michigan, Ann Arbor, Michigan 48109-1055

Attenuation of dopamine surface-enhanced Raman scattering (SERS) spectra at silver electrodes by protein adsorption is described. Polymer-modified electrodes eliminate protein adsorption effects. Partially hydrolyzed cellulose acetate coatings prevent protein adsorption and allow transport of dopamine to and from the electrode surface. Dopamine SERS spectra from these electrodes are similar to those obtained at uncoated electrodes. Perfluorosulfonate (Nafion) coatings also prevent protein adsorption. However, dopamine transported to the electrode remains trapped inside the coating and cannot be removed.

INTRODUCTION

In the years immediately following the discovery of surface-enhanced Raman scattering (SERS) (*1*), most research focused on elucidation of SERS enhancement mechanisms and descriptions of applicable substrates (*2–5*). As the technique has matured, attention has shifted to application of SERS, in analytical chemistry and other fields. SERS has been proposed for the analysis of nitro polynuclear aromatic compounds (*6*), pesticides (*7*), and groundwater contaminants (*8, 9*). SERS has also been proposed as a detector for high-performance liquid chromatography and flow-injection analysis systems (*10, 11*).

Coincident with the changing interest in SERS, chemists have begun to concentrate on aspects of the technique that directly affect its performance as an analytical tool. For example, Laserna and co-workers (*12*) have recently shown that coadsorption of analytes leads to nonlinear working curves and a reduced concentration range.

We have previously reported the SERS spectra of the catecholamine neurotransmitters and related compounds (*13*). We have shown that dopamine and norepinephrine give intense SERS at silver electrodes at physiological pH. The catecholamines are adsorbed as cations at this pH. Anionic catecholamine metabolites are SERS inactive under the conditions of the measurement.

Most SERS measurements are performed in simple synthetic electrolyte solutions. For SERS to be an effective analytical technique in neurochemistry, however, it is necessary to confront the matrix effects that may be present in neurochemical samples. Electrode fouling by proteins will make conventional SERS measurements of catecholamines difficult or impossible in brain extracellular fluid, cell extracts, brain slices, or any other protein-rich medium.

We have reported the effects of serum albumin addition on dopamine SERS intensity using an electrode that is negatively biased prior to addition of the sample (*14*). We have shown that SERS spectra of dopamine in perfusion dialysates are nearly the same as those obtained in inorganic buffers (*14*). Perfusion dialysis reduces the protein burden and eliminates the surfactant effect (*15, 16*). However, development of a SERS probe which could work directly in complex matrices without a separation step would be advantageous.

Analytical electrochemists use polymer-coated electrodes extensively for protection from electrode fouling by large surfactant molecules or ions (*17–20*). Coatings may also improve stability, selectivity, and sensitivity of the electrode. Nafion, cellulose acetate, and poly(vinyl chloride) are among the polymers commonly used.

Nafion (Du Pont) is a perfluorinated ionomer which has a large ion-exchange affinity for organic cations relative to simple inorganic cations (*21*). Because of the large selectivity coefficients for hydrophobic cations (10^3–10^6), Nafion has been used to preconcentrate organic cations at electrode surfaces prior to voltammetric detection (*21, 22*). Porous coatings also serve to block polymeric solutes by size exclusion.

Cellulose acetate coatings offer similar size-exclusion protection from electrode fouling by large molecules. Unlike Nafion, cellulose acetate is not an ion exchanger. In principle, any small anion or cation can diffuse through a cellulose acetate membrane. Wang and co-workers have recently used controlled base-hydrolysis of cellulose acetate films to manipulate size selectivity (*19, 20*), Weber et al. generate cellulose acetate coatings by using a phase inversion method (*17*).

In this paper, we discuss the effect of albumin addition on SERS measurements in which the working electrode bias has not been established prior to sample addition. This experiment more closely represents conditions under which useful neurochemical measurements must be made. We report dopamine SERS at Nafion and cellulose acetate coated silver electrodes and demonstrate application to protein-rich matrices.

EXPERIMENTAL SECTION

Apparatus. Spectra were obtained with a Spex 1877 triple spectrograph fitted with an 1800 grooves/mm grating in the spectrograph stage and a PAR OMA III intensified diode array or Photometrics series 200 cryogenically cooled CCD detector. Spectra were obtained with 25–100 mW Ar^+ 514.5-nm or Nd/YAG 532-nm excitation at the sample. Integration times were 120 s. SERS measurements were obtained in a two-electrode electrochemical cell. Illumination and scattered light collection were through a fiber optic probe (*25*) or an inverted research microscope (Olympus, IM-2) using a 10× ultralong working distance objective. Sample size was 0.25 mL. All measurements were made at −0.9 V vs Ag/AgCl unless otherwise noted. All spectra were prepared for presentation by using a 13-point Savitzky–Golay quadratic/cubic smooth.

The working electrode was a 2 mm diameter silver disk formed by epoxy cementing a silver (Alfa 99.99%) wire into a glass tube. The reference electrode was an anodized, Teflon-coated silver (Medwire 99.99%) wire which also acted as the counter electrode.

Reagents. Dopamine hydrochloride and bovine serum albumin (Sigma) were used as received. Cellulose acetate (Scientific Polymer Products, 39.8% acetyl content) and Nafion (Aldrich, 1100 E.W., solution in lower aliphatic alcohols) were used as received. All other compounds were ACS reagent grade. Analyte solutions were prepared with type I water. These solutions were buffered to pH 7.2 with 0.1 M phosphate unless otherwise noted. Solutions contained 0.1 M potassium chloride and excess ascorbate to prevent oxidation. A 1.25% cellulose acetate solution was prepared in a 1:1 mixture of acetone and cyclohexanone.

Procedure. Uncoated 2 mm diameter silver electrodes were polished and conditioned by using an oxidation–reduction cycle (ORC) as previously described (*13*). Nafion-coated electrodes were formed by first generating a SERS-active electrode using the same

0003-2700/90/0362-0846$02.50/0

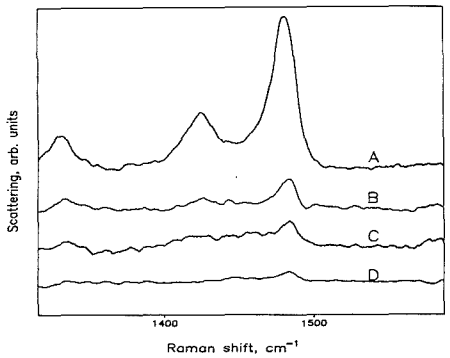

Figure 1. Effect of bovine serum albumin (BSA) addition on the SERS spectrum of 1×10^{-4} M dopamine in pH 7.2 buffer at −0.9 V: (A) 0.0% BSA, (B) 0.1% BSA, (C) 0.2% BSA, (D) 0.3% BSA.

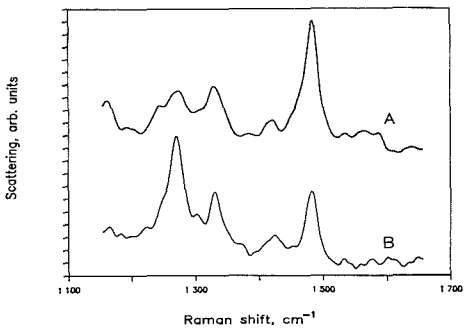

Figure 2. 1×10^{-4} M dopamine SERS spectra (A) at pH 8.6, −0.5 V vs Ag/AgCl, and (B) at pH 7.2, −0.9 V vs Ag/AgCl.

procedure. The roughened electrode was allowed to dry in air and dip-coated in the Nafion solution. The electrode was dried for 5 min under a gentle air stream at room temperature and placed in a sealed vial overnight before use.

Cellulose acetate coatings were formed by using a modification of the procedure of Wang et al. (*19*). Two microliters of 1.25% cellulose acetate was applied by syringe to the top of a polished working electrode and allowed to dry for 30 min in air. The film was then hydrolyzed in a stirred 0.07 M KOH solution for 60 min. The electrode was rinsed with distilled water, placed in the electrochemical cell, and conditioned by using the ORC for a bare electrode.

RESULTS AND DISCUSSION

Figure 1 shows the effects of albumin addition on the dopamine SERS spectrum obtained at a silver electrode biased to −0.9 V after immersion in the solution. Although the effect is similar to that obtained by using a prebiased electrode, complete suppression of dopamine SERS occurs at a lower protein burden. At 0.1% bovine serum albumin (BSA), the SERS intensity drops to less than half of that obtained in a protein-free solution. Above 0.3%, the spectrum is completely eliminated. Using a pre-biased electrode, we have previously shown a residual signal at 1.0% BSA. The present experiment is carried out under conditions more commonly encountered in practice.

Figure 2 shows dopamine SERS spectra at uncoated electrodes at pH 7.2 and 8.6. At pH 7, the C—O stretch (1269 cm^{-1}) and ν_{19b} (1479 cm^{-1}), which is primarily a phenyl C=C stretch, have similar intensities and maximize at −0.9 V vs Ag/AgCl, near the point of zero charge (*26*). However, between pH 8.6 and 10, ν_{19b} is more intense than any other band in this region and maximizes at −0.5 V vs Ag/AgCl, where the electrode surface bears a net positive charge. Similar effects are observed with catechol itself.

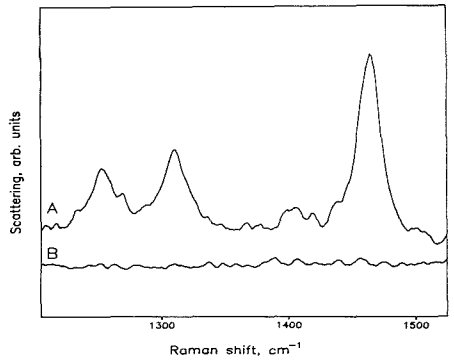

Figure 3. 1×10^{-4} M dopamine SERS spectra (pH 7.2) at −0.5 V in the presence of 0.5% BSA using (A) a Nafion-coated electrode and (B) an uncoated electrode.

Because the pK_1 and pK_2 of dopamine (catechol hydroxyl and ethyl ammonium, respectively) are 8.87 and 10.63 (*27*), the catecholate/ethylammonium zwitterion is an important species between pH 8.6 and pH 10. There is no change in SERS frequencies which might suggest a change in the adsorbed species at alkaline pH. A tentative explanation is that the relative intensity changes at higher pH may be due to differences in surface orientation between the cation and zwitterion.

Figure 3a shows the dopamine SERS spectrum obtained in pH 7.2 buffer in the presence of 0.5% bovine serum albumin (BSA) at a Nafion-coated electrode. The effect of 0.5% BSA on an uncoated electrode is to eliminate the spectrum completely, as shown in Figure 3b. Therefore, the Nafion coating is adequate to protect the electrode surface from fouling. The spectrum has at least twice the intensity of the spectrum of dopamine at the same concentration adsorbed onto a bare silver electrode. The preconcentration effect is similar to that reported previously in voltammetry (*21*, *22*). No Nafion bands are visible in the dopamine spectrum of Figure 3a. Although one might expect to see at least some aromatic ring vibrations, Nafion is a polyanion which is desorbed at the potential of this experiment.

The relative band intensities of dopamine at a Nafion-coated electrode are those observed at pH 8.6 or higher at a bare electrode. In addition, band intensities maximize around −0.5 V vs Ag/AgCl, rather than around −0.9 V. This behavior is curious, because the internal pH of Nafion is more acidic than the solution pH (*23*, *24*). These pieces of evidence suggest adsorption of a catecholate zwitterion or possibly to an orientation of the ammonium cation on the coated surface which is very different from that on the bare electrode surface.

Once dopamine has been taken up by a Nafion-coated electrode, it is very difficult to remove it. A Nafion-coated electrode, immersed in 1×10^{-4} M dopamine, and then transferred to a dopamine-free buffer continues to show an unattenuated dopamine SERS spectrum. Even vigorous stirring leaves the spectrum unchanged. The intensity can be manipulated by potential change, but there is no evidence that dopamine leaves the interior of the coating. Similar behavior has been reported by Espenscheid et al. (*28*).

The behavior of cellulose acetate coated electrodes is quite different from that of Nafion-coated electrodes, as shown in Figure 4. The spectrum shown in Figure 4a demonstrates

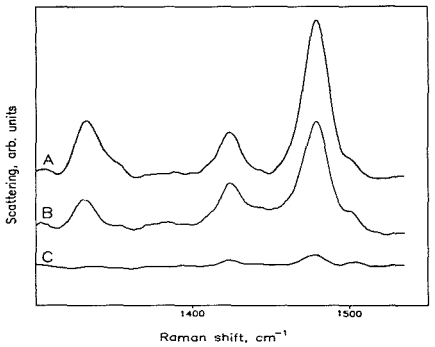

Figure 4. Dopamine SERS spectra obtained by using a cellulose acetate coated electrode at −0.9 V after (A) immersion in 1×10^{-4} M dopamine, (C) 120-s wash in stirred 0.1 M KCl, and (B) reimmersion in 1×10^{-4} M dopamine.

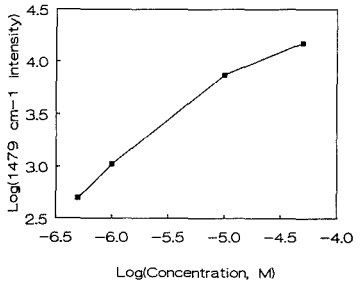

Figure 5. Concentration dependence of dopamine 1479-cm^{-1} SERS intensity in the presence of 0.5% BSA using a cellulose acetate coated electrode.

that cellulose acetate protects the electrode against BSA adsorption. However, the SERS intensities and band ratios remain those of dopamine at a bare electrode at pH 7. This behavior is consistent with the operation of cellulose acetate as a size exclusion membrane with no ion-exchange function. The absolute intensity of the spectrum is about the same as that encountered at a bare electrode at the same concentration. There is little, if any, preconcentration of dopamine in this membrane.

Dopamine can be removed from cellulose acetate coated electrodes. Transfer of an electrode from a buffer containing 1×10^{-4} M dopamine to a dopamine-free buffer causes attenuation of the spectrum (Figure 4c) to an intensity commensurate with release of 99% of the analyte. The signal decay occurs within 90 s if the solution is gently stirred. If the electrode is reimmersed in the original dopamine-containing buffer, about 60% of the activity is recovered (Figure 4b). This percentage recovery is similar to that which we observe on bare silver electrodes which have been cycled between 0.0 and −0.9 V.

Figure 5 summarizes the concentration dependence of dopamine spectral intensities obtained in the presence of 0.5% BSA using cellulose acetate coated electrodes. The behavior is essentially the same as previously reported (*13*) for bare electrodes in protein-free buffers. Analytically useful signals are obtained in the physiological concentration region.

We were unable to produce cellulose acetate coated electrodes by applying the polymer layer after an ORC, as with Nafion coatings. Control experiments with uncoated electrodes show that SERS activity is lost during the alkaline hydrolysis step. Consequently, cellulose acetate coatings were applied prior to the ORC.

Attempts at producing more robust membranes from higher concentrations of cellulose acetate have proven less successful. At 5.0% cellulose acetate, electrode response is sluggish and requires more than 20 min of vigorous stirring for analyte removal. On the other hand, attempts to decrease response times with thinner coatings from less concentrated polymer solutions or with longer hydrolysis times produced electrodes with unstable and protein-permeable coatings. This behavior suggests that a careful optimization of coating conditions will be necessary. Other cellulose acetate coating procedures that produce thinner membranes and faster response times (*17*) in voltammetric applications may also prove useful here.

CONCLUSIONS

The electrode-coating technologies employed in analytical electrochemistry can be used to protect SERS electrodes. Dopamine response is preserved in the presence of protein burdens much higher than those encountered in brain extracellular fluid. In neurochemical applications, Nafion and other ion exchangers may prove practical on gold electrodes, which can be operated at anodic potentials positive enough to oxidize catecholamines to neutral *o*-quinones. Because the inherent selectivity of vibrational spectroscopy reduces the need for ion exchange selectivity, a perm-selective coating such as cellulose acetate may often be all that is needed.

Polymer coatings may prove generally useful to protect SERS-active metals in matrices where bare metal surfaces are fouled by surfactant adsorption. Both ion exchangers and perm-selective coatings may prove valuable to protect surfaces intended for one-time use. Silver island films, coated fumed silica, or other similar materials could easily be precoated with a polymer layer. The barrier function would extend the range of applications and the preconcentration effects of ion exchangers might lower detection limits. Colloidal silver (*29*) and platinum (*30*) imbedded in a Nafion membrane have already been prepared. A successful Nafion coating procedure for colloidal silver could be especially useful, because the polyanion might stabilize these colloids indefinitely.

LITERATURE CITED

(1) Fleischmann, M.; Hendra, P. J.; McQuillan, A. *Chem. Phys. Lett.* **1974**, *26*, 163–166.
(2) Campion, A. *Annu. Rev. Phys. Chem.* **1985**, *36*, 549–572.
(3) Garrell, R. L. *Anal. Chem.* **1989**, *61*, 401A–411A.
(4) Moskovits, M. *Rev. Mod. Phys.* **1985**, *57*, 783–826.
(5) *Surface Enhanced Raman Scattering*; Furtak, T. E., Chang, R. K., Eds.; Plenum Press: New York, 1982.
(6) Enlow, P. D.; Buncick, M.; Warmack, R. J.; Vo-Dinh, T. *Anal. Chem.* **1986**, *58*, 1119–1123.
(7) Alak, A. M.; Vo-Dinh, T. *Anal. Chem.* **1987**, *459*, 2149–2153.
(8) Carrabba, M. M.; Edmonds, R. B.; Rauh, R. D. *Anal. Chem.* **1987**, *59*, 2559–2563.
(9) Angel, S. M.; Katz, L. F.; Archibald, D. D.; Lin, L. T.; Honigs, D. E. *Appl. Spectrosc.* **1988**, *42*, 1327–1331.
(10) Torres, E. L.; Winefordner, J. D. *Anal. Chem.* **1987**, *59*, 1626–1632.
(11) Force, R. K. *Anal. Chem.* **1988**, *60*, 1987–1989.
(12) Laserna, J. J.; Campiglia, A. D.; Winefordner, J. D. *Anal. Chem.* **1989**, *61*, 1697–1701.
(13) Lee, N. S.; Hsieh, Y. Z.; Paisley, R. F.; Morris, M. D. *Anal. Chem.* **1988**, *60*, 442–446.
(14) McGlashen, M. L.; Davis, K. L.; Morris, M. D. *AIP Conf. Proc., Adv. Laser Sci.-IV* **1989**, 707–712.
(15) Wightman, R. M.; May, L. J.; Michael, A. C. *Anal. Chem.* **1988**, *60*, 769A–779A.
(16) Wages, S. A.; Church, W. H.; Justice, J. B., Jr. *Anal. Chem.* **1986**, *58*, 1649–1656.
(17) Kuhn, L. S.; Ismail, K. Z.; Weber, S. G. *Anal. Chem.* **1989**, *61*, 303–309.
(18) Kristensen, E. W.; Kuhr, W. G.; Wightman, R. M. *Anal. Chem.* **1987**, *59*, 1752–1757.
(19) Wang, J.; Hutchins, L. D. *Anal. Chem.* **1985**, *57*, 1536–1541.
(20) Wang, J.; Hutchins-Kumar, L. D. *Anal. Chem.* **1986**, *58*, 402–407.
(21) Szentirmay, M. N.; Martin, C. R. *Anal. Chem.* **1984**, *56*, 1898–1902.
(22) Nagy, G.; Gerhardt, G. A.; Oke, A. F.; Rice, M. E.; Adams, R. N.; Moore, R. B., III; Szentirmay, M. N.; Martin, C. R. *J. Electroanal. Chem. Interfacial Electrochem.* **1985**, *188*, 85–94.
(23) Sondheimer, S. J.; Nigel, J. B.; Lemke, M. E.; Fyfe, C. A. *Macromolecules* **1986**, *19*, 339–343.

(24) Schmidt, M. H., Lewis, N. S. J. Phys. Chem. 1988, 92, 2018–2022.
(25) Scott, S. D.; McCreery, R. L. Anal. Chem. 1984, 56, 2199–2204.
(26) Leikis, D. I.; Rybalka, K. V.; Sevastyanov, E. S.; Frumfin, A. N. J. Electroanal. Chem. Interfacial Electrochem. 1973, 46, 161–169.
(27) Lewis, G. P. Br. J. Pharmacol. 1954, 9, 488–493.
(28) Espenscheid, M. W.; Ghatak-Roy, A. R.; Moore, R. B., III; Penner, R. M.; Szentirmay, M. N.; Martin, C. R. J. Chem. Soc., Faraday Trans. 1 1986, 82, 1051–1070.
(29) Lee, P. C.; Meisel, D. J. Catal. 1981, 70, 160–167.
(30) Liu, H. Y.; Anson, F. C. J. Electroanal. Chem. Interfacial Electrochem. 1983, 158, 181–185.

RECEIVED for review November 1, 1989. Accepted January 19, 1990. This work supported in part by Public Health Service Grant NS-26160.

A Simple and Robust Flow Injection Analysis Method for Determination of Free Acid and Metal Concentrations in Hydrolyzable Metal Solutions

Walter Lindberg, Gregory D. Clark,[1] Christopher P. Hanna, David A. Whitman,[2] Gary D. Christian,* and Jaromir Ruzicka

Department of Chemistry, BG-10, University of Washington, Seattle, Washington 98195

A single-line flow injection analysis (FIA) system for simultaneous determination of hydrolyzable metals and free acid has been developed. As a model for hydrolyzable metals iron was chosen. The setup allows determination of 0.5–6 M acid and 0.1–1.6 M iron. The resulting prediction error is 7% for acid and 3.8% for iron. Data were obtained by using a diode array detector. The calibration models were developed by using partial least-squares (PLS) regression. These results were compared with results obtained by traditional univariate calibration. The project aimed at developing a simple and robust FIA system to be applicable in an industrial process setting. Necessary modifications of present FIA instrumentation to fit such an environment are discussed.

INTRODUCTION

Analysis of free acid in hydrolyzable metal solutions is often fraught with difficulties because of interference from the formation of hydrogen ions from hydrolysis of the metal. This analysis problem often occurs in nuclear fuel processing where an accurate acid content is mandatory for solvent extraction, ion exchange, and precipitation reactions that separate and purify the radioactive material. This difficulty has basically been dealt with in two ways: (1) removal of the metal by precipitation, ion exchange, or solvent extraction or (2) complexation of the metal with a weak acid. A discussion of these methods can be found in the paper by Ryan et al. (*1*) and references therein.

In a recent paper (*2*) the metal hydrolysis interference was tackled by, in addition to adding a complexant, performing the acid determination by standard addition of acid rather than base, thereby avoiding hydrolysis. pH was measured by a conventional glass electrode and the equivalence point was evaluated by calculations based on the equilibrium equation, such as the Nernst equation or the Gran plot. In another recent work, multivariate methods (partial least-squares regression) were used for determination of plutonium and acid using spectrophotometry (*3*). Both plutonium and free acid could be estimated by recording the visible spectra of the solutions and taking advantage of the influence of the acid concentration on the plutonium spectrum.

The intention of this work was to develop a simple and robust flow injection analysis (FIA) system for rapid at-line (*4*) analysis of toxic and hazardous samples such as plutonium and uranium solutions. By at-line we mean manual sampling using an instrument that can be installed in close proximity to the process line. Due to safety reasons, iron was used in place of plutonium or uranium, as a model which has similar propreties with respect to hydrolysis. The desirable FIA setup should allow both acid and iron determinations in the concentration ranges from 0.5 to 6 M acid and 0.1 to 1.6 M iron. Because of the high concentrations involved, a part of the project dealt with the development of a suitable system for sample dilution. Since the FIA apparatus should be adaptable to process environments, an overall goal was to keep the instrument as robust and mechanically simple as possible.

EXPERIMENTAL SECTION

Apparatus. A peristaltic pump was used for solvent delivery (Alitea, USA, P.O. Box 26, Medina, WA 98039). For sample injection either a Rheodyne Model 7010 or Model 7314 injection valve was used. They were equipped with a 20-μL and a 0.5-μL sample loop, respectively. For mixing (dispersion), a mixing chamber combined with a reactor was used (see Figure 1). The chamber was a tube of 1.5 mm i.d. and 10 mm length containing a micro stirring bar, which was vibrated with a stirring motor. Microline tubing with 0.51 mm i.d. was used for coils and connecting lines. A HP8452 diode array spectrophotometer equipped with a flow cell was used for detection. Data from the diode array detector was converted to SIMCA data format and was analyzed by the SIMCA-3B package (Sepanova AB, Östrandsvägen 14, S-122 43 Enskede, Sweden, or Principal Data Components, Shepards Blvd., Columbia, MO 65201). Univariate calibration was done by programs written using the Matlab package (The MathWorks, Inc., 21 Eliot St., South Natick, MA 01760).

Chemicals. Standard solutions were prepared from $Fe^{III}(NO_3)_3 \cdot 9H_2O$ (Aldrich) and concentrated HNO_3 (J. T. Baker), both of reagent grade quality. Cresol red (Aldrich) was dissolved in a small volume of 0.1 M NaOH and then diluted with distilled water to a 0.04% (w/v) stock solution.

Procedure. Solutions were prepared to cover the range of combinations of iron (0.1–1.6 M) and nitric acid (0.5–6 M) studied. Altogether 20 to 40 sample solutions were prepared. The samples were analyzed in random order so as to not introduce spurious

[1] Present address: Department of Laboraboty Medicine, SB-10, University of Washington, Seattle, WA 98195.
[2] Present address: Department of Laboratory Medicine and Pathology, University of Minnesota, Box 198 UMHC, 420 Delaware St. S.E., Minneapolis, MN 55455.

0003-2700/90/0362-0849$02.50/0

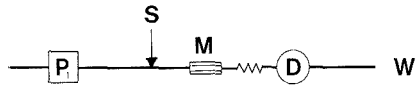

Figure 1. Single-line FIA manifold: P, peristaltic pump; S, 0.5-μL injection valve; M, mixing devices; D, diode array detector connected to a personal computer; W, waste.

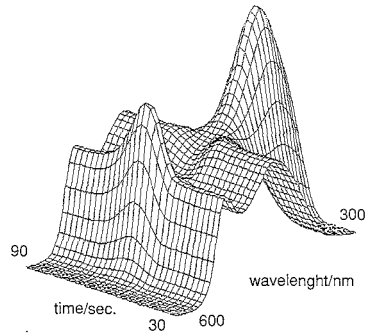

Figure 2. 3D FIA peak profile obtained by using single-line manifold and diode array detection. The spectrum ranges from 300 to 600 nm and the time from 30 to 90 s. The background spectrum (seen in the middle) is from the indicator in the carrier solution, the front peak the acid form spectrum of the indicator, and the rear peak the iron absorption. The trough between the peaks is due to the decrease of the base form of the indicator.

correlations in data. In the data analysis the data set was divided, some to be calibration samples and some to be test samples. By use of a diode array detector the whole spectrum of interest could be scanned, which gave great flexibility in the further data analysis. A typical readout is shown in Figure 2. Partial least-squares regression (PLS) (*5, 6*) was done by extracting either a suitable spectrum (usually at the peak maximum) or FIA time profiles (corresponding to the absorbing regions for the acid and iron) from each sample data matrix. The vectors thus obtained were then combined to a matrix to represent the calibration set and the test set. In cases where appropriate, analyte concentrations and absorbances were also modeled using univariate inverse least-squares regression. The detector was zeroed against carrier solution without indicator and thereafter indicator was added to give approximately 1 absorbance unit for the peak maximum. The injector was connected to a microswitch that automatically started the scan as the sample was injected. This was done by using the sipper switch feature of the instrument (pin 18 and 29 on the GP-IO interface).

RESULTS AND DISCUSSION

In most process monitoring environments, the information value and the cost of the analysis are the two determining factors of the utility of the analysis method. In this context, this means obtaining sufficiently accurate concentration estimates of the analytes of interest using an instrumental setup that is as simple as possible to minimize instrument downtime. In analyzing these highly concentrated solutions, it is necessary to dilute the samples prior to detection. On-line dilution systems have recently been developed in FIA (ref 7 and references therein). They consist of a mixing chamber connected to an injection valve in which a small volume of the dispersed injected sample from the mixing chamber is injected into another carrier stream, thereby splitting off a small portion of the sample for analysis, while the rest is transported to waste. However, in this case, considering the amount of dilution that was needed and the strong desire for simplicity of the FIA system, we chose to simply reduce the volume of the injected sample to much smaller volumes than are commonly used in FIA. The dispersion could then be adjusted to the desired value by simply using coils and mixing chambers. When a 0.5-μL injection volume was used, the required dispersion could be obtained in a single line FIA system. Another advantage of this approach is that if the sample is environmentally hazardous or harmful for the instrumentation, it is safer if the amount of sample solution circulated through the system is kept to a minimum.

Oxalate Carrier. In the initial experiments, we attempted to develop a FIA method based on complexation with 0.15 M sodium oxalate as carrier, in accordance with earlier described literature concerning batch titrations of free acid in hydrolyzable metal solutions (*1*). The measurement of the acid was done according to the "single point titration" concept (*8, 9*), where the pH change of a buffer solution is a function of the acid content of the sample added. For detection, a pH-sensitive indicator was added with a pK_a similar to the pK_a of the buffer, thereby allowing spectrophotometric monitoring of the pH changes of the buffer. When 0.15 M oxalate was used as buffer (pH 7.2), bromophenol blue was chosen as indicator. Its pH transition interval is 3.0–4.6 (*10*), while the two pK_a values of oxalic acid are 1.2 and 4.2. Iron was in all cases detected by its own yellowish color.

A number of FIA manifolds (e.g., single line, double line) were tested for these measurements, and in none was a satisfactory prediction of both free acid and metal concentrations obtained using PLS (prediction error 11.2% for the acid and 6.6% for iron). A probable reason is that the determination of each species is not independent of the other. This is so because the amount of oxalate accessible for complexation with iron is dependent of the pH of the sample solution. Likewise, the amount of oxalate buffer that affects the pH change when the sample is added is also influenced by the amount complexed with the iron in the solution. A less serious difficulty using this approach might also be the necessity of matching the pK_a of the indicator with the buffer pH since the absorbance of the indicator as a function of the amount of acid added may not be a linear function over the whole concentration range of interest.

HCl Carrier. Another approach to avoid interference from hydrolysis is to make the analysis in an acidic medium as suggested by Baumann and Torrey (*2*). Since iron starts forming hydroxy complexes around pH 2 (*11*), a 0.01 M HCl solution was tested as the carrier stream in a single-line FIA system (Figure 2). Detection of the acid was facilitated by using cresol red as indicator, which has a color change from yellow to red at pH below 2 (*10*). The calibration interval was, in the case of iron, restricted to include only concentrations from 0 to 0.4 M in order to simplify the system. Despite this simplification, the relative root mean square error of prediction (RRMSEP, see tables for definitions) (*12*) of the iron prediction error was 29%, which was an unreasonably large error. The corresponding error of the acid prediction was 7.8%, which we regarded as acceptable. The data analysis was done by extracting the spectrum corresponding to the peak maximum from the three-dimensional data profile. The spectra from the different samples were then combined to form a data matrix. Calibration and prediction were subsequently done by partial least-squares modeling. The difference in prediction errors of acid and iron also indicated that the large prediction error for iron was not related to the construction of the manifold but rather indicated a chemical problem.

After careful inspection of the FIA peaks, it was observed that while the peak of the indicator, detecting the acid, was smooth and had the shape of a normal FIA peak, the iron peak from the same run showed a different shape approaching a peak with two maxima (Figure 3). This finding shows that there are two types of mechanisms going on simultaneously

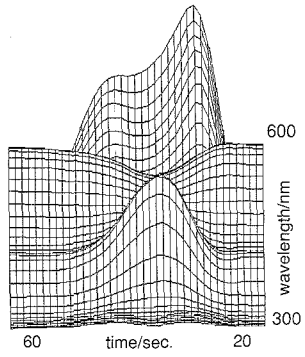

Figure 3. FIA peak profiles using 0.01 M HCl as carrier. The peak in the front shows the acid form of the indicator and the rear peak the profile from iron. The 3D FIA peak profile illustrates the difference between the physical dispersion of a sample zone and chemical reactions taking place along the gradient. The dispersion was 180 in this experiment.

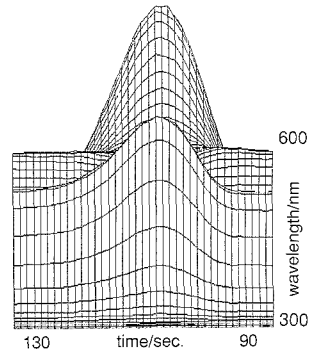

Figure 4. FIA profiles of acid and iron with 0.01 M HCl and 1 M NaCl as carrier. In comparison with Figure 3 the double peak feature of the iron has disappeared and both peaks have the same shape.

in the solution. In the case of the acid, the indicator acts as a sensor probing the acid concentration, whereas for iron the metal reacts with chloride to form complexes that are indicated by their absorption. This means that because chloride concentration was too low, different complexes were formed. The complex formed depends on the sample/carrier stoichiometry along the concentration profile. This was a likely source of error because with different sample composition the iron complex composition would change and consequently the absorbance spectra would reflect different combinations of complexes from sample to sample.

HCl/NaCl Carrier. As a remedy a carrier containing 0.01 M HCl and 1 M NaCl was prepared to assure an excess of Cl^- (Figure 4). The dispersion was adjusted in this experiment to 800 to bring the absorbance level of iron down to be within a linear range. The dispersion was obtained by using one micro stirring bar and coils and connecting lines to a total system volume of 1 mL. The flow rate was 0.58 mL min^{-1}. By this measure the error was 5.8% for acid and 2.1% for iron, which is a considerable improvement in iron prediction in comparison with the previous experiment. These data also showed no interaction between acid and iron; i.e., the absorbance of iron was independent of acid concentration and likewise the absorbance of the indicator was independent of the amount of iron in the sample. This means that univariate

Table I. Root Mean Square Error o[illegible] Using the Same Calibration Set (13 sa[illegible] Different Numbers of Wavelengths[a]

		acid		
	no. of wavelengths	RMS-EP	RRMS-EP, %	
univariate (300 518)	2	0.216	7.2	0.13[illegible]
PLS (6)	6	0.182	6.9	0.0193
PLS (101)	101	0.184	7.0	0.0191

[a] For ease of comparison the relative error is also giv[illegible] (RRMSEP). RMSEP calculated as: $(\mathrm{SUM}(x_{pred} - x_{true})^2/n)^{0.5}$. RRMSEP calculated as: $\mathrm{RMSEP}/x_{mean} \times 100$.

calibration curves are applicable. The absorbance of iron was measured at its peak maximum (336 nm) and the calibration curve was a straight line, whereas the calibration plot for acid is slightly curved, using the peak maximum of the indicator (518 nm). If the same samples for calibration and testing as used with PLS calibration above were used with a univariate evaluation method, the prediction errors were 5.1% and 2.7% for acid and iron, respectively. These results indicate that univariate calibration is adequate and is preferable if simplicity is the priority.

A natural extension of the previous experiment is to increase the amount of chloride to extend the range of analysis for iron. Therefore, the amount of chloride was increased 4 times by using 4 M NaCl in the carrier, which then would allow determination of iron up to 1.6 M compared to 0.6 M with 1 M NaCl. The dispersion of the manifold was increased to 1200 in order to somewhat alleviate the very high absorbances from iron. This was done by adding one additional mixing chamber and coils to a total system volume of 1.2 mL. The flow rate was 1.2 mL min^{-1}. As before, the spectrum giving the highest absorbance was selected for analysis.

Calibration Method. In order to investigate the influence of the calibration method on the prediction error, different calibration alternatives were evaluated. Table I illustrates the effect from the number of measurement wavelengths. In univariate calibration the indicator peak maximum was taken as the wavelength for the acid, and in the case of iron the wavelength chosen was that which was most selective but for which the absorbance was low enough for measurement (300 nm). The most striking feature is the poor prediction of iron using a univariate approach (second degree polynomial). This is because there is no wavelength in the spectrum that both gives a sufficiently low absorbance to cover the calibration range without giving too high absorbances and does not overlap with the indicator. This means that a fully selective signal cannot be obtained.

The spectral overlap problem can, however, be resolved by using a multivariate approach, as is demonstrated from the use of PLS. In this context it is important to note why PLS calibration works in this case but not in the experiment with only 0.01 M HCl as a carrier. In the present case the same complex is formed, whose *spectrum overlaps* with another spectrum (the indicator) while in the previous case different *chemical complexes* were formed, which means that we actually attempted to calibrate having *different* constituents in the different samples. This illustrates the fact that multivariate methods do not provide any solution to the basic questions in chemistry but provide a more powerful tool to reveal information in data than do more traditional methods.

The spectral overlap could also possibly be solved by methods other than multivariate modeling. These include further diluting the sample by increased dispersion via longer coils or using a flow cell with a shorter path length, thereby decreasing the sensitivity. In this way it would be possible

II. Root Mean Square Error of Prediction (RMSEP), a Calibration Set of 24 Samples[a]

	no. of wavelengths	acid		iron	
		RMSEP	RRMSEP, %	RMSEP	RRMSEP, %
'LS(151)	151	0.340	13.1	0.0316	6.3
PLS(101)	101	0.163	6.3	0.0179	3.6

[a] The 151 wavelength data set contains measurements with absorbances clearly out of the linear range. In the 101 variable data set these have been eliminated. For ease of comparison the relative serror is also given (RRMSEP). RMSEP calculated as: $(\mathrm{SUM}(x_{\mathrm{pred}} - x_{\mathrm{true}})^2/n)^{0.5}$. RRMSEP calculated as: $\mathrm{RMSEP}/x_{\mathrm{mean}} \times 100$.

to make measurements at the peak maximum of iron (336 nm), where no interference from the indicator is present. The former approach will increase the total volume flow, which probably makes changing the flow cell a better solution. A third, feasible method would be to choose a time corresponding to the trailing edge of the peak for measurement. A slight disadvantage can be that a time-based measurement must be used, which will cause problems if the flow rate varies, but the advantage of the high sample throughput could be maintained also in this case. Table II shows a comparison between only using wavelengths giving linear response with concentration (101 wavelengths) and those wavelengths that, due to high absorbance values (151 wavelengths), do not give linear response. The results show that by removing data that are not linear before calibration, an improved result is obtained.

CONCLUSIONS AND SUGGESTIONS FOR FURTHER WORK

We have shown that it is possible to determine both iron and free acid simultaneously by using a single-line FIA system and a UV–vis diode array detector. The relative prediction errors are, in our case, better for acid and worse for the metal, than those recently published by Carey et al. (*3*). However, our calibration range is 13 times higher for the metal and twice as high for the acid. Further work in this project should be to investigate whether the same or similar type of chemistry as employed in this work also applies in the analysis of mixtures of free acid in plutonium/uranium solutions.

An area where multivariate calibration will be useful in FIA is in compensating base-line shifts under the peak due to difference in refractive index between carrier and sample (*13*). This problem is analogous to a curve overlap interference as described above. The refractive index can thus be compensated by varying the refractive index of the samples in the calibration set. Thereby the interference can be modeled and taken into account in the prediction of unknown samples.

If this method is to be useful in an industrial setting, we believe that the FIA system has to be constructed in a more robust fashion than described in this work. Particular concern has to be given the pump and the injector. It is likely that the peristaltic pump whose tubings wear easily would have to be replaced with some other pump that needs less attention and maintenance. In the injector the small bore of the loop and the rotor seal may also be a source of problem, with certainty if the samples contain particulate matter. In order to solve this problem, one has to investigate what is the narrowest injector bore that is likely to give a maintenance-free run. If these dimensions do not allow a low-volume (e.g., 0.5 μL) injector to be constructed, the desired dispersion can be achieved by increasing the dimensions of the connecting lines, thereby allowing larger injected volumes. This approach will of course increase reagent consumption, but since none of the chemicals involved are expensive, this factor is probably not critical.

LITERATURE CITED

(1) Ryan, Jack L.; Bryan, Garry H.; Burt, Merrill C.; Constanzo, Dan A. *Anal. Chem.* **1985**, *57*, 1423–1427.
(2) Baumann, Elizabeth, W.; Torrey, Benjamin H. *Anal. Chem.* **1984**, *56*, 682–685.
(3) Carey, W. Patrick; Wangen, Lawrence E.; Dyke, James T. *Anal. Chem.* **1989**, *61*, 1667–1669.
(4) Callis, James B., Illman, Deborah L.; Kowalski, Bruce R. *Anal. Chem.* **1987**, *59*, 624A–637A.
(5) Geladi, Paul; Kowalski, Bruce R. *Anal. Chim. Acta* **1986**, *185*, 1–17.
(6) Höskuldsson, Agnar *J. Chemom.* **1988**, *2*, 211–228.
(7) Clark, Gregory D.; Ruzicka, Jaromir; Christian, Gary D. *Anal. Chem.* **1989**, *61*, 1773–1778.
(8) Johansson, Gillis; Backén, Wilbert *Anal. Chim. Acta* **1974**, *69*, 415–424.
(9) Åström, Ove *Anal. Chim. Acta* **1978**, *97*, 259–267.
(10) *CRC Handbook of Chemistry and Physics*, 68th ed.; Weast, R. C., Ed.; CRC Press: Boca Raton, FL, 1987; p D-147.
(11) Ringbom, Anders *Complexation in Analytical Chemistry*; Interscience Publishers: New York, 1963.
(12) Martens, Harald; Naes, Tormod Multivariate calibration by data compression. In *Near Infrared Technology*; Williams, P., Norris, K., Eds.; American Association of Cerial Chemists, Inc.: St. Paul, MN, 1987; Chapter 4.
(13) Zagatto, E. A. G.; Arruda, M. A. Z.; Jacintho, A. O.; Mattos, I. L. *Anal. Chim. Acta*, in press.

RECEIVED for review October 10, 1989. Accepted January 19, 1990. Financial support from Battelle Northwest Laboratories, Richland, WA, is gratefully acknowledged. W.L. thanks the Swedish Natural Science Research Council (NRF) for a traveling stipend and J. O. Nauclérs Minnesfond and the Swedish Board for Technical Development (STU) for financial support.

Helium Discharge Detector for Quantitation of Volatile Organohalogen Compounds

David A. Ryan, Suzanne M. Argentine, and Gary W. Rice*

Department of Chemistry, College of William and Mary, Williamsburg, Virginia 23185

A helium discharge has been evaluated as an element-selective, gas chromatographic detector for volatile organohalogen compounds. Absolute limits of detection ranged from 3 pg for chloroform to 29 pg for *p*-dibromobenzene with a linear response of 10^3–10^4. The relative response of the detector was determined to be based solely on the mass of the halogen species present. This feature allowed for relatively simple quantitation of chlorinated and brominated haloform species in water samples by the addition of a single internal standard for calibration of the halogen response.

INTRODUCTION

Halogenated organic compounds constitute the largest fraction of priority pollutants as designated by the U.S. Environmental Protection Agency, with over 50% of the compounds or compound classes containing chlorine, bromine, or some combination. There are currently a number of different detectors available for gas chromatography that provide varying degrees of selective detection for halogenated compounds.

The electron capture detector (ECD) is the most widely used GC detector for trace analysis of halogenated compounds, especially since low femtogram detection levels are possible using capillary GC (*1*, *2*). The drawbacks of the ECD are numerous and well documented. The response of the ECD is very dependent on compound structure, number of halogen atoms in the compound, carrier gas purity, and detector temperature (*3*–*6*). Response factors from an ECD can vary over short time spans, as well as being markedly different relative to another ECD.

A modified flame photometric detector (FPD) can be used by detecting photoemission from indium halide species produced from the combustion of halogenated compounds in the presence of an indium pellet (*7*, *8*). The detector and carrier gas flows must be finely controlled to minimize variations in detector sensitivity, and substantial solvent elution can cause flame extinguishment (*9*).

The electrolytic conductivity detector (ECOD) provides a wide linear range (typically 10^4–10^5), picogram limits of detection, and a response that is dependent only on the gram amount of halogen present (*10*, *11*). Periodic cleaning of the reactor tube is required to avoid baseline drift and loss of response over extended time periods. Solvent venting is necessary in capillary systems to prevent reactor tube contaminations (*11*, *12*).

The microwave induced plasma (MIP) is a very promising element-selective detector, a commercial version of which is now available (*13*, *14*). Limits of detection for the halogens are 20–30 pg with a linear range 3 to 4 orders in magnitude. Response is dependent only on the gram amount of halogen present and selectivity relative to other elements is excellent. The MIP still has several drawbacks. Synchronized valves must be incorporated between the column and plasma source to vent excessive amounts of solvent or eluents that may extinguish the plasma (*15*, *16*). Water cooling is required around the quartz plasma containment tube to prevent devitrification (*17*). The optimum limits of detection for each element are dependent on plasma flow rates, observation point, power, and a mixture of doping gases (*18*, *19*).

Detectors such as the MIP offer the greatest versatility with respect to simplifying chromatographic detection in complex mixtures with minimal sample preparation. The other detectors mentioned are still limited in scope to the number of elements detected and element selectivity. A detector is still needed with advantages comparable to the MIP that is simpler in operation and free of the associated problems discussed.

A detector developed in this laboratory which possesses features similar to the MIP is the helium discharge detector (HDD). The HDD does not require extensive optimization for each element, is not prone to extinguishment from excessive sample volumes, and does not require additional cooling. Detection limits of 8 pg for Cl and 20 pg for Br have been reported (*20*).

Previous work in this laboratory has demonstrated that the response of the HDD is also dictated by the gram amount of halogen present (*21*). Polychlorinated biphenyl congeners were quantitated by incorporating a single internal standard into chromatographed solutions to calibrate the area generated per gram amount of Cl present. These solutions only contained aromatic compounds, and no attempt was made to determine if the same methodology could be applied to a broader class of organohalogen compounds.

The objectives of this work were to determine the limits of detection, linear range of response, selectivity, and molar response for halogenated compounds commonly found or designated as priority pollutants. The determination of haloforms in drinking water is also demonstrated.

EXPERIMENTAL SECTION

Instrumentation. The construction and operation of the HDD have been described (*20*, *21*). The HDD was mounted onto a Carlo Erba Model 4180 GC equipped with a capillary on-column injector. An IBM-PS/2 Model 30-E21 computer equipped with an Axxiom Chromatography Data System was used for data collection and analysis. An overview of the instrumentation and operating parameters used in this study is given in Table I.

Standard Solutions. Several solutions were prepared that contained mixtures of chloro-, bromo-, and bromochloro-organic compounds for the evaluation of limits of detection, linear range of response, and molar response factors. Each compound was added in 0.100-g amounts to a 10.0-mL volumetric flask and diluted to volume with pentane. Serial dilutions of the stock solutions were made to give concentrations of 100, 10, 1.0, 0.3, 0.1, 0.03, and 0.01 μg/mL. The pentane was purified by stirring overnight over sodium followed by distillation to remove trace levels of several chlorinated hydrocarbons observed in pentane chromatograms.

Selectivity at the Cl analytical wavelength over Br and hydrocarbon species was evaluated by preparing a solution containing 20 ng/mL carbon tetrachloride, 200 μg/mL dibromomethane, and 200 μg/mL of octane. A similar solution containing 80 ng/mL dibromomethane, 200 μg/mL carbon tetrachloride, and 200 μg/mL octane was prepared for evaluating the selectivity at Br analytical wavelengths.

*Author to whom all correspondence should be sent.

0003-2700/90/0362-0853$02.50/0

Table I. Instrumentation and Operating Parameters for the GC–HDD System

(A) Helium Discharge Detector	
Helium flow rate	60 mL/min
voltage[a]	6500 V RMS
frequency[a]	176 kHz
load power[a]	60 W
(B) Spectrometric System	
monochromator	0.5 m (Minuteman, Model 305M)
band-pass (fwhm)	0.35 nm
analytical wavelengths	837.6 nm (Cl), 827.2 nm (Br)
photomultiplier tube	R758 (Hamamatsu)
PMT voltage	1080 V (Keithley Model 247)
amplifier	Keithley Model 485 picoammeter
integrator	IBM PS/2 Model 30-E21 w/Axxiom Chromatography Data System
(C) Gas Chromatographic System	
GC	Carlo Erba Model 4180
injection mode	on-column
injection volume	0.5–1.0 μL
carrier gas	helium
temperature program	35 °C (2 min), 5 °C/min, 150 °C
column	DB-5, 30 m × 0.25 mm i.d. (J&W)

[a] Model HPG-2 (ENI Power Systems)

Table II. Absolute Limits of Detection (pg) for Selected Organohalogen Compounds Using the HDD

compound	limit, pg	compound	limit, pg
dichloromethane	4	*p*-dichlorobenzene	9
chloroform	3	*o*-dichlorobenzene	12
carbon tetrachloride	3	dibromomethane	9
1,1,1-trichloroethane	5	bromoform	12
trichloroethylene	4	1,2-dibromoethane	10
1,1,2,2-tetrachloroethane	10	1,1,2,2-tetrabromoethane	26
tetrachloroethylene	8	1,3-dibromobutane	18
1,2-dichloropropane	9	*p*-dibromobenzene	29
chlorobenzene	12	bromochloromethane	9
		bromodichloromethane	18
		chlorodibromomethane	16
		bromotrichloromethane	13

Solutions were also prepared to generate 10-point calibration curves from two injections. Solutions containing five chlorine or bromine compounds were prepared to give halogen concentrations of 2, 6, 20, 40, and 80 ng/μL, with the first eluting compound having the lowest concentration and each subsequent one increasing in concentration. These solutions were diluted to give concentrations of 20, 60, 200, 400 and 800 pg/μL as well.

Water Sampling Procedures. A 15-mL volume of pentane was added to 100-mL water samples in 250-mL separatory funnels and vigorously shaken for 2 min. The water was removed and 50 mL of 1 M NaOH added to extract organic acids back into the water layer. The pentane was then transferred to a 25-mL Erlenmeyer flask and anhydrous sodium sulfate added to remove residual water. The pentane was then transferred to a graduated conical centrifuge tube, chilled in an ice bath, and evaporatively concentrated to ~0.8 mL under a stream of dry nitrogen. A 100-μL spike containing 2.0 μg/mL of 1-chloro-2-bromopropane in pentane was then added and the volume adjusted to 1.0 mL. All chromatograms were obtained under the conditions described in Table I.

RESULTS AND DISCUSSION

Limits of Detection and Linear Range. Limits of detection were estimated from chromatograms of the most dilute solutions that could be detected. Concentrations that would give peak heights 3 times greater than the standard deviation in the background signal were calculated. log–log plots were prepared of the relative area versus the picogram amount of

Table III. Selectivity Ratios for Br and Cl at Selected Analytical Wavelengths

wavelength, nm	selectivity ratio relative to C_8H_{18}	CH_2Br_2	CCl_4
837.2 (Cl)	1150	9100	
827.2 (Br)	60		470
863.9 (Br)	180		1560
882.5 (Br)	310		580
889.8 (Br)	580		nd[a]

[a] Not detected.

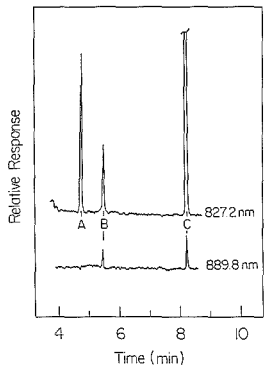

Figure 1. Chromatograms for bromine selectivity at 827.2 nm (top) and 889.8 nm (bottom): (A) CCl_4 (100 ng); (B) CH_2Br_2 (40 pg); (C) C_8H_{18} (100 ng).

The limits of detection obtained for a number of Cl, Br, and Br/Cl compounds are given in Table II, with values ranging from 3 pg for chloroform and carbon tetrachloride to 29 pg for *p*-dibromobenzene. One would expect a much smaller range of values if the detector is mass dependent; however no attempt was made to selectively improve the limits of detection by reducing the retention times of the more highly retained compounds, which would result in sharper peaks and higher peak response. Nevertheless, the limits of detection appear to be comparable to capillary chromatographic detection with the EOCD (*11*) and are significantly better than the MIP. Detection limits reported for a number of halocarbons with the ECD are superior by 2 to 3 orders of magnitude (*2*).

The linear range obtained for all compounds studied ranged from $10^{3.5}$ to 10^4 for chlorinated compounds and 10^3 to $10^{3.5}$ for brominated species. Correlation coefficients calculated from least-squares fits ranged from 0.9972 to 0.9996, with slopes of 0.912–1.043. These values are very good considering that the reproducibility of manual injections at the microliter level can vary by as much as 5–10%.

Selectivity. The selectivities obtained at Cl and Br analytical wavelengths are given in Table III. Selectivity ratios were calculated on the basis of the quantity of nonanalyte species that would be required to obtain a peak area equivalent to that produced by the analyte element of interest in each chromatogram. The selectivity of Cl over Br and octane exceeded 1000 in both cases. The selectivity of Br was determined at several analytical wavelengths due to poor selectivity over octane at 827.2 nm. Apparently there is substantial background emission from molecular CO and CN species produced in the discharge from impurities in the gas stream. Substantial improvements in selectivity were obtained by going to higher wavelengths, as illustrated in Table III. There is however a trade off in the limit of detection as il-

Table IV. Detector Response for Br and Cl Compounds

compounds	calcd value[a]	exptl value[b]	rel error, %
	Cl Mix 1		
chloroform	1.80	1.80	0.0
1,1,1-trichloroethane	1.63	1.66	1.8
1,2-dichloropropane[c]	1.00		
1,1,2-trichloroethane	1.59	1.57	−1.5
tetrachloroethylene	1.73	1.78	2.9
1,1,2,2-tetrachloroethane	1.87	1.83	−2.3
	Cl Mix 2		
carbon tetrachloride	2.31	2.25	−2.8
trichloroethylene	1.86	1.85	−0.7
chlorobenzene	0.57	0.56	−1.9
1,4-dichlorobutane[c]	1.00		
p-dichlorobenzene	0.95	0.95	0.0
o-dichlorobenzene	0.95	0.97	2.1
	Br Mix		
1-bromopropane	0.82	0.83	1.2
dibromomethane	1.16	1.15	−0.9
1,2-dibromoethane	1.07	1.09	1.9
bromoform	1.20	1.25	4.2
2,3-dibromobutane	0.93	0.91	−2.2
1,3-dibromopropane[c]	1.00		
carbon tetrabromide	1.22	1.23	0.8
1,4-dibromobutane	0.93	0.94	1.1
p-dibromobenzene	0.86	0.86	0.0
1,1,2,2-tetrabromoethane	1.17	1.16	−0.9

[a] Ratio of gram amount of halogen in each compound to that of the internal standard in each mixture. [b] Average of three determinations based on peak area ratios. [c] Used as the internal standard.

lustrated in Figure 1. This factor is primarily due to the poor response of the photomultiplier tube used in these studies at higher, near-IR wavelengths. Earlier work in our laboratory has indicated that the 889.8-nm line is actually 2 times as intense as the 827.2-nm line when the intensity is adjusted for grating efficiency and detector response (*22*). The incorporation of a detector with significantly greater efficiency in the 900-nm region would alleviate the selectivity problem associated with Br at 827.2 nm without compromising sensitivity.

Relative Response. The response of the HDD should be based solely on the mass of the Cl or Br present and not dependent on any other factors such as the chemical environment or substitution patterns within a compound. This deduction is based on the assumption that the compounds are dissociated into free atoms from which atomic emission is observed. Some recombination reactions may be occurring between O and N impurities in the discharge gas and C from the dissociated compounds, which could give rise to such species as CO and CN. Such effects would not be expected from the halogens. Thus the quantitation of halogenated compounds from a single calibrated internal standard could be achieved provided that the identity of the compounds of interest are known to correlate the halogen signal to the amount of compound present.

Several mixtures containing 1.0 μg/mL of each organohalogen compound were chromatographed with one compound in each mixture selected as an internal standard. A ratio of the gram amount of halogen present in each compound relative to the halogen content in the internal standard was calculated. If the detector response is truly based on the gram amount of each halogen present, then the ratio of the areas produced in the chromatograms should be the same as the gram ratios calculated for each mixture.

The results of this study are given in Table IV. The average error for the calculated ratios was 1.5%, which was well within experimental errors expected due to inaccuracies in solution preparations as well as no consideration for possible impurities in the compounds used. Similar results were obtained at concentrations of 10 μg/mL. At lower concentrations (<0.2 μg/mL) the relative errors were as high as 15%, which we attribute to inaccuracies in the peak integrations due to the increased background noise associated with the signal amplifications necessary for detection. Nevertheless, the results of this experiment strongly support the fact that the HDD response is based solely on the gram amount of halogen present and independent of compound structure.

Table V. Cl/Br Ratios in Bromochloro Compounds as Determined by the HDD

compound	Cl/Br (expected)	rel[a] mol of Cl	rel[a] mol of Br	Cl/Br (found)
bromochloromethane	1.00	1.45	1.48	0.98
bromodichloromethane	2.00	1.25	0.61	2.05
chlorodibromomethane	0.50	1.13	2.24	0.50
bromotrichloromethane	3.00	2.89	0.97	2.98
1-bromo-4-chlorobutane	1.00	0.82	0.78	1.05
2-bromochlorobenzene	1.00	0.80	0.83	0.96
1-bromo-2,3-dichlorobenzene	2.00	0.91	0.44	2.07

[a] 2-Bromo-1-chloropropane used as internal standard

Halogen ratios were also determined from a group of bromochloro-containing compounds. A solution containing six compounds at concentrations of 1.0 μg/mL was chromatographed in triplicate on both the Br and Cl analytical wavelengths. The relative number of moles of Br and Cl in each compound was determined by using 2-bromo-1-chloropropane as the internal standard. The experimental Cl/Br ratios obtained are given in Table V and in all cases agreed very well with the expected values. The only optimization required was the wavelength setting. Such capabilities are not possible with such detectors as the ECD, and the MIP must be optimized for several variables in order to obtain the maximum sensitivity for each element at trace levels. No attempt was made to see if carbon and hydrogen ratios could be obtained to generate a complete empirical formula, as significant background emission from these species as well as suspected recombination effects as previously discussed prevents such determinations at this time.

The response of the HDD was also tested by generating a 10-point calibration curve covering 3 to 4 orders of magnitude in halogen concentrations from two 0.5-μL injections. A typical chromatogram from the Cl calibration is shown in Figure 2. A plot of the Cl and Br calibration curves is shown in Figure 3. The correlation coefficients (0.9995 for Cl and 0.9998 for Br) and the slopes (0.945 for Cl and 0.987 for Br) clearly indicate that the peak areas obtained are independent of the concentration range studied as well as the chemical environment of the halogen species in the compounds. This feature has a significant advantage over detectors such as the flame ionization detector or electron capture detector, where response factors relative to a designated internal standard must be accurately known or calibration curves must be obtained for every individual compound.

Applications. The HDD would appear to be an excellent detector for the determination of organohalogen compounds produced from the chlorination of drinking water. The current method of choice for the isolation of volatile organic compounds from water samples is the purge and trap technique (*22–26*). Such an apparatus was not available in this labo-

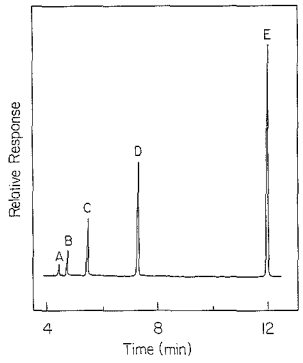

Figure 2. Chromatogram obtained for generating a multipoint calibration curve: (A) carbon tetrachloride (10 pg); (B) 1,1,1-trichloroethane (30 pg); (C) trichloroethylene (100 pg); (D) 1,1,2-trichloroethane (200 pg); (E) 1,1,2,2-tetrachloroethane (400 pg). Amounts given are for picograms of Cl present in each peak.

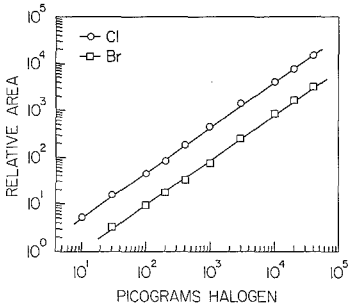

Figure 3. Ten-point calibration curves obtained from the injection of two standards each for Cl and Br.

ratory; thus a simple and reproducible extraction procedure was developed that was similar in design to other investigations (27, 28).

Preliminary screenings of water samples indicated that the primary species present were the haloform species. Deionized water was spiked with known concentrations of each haloform and extracted with the previously described procedure to determine the recovery efficiency and reproducibility for each species. Recoveries ranged from 40% for chloroform to 70% for dibromochloromethane with an average deviation of 2–4%. No halogenated species were detected in unspiked water samples; thus no black corrections were required.

A typical chromatogram showing the element-selective nature of the detector is shown in Figure 4 from a Williamsburg, VA, tap water sample. The results of this study from duplicate determinations on two different water sources are given in Table VI. Quantitation for bromodichloro- and chlorodibromomethane was performed on both the Br and Cl wavelengths to check the viability of using a single internal standard for quantitation. The reproducibility was excellent regardless of whether quantitation was based on the Br or Cl unit area generated by the internal standard. The estimated relative limits of detection for the technique are given at the bottom of Table VI and based on a 100-mL water sample concentrated to 1.0 mL, a 1.0-μL injection volume, and a signal to noise ratio of 3. All of the haloforms can be detected at sub-part-per-million levels. These studies are only preliminary in nature and intended to demonstrate the capabilities of the HDD for quantitative determinations as applied to real situations. The limits of detection could be significantly enhanced by incorporating purge/trap techniques.

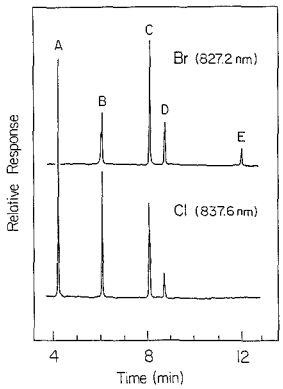

Figure 4. Chromatograms obtained from the extraction of a Williamsburg, VA, water sample at the Br (top) and Cl (bottom) wavelengths: (A) $CHCl_3$; (B) $CHBrCl_2$; (C) $ClCH_2CHBrCH_3$ (internal standard); (D) $CHBr_2Cl$; (E) $CHBr_3$.

Table VI. Haloform Concentrations (ppb) Determined in Drinking Water Using the HDD

sample		$CHCl_3$	$CHBrCl_2$	$CHBr_2Cl$	$CHBr_3$
Williamsburg, VA	1 (Cl)	28.1	20.2	6.8	
	(Br)		18.3	7.0	1.6
	2 (Cl)	28.1	19.8	7.6	
	(Br)		20.4	7.7	1.9
	av	28.1	19.7	7.3	1.8
Nags Head, NC	1 (Cl)	17.9	27.0	22.1	
	(Br)		27.4	22.0	4.2
	2 (Cl)	16.7	25.4	20.9	
	(Br)		27.1	21.8	4.0
	av	17.3	26.7	21.7	4.1
rel limits of det, ppb		0.13	0.15	0.18	0.23

CONCLUSION

The attributes of the HDD make it a viable alternative for trace analysis of organohalogen compounds. Although the detection limits are substantially poorer than those for ECD, the ease and confidence through which compounds can be quantitated with the HDD are significantly better. Continued research is warranted for improved methods of gas purification, as well as evaluation of other analytical wavelengths in the near-IR region to improve the selectivity and limits of detection once a more sensitive photodetector is obtained.

LITERATURE CITED

(1) Patterson, P. L. *J. Chromatogr.* **1977**, *134*, 25.
(2) Ecklund, G.; Josefsson, B.; Ross, C. *HRC CC, J. High Resol. Chromatogr. Chromatogr. Commun.* **1978**, *1*, 34.
(3) T. Cairns, T.; Seigmond, E. *Anal. Chem.* **1981**, *53*, 1183A.
(4) Nicholson, A. A.; Meresz, O.; Lemyk, B. *Anal. Chem.* **1979**, *49*, 814.
(5) van de Wiel, H. J.; Tommassen, P. *J. Chromatogr.* **1972**, *71*, 1.
(6) Chen, E. C.; Wentworth, W. E. *J. Chromatogr.* **1972**, *68*, 302.
(7) Overfield, C. V.; Winefordner, J. D. *J. Chromatogr. Sci.* **1970**, *8*, 233.
(8) Bowman, M. C.; Beroza, M.; Nickless, G. *J. Chromatogr. Sci.* **1971**, *9*, 44.
(9) Moseman, R. F.; Aue, W. A. *J. Chromatogr.* **1971**, *63*, 229.
(10) Anderson, R. J.; Hall, R. C. *Amer. Lab.* **1980**, *12*, 108.
(11) Piringer, O.; Wolff, E. *J. Chromatogr.* **1984**, *284*, 373.
(12) Goo, R. K. S.; Kanai, H.; Inouye, V.; Watatsuki, H. *Anal. Chem.* **1980**, *52*, 1003.
(13) Quimby, B. D.; Sullivan, J. J. Papers 736 and 902 presented at the 1989 Pittsburgh Conference and Exposition, Atlanta, GA, March 6–10, 1989.
(14) Wylie, P. L. Paper 738 presented at the 1989 Pittsburgh Conference and Exposition, Atlanta, GA, March 6–10, 1989.

(15) Layman, L. R.; Hieftje, G. M. *Anal. Chem.* **1975**, *47*, 194.
(16) Estes, S. A.; Uden, P. C.; Barnes, R. M. *Anal. Chem.* **1981**, *53*, 1336.
(17) Quimby, B. D.; Sullivan, J. J. Paper S7 presented at the 1988 Winter Conference on Plasma Spectrochemistry, San Diego, CA, Jan 3–9, 1988.
(18) Risby, T. H.; Talmi, Y. *CRC Crit. Rev. Anal. Chem.* **1983**, *14*, 231.
(19) Estes, S. A.; Uden, P. C.; Barnes, R. M. *Anal. Chem.* **1981**, *53*, 1829.
(20) Rice, G. W.; D'Silva, A. P.; Fassel, V. A. *Spectrochim. Acta* **1985**, *40B*, 1573.
(21) McAteer, P. J.; Ryerson, T. B.; Argentine, M. D.; Ware, M. L.; Rice, G. W. *Appl. Spectrosc.* **1988**, *42*, 586.
(22) Ware, M. L. Masters Thesis, College of William and Mary, Aug 1988.
(23) Grob K.; Grob, G. *J. Chromatogr.* **1974**, *90*, 303.
(24) Murray, A. J.; Riley, J. P. *Anal. Chim. Acta* **1974**, *65*, 261.
(25) Bellar, T. A.; Lichtenburg, J. J. *J. Am. Water Works Assoc.* **1974**, 703.
(26) Quimby, B. D.; Delaney, M. F.; Uden, P. C.; Barnes, R. M. *Anal. Chem.* **1980**, *52*, 259.
(27) Goldberg, M. C.; DeLong, L.; Sinclair, M. *Anal. Chem.* **1973**, *45*, 89.
(28) Grob, K.; Grob, K., Jr.; Grob, G. *J. Chromatogr.* **1975**, *106*, 299.

RECEIVED for review August 28, 1989. Revised manuscript received January 9, 1990. Accepted January 12, 1990. The authors gratefully acknowledge financial support for this research from the Thomas F. and Kate M. Jeffress Memorial Trust. This work was presented in part at the 1989 Federation of Analytical and Spectroscopy Societies Conference, October 1–6, 1989, Chicago, IL.

Minimization of Interferences in Inductively Coupled Plasma Mass Spectrometry Using On-Line Preconcentration

E. M. Heithmar* and T. A. Hinners

U.S. Environmental Protection Agency, P.O. Box 93478, Las Vegas, Nevada 89193-3478

J. T. Rowan

Lockheed Engineering and Sciences Company, 1050 East Flamingo Road, Las Vegas, Nevada 89119

J. M. Riviello

Dionex Corporation, 1228 Titan Way, P.O. Box 3603, Sunnyvale, California 94088-3603

A semiautomated system is used to preconcentrate Ti, V, Mn, Fe, Co, Ni, Cu, Cd, and Pb, in order to remove high salt matrices. The preconcentration system accepts digests with acid concentrations equivalent to 0.8–1.4% HNO_3, neutralizes them, and loads them onto a macroporous iminodiacetate resin. The alkali and alkaline-earth metals, along with deleterious anions such as chloride, are washed off the resin before and analyte metals are eluted with nitric acid. A total of 13 isotopes of the analytes are measured. An examination of the apparent concentration efficiencies, as well as the behavior of two internal standard elements added to the eluate stream, indicates that the elution front matrix enhances the inductively coupled plasma mass spectrometry response of the analytes. Investigation of the nature of the blank signals suggests that the detection limits of several of the isotopes could benefit by much larger preconcentration factors, while those of vanadium, copper, cadmium, and lead are currently limited by reagent purity and laboratory contamination. The preconcentration system is evaluated on several simple synthetic matrices, as well as on synthetic seawater and three wastewaters. Digestion of samples containing natural organic chelators is required.

The analysis of environmental samples for trace elements poses two major problems. First, regulatory action-levels for environmental concentrations of many metals are in low part-per-billion level. In order to ensure that "false-negatives" are not caused by slight variations in method performance, it is desirable to have detection limits at least 10-fold lower than these levels. Second, the matrices encountered in environmental samples are diverse and often complex. Because of the need for low detection limits, graphite furnace atomic absorption spectrometry (GFAAS) and, more recently, inductively coupled plasma mass spectrometry (ICP-MS) have been employed in environmental analysis (*1*, *2*). ICP-MS has the advantage over GFAAS of being a multielemental technique, but it has not yet been accepted for analyses related to regulatory compliance.

One of the major drawbacks of ICP-MS, compared to such robust techniques as inductively coupled plasma atomic emission spectrometry (ICP-AES), is the interferences often exhibited with the complex matrices encountered in environmental analysis. These interferences can be spectral (*2*, *3*), or physicochemical (*4*, *5*), in nature. The former have been treated mathematically, by the use of various fundamental or empirical correction terms in the calibration function. The physicochemical effects can be ameliorated to a certain extent by the use of internal standardization (*4*) or alternative sample introduction techniques, such as flow injection analysis (*5*). All of these approaches decrease the signal-to-noise ratio to some extent, and none of them is completely adequate for complex matrices.

Preconcentration can be used to separate analytes from interferences prior to analysis. The analytes are generally complexed with some chelating agent. Separation can be effected by solvent extraction (*7*), precipitation (*8*), or the use of an immobilized form of the chelating agent, such as with a resin. The last approach has become increasingly popular in the last few years. The resin can be digested to liberate the trace elements (*9*) or the analytes can be released by changing the ionic form of the resin. The latter method allows semiautomated methods to be developed that make use of resin-packed columns. Many such methods have been described (*10–17*). Although some methods have employed chelating agent adsorbed on hydrophobic resins (*10*), acidic

0003-2700/90/0362-0857$02.50/0

Table I. ICP-MS Conditions

torch: normal "short" type
gas flows: plasma, 12 L/min; auxiliary, 1.8 L/min; nebulizer, 1.1 L/min
foreward power: 1200 W
reflected power: <5 W
sample flow (by peristaltic or high pressure pump): 1.0 mL/min
sampler position: 18 mm above load coil
sampler/skimmer: platinum (1.1 mm sampler orifice, 0.9 mm skimmer orifice)
lens settings: first and third Einzel lenses, −18.1 V; Bessel box plates, −9.7 V; Bessel box barrel, +2.1 V; Bessel box stop lens, −5.3 V
interface pressure: 2 Torr
mass spectrometer pressure: 2.5×10^{-5} Torr
resolution: 0.95–1.0 m/z units at 10% peak height
typical sensitivities: ^{7}Li, 1000 s^{-1} μg^{-1} L; ^{59}Co, 1500 s^{-1} μg^{-1} L; ^{115}In, 3000 s^{-1} μg^{-1} L; ^{205}Tl, 1000 s^{-1} μg^{-1} L
peaks monitored during routine analysis: m/z 46, 48, 49, 51, 52, 54, 55, 57, 60, 62, 63, 65, 89, 111, 208, and 209; m/z 53 substituted for m/z 46 during direct nebulization experiments to allow correction for $(^{35}Cl^{16}O)^{+}$ on ^{51}V
measurements/peak: 1
measurement time: 81 ms
dwell time: 27 ms (three dwells per measurement)

or basic alumina (*14–16*), or ion-pairing and adsorption on nonpolar resin (*17*), the largest number have used some form of an iminodiacetate copolymer (*11–13*). These resins were previously used in the batch mode for preconcentration and matrix elimination prior to GFAAS (*18*) or neutron activation analysis (*19*).

Preconcentration techniques in ICP-MS have not been widely used. McLaren et al. (*20*) and Beauchemin et al. (*21*) used 8-hydroxyquinoline immobilized on silica. They were able to determine several trace elements in a coastal seawater and a river water. The immobilized hydroxyquinoline is efficient; it allows preconcentration from large quantities of water, and some separation from magnesium and calcium can be achieved. An on-line procedure based on the immobilized 8-hydroxyquinoline has been reported (*22*). Plantz et al. (*17*) developed an on-line method using complexation in solution and adsorption of the metal bis(carboxymethyl)dithiocarbamate on a nonpolar resin (*17*). This approach worked well for moderately high salt concentrations, and the levels of four trace elements in seawater and urine were determined.

Although iminodiacetate copolymers are effective resins for the separation of a number of trace elements from the alkali and alkaline-earth metals, their routine use suffers from two drawbacks. First, many formulations of the resin exhibit pronounced changes in volume upon changing ionic form (*23*). This can impede the flow of sample. Second, the resin exhibits its best discrimination against alkali and alkaline-earth metals at pH values from 5.0 to 5.8. Several trace element species, especially Fe^{3+} and Cu^{2+}, hydrolyze and precipitate at these pH values. The present work uses a commercially available highly cross-linked copolymer with reduced tendency to swell, and a flow-injection approach to sample neutralization and buffering which minimizes hydrolysis. A preconcentration system based on the same resin has recently been used in conjunction with ion chromatography (*24*). Postcolumn internal standard addition is employed to examine high apparent preconcentration efficiency and to correct for instrumental drift. The efficacy of on-line preconcentration from several synthetic and natural matrices is investigated for titanium, vanadium, manganese, iron, cobalt, nickel, copper, cadmium, and lead.

EXPERIMENTAL SECTION

Instrumentation. The inductively coupled plasma mass spectrometer used is the Sciex/Perkin-Elmer ELAN Model 250, equipped with mass-flow controllers and upgraded ion optics. The instrumental conditions employed for preconcentration (Table I) are optimized for high sensitivity, rather than for minimum molecular ion interferences, since many molecular ions would be minimized by matrix elimination (i.e., the parameters given in Table I reflect rather "cool" plasma conditions).

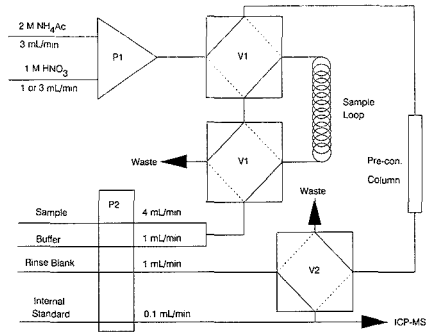

Figure 1. On-line preconcentration device: P1, high-pressure pump; P2, peristaltic pump; V1 and V2, four-way valves (V1 shown in the "A" position, V2 in "B" position).

The preconcentration device is shown schematically in Figure 1. The system is based on a high-pressure, programmable pump (Model GPM), four-way high-pressure slider valves, and a prototype iminodiacetate resin column, all from Dionex Corp., Sunnyvale, CA, and a 16-channel peristaltic pump (Model 1200, Lachat Instruments, Mequon, WI). The column is 9 mm i.d. by 25 mm long, and contains approximately 1.5 mL of resin. Both a 2.5-mL and a 10-mL sample loop (TFE tubing) were used in various parts of the study. The operation of the preconcentration device is controlled by the high-pressure pump program and is described in the procedure subsection.

Reagents. Distilled, doubly deionized water and sub-boiling distilled-in-quartz concentrated nitric acid, acetic acid, and ammonia (Seastar, Sidney, B.C.) were used throughout the study. Stock analyte solutions of titanium, vanadium, manganese, iron, cobalt, nickel, copper, cadmium, and lead in 1% (v/v) nitric acid and an internal standard solution containing yttrium and bismuth at 1 mg/L in 5% nitric acid were prepared from commercial multielement plasma standards (Spex Industries, Metuchen, NJ).

A solution of approximately 2 M ammonium acetate at a pH of 5.5 was prepared from 4 M stock solutions of the Seastar reagents. This was one of the resin eluant solutions. The second eluant solution was 1 M nitric acid. A second ammonium acetate solution of approximately 2 M concentration was prepared, and its pH was adjusted with 4 M ammonia or acetic acid so that, when mixed on-line with a 1% nitric acid sample (see Figure 1), the pH of the resulting solution was 5.5.

Synthetic matrix solutions of 2000 mg/L sodium, potassium, magnesium, or calcium were prepared in 1% nitric acid from the chlorides with minimum purities of 99.99+% (Aldrich Chemicals, Milwaukee, WI). Similarly, synthetic seawater solution was prepared from these chloride salts and sub-boiling, distilled-in-quartz sulfuric acid (J. T. Baker Chemicals, Phillipsburg, NJ) and nitric acid so that the final solution contained 10560 mg/L sodium, 1270 mg/L magnesium, 400 mg/L calcium, 380 mg/L potassium, 21 000 mg/L chloride, and 880 mg/L sulfur. This solution had the same matrix as a seawater sample acidified with 0.5% hydrochloric acid and 1% nitric acid.

Sample Preparation. Municipal wastewater samples were obtained from the primary effluent discharge line and the secondary effluent stream at the Clark County, NV, Sanitation District Water Treatment Plant. A water sample from the Las Vegas Wash was also obtained from a point 5 km south of the Advanced Water Treatment Plant of the Sanitation District. These samples were filtered through 0.45-μm cellulose filters and then acidified with 1% nitric acid.

Dissolved organic carbon (DOC) was determined on each sample. DOC values were 13, 22, and 33 mg/L for the wash water,

secondary effluent, and primary effluent, respectively. The alkali and alkaline-earth metal concentrations of the samples were determined by ICP-AES (Plasma II, Perkin-Elmer) using routine procedures (25). These concentrations were all consistent among the samples at 210 ± 10 mg of Na/L, 22 ± 2 mg of K/L, 52 ± 3 mg of Mg/L, and 115 ± 8 mg of Ca/L.

A 45-mL aliquot of each filtered sample was placed in a sealed TFE digestion vessel (CEM, Matthews, NC) with 5 mL of concentrated nitric acid and digested in a microwave oven (Model 81D, CEM, Matthews, NC). The microwave power was maintained at 545 W for 10 min and then lowered to 345 W for an additional 10 min. The cooled digestate was diluted 10-fold in water. Both the undigested (referenced as "raw") samples and the diluted digests were analyzed without further treatment.

Procedure. (Refer to Figure 1. Valve 1 in the figure is shown in the "A" position and valve 2 is shown in the "B" position.) The preconcentration procedure begins by placing the sample-uptake line in acidified sample. The sample, at 4.0 mL/min, is mixed with ammonium acetate at 1.0 mL/min and passed through the sample loop to waste via valve 1 in the "A" position. During this time, the resin is being preconditioned to the ammonium form at pH 5.5 with 2 M ammonium acetate. With valve 2 in the "B" position, the ammonium acetate passes to waste, and 2% nitric acid rinse solution is delivered to the plasma. The sample does not remain at pH 5.5 for more than 3.4 min when the 10-mL loop is used (50 s when the 2.5-mL loop is used).

At $t = 0.0$ min (all times are given for 10-mL samples; subtract 3 min from all subsequent times for 2.5-mL samples), the preconcentration program is initiated, valve 1 turns to the "B" position, and the high-pressure pump sweeps the sample to the resin column with 2 M ammonium acetate at 3 mL/min, preconcentrating the analytes, and passing the sample to waste. At 4.0 min, valve 1 turns to the "A" position, and the high-pressure pump continues to pass 2 M ammonium acetate through the column to waste. This wash-out period replaces chelated Mg^{2+} and Ca^{2+} with NH_4^+. At 6.0 min, the high-pressure pump switches to 1 M HNO_3 at 3 mL/min. At 6.7 min, the pump slows to 1 mL/min and valve 2 turns to the "A" position, passing the eluted trace metals to the ICP-MS. Internal standard solution is mixed with the eluate in an approximately 1:10 ratio, yielding 100 μg/L concentrations of Y and Bi internal standards.

After the analyte peaks pass (at 8.7 min), valve 2 turns to the "B" position and 3 mL/min of 2 M ammonium acetate is passed through the column to waste for 1 min. This is followed by successive 3-mL rinses with nitric acid, ammonium acetate, nitric acid, and finally ammonium acetate again, each at a rate of 3 mL/min. The resin is now reconditioned, and ready for the next sample, which generally is already passing through the sample loop. The reason for the alternating rinses with nitric acid and ammonium acetate is described in Results and Discussion. The entire preconcentration procedure is conducted with two reagent blanks at the beginning of each day, as the first preconcentration cycle generally exhibits elevated ICP-MS backgrounds, especially at m/z 51 and 55.

The mass spectra are obtained by using the "Multiple Elements" program of the ELAN ICP-MS. The measurement routine described in Table I allows the observation of each peak every 0.67 s and a temporal display resolution of 2 s. The acquisition of the spectrum is initiated at 6.7 min in the preconcentration program. The analyte peaks appear in about 50 s and reach near the base line before valve 2 switches to the "B" position and data acquisition ceases. The spectrum is converted to an ASCII file and automatically sent via the Kermit communications protocol to an 80386-based microcomputer for processing. The spectrum is placed in a commercial spreadsheet by a macro that automatically finds the analyte peaks and integrates each over the optimal detection period. Because there is some variability in the elution time of the peaks, relative to the start of the data acquisition, the $(^{40}Ar^{12}C)^+$ intensity at m/z 52 is used as an approximate time reference for the analyte peaks. Descriptions of the communications, peak location, and calculations algorithms are available upon request.

RESULTS AND DISCUSSION

Effect of Buffer Ionic Strength. Initial experiments with off-line buffering involved varying the buffer concentrations

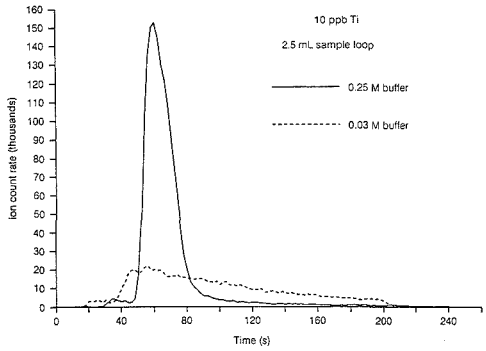

Figure 2. Effect of buffer concentration on preconcentration profile of titanium (m/z 48 shown).

from the minimum amount that would neutralize 0.1% nitric acid solutions (about 0.03 M ammonium acetate) up to 1 M ammonium acetate. Figure 2 shows the preconcentration elution profiles for ^{48}Ti at 0.03 and 0.25 M buffer concentrations. It is apparent that the lower-concentration solution exhibited pronounced tailing. This was eliminated by the use of 0.25 M buffer. Concentrations above 0.25 M had little further effect. Similar results were obtained for isotopes of vanadium, iron, and lead. Other analytes were less affected. Since the pH values of both solutions were well within the optimal pH range, the effect was apparently related to ionic strength. Titanium, vanadium, and iron all have multiple oxidation states with varying affinities for iminodiacetate, but it is unknown if this was a factor here. Plantz et al. (17) noted a similar phenomenon of poor preconcentration in dilute solutions and attributed it to a "salting out" effect, but the chemistry of that system was different; neutral metal chelate was adsorbing on a neutral resin. The reason for the effect of the buffer concentration in this study is not currently known.

Whatever the reason for the tailing phenomenon at low ionic strength, the on-line buffer was made 2 M, in order to produce a 0.4 M final buffer concentration in the sample. Two important considerations were the possibility of elevated analyte blanks at high buffer concentration and the lack of ability to withstand variations in sample acidity at low buffer concentrations. The 2 M buffer produced acceptable blanks, and it adequately buffered solutions ranging from 0.8% to 1.4% HNO_3 to a pH of 5.4 ± 0.2.

Preconcentration Efficiency. The efficiency of the preconcentration system was determined by bypassing the column and using the sample loop for flow-injection sample introduction directly to the nebulizer. The integrated signals for 10 μg/L solutions of each of the analytes in 1% nitric acid were compared with the integrated signals after preconcentration. Both analyses were performed in duplicate and the integrated intensities were corrected for background. Since the integrated intensities, not the peak heights, were compared, the two values should be the same, irrespective of the preconcentration factor, if the preconcentration was 100% efficient and the sensitivity remained constant.

Table II gives the results of that comparison. It is obvious that the preconcentration system is yielding enhanced absolute sensitivity relative to direct aspiration in a 1% nitric acid matrix. This phenomenon is confirmed by Figure 3, which shows the elution profile of 10 μg/L cobalt and the corresponding internal standard intensities. At the front edge of the ^{59}Co elution, the ^{89}Y intensity suddenly increases, followed by a similar increase in the ^{209}Bi intensity. The measurement cycle (Table I) provides for a maximum time difference be-

Table II. Integrated Preconcentration Intensities Compared to Integrated Direct Nebulization Intensities[a]

element	% relative signal	element	% relative signal
Ti	150	Ni	150
V	130	Cu	150
Mn	130	Cd	120
Fe	140	Pb	130
Co	150		

[a] Direct nebulization of 1% HNO_3 solution = 100%. Relative signals are ±10% (N = 2).

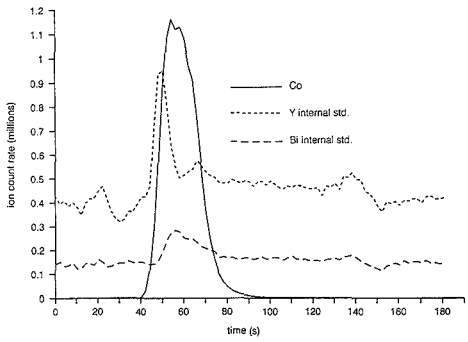

Figure 3. Typical elution profile for cobalt, along with the intensities of the two postcolumn internal standards.

tween the observation of two masses of 0.67 s. Therefore, the difference in the temporal behavior of these effects is real and indicates that they are not due to mixing anomalies caused by the change in eluant viscosity. The cobalt elution profile (as well as those of the other analytes) overlaps these intensity enhancements, so a signal enhancement of the analyte peaks due to the solution matrix should be expected. Both enhancements and suppressions due to sample matrix have been reported in ICP-MS (*26*).

In order to establish conclusively that the matrix at the elution front causes an ion-signal enhancement, three different matrices spiked with 25 μg/L of analytes and internal standards were directly nebulized. The first matrix, used as a reference, was 1% nitric acid. The second was 1 M nitric acid. The third matrix was 0.8 M ammonium nitrate in 0.2 M nitric acid. The background-corrected intensities for the analytes and internal standards in the latter two solutions, referenced to intensities in 1% nitric acid, are given in Table III. Ammonium nitrate causes a pronounced enhancement of most signals. The proportions of the various matrix components at the exact time of analyte elution are not known and in fact are highly transient. It is probable, however, that the eluant contains an appreciable concentration of ammonium ion at this time, due to the conversion of resin sites from the ammonium to the hydronium form. The effect of ammonium ion on analyte sensitivities shown by the data in Table III is consistent with the enhancement observed during analyte elution.

Detection Limits. The detection limits obtained with any preconcentration system depend on the mode of peak detection (area vs peak height), and the integration time (or time constant, in the case of peak-height measurement). As a result of preliminary studies, it was decided that peak areas would be used for quantitation. Peak widths, and therefore peak heights, sometimes varied by ±15% during the day. Peak areas, conversely, were reproducible. In order to establish optimal measurement parameters, the integration time was

Table III. Relative Analyte Intensities with Direct Nebulization of Various Matrices[a]

element	1 M HNO_3	NH_4NO_3/ HNO_3	element	1 M HNO_3	NH_4NO_3/ HNO_3
Ti	115	141	Cu	106	125
V	114	140	Y	114	136
Mn	115	139	Cd	92	100
Fe	115	138	Pb	113	128
Co	113	136	Bi	116	127
Ni	102	130			

[a] 1% nitric acid matrix = 100%. Precision of percent ratios is ≤8% (N = 4).

Table IV. Detection Limits (μg/L, 3σ Criterion, N = 5) for Preconcentration System

isotope	2.5-mL sample	10-mL sample
^{48}Ti	0.1	0.04
^{49}Ti	0.05	0.02
^{51}V	0.08	0.006
^{55}Mn	0.03	0.006
^{54}Fe	20	1
^{57}Fe	2	0.3
^{59}Co	0.002	0.0004
^{60}Ni	0.1	0.01
^{62}Ni	0.1	0.02
^{63}Cu	0.05	0.004
^{65}Cu	0.05	0.007
^{111}Cd	0.03	0.006
^{208}Pb	0.08	0.005

varied from 20 to 60 s, with different starting points for the integration window. Since a maximum in the m/z 55 signal was present in all elution profiles shortly after the maximum in the $(^{40}Ar^{12}C)^+$ signal, the starting points in standards and samples could be precisely matched. Two low-concentration standards and five blanks were analyzed using each set of timing parameters. The detection limits obtained exhibited a broad minimum for nearly every element from 20 to 50 s integration time, with an optimal starting point of 10 s before the m/z 55 maximum. Since the widths of the peaks could vary from 14 to 20 s (fwhm), a conservative integration time of 40 s was determined. Table IV gives the detection limits found for each isotope for both the 2.5-mL loop and the 10-mL loop.

Two complementary approaches can be taken to improving these detection limits. If the blank noise is predominantly from sources other than analyte signal, increasing the sample size should provide a virtually linear improvement in signal to noise. On the other hand, if the analyte is the major contributor to blank noise, further cleanup of reagents should yield lower blanks, and consequently lower detection limits. The latter case was of concern to us, as the reagents were all used without further purification, and all operations were performed in a general-purpose instrumentation laboratory. Examination of the elution profiles of the blanks helped to establish the predominant blank contributions.

Figure 4a shows a representative blank for ^{48}Ti, along with the signal obtained for 0.5 μg/L Ti. Although there appears to be a substantial peak in the blank corresponding to the elution time of the titanium, the maximum contribution to this by the analyte (equivalent to about 0.02 μg/L Ti) can be seen by multiplying the ^{49}Ti blank profile by 13.4. The result is shown at the bottom of the figure and accounts for no more than 30% of the blank. The rest of the blank must be molecular in nature. Two contributions that can be accounted for directly are those from $(^{14}N^{16}O^{18}O)^+$ and $(^{36}Ar^{12}C)^+$. The m/z 46 peak is predominantly from $(^{14}N^{16}O^{16}O)^+$ in the blank (contributions from $^{46}Ti^+$ and $^{46}Ca^+$ impurities were insig-

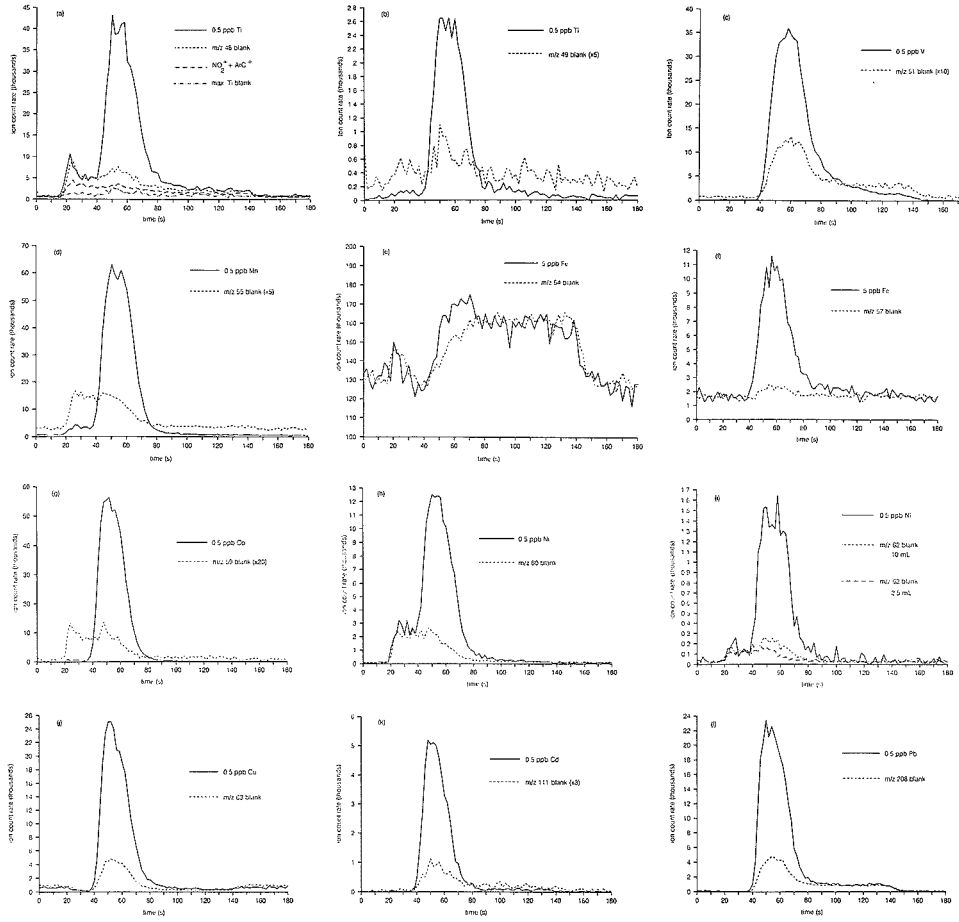

Figure 4. Typical blanks and 0.5 μg/L standard responses with the 10-mL sample loop (unless otherwise indicated in the legend) for (a) ^{48}Ti, (b) ^{49}Ti, (c) V, (d) Mn, (e) ^{54}Fe, (f) ^{57}Fe, (g) Co, (h) ^{60}Ni, (i) ^{62}Ni, (j) ^{63}Cu (^{65}Cu similar), (k) ^{111}Cd, and (l) ^{208}Pb.

nificant). Multiplying the m/z 46 intensity by 0.004 gives an estimate of the NO_2^+ contribution to m/z 48. Similarly, the m/z 52 intensity during the blank elution is almost entirely due to $(^{40}Ar^{12}C)^+$ from the residual acetate carbon introduced into the plasma at this time. The $(^{36}Ar^{12}C)^+$ contribution at m/z 48 is estimated by multiplying the m/z 52 intensity by 0.0034. The resulting sum of $(^{14}N^{16}O^{18}O)^+$ and $(^{36}Ar^{12}C)^+$ intensities is shown in Figure 4a. The remainder of the m/z 48 blank is of noncharacterized molecular origin.

The similarity of blank and 0.5 μg/L sample profiles in Figure 4b shows that, unlike its sister isotope, preconcentrated ^{49}Ti apparently accounts for the majority of its 0.02 μg/L blank. Figure 4c demonstrates that the m/z 51 blank is also probably dominated by approximately 0.015 μg/L preconcentrated analyte. Figure 4d for m/z 55, on the other hand, exhibits a blank profile that is dominated by molecular contribution, possibly $(^{40}Ar^{14}NH)^+$.

The two iron profiles in Figure 4, parts e, m/z 54, and f, m/z 57, are quite a contrast. A 5 μg/L quantity of Fe creates just a small shoulder on the m/z 54 blank, which is dominated by the $(^{40}Ar^{14}N)^+$ surge from the high concentration of nitrogen in the eluant. The m/z 57 blank shows a small peak corresponding to approximately 0.5 μg/L preconcentrated iron on top of the constant $(^{40}Ar^{16}OH)^+$ background. These two figures demonstrate the reason for the superior ^{57}Fe detection limit.

The m/z 59 blank (Figure 4g) shows another large contribution from an identified transient molecular ion, although there may also be a small analyte contribution (≤0.002 μg/L) as well. The m/z 60 blank (Figure 4h) is apparently dominated by unidentified transients, while the m/z 62 blank in Figure 4i has a higher relative contribution from approximately 0.04 μg/L analyte, judging from the smaller size of the second half of the 2.5-mL blank. Blanks for both copper isotopes are dominated by a nearly 0.1 μg/L analyte contribution (see Figure 4j for m/z 63), as could be expected for this common contaminant. Figures 4k and 4l are also dominated by ^{111}Cd (approximately 0.03 μg/L) and ^{208}Pb (approximately 0.1 μg/L), respectively.

It is apparent from these blank profiles that in the cases of vanadium, copper, cadmium, and lead, as well as ^{49}Ti, rigorous reagent purification and stringent clean-room conditions could significantly improve detection limits. Conversely, the detection limits of the other isotopes would definitely improve with larger sample sizes. Even in the cases of the elements with analyte-limited blanks, blank areas did

Table V. Effect of Cycling Acid and Buffer Postanalysis Rinses[a]

element	4-min acid rinse	two 2-min acid/buffer cycles
Ti	0.05	ND
V	0.15	0.06
Co	0.03	0.01
Cu	0.12	ND

[a] Only elements exhibiting detectable memory are listed. Values given are apparent concentrations (μg/L) in first blank after 10 μg/L standard.

not increase by a factor of 4 from the 2.5-mL sample loop to the 10-mL loop, so some improvement with increased sample size is still possible.

Zinc was not included among the elements studied in this work, although it is efficiently retained and eluted from the iminodiacetate resin. Early experiments produced such large zinc blanks that quantitation at the low microgram per liter level was impossible. Since concentrations of zinc encountered in our laboratory are usually relatively high, preconcentration of that element was not pursued further.

Residual Signal. Early experiments with the preconcentration system used a continuous postanalysis rinse with 1 M nitric acid for 4 min at 3 mL/min, prior to the column reconditioning with 1 min of ammonium acetate. Considerable residual signal was apparent for some analytes, particularly vandium, in the first blank after a high concentration standard. Successive blanks decreased until a base line was reached after two or three blanks. Since the degree of memory did not appear to be greatly affected by length of nitric acid rinse or of ammonium acetate reconditioning, the alternation between ionic forms was probably the essential factor in decreasing the blank. Various programs of alternating rinse times were tested, and the regime described in the Procedure was chosen as the best compromise between speed of analysis and freedom from increased blank signals. Table V shows the apparent residual signals in the first blank analyzed after a 10 μg/L standard, for the original program of 4 min of acid wash, and for the 4 min of alternating 1 min acid and buffer segments. It is not clear why vanadium, and to a lesser extent titanium, cobalt, and copper, exhibit memory.

Linearity and Precision. Calibration curves were determined for each of the analytes from 0.3 to 30 μg/L, using the 2.5-mL sample loop, and from 0.3 to 10 μg/L, using the 10-mL sample loop. (The iron calibration curves were determined by using 10 times these concentrations.) All 13 isotopic calibrations were linear, with correlation coefficients ranging from 0.998 to 0.9999. Table VI gives the precision obtained at 10 and 0.5 μg/L with the 2.5-mL sample loop and at 0.5 μg/L with the 10-mL sample loop. Even at the lower concentration, the precision was usually analyte-noise limited, so there is no correlation between precision and detection limits. The long-term precision of the method was good, but the sensitivity for lead tended to drift during the day. Lead calibrations and analyses used the internal standard intensity of bismuth to correct this drift.

Simple Synthetic Matrices. The degree of residual interferences from molecular ions of alkali and alkaline-earth metals, as well as chloride, was examined as a function of preelution wash-out time. Solutions (2000 mg/L) of each major alkali and alkaline-earth metal were preconcentrated, and the ammonium acetate wash-out times were varied from 1 to 6 min. Only 2000 mg/L calcium produced residual spectral interferences greater than the detection limits given in Table IV at wash-out times greater than 1 min. After 2 min wash-out, the calcium solution produced an apparent Ti

Table VI. Precision as a Function of Concentration and Sample Size[a]

	2.5-mL sample		10-mL sample
element	10 μg/L	0.5 μg/L	0.5 μg/L
^{48}Ti	0.5	7.2	4.0
^{49}Ti	2.0	4.7	1.9
^{51}V	0.7	2.5	3.3
^{55}Mn	0.5	3.2	0.8
^{54}Fe[b]	2.1	ND[c]	15
^{57}Fe[b]	3.3	6.3	6.5
^{59}Co	2.0	3.2	2.1
^{60}Ni	2.0	3.2	2.7
^{62}Ni	1.9	5.9	5.7
^{63}Cu	3.7	9.6	5.1
^{65}Cu	3.5	10.9	5.4
^{111}Cd	1.1	3.4	3.4
^{208}Pb	2.2	2.7	2.3

[a] Percent relative standard deviation (N = 4). [b] Concentrations of iron were 100 and 5 μg/L. [c] Concentration near detection limit at this sample size. Precision not determined.

Table VII. Spectral Interferences Observed in Flow-Injection Direct Nebulization of Simple Synthetic Matrices[a]

	matrix element			
analyte	Na	K	Mg	Ca
^{48}Ti	ND[b]	ND	2.9	c
^{49}Ti	12	8	27	14
^{51}V	15	11	40	20
^{55}Mn	ND	6	0.4	0.6
^{54}Fe	ND	ND	ND	ND
^{57}Fe	ND	52	51	22000
^{59}Co	ND	ND	2	15
^{60}Ni	1.2	0.4	1.2	270
^{62}Ni	62	ND	2.7	6.6
^{63}Cu	21	1.4	0.2	ND
^{65}Cu	ND	0.8	0.5	13

[a] Apparent concentration of analyte (μg/L) caused by 2000 mg/L matrix element and associated chloride. [b] Not detected at the detection limit of flow-injection direct nebulization method. [c] Not measured, exceeded dynamic range of ICP-MS.

signal at m/z 48 corresponding to 75 μg/L Ti. This is caused by residual ^{48}Ca in the resin, equal to about 1.5% of the original Ca concentration. The only molecular spectral interferences remaining after 2 min of wash-out were the equivalent of 270 μg/L iron at m/z 57 ($^{40}Ca^{16}OH^+$), the equivalent of 0.1 μg/L cobalt at m/z 59 ($^{42}Ca^{16}OH^+$, $^{40}Ca^{18}OH^+$, etc.), and the equivalent of 1 μg/L nickel at m/z 60 ($^{44}Ca^{16}O^+$). No molecular interferences remained after 6 min of wash-out, and only the equivalent of 1.8 μg/L Ti remained at m/z 48, corresponding to 0.03% of the original Ca concentration. It should be noted that the 2000 mg/L synthetic matrices also contained up to 5900 mg/L chloride, which never produced any molecular interferences.

The 2000 μg/L synthetic matrices were also analyzed by direct nebulization. In these experiments, the column was again bypassed and a 300-μL sample loop was installed on valve 1. This flow-injection system minimized the buildup of solids on the sampler orifice (6). The calibration was based on the ratios of signals to the on-line ^{89}Y and ^{209}Bi internal standards, as the sodium and potassium matrices caused significant signal suppression. Table VII lists the apparent concentrations of analytes caused by direct nebulization of the four simple synthetic matrices. As expected, all of the solutions produce strong interferences on m/z 51, due mainly to $(^{35}Cl^{16}O)^+$, when aspirated directly. $(^{35}Cl^{14}N)^+$ also interferes at m/z 49. Sodium produces an interference at m/z 62 due

Table VIII. Percent Recoveries from Simple Synthetic Matrices[a]

	matrix element							
	Na		K		Mg		Ca	
analyte	PC[b]	FIA[c]	PC	FIA	PC	FIA	PC	FIA
^{48}Ti	106	104	103	105	98	101	−34	189
^{49}Ti	105	103	104	110	100	106	96	104
^{51}V	104	130	103	104	110	104	98	107
^{55}Mn	102	86	101	88	88	89	81	94
^{54}Fe	103	23	107	20	95	28	99	38
^{57}Fe	103	74	102	85	99	82	96	−2300
^{59}Co	101	85	100	92	97	84	93	80
^{60}Ni	102	77	99	81	95	68	90	−230
^{62}Ni	104	103	102	76	100	68	90	82
^{63}Cu	103	78	94	64	99	72	90	75
^{65}Cu	103	69	94	70	97	73	89	73
^{111}Cd	102	69	101	74	96	73	93	79
^{208}Pb	100	70	92	65	89	74	98	79

[a] 10 μg/L spike of each analyte (100 μg/L spike of iron). [b] Preconcentration ICP–MS. [c] Flow-injection direct nebulization ICP-MS.

Table IX. Apparent Analyte Concentrations in Nonspiked Synthetic Seawater Matrix by Preconcentration and by Flow-Injection Direct Nebulization[a]

analyte	preconcentration	flow injection
^{48}Ti	39	1120
^{49}Ti	ND	120
^{51}V	ND	ND
^{55}Mn	ND	ND
^{54}Fe	ND	ND
^{57}Fe	130	3330
^{59}Co	ND	1.3
^{60}Ni	ND	19
^{62}Ni	ND	500
^{63}Cu	ND	52
^{65}Cu	ND	15

[a] Concentrations in μg/L.

to $(^{23}Na_2{}^{16}O)^+$ and a smaller effective interference on ^{63}Cu from $(^{23}Na^{40}Ar)^+$. In the potassium matrix, $(^{39}K^{16}O)^+$ causes an interference at m/z 55. $^{24}Mg_2{}^+$ could explain a small interference at m/z 48 in the magnesium matrix. In the same solution, $(^{24}Mg^{35}Cl)^+$ accounts for the signal at m/z 59 and $(^{25}Mg^{37}Cl)^+$ produces a signal at m/z 62. In the calcium matrix, the strongest interferences are the $(^{40}Ar^{16}OH)^+$ effect at m/z 57, the $(^{44}Ca^{16}O)^+$ signal at m/z 60, and, of course, the $^{48}Ca^+$ interference on ^{48}Ti. In short, every isotope between m/z 48 and m/z 65 is subject to a spectral interference by one of the four matrices, except ^{54}Fe.

Percent recoveries of 10 μg/L spikes of the simple synthetic matrices for preconcentration sample introduction are compared to the percent recoveries for flow-injection direct nebulization in Table VIII. All but two of the recoveries for preconcentration sampling fall between 85% and 115%. One of these is for manganese in the calcium solution. Recoveries of manganese with iminodiacetate resins are known to be adversely affected by high calcium concentrations (*23*). If manganese is to be determined in such matrices, standards similar in composition to the samples should be prepared, or the method of standard addition can be employed. The isobaric ^{48}Ca interference on ^{48}Ti caused a negative recovery, due to slight variability in the efficiency of the ammonium acetate wash-out between the spiked and nonspiked samples. Of the directly nebulized samples, more than half of the recoveries fall outside a 85% to 115% acceptance window. It was impossible to distinguish any analyte signals on top of the intense $(^{40}Ca^{16}OH)^+$ and $(^{44}Ca^{16}O)^+$ interferences.

Table X. Percent Recoveries from Spiked Synthetic Seawater by Preconcentration and by Flow-Injection Direct Nebulization[a]

analyte	preconcentration	flow injection
^{48}Ti	110	−71
^{49}Ti	98	75
^{51}V	108	117
^{55}Mn	85	68
^{54}Fe	109	61
^{57}Fe	118	−104
^{59}Co	98	54
^{60}Ni	99	41
^{62}Ni	97	−330
^{63}Cu	95	47
^{65}Cu	95	35
^{111}Cd	94	48
^{208}Pb	97	72

[a] 10 μg/L spike of each analyte (100 μg/L spike of iron).

Table XI. Percent Recoveries of Trace Metals from Wastewaters and Wastewater Digests[a]

	Las Vegas wash		secondary effluent		primary effluent	
analyte	raw	digest	raw	digest	raw	digest
^{48}Ti	106	95	100	92	0	95
^{49}Ti	86	93	52	100	27	96
^{51}V	104	99	110	102	110	101
^{55}Mn	97	94	100	96	97	94
^{54}Fe	90	90	81	106	97	90
^{57}Fe	150	94	139	97	97	95
^{59}Co	99	97	101	99	98	97
^{60}Ni	100	97	101	99	103	95
^{62}Ni	103	101	94	101	99	100
^{63}Cu	78	97	54	106	37	99
^{65}Cu	78	98	57	105	38	99
^{111}Cd	95	100	94	96	66	96
^{208}Pb	83	95	67	92	28	90

[a] 10 μg/L spike of each analyte (100 μg/L spike of iron).

Synthetic Seawater. The results of the preconcentration ICP-MS analysis of nonspiked synthetic seawater are compared with the results from flow-injection direct nebulization in Table IX. The only spectral interferences remaining after preconcentration and a 6-mL wash-out with ammonium acetate are relatively small residual $^{48}Ca^+$ and $(^{40}Ca^{16}OH)^+$ peaks. Conversely, strong interferences from $^{48}Ca^+$, $(^{35}Cl^{14}N)^+$, $(^{24}Mg^{35}Cl)^+$, $(^{40}Ca^{16}OH)^+$, $(^{44}Ca^{16}O)^+$, $(^{23}Na_2{}^{16}O)^+$, $(^{23}Na^{40}Ar)^+$, and $(^{32}S^{16}O_2H)^+$ are evident in the flow-injection results. A comparison of the percent recoveries in the spiked seawater sample by the two methods is shown in Table X. Again, recoveries for the preconcentration technique are superior to those for flow-injection direct nebulization, even though the former technique only used internal standardization for lead, while the latter required the use of internal standardization for every analyte. The poor, and sometimes even negative (i.e., spiked samples yielding lower signal than unspiked samples), recoveries obtained with the flow-injection experiment are due to drift in the ICP-MS sensitivity caused by the exposure to the high dissolved solids matrix.

Wastewater Recoveries. A major drawback to preconcentration methodologies is the low recoveries obtained in the presence of certain organic chelators. In natural waters and wastewaters, colloids often sequester analyte and must be destroyed by appropriate treatment prior to preconcentration (*18*). Table XI presents the percent recoveries for both the raw and the microwave-digested wastewater samples. It can be seen that, especially in the case of the primary effluent, titanium, copper, cadmium, and lead show poor recoveries in the raw material. The simple microwave digestion procedure,

however, is sufficient to liberate the bound metals and restore full recoveries.

Current Work. Currently, the on-line procedure described in this report is being investigated for very low concentration determinations. This work involves approaches for minimizing both molecular and analyte contributions to the blanks. An interface for automated analysis by preconcentration is also being developed. Unfortunately, the current status of ICP-MS software makes complete automation of preconcentration techniques problematic. Not only is satisfactory support for transient signals lacking but so is the hardware and software, which would make interfacing a less daunting task. Several approaches to this aspect of the problem are being investigated.

LITERATURE CITED

(1) Henshaw, J. M.; Heithmar, E. M.; Hinners, T. A. *Anal. Chem.* **1989**, *61*, 335-342.
(2) McLaren, J. W.; Beauchemin, D.; Berman, S. S. *Anal. Chem.* **1987**, *59*, 610-613.
(3) Lyon, T. D. B.; Fell, G. S.; Hutton, R. C.; Eaton, A. N. *J. Anal. At. Spectrom.* **1988**, *3*, 265-271.
(4) Beauchemin, D.; McLaren, J. W.; Berman, S. S. *Spectrochim. Acta, Part B* **1987**, *42B*, 467-490.
(5) Douglas, D. J.; Kerr, L. A. *J. Anal. At. Spectrom.* **1988**, *3*, 749-752.
(6) Hutton, R. C.; Eaton, A. N. *J. Anal. At. Spectrom.* **1988**, *3*, 547-550.
(7) Van Loon, J. C. *Selected Methods of Trace Metal Analysis*; Wiley-Interscience: New York, 1985; pp 104-106.
(8) Xiao-quan, S.; Tie, J.; Xie, G. *J. Anal. At. Spectrom.* **1988**, *3*, 259-263.
(9) Chung, Y. S.; Barnes, R. M. *J. Anal. At. Spectrom.* **1988**, *3*, 1079-1082.
(10) Brajter, K.; Dabek-Zlotorzynska, E. *Analyst* **1988**, *113*, 1571-1574.
(11) Olsen, S.; Pessenda, L. C. R.; Ruzicka, J.; Hansen, E. H. *Analyst* **1983**, *108*, 905-917.
(12) Hirata, S.; Yoshima, U.; Masahiko, I. *Anal. Chem.* **1986**, *58*, 2602-2606.
(13) Hirata, S.; Honda, K.; Kumamaru, T. *Anal. Chim. Acta* **1989**, *221*, 65-76.
(14) McLeod, C. W. *J. Anal. At. Spectrom.* **1987**, *2*, 549-552.
(15) Furuta, N.; Brushwyler, K. R.; Helftje, G. M. *Spectrochim. Acta, Part B* **1989**, *44B*, 349-358.
(16) Karakaya, A.; Taylor, A. *J. Anal. At. Spectrom.* **1989**, *4*, 261-263.
(17) Plantz, M. R.; Fritz, J. S.; Smith, F. G.; Houk, R. S. *Anal. Chem.* **1989**, *61*, 149-153.
(18) Kingston, H. M.; Barnes, I. L.; Brady, T. J.; Rains, T. C.; Champ, M. A. *Anal. Chem.* **1978**, *50*, 2064-2070.
(19) Greenberg, R. R.; Kingston, H. M. *Anal. Chem.* **1983**, *55*, 1160-1165.
(20) McLaren, J. W.; Mykytiuk, A. P.; Willie, S. N.; Berman, S. S. *Anal. Chem.* **1985**, *57*, 2907-2911.
(21) Beauchemin, D.; McLaren, J. W.; Mykytiuk, A. P.; Berman, S. S. *Anal. Chem.* **1987**, *59*, 778-783.
(22) Beauchemin, D.; Berman, S. S. *Anal. Chem.* **1989**, *61*, 1857-1862.
(23) Werefridus, W. V. B.; Overbosch, A. W.; Feenstra, G.; Maessen, F. J. M. J. *J. Anal. At. Spectrom.* **1988**, *3*, 249-257.
(24) Sirivaks, A.; Kingston, H. M.; Riviello, J. M. *Anal. Chem.*, in press.
(25) Method 6010. In *Test Methods for Evaluating Solid Waste*; SW-846; U.S. Environmental Protection Agency: Washington, DC, 1986.
(26) Beauchemin, D.; McLaren, J. W.; Berman, S. S. *Spectrochim. Acta* **1987**, *42B*, 467-490.

RECEIVED for review September 6, 1989. Accepted January 16, 1990. Although the research described in this article has been funded by the United States Environmental Protection Agency, it has not been subjected to Agency review and therefore does not necessarily reflect the views of the Agency. No official endorsement should be inferred. Mention of trade names or commercial products does not constitute endorsement or recommendation for use.

Automatic Phase Correction of Fourier Transform Nuclear Magnetic Resonance Spectroscopy Data and Estimation of Peak Area by Fitting to a Lorentzian Shape

F. Montigny, K. Elbayed, J. Brondeau, and D. Canet*

Laboratoire de Méthodologie RMN (U.A. CNRS 406-LESOC), Université de Nancy I, B.P. 239, 54506 Vandoeuvre lès Nancy Cedex, France

The proposed method for automatically phasing NMR spectra (zero-order and first-order corrections) involves two (possibly three) stages. The first stage deals with the relation between real and imaginary amplitudes of the peak maximum, whose location is deduced from the power spectrum. Because of digitization, it is generally necessary to refine the phase angle by making use of the data points above peak half-height in the magnitude spectrum (second stage). A further refinement (third stage) is carried out by an iterative fitting procedure applicable only to Lorentzian lines. This latter procedure, computationally very fast, allows as well a reliable estimation of peak areas, especially useful for the sequential listing of peak characteristics in multiline spectra.

INTRODUCTION

Phasing an NMR spectrum after Fourier transform of its free induction decay (denoted thereafter by fid) is still time-consuming and tedious with most existing software. This is generally accomplished by trial and error until the real part of the Fourier transformed spectrum (denoted thereafter by Re; Im for the imaginary part) appears globally as a pure absorption spectrum. The criterion to be met is left to the spectroscopist's appreciation or experience. Several methods have already been devised in order to get free from this task by using (i) maximization or minimization of peak areas (*1-4*) or (ii) the dispersion vs absorption representation (*5-8*) according to the DISPA technique introduced by Marshall and Roe (*9*). Generally, these procedures involve important computing time and/or complicated algorithms and do not seem to be so reliable, as claimed quite recently by Brown et al. (*10*) who proposed using as a criterion the flattest possible base line. Moreover, in most of these methods, use is made of *all* the data points pertaining to the lines which serve to calculate phase angles, with the drawback of introducing artifacts associated with points close to the base line; the latter may be of low significance because of noise and/or an ill-defined base line due for instance to the presence of broad components. We describe here an alternative procedure that is easy to implement and whose simplicity stems from a systematic use of the magnitude spectrum; this permits, inter alia, the selection of data points above half-height. An eventual re-

0003-2700/90/0362-0864$02.50/0

finement, performed by the resolution of nonlinear equations on the real and imaginary parts and based on the assumption of Lorentzian lines, adds little computing time since it operates at the ultimate stage of the phase correction process. An additional advantage of this latter algorithm lies in its ability to provide an reliable estimation of peak areas.

PHASE CORRECTIONS OF FT NMR SPECTRA

The amplitudes $A(x)$ and $D(x)$ of pure absorption and dispersion spectra are related to $\mathrm{Re}(x)$ and $\mathrm{Im}(x)$ by (*11*)

$$A(x) = \cos\phi\ \mathrm{Re}(x) + \sin\phi\ \mathrm{Im}(x) \quad (1a)$$

$$D(x) = \sin\phi\ \mathrm{Re}(x) - \cos\phi\ \mathrm{Im}(x) \quad (1b)$$

These equations apply to a single peak; x is equal to $\nu - \nu_0$, where ν_0 is the resonance frequency and ν the frequency of the considered data point in the digitized spectrum. The phase angle ϕ is of course specific of the relevant peak since most spectra involve a phase correction linearly dependent on the frequency (we shall disregard here corrections of higher order (*3*)). For this reason, two lines of frequency ν_1 and ν_2 have to be selected; they yield two phase angles ϕ_1 and ϕ_2, from which it is possible to derive the two global phase corrections (applicable to the whole spectrum), denoted by $\phi^{(0)}$ for zero order and $\phi^{(1)}$ for first order and such that the phase correction to be applied to a signal at frequency ν has the form $\phi = \phi^{(0)} - [(\nu - \nu_{max})/2\nu_{max}]\phi^{(1)}$

$$\phi^{(0)} = [\phi_1(\nu_2 - \nu_{max}) - \phi_2(\nu_1 - \nu_{max})]/(\nu_2 - \nu_1) \quad (2a)$$

$$\phi^{(1)} = 2\nu_{max}(\phi_1 - \phi_2)/(\nu_2 - \nu_1) \quad (2b)$$

where ν_{max} is the Nyquist frequency. These formulas are valid in the case of Fourier transform of a complex fid; with a real fid, $2\nu_{max}$ has to be replaced by ν_{max}. Within the software possessing the automatic phase correction to be described below, the user positions the cursor at two different locations in the initial (noncorrected) spectrum where two visible peaks are as isolated and as far away as possible. The exact location of the cursor does not matter since the maximum of the two relevant peaks will be looked for in the magnitude spectrum. However, the user is asked for the sign of each of these two peaks in the forthcoming absorption spectrum. This feature has been purposely implemented to treat spectra involving both positive and negative lines (edited spectra, antiphase multiplets, signals with negative or positive NOE ...). Once these decisions have been made, and having at hand eqs 2, it is clear that it only remains to determine the angle ϕ of eqs 1.

THE AUTOMATIC PHASING PROCESS

First Stage (Peak Maximum). Let us suppose, as a first approximation, that the maximum of the relevant peak in the magnitude spectrum corresponds exactly to the resonance frequency, i.e. $x = 0$. Of course, this is almost never true because of the interpolations resulting from data digitization (*12*, *13*) or because of possible overlap with neighboring peaks (*14*). (Zero-filling would not cure these problems (*15*).) This is the reason why this first stage cannot generally yield an accurate phase correction but is able to provide a starting basis for further refinements. In practice, the magnitude (or rather the power) spectrum will be calculated locally in the vicinity of the cursor position and its maximum determined in the following way: (i) starting from the cursor position, determine in which direction the spectrum amplitude increases and (ii) keep moving in that direction until the spectrum amplitude decreases by an amount greater than a quantity reflecting the mean noise. This quantity is estimated by computing the average, over the whole spectrum, of the difference in amplitude of two consecutive data points. Let us recall that *the magnitude spectrum, defined as* $[(\mathrm{Re})^2 + (\mathrm{Im})^2]^{1/2} = [A^2 + D^2]^{1/2}$, *is independent of the phase angle* (the power spectrum is just the square of the magnitude spectrum and requires less computing time). From eq 1b $D(0) = 0$, and the first estimate ϕ_0 of the phase angle is given by

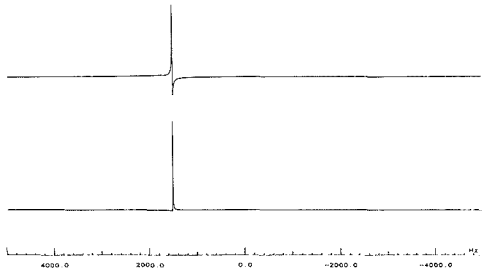

Figure 1. (Top) Dephased synthetic spectrum (10000 Hz for 2048 points). (Bottom) After phase correction performed with stages 1 and 2 of the proposed procedure.

$$\phi_0 = \tan^{-1}[\mathrm{Im}(0)/\mathrm{Re}(0)] + \{\pi\} \quad (3)$$

If we assume, as this is usually the case, that the function $\tan^{-1}$ *returns an angle whose value lies in the range* $[-\pi/2, \pi/2]$, there remains an ambiguity of an angle π (represented by the braces of eq 3) which can be resolved by noticing that from eq 1a

$$\cos\phi = \mathrm{Re}(0)/A(0) \quad (4)$$

The sign of $\mathrm{Re}(0)$ is of course known whereas the sign of $A(0)$ has been chosen by the user (see above). This provides the sign of $\cos\phi$ and hence the situation for which an angle π has to be added to $\tan^{-1}[\mathrm{Im}(0)/\mathrm{Re}(0)]$

$$\text{if } \mathrm{Re}(0)/A(0) > 0 \text{ then } \phi_0 = \tan^{-1}[\mathrm{Im}(0)/\mathrm{Re}(0)] \quad (3a)$$

$$\text{if } \mathrm{Re}(0)/A(0) < 0 \text{ then } \phi_0 = \tan^{-1}[\mathrm{Im}(0)/\mathrm{Re}(0)] + \pi \quad (3b)$$

Equations 3 would therefore permit solving the problem in a straightforward manner if the data point at exactly $x = 0$ was available. Because of digitization, this can occur only by chance and usually ϕ_0 must be refined as indicated in the next section.

Second Stage (Data Points above Half-Height). In order to compensate for the error of digitization affecting the data point corresponding to the maximum in the magnitude spectrum, further points around this maximum need obviously to be considered, since it can be hoped that effects of digitization error will tend to average out. For avoiding artifacts due to base-line distortion or to possible overlap with a neighboring peak, we have found it convenient to select those points whose *amplitudes in the magnitude spectrum are above half-height* (plus, for security reasons, one point on each side below this half-height). Furthermore, still with the objective to reduce the artifacts mentioned above, each of these points is *weighted by its amplitude* h_k *in the magnitude spectrum* so that an improved value of the phase angle ϕ is obtained by looking for a maximum (or a minimum if the peak is going to be negative) of the quantity $\sum_k h_k[\cos\phi\ (\mathrm{Re})_k + \sin\phi\ (\mathrm{Im})_k]$. This is accomplished in the following way: (i) starting from ϕ_0, determine the direction corresponding to the desired variation (maximum or minimum) and (ii) increment (or decrement) ϕ by step of 0.1° until the extremum is reached. The resulting phase correction may still be not correct as illustrated by the spectrum of Figure 1, which shows a synthetic spectrum purposely dephased and then subjected to the procedures just described (stages 1 and 2). This example clearly reveals the difficulties associated with digitization when

dealing with a limited number of data points. A further refinement is therefore necessary. Since at this point one is close to the exact solution, this enables the third stage to be executed rapidly and to simplify the relevant calculations thanks to the small value of the remaining phase correction.

Third Stage (Fit to a Lorentzian Shape). This will be applied to a spectrum phase-corrected according to stages 1 and 2 and needs a hypothesis concerning line shape. As a consequence, this approach is meaningful as long as a sufficient number of points surrounding the maximum is available. In practice, this step is skipped (with a message warning the user) if the magnitude spectrum possesses less than three points above half-height. This condition is dictated by the three unknowns to be determined below and outlines again the usefulness of the magnitude spectrum. We shall make in the following the hypothesis of *Lorentzian lines*. This implies also that the fid has been acquired in a time sufficiently long so as to avoid truncation and the subsequent deviation from a true Lorentzian line shape; however, in any event, a strong exponential multiplication can circumvent this problem and thus permit determination of the proper phase correction parameters which can then be applied to the spectrum obtained with the usual exponential multiplication. T_2 standing for the effective transverse relaxation time, and $\mathcal{A}$ for *the fid amplitude which is also the peak area*, the absorption and dispersion functions can be written as

$$A(x) = \mathcal{A}T_2/(1 + 4\pi^2T_2^2x^2) \quad (5a)$$

$$D(x) = -2\pi\mathcal{A}T_2^2x/(1 + 4\pi^2T_2^2x^2) \quad (5b)$$

and consequently

$$D(x) = -2\pi T_2xA(x) \quad (6)$$

From eqs 1, one obtains for ϕ (assuming, as this can be expected at this point, that $\sin\phi \approx \phi$ and $\cos\phi \approx 1$)

$$\phi = [\mathrm{Im}(x) - 2\pi T_2x\mathrm{Re}(x)]/[\mathrm{Re}(x) + 2\pi T_2x\mathrm{Im}(x)] \quad (7)$$

ϕ can therefore be derived from any data point at abscissa x provided that T_2 is known. At this stage, we must introduce explicitly a quantity associated with the third unknown ν_0 ($x = \nu - \nu_0$). The frequency interval between two consecutive data points is constant and given by $\Delta = 1/2\mathrm{Dw}$, where Dw is the sampling interval (dwell time). We shall assign the index k to data points on each side of the maximum of the magnitude spectrum so that $k = 0$ corresponds to this maximum, $k = 1$ to the first point on the right, $k = -1$ to the first point on the left, and so on. With this notation x_0 (which is substituted to the unknown ν_0) reflects the position of the maximum with respect to the resonance frequency whereas the abscissa pertaining to data point k can be expressed as

$$x_k = x_0 + k\Delta \quad (8)$$

For convenience, we shall also use the following notations:

$$X_k = X_0 + 2\pi T_2k\Delta \text{ and } X_0 = 2\pi T_2x_0 \quad (9)$$

This yields for eq 7

$$\phi = [(\mathrm{Im})_k - X_k\,(\mathrm{Re})_k]/[(\mathrm{Re})_k + X_k\,(\mathrm{Im})_k] \quad (10)$$

where the three unknowns ϕ, X_0, and T_2 (among which ϕ is really useful) require at least three data points. This is reminiscent of the method of Giancaspro and Comisarow (*16*) aimed at determining the exact resonance frequency from three data points; this method has been recently further discussed with regard to experimental conditions (*17*). In practice, all data points which are above half-height in the magnitude spectrum will be retained. Since eq 10 (for different subscripts k) is highly nonlinear with respect to these three unknowns, its resolution is better carried out iteratively. The following algorithm has been found efficient and reliable. Notice that the point at $k = 0$ is used for evaluating X_0, whereas the other data points serve for refining T_2.

Step 0: $\phi = 0$.

Step 1: Calculate X_k from $(\mathrm{Im})_k$ and $(\mathrm{Re})_k$ by means of eq 10 for all k available, at least for $k = 0$, $k = +1$, $k = -1$.

Step 2: For all $k \neq 0$, calculate T_2 by means of eq 9 and take its average: $\langle T_2 \rangle$.

Step 3: With the value of X_0 obtained in step 1, recalculate new $X_k (k \neq 0)$ by substituting $\langle T_2 \rangle$ to T_2 in (9). Reapply eq 10 to each "new" X_k for determining ϕ. Take the average value: $\langle \phi \rangle$.

Step 4: Set $\phi = \langle \phi \rangle$ and return to step 1 for iteration unless the whole set of unknowns (ϕ, T_2, X_0) has little changed with regard to the previous iteration. In that case, exit.

The efficiency of the third stage is demonstrated in Figure 2. The whole procedure (stages 1, 2, and 3) is illustrated by the experimental spectra of Figures 3 and 4. The former demonstrates the quality of the phase correction when a broad resonance entails an apparent distorted base line. The latter concerns a spectrum possessing a flat base line but exhibiting several resonances of very different line widths. The two narrowest lines have been selected for automatic phasing, which involves both zero- and first-order phase corrections; it can be seen that the algorithm has worked perfectly in spite of the partial overlap of one of the selected peaks with broader resonances. This example further stresses the interest of considering data points located around the resonance frequency. A final example is provided by Figure 5, which demonstrates the efficiency of the method in the case of a crowded spectrum involving a poor signal-to-noise ratio. It can be noticed that the last line at the right extremity of the spectrum remains slightly unphased. This may be unavoidable

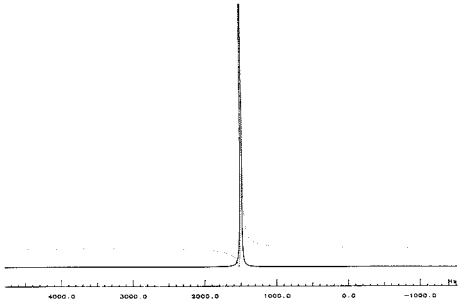

Figure 2. (Dotted trace) The spectrum of the bottom of Figure 1 with an 8-fold vertical expansion. (Full trace) With the same vertical expansion but phase corrected according to the third stage of the proposed procedure.

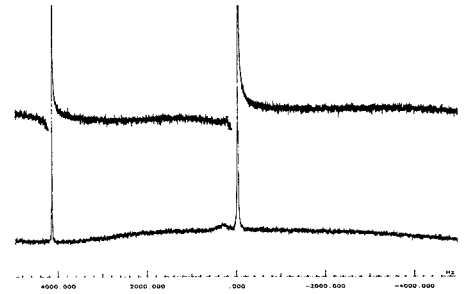

Figure 3. (Top) A raw experimental spectrum (51.86-MHz ^{27}Al spectrum, 10 000 Hz for 4096 points) exhibiting base-line distortions, outlined by a vertical expansion. (Bottom) The same spectrum phase corrected according to the whole procedure described in this paper.

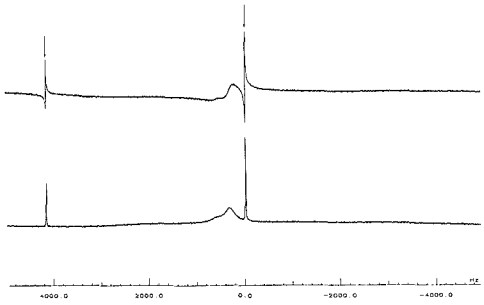

Figure 4. (Top) A raw experimental spectrum (51.86-MHz ^{27}Al spectrum, 10 000 Hz for 4096 points) comprising resonances of different line widths. (Bottom) The sampe spectrum phase corrected according to the whole procedure described in this paper. (Arrows indicate lines selected for calculating phase angles.)

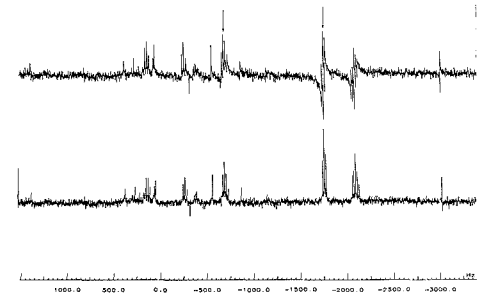

Figure 5. (Top) A raw experimental spectrum (200-MHz ^{13}C spectrum, 10 000 for 8192 points) including many lines with a modest signal-to-noise ratio. (Bottom) The same spectrum phase corrected according to the whole procedure described in this paper. (Arrows indicate lines selected for calculating phase angles.)

due to truncation of the time domain signal corresponding to that line (*18*).

CALCULATION OF PEAK AREAS

After the phase correction operations, the preceding algorith (stage 3) can be applied to any line in the spectrum. This yields a reliable estimate of both X_0 and T_2, which can in turn be inserted into eqs. 9 and 5a to derive, for each data point, an estimation of the peak area

$$\mathcal{A}_{(k)} = 2\pi A_k[1 + (X_0 + 2\pi T_2 k\Delta)^2]/2\pi T_2 \qquad (11)$$

The final value retained for the peak area is the average of the $\mathcal{A}_{(k)}$ for all available k. This method compares favorably well with direct numerical integration between two locations bracketing the peak of interest, provided that overlap with neighboring resonances is not too severe. Tests have been performed on synthetic spectra with possibly random noise added and the amplitude of the synthesized fid (equal to the peak area) was always retrieved within a few percent. Further tests applied on experimental spectra consist in calculating the ratio of the total area of all lines in a triplet to the total area of the corresponding quartet, the triplet and the quartet corresponding to an ethyl group (200 MHz proton spectrum). In one instance, where the signal-to-noise ratio was relatively low, we found 1.45 from the present algorithm vs 1.46 by direct numerical integration of each of the two patterns. For a higher signal-to-noise ratio, the relevant figures were respectively 1.49 vs 1.475. After application of a line broadening of 2 Hz (for a multiplet splitting of 7 Hz), in order to simulate overlap, this ratio was found to be in error by only 5%.

The present method is especially valuable in the context of the so-called peak list routines which usually look for peak positions and heights in a sequential fashion, thus preventing direct numerical integration since the limits of this integration have to be set for each peak. No such restriction exists with the present algorithm which has been implemented in our peak-printout software, yielding analytical information without the need of repetitive and tedious numerical integrations.

LITERATURE CITED

(1) Ernst, R. R. *J. Magn. Reson.* **1969**, *1*, 7–26.
(2) Siegel, M. M. *Anal. Chim. Acta* **1981**, *133*, 103.
(3) Daubenfeld, J.-M.; Boubel, J.-C.; Delpuech, J.-J. *J. Magn. Reson.* **1985**, *62*, 195–208.
(4) Cieslar, C.; Clore, G. M.; Gronenborn, A. M. *J. Magn. Reson.* **1988**, *79*, 154–157.
(5) Sotak, C. F.; Dumoulin, C. L.; Newsham, M. D. *J. Magn. Reson.* **1984**, *57*, 453–462.
(6) Herring, F. G.; Phillips, P. S. *J. Magn. Reson.* **1984**, *59*, 489–496.
(7) Craig, E. C.; Marshall, A. G. *J. Magn. Reson.* **1988**, *76*, 458–475.
(8) Wachter, E. A.; Diskey, G. Y.; Farrar, T. C. *J. Magn. Reson.* **1988**, *82*, 352–359.
(9) Marshall, A. G.; Roe, D. G. *Anal. Chem.* **1978**, *50*, 756–763.
(10) Brown, D. E.; Campbell, T. W.; Moore, R. N. *J. Magn. Reson.* **1989**, *85*, 15–23.
(11) For all general formulas concerning FT NMR signals, see for instance: Canet, D. *J. Chim. Phys.* **1988**, *85*, 657–668, and references therein.
(12) Chow, K. H.; Comisarow, M. B. *Comput Chem.* **1989**, *13*, 291–296.
(13) Keefe, C. D.; Comisarow, M. B. *Appl. Spectrosc.* **1989**, *43*, 605–607.
(14) Lee, J. P.; Comisarow, M. B. *J. Magn. Reson.* **1987**, *72*, 139–142.
(15) Comisarow, M. B.; Melka, J. D. *Anal. Chem.* **1979**, *51*, 2198–2203.
(16) Giancaspro, C.; Comisarow, B. *Appl. Spectrosc.* **1983**, *37*, 153–166.
(17) Verdun, F. R., Giancaspro, C.; Marshall, A. G. *Appl. Spectrosc.* **1988**, *42*, 715–721.
(18) Comisarow, M. B. *J. Magn. Reson.* **1984**, *58*, 209–218.

RECEIVED for review July 27, 1989. Accepted January 12, 1990.

Laser Desorption Electron Impact: Application to a Study of the Mechanism of Conjugation of Glutathione and Cyclophosphamide

Zhi-min Yuan, Catherine Fenselau,* D. M. Dulik, William Martin, W. Bart Emary, R. B. Brundrett, O. M. Colvin, and R. J. Cotter

Department of Chemistry and Biochemistry, University of Maryland Baltimore County, Baltimore, Maryland 21228, and Department of Pharmacology and Molecular Sciences, Johns Hopkins University, Baltimore, Maryland 21205

Toward the objective of producing ion radical species from involatile and thermally labile samples, we have combined laser desorption of neutral molecules with electron impact ionization on a time-of-flight mass analyzer with a delayed draw-out pulse. The analytical capabilities of this method are tested in the analysis of isotope labels in the involatile product in a mechanistic study of both the chemical and the enzyme catalyzed reactions of cyclophosphamide with glutathione.

INTRODUCTION

Isotope analysis and other applications of mass spectrometry require cleavage of carbon–carbon bonds within a molecule. Such bond scissions are prevalent in the ion radical species produced by electron impact ionization, as for example, cleavage of bonds α to a *heteroatom* and the *McLafferty rearrangement* (*1*). Ion radicals and their fragmentation pathways are not usually initiated by the newer *desorption* methods and have thus far been confined to samples sufficiently volatile for electron impact ionization. *Fast atom bombardment*, for example, produces even electron ions in most cases, which do not usually undergo homolytic or other carbon–carbon bond scission unimolecularly (*2*). Thus, we have combined laser desorption of neutral molecules with electron impact ionization (*3, 4*) as a means for producing ion radical species from involatile samples.

As part of continuing studies of the formation of glutathione conjugates as deactivated metabolites of anticancer alkylating mustards (*5*), we have designed an isotope labeling experiment to distinguish whether glutathione conjugation with cyclophosphamide takes place via *direct displacement* of chloride (reaction 1 in Figure 1), or by opening a cyclic *aziridinium* ion (reaction 2 in Figure 1). Direct halide displacement is the accepted mechanism for glutathione conjugation of halocarbons (*6*); however, kinetic (*7*) and isotope labeling evidence (*8*) indicate that many reactions of sulfur and nitrogen mustards take place subsequent to internal displacement and formation of the cyclic aziridinium intermediate.

As indicated in Figure 1, cyclophosphamide labeled with deuterium isotopes in the terminal methylene group of each mustard arm would bond with glutathione in the two reaction schemes to produce products in which the isotope labels have different positional distributions. The fragmentation pattern observed for the cyclophosphamide family in classical electron impact spectra (*9*) features bond scission between the two methylene groups in question (Figure 1) and would permit distinction of the patterns of labels in the two products (*8*). Nonselective opening of the aziridinium ring (path 2 in Figure 1) would be revealed by a 50:50 split in the peaks, i.e., m/z 213 and 215 for the ^{35}Cl species and 215 and 217 for the ^{37}Cl species. Glutathione conjugates are involatile and thermally labile, and they have not been successfully analyzed by electron impact, even derivatized. The monoglutathione conjugate derived from cyclophosphamide by both chemical and enzyme-catalyzed reactions, and reported here for the first time, was no exception, and this isotope labeling study was selected as an excellent candidate for the laser desorption electron impact method.

EXPERIMENTAL SECTION

Materials. Cyclophosphamide and 2′,2′,2″,2″-tetradeuterocyclophosphamide had been synthesized previously (*10*). Glutathione was purchased from Sigma Chemical Co. (St. Louis, MO). All other chemicals were reagent grade and used without further purification.

Conjugation Reactions. The chemical reaction was carried out by mixing cyclophosphamide (0.1 M) and glutathione (1.0 M) in aqueous solution adjusted to pH 10 with ammonium hydroxide, for 24 h at room temperature.

The conjugation reaction was also carried out under catalysis by immobilized rabbit liver microsomal glutathione *S*-transferases (*11*). The incubation mixture contained cyclophosphamide (1.0 mM), glutathione (5.0 mM), and 15 mL of microsomal protein immobilized to beaded Sepharose in phosphate buffer (0.1 M, pH 7.4). The total volume was 20 mL. This incubation was carried out for 24 h at 37 °C and terminated by addition of enough trifluoroacetic acid to bring the pH to 3.0. Conjugation was not observed at pH 7.4 in a control incubation run without immobilized protein.

The monoglutathione products from both the chemical and the enzymatic reactions were purified by high-pressure liquid chromatography on a Beckman/Altex (Fullerton, CA) liquid chromatograph using a RP-C18 Brownlee Labs (Santa Clara, CA) column (250 × 4.6 mm) and a gradient mobile phase (A, 0.1% trifluoroacetic acid (TFA); B, 60/40 acetonitrile–0.1% TFA, B from 10% to 30% in 25 min) at a flow rate of 2.0 mL/min. Ultraviolet detection was used at 215 nm. Molecular weights of the conjugates were obtained by fast atom bombardment mass spectrometry on a Kratos (Manchester, U.K.) MS-50 mass spectrometer operating at 3000 resolution.

Laser Desorption Electron Impact Mass Spectrometry. LDEI mass spectra were obtained on a modified CVC Products (Rochester, NY) Model 2000 time-of-flight mass spectrometer fitted with a Tachisto (Needham, MA) Model 215G pulsed carbon dioxide laser (*3*). The laser wavelength was 10.6 μm with a pulse width of 40 ns and energy of 100 mJ. This instrumental configuration has been described in detail (*12*) and has been used for the recording of ions produced directly by the laser (LD) as well as those produced by electron impact ionization of desorbed neutrals (*3*). In the LDEI method, desorption of neutral species was initiated with the *instantaneous power density* of the pulsed laser reduced below ca. 10^7 W/cm^2. When the laser power is reduced, few ions are evident unless the electron beam is turned on. Thus, after a 90-μs delay, each laser pulse was then followed by an 0.5 μs 30-eV electron beam pulse, a second delay of approximately 8 μs, and a *drawout* pulse. The second time delay provides *time lag focusing* (*13*) for optimizing the mass resolution. In this case, resolution was about 1/200. The drawout pulse extracts the ions from the ion source and initiates their acceleration into the 1-m drift region. The drawout pulse also provides the trigger pulse for a LeCroy (Spring Valley, NY) Model 3500SA

0003-2700/90/0362-0868$02.50/0

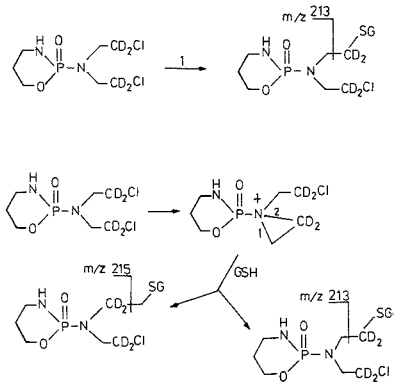

Figure 1. Alternative reactions for conjugation of glutathione (GSH) and 2′,2′,2″,2″-tetradeuterocyclophosphamide.

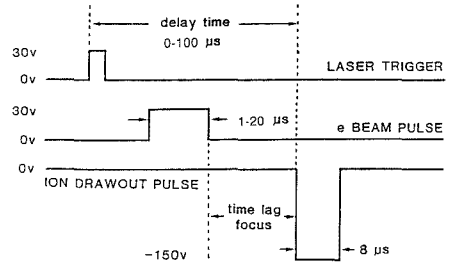

Figure 2. Timing sequence of the laser desorption electron ionization instrument used for this study.

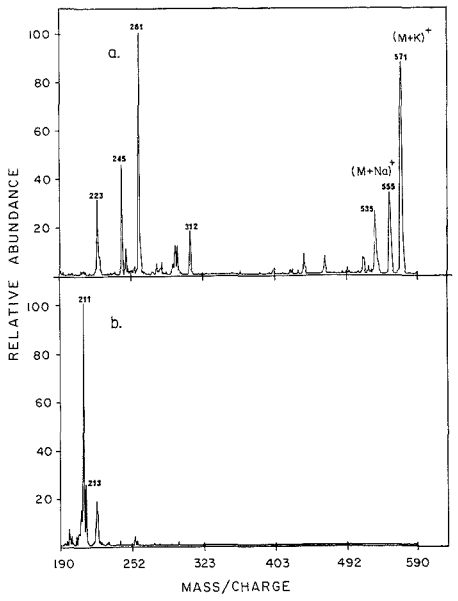

Figure 3. Laser desorption (a) and laser desorption electron impact (b) spectra of cyclophosphamide glutathione produced by chemical reaction.

transient recorder and signal averager, which records the mass spectrum from each laser pulse. Signal-averaged mass spectra

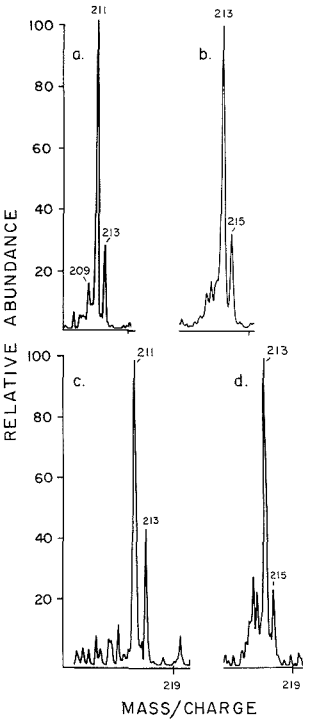

Figure 4. Partial laser desorption electron impact spectra of (a) chemically formed cyclophosphamide glutathione, (b) chemically formed 2′,2′,2″,2″-tetradeuterocyclophosphamide glutathione, (c) enzymatically formed cyclophosphamide glutathione, and (d) enzymatically formed 2′,2′,2″,2″-tetradeuterocyclophosphamide glutathione.

are obtained by repeating this cycle.

RESULTS AND DISCUSSION

A schematic representation of the timing sequence is shown in Figure 2. The time intervals between desorption and ionization and between ionization and drawout can be regarded as experimental variables (*4*), which in this case were adjusted to optimize the abundances and resolution (respectively) of the ions of interest.

The laser desorption (LD) mass spectrum of the cyclophosphamide glutathione conjugate is shown in Figure 3a. Consistent with previous studies using the CO_2 laser (*3*), molecular ions are formed as their sodium or potassium adducts (555 and 571 amu). Signals for the chloride isotopes in the heavier ions are not resolved in this spectrum, and the mass values indicated are average masses. Fragment ions are formed by the loss of HCl from molecular ion adducts, mass 535 for the kalinated species. The spectra of the tetradeutero analogues (not shown) indicate that ions of mass 312 are derived from kalinated glutathione, apparently by elimination of RSH, R being the cyclophosphamide moiety. The base peak at m/z 261 corresponds to a kalinated ion resulting from both of these processes and is shown in Chart I. This ion and its natriated and protonated analogues (245 and 223 amu) appear at mass values increased by four in the laser desorption spectrum of the tetradeuterated conjugate.

The electron impact spectrum (Figure 3b) of cyclophosphamide glutathione ablated by the laser beam has quite a different appearance. Potassium and sodium adduct ions are not observed. Consistent with previously published

Chart I. Laser Desorption Fragment Ions

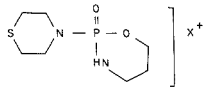

X	m/z
K	261
Na	245
H	223

electron impact spectra of cyclophosphamide (*9*), molecular ion radicals (masses 531 and 533) are also not detected in the laser desorption electron impact spectrum. Facile cleavage between the methylene groups in the mustard arm (Figure 1) leads to the base peak at m/z 211 and its ^{37}Cl satellite at 213, illustrated more clearly in Figure 4. Additional ions occur at masses 209, 222, and 223, which appear to be formed in part by pyrolytic processes, since their relative intensities vary from spectrum to spectrum.

The fragment ions of major interest in this study are those of mass 211 and 213 amu. In the LDEI spectra of the tetradeutero analogues formed either chemically or enzymatically (Figure 4b,d), this pair of peaks occurs at m/z 213 and 215, recorded with approximately the 3:1 intensity ratio characteristic of chlorine isotopes. The absence of signals at m/z 217 confirms the retention of only two deuterium labels in the ions. This in turn excludes the symmetrical aziridinium ion as a reaction intermediate in either the chemical reaction (pH 10) or the enzyme catalyzed reaction. The isotope distribution in both cases is consistent with conjugation by direct displacement of one chloride.

LITERATURE CITED

(1) McLafferty, F. W. *Interpretation of Mass Spectra*; University Science Books: Mill Valley, VA, 1980.
(2) Fenselau, C.; Cotter, R. J. *Chem. Rev.* **1987**, *87*, 501-512.
(3) VanBreeman, R. B.; Snow, M.; Cotter, R. J. *Int. J. Mass Spectrom. Ion Phys.* **1983**, *49*, 35-50.
(4) Fenselau, C.; Emary, W. B.; Cotter, R. J. *Org. Mass Spectrom.* **1989**, *24*, 694-698.
(5) Colvin, M.; Russo, J. E.; Hilton, J.; Dulik, D. M.; Fenselau, C. *Advances in Enzyme Regulation* **1988**, *27*, 211-221.
(6) Mannervik, B.; Danielson, U. H. *CRC, Crit. Rev. Biochem.* **1988**, *23*, 283-337.
(7) Peterson, L. A.; Harris, T. M.; Guengerich, F. P. *J. Am. Chem. Soc.* **1988**, *110*, 3284-3291.
(8) Colvin, M.; Brundrett, R. B.; Kan, M. N.; Jardine, I.; Fenselau, C. *Cancer Res.* **1978**, *36*, 1121-1126.
(9) Fenselau, C. In *Physical Methods in Modern Chemical Analysis*; Kuwana, T., Ed.; John Wiley and Son: New York, 1978, Vol. I, pp 123-125.
(10) Jardine, I.; Fenselau, C.; Appler, M.; Kan, M. N.; Brundrett, R. B.; Colvin, M. *Cancer Res.* **1978**, *38*, 408-415.
(11) Pallante, S.; Lisek, C. A.; Dulik, D. M.; Fenselau, C. *Drug Metab. Disp.* **1986**, *14*, 313-318.
(12) Olthoff, J. K.; Lys, I.; Demirev, P.; Cotter, R. J. *Anal. Instrum.* **1978**, *16*, 93-115.
(13) Wiley, W. C.; McLaren, I. H. *Rev. Sci. Instrum.* **1955**, *26*, 1150.

RECEIVED for review November 10, 1989. Accepted January 24, 1990. This research was supported by grants from the National Institutes of Health, GM 21248 (to C.F.) and CA 16783 (to O.M.C.), and from the National Science Foundation, BBS 85-15390 (to R.J.C.). This work was presented in part at the Thirty-Seventh Annual Conference on Mass Spectrometry and Allied Topics, Miami Beach, FL, 1989

Quantitative Static Secondary Ion Mass Spectrometry of Molecular Ions from 1-β-3,4-Dihydroxyphenylalanine (L-DOPA) and Indolic Derivatives

Michael B. Clark, Jr.,[1] and Joseph A. Gardella, Jr.*[,2]

Department of Chemistry and Surface Science Center, State University of New York at Buffalo, Buffalo, New York 14214

Traditionally, static secondary ion mass spectrometry (SIMS) is believed to yield qualitative information and very little quantitative information. A method to obtain quantitative molecular ion data from organic static SIMS analysis of L-DOPA and related compounds is presented. Linear calibration curves have been constructed by integrating the protonated molecular ion to silver ion peak area ratios over a known ion dosage and plotting versus the original sample concentration.

INTRODUCTION

Secondary ion mass spectrometry (SIMS) is a simple and very powerful surface analytical technique. Typically, a primary ion beam of 0.5-30 keV energy bombards a solid surface, and the sputtered secondary ions are mass analyzed (*1*). The interested reader is referred to ref 2 for an excellent description of the basic concepts and applications of the SIMS technique. As a surface analytical technique, SIMS has several advantages over ESCA (electron spectroscopy for chemical analysis) and Auger electron spectroscopy (*2*, *3*). These advantages include detection of all elements and their isotopic distributions, and a low detection limit, microgram per gram and nanogram per gram for elements and attomolar concentrations for molecular species (*2*). Unfortunately, SIMS suffers from so-called matrix effects, producing vastly different ion yields from different chemical structures and preparations.

The SIMS experiment can be performed with several different types of experimental conditions, divided loosely into "dynamic" or "static" modes. There are several review articles (*2-4*) comparing and contrasting these two modes of SIMS. High current densities, greater than 1 $\mu A/cm^2$, can be used to gain elemental information as a function of sputter depth into the bulk. In addition, elemental maps or imaging can be obtained by focusing the ion beam to small (1-3 μm) spot sizes ("ion microprobe") or by illuminating the sample with a large-diameter ion beam and using ion optics to preserve

* To whom correspondence should be addressed.
[1] Current address: Rohm and Haas Co., Norristown Rd., Spring House, PA 19477.
[2] Current address: Analytical and Surface Chemistry Program, Chemistry Divison, National Science Foundation, Washington, DC 20550.

0003-2700/90/0362-0870$02.50/0

the spatial distribution of secondary ions ("ion microscope"). Because of the high current densities used in dynamic SIMS, essentially all molecular information is lost. In the static or low damage mode, low current densities and ion dosages (less than 1 nA/cm^2 and 1×10^{13} ions/cm^2, respectively) yield a very small probability that a primary ion will strike the same molecule or surface region twice in a typical analysis time. Therefore, molecular information can be obtained by this technique because structure and bonding information are not damaged by the primary ion beam.

Static SIMS was first described in 1970 by Benninghoven (*5*). With current density lowered to less than 10 nA/cm^2 and defocused ion beams, molecular secondary ions were obtained for organic carboxylic acid compounds. In 1976–1977, static SIMS speectra of 15 amino acids (*6*, *7*), displaying parentlike molecular ions, were published, causing a renewed interest in the technique. From that time, static SIMS has been used to analyze a wide variety of synthetic polymers (*8–12*), biomolecules (*13*, *14*), and pharmaceuticals (*14*, *15*). The focus of a majority of these studies was to investigate secondary ion emission mechanisms and/or show the capability of static SIMS to provide a mass spectrum of a large, thermally labile organic compound. In the past few years, the application of static SIMS to characterize the changes in the molecular structure of the surface of plasma modified polymers has been investigated (*16*, *17*), to take advantage of the surface sensitivity of SIMS, which other desorption–ionization mass spectrometric methods do not have.

The major disadvantage of static SIMS is the difficulty in obtaining reproducible, accurate quantitative information. Quantitative information with a precision between a factor of 2 and 15% is considered obtainable from only the elemental ions produced in dynamic SIMS (*18*). Still, the ability to provide elemental quantitative information through secondary ion yields is complicated by the variation by 4 orders of magnitude across the periodic table. In addition, matrix effects, instrumental parameters, and ion collection efficiences influence secondary ion yields and must be considered when attempting to quantitate SIMS data (*18*). There are several quantitative methods or models in the literature (*18*, *19*). One approach is based on primary ion induced Saha-Eggert "thermal" desorption of elemental secondary ions (*18*). Local thermal equilibrium (LTE) (*20–22*) and collision cascade (*23–25*) models can be used to obtain "semi"quantitative (error factor $\approx$2) data. However, these are inadequate because they do not take into account matrix effects and exact instrumental parameters (i.e. mass-dependent transmission function) (*18*). The use of absolute or relative sensitivity factors derived from standard reference materials is an alternative method of obtaining elemental data from SIMS (*19*). Matrix effects can be overcome by using reference materials with compositions equivalent to the sample of interest. However, the availability of standard microscopically homogeneous calibration materials with representative matrices is very limited.

One technique to overcome these types of matrix effects was suggested by Morrison and co-workers. This technique involves implanting known concentrations of a reference material (e.g. an isotope of the element of interest) in the sample to be analyzed (*26*, *27*). The sample is then sputtered depth profiled and the reference material's signal is integrated over the sputter time. The integrated ion intensity of the reference material is directly related to its known concentration, and the relative concentrations of other elements can be calculated. This method of quantitation has been used to determine the amount of Al and Si impurities in steel and Te impurities in GaAs (*27*), dopant concentrations in $Al_xGa_{1-x}As$ matrices (*28*), and the calcium distribution in biological samples (*29*). In the present work, a modified version of this "standard addition" approach has been applied to static SIMS analysis of organic overlayers of L-DOPA and related indolic compounds and the results are presented.

Table I. Model Compounds Used in the SIMS Experiments

name	structure	mol wt, g/mol
L-DOPA	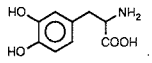	197
DHI	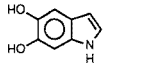	149
dopamine	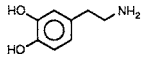	153

The possibility of obtaining quantitative molecular information directly from static SIMS would be a major advancement in the technique. To date, the literature contains only a few reported attempts to obtain quantitative information from static SIMS of organic compounds. One such study of quantitation by static SIMS related absolute molecular ion intensities to initial concentration of amino acids (*30*). This study reported a linear relationship between the secondary ion intensity and a surface concentration of 1×10^{13} to 5×10^{14} arginine molecules/cm^2. Below 1×10^{13} molecules/cm^2 instrumental noise limited the detection of the secondary ion and above 5×10^{14} molecules/cm^2 the intensity became relatively constant. The authors attributed these results to a complete monolayer of arginine being formed with 5×10^{14} molecules/cm^2 with multiple layers formed at higher concentration. Because the number of molecules that can be ionized due to direct interactions with the substrate is limited with increasing concentrations, the secondary ion intensity becomes constant. A second study reported taking peak intensity ratios of ions from fragmentation mechanisms unique to the soft and hard segments of polyurethanes (*31*). These ratios were found to correlate very well with quantitative ESCA and bulk analysis. Also recently, time of flight static SIMS results (in particular the intensity of H^+) were correlated to Fourier transform infrared (FTIR) and NMR results to determine the hydrogen content in a series of perfluorinated polyalkyl ethers (*32*). Although these latter two studies use the word "quantitative" the static SIMS data were correlated to results obtained from other bulk techniques and involve atomic ions or ions from fragmentation mechanisms.

In the present study, we show that the integration of total molecular ion signal, normalized to substrate ion yield, can be directly correlated to the amount of material on the surface of a simple system. Normalizing the molecular ion's peak area ratio to a substrate ion area eliminates the changes in the instrumental parameters.

EXPERIMENTAL SECTION

Sample Preparation. The compounds used in this study are listed in Table I. Details of the sample synthesis or source of purchase have been given previously (*33*). Stock solutions (1.0×10^{-4} M) of the model compounds were prepared by dissolving the compound in triply distilled (in quartz) water which was adjusted to a pH = 4.0 by addition of HCl. A modification of the sample preparation scheme developed by Benninghoven (*30*) was employed. Sample concentrations of 5.0×10^{13} to 5.0×10^{15} molecules/cm^2 were produced by pipetting 20 μL of the compound solution, diluted to the appropriate concentration, from a disposable micropipet onto an acid-etched sputter-cleaned silver coupon (Alfa Products, 99.999% purity) and allowing the solvent to slowly dry. The silver coupon was prepared by treatment with nitric acid (40% by volume) to clean and etch the silver coupon. The silver coupon was then Ar^+ ion sputtered at 200 nA/cm^2 for 20–30 min in the SIMS instrument to remove hydrocarbon contamination to below the detection limits of the instrument.

Table II. Masses and Relative[a] Intensities for the Secondary Molecular Ions of the Model Compounds Detected in SIMS

molecular ion	mass[b] (relative intensity) L-DOPA	DHI	dopamine
$(M + H)^+$	198 (0.094)	150 (0.280)	154 (0.734)
$(M - H)^-$	196	148	nd[c]
$(M + H - NH_3)^+$	181 (0.089)	nd	137 (1.975)
$(M + H - H_2O)^+$	nd	132 (0.183)	nd
$(M - 45)^+$	152 (0.344)	na[d]	na
$(M + Ag)^+$	304, 306 (0.027)	256, 258 (0.027)	nd
$(M + Ag - 45)^+$	259, 261 (0.014)	na	na

[a] Relative to the ^{107}Ag intensity. [b] Mass units are daltons. [c] nd, not detected. [d] na, not applicable to the compound.

Instrumentation. The SIMS data were collect with a Leybold-Heraeus LHS 10 SIMS100. This quadrupole-based instrument was modified for organic SIMS by incorporation of a special low kinetic ion energy pass filter into the optics. This instrument is turbomolecular pumped with a base pressure of 5×10^{-10} mbar. A Balzers quadrupole mass filter (3–1000 amu) modified with a Kramer off-axis multiplier was used for mass separation and detection. Samples were mounted on an isolated bias rod with a bias of ±13 V (in the positive/negative mode) to assist in the extraction of organic ions. A Leybold-Heraeus Model 12-38 differentially pumped ion gun (0.5–5 kV continuous) was used to ionize 99.9995% argon gas (Airco) accelerated to 4 kV as the primary ion beam. The ion beam produced was defocused and rastered over a 4 × 4 mm area resulting in an ion current density of less than 5 nA/cm², referenced to a Faraday cup. Total current measurements were taken for each sample with a Keithley Model 480 picoammeter and were found to be in good agreement with the Faraday cup measurements.

Data collection was accomplished with a custom interface system designed by Assmuth and Muelhoff, Inc. (Wilkensburg, PA). The interface uses a commercially available "Slicer" single board computer which communicates with an IBM PC. The interface is responsible for quadrupole control and data acquisition. With this system, signal averaging was made possible yielding organic SIMS spectra with improved signal-to-noise ratios. All data manipulations (peak areas and positions) were carried out with the SIMS software provided by Assmuth and Muelhoff, Inc.

The low-resolution survey scans (3–900 daltons) were collected with four data points per mass unit (i.e. resolution of 0.25 daltons) at a rate of 5 ms per mass unit. Typically, 5–10 scans were signal averaged per survey scan. The high-resolution spectra were collected at a resolution of 0.1 D at a rate of 10 ms per mass unit. In general, 10–50 high-resolution scans were signal averaged, depending on the level of the signal to noise.

RESULTS AND DISCUSSION

Positive static SIMS spectra of the model compounds can be found in Figure 1. The most important molecular ions are labeled and are simply related to protonation, silver ion cationization, and simple neutral molecule loss from these these ions. Detailed discussions of these spectra have been presented elsewhere (*34*). A summation of the static SIMS results obtained for the compounds used in these studies can be found in Table II. Initial experiments were carried out to investigate how the secondary molecular ion intensities varied with concentration in a manner similar to Benninghoven et al. (*30*). Specifically, the peak areas of the molecular secondary ions were monitored versus ion dosage, i.e. number of primary ions per sample (target) area. The total or final ion dosages presented in this section correspond to bombardment ("sputter") times of 45–60 min.

The results of various concentration studies of L-DOPA are plotted in Figure 2. The protonated molecular ion peak area was ratioed to the silver peak area in order to correct for any

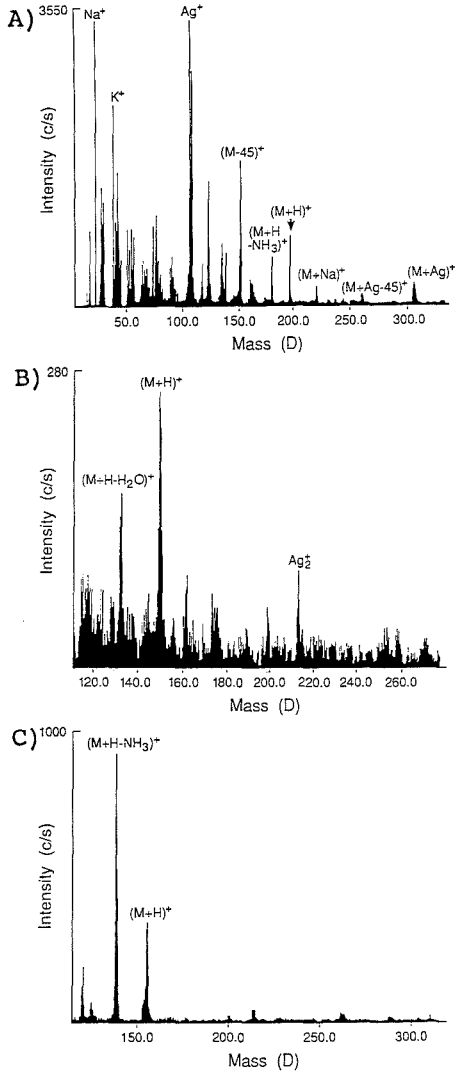

Figure 1. (A) Positive SIMS survey spectrum of L-DOPA on Ag (3–325 daltons, linear scale). (B) Positive SIMS survey spectrum of DHI on Ag (115–280 daltons, linear scale). (C) Positive SIMS survey spectrum of dopamine on Ag (115–315 daltons, linear scale).

variation in instrumental parameters and this ratio was monitored with ion dosage. Typically, the peak areas of the protonated molecular ion of L-DOPA and the silver ions were obtained by integrating between 196 and 200 daltons and 105 and 111 daltons, respectively. For five replicate analyses, the peak area ratios reported are reproducible within a relative standard deviation of ±15%. From Figure 2, it is obvious that there is a nonlinear increase in the $(M + H)^+/Ag^+$ ratio versus L-DOPA concentration taken initially or at any particular time. In addition, the $(M + H)^+/Ag^+$ peak area ratio varied with ion dosage. According to Benninghoven (*30*), concentrations of 5.0×10^{14} arginine molecules/cm² correspond to a mono-

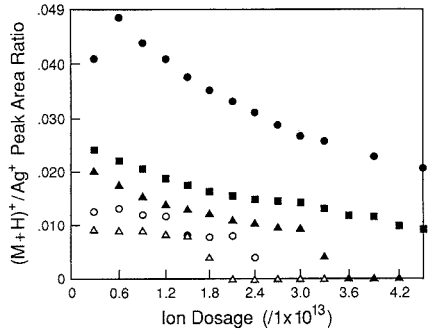

Figure 2. Plot of static SIMS $(M + H)^+/Ag^+$ peak area ratio versus ion dosages for several concentrations (molecules/cm^2) L-DOPA on Ag: (△) 1.0×10^{14}, (○) 2.5×10^{14}, (▲) 5.0×10^{14}, (■) 7.0×10^{14}, and (●) 1.0×10^{15} molecules of L-DOPA/cm^2 of Ag.

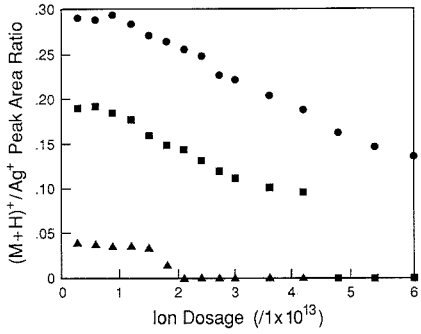

Figure 3. Plot of static SIMS $(M + H)^+/Ag^+$ peak area ratio versus ion dosage for several concentrations (molecules/cm^2) of DHI on Ag: (▲) 1.0×10^{14}, (■) 5.0×10^{14}, and (●) 1.0×10^{15} molecules of DHI/cm^2.

layer coverage. With this value as a general guideline for a "monolayer", for concentrations corresponding to greater than a monolayer (i.e. 7.0×10^{14} and 1.0×10^{15} L-DOPA molecules/cm^2), the protonated molecular ion was detected after ion dosages corresponding to 5×10^{13} ions/cm^2. For concentrations corresponding to that below monolayer coverages, the $(M + H)^+/Ag^+$ peak area ratios systematically fell to zero at smaller dosages (i.e. shorter irradiation times) because of the depletion or consumption of the protonated molecular ion.

The results of the analysis of various concentrations of 5,6-dihydroxyindole (DHI) are presented in Figure 3. The concentration/ion dose study results of DHI are very similar to those found for the L-DOPA study. A nonlinear increase in the $(M + H)^+/Ag^+$ peak area was found with an increase in DHI concentration. Because of the relatively constant $(M + H)^+/Ag^+$ peak area ratio at the concentration of 1.0×10^{14} DHI molecules/cm^2 of Ag, a monolayer coverage was assumed to occur between this concentration and 5.0×10^{14} molecules of DHI/cm^2 Ag. Combining the number of DHI molecules/monolayers with the geometric area of the silver coupon (1.5 cm^2), the area occupied per DHI molecule was approximately 40–100 Å^2, which agrees with published values (*35*, *36*). The $(M + H)^+/Ag^+$ peak area ratios of 1.0×10^{14} and 5.0×10^{14} molecules of DHI/cm^2 of Ag also went to zero as a function of ion dosage indicating the depletion or consumption of the protonated molecular ion. The $(M + H)^+/Ag^+$ peak area ratios of DHI were found to be greater than for L-DOPA, for the same concentration. This increase may be a function of the quadrupole's transmission function but a more likely explanation is the DHI molecular ion may be more stable than the L-DOPA molecular ion due to additional aromaticity present in the DHI structure.

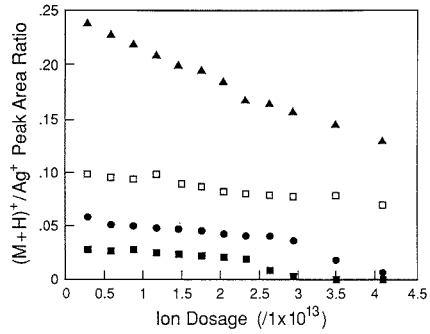

Figure 4. Plot of static SIMS $(M + H)^+/Ag^+$ peak area ratio versus ion dosage for several concentrations (molecules/cm^2) of dopamine on Ag: (■) 5.0×10^{13}, (●) 1.0×10^{14}, (□) 5.0×10^{14}, and (▲) 1.0×10^{15} molecules of dopamine/cm^2.

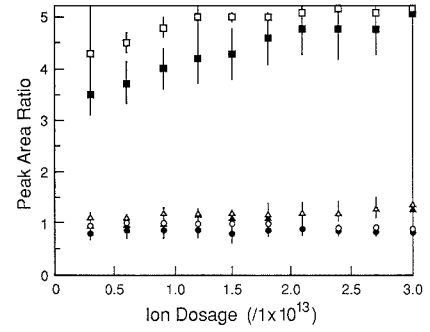

Figure 5. Relative $(M - 45)/(M + H)^+$, $(M + H - NH_3)^+/(M + H)^+$, and $(M + Ag)^+/(M + H)^+$ peak area ratios versus ion dosage for 1.0×10^{15} and 5.0×10^{14} molecules of L-DOPA/cm^2 Ag: (▲) $(M + H - NH_3)^+/(M + H)^+$, 1.0×10^{15}; (■) $(M - 45)/(M + H)^+$, 1.0×10^{15}; (●) $(M + Ag)/(M + H)^+$, 1.0×10^{15}; (▲) $(M + H - NH_3)^+/(M + H)^+$, 5.0×10^{14}.

The concentration/ion dose results for dopamine were slightly different than the results found for the L-DOPA and DHI studies. The results of the dopamine studies can be found in Figure 4. The most interesting result of the dopamine studies is the relatively constant $(M + H)^+/Ag^+$ peak area ratio versus ion dose for concentrations of 5.0×10^{13} to 5.0×10^{14} dopamine molecules/cm^2. Unlike the previous studies, the $(M + H)^+$ intensity of dopamine was detectable over the background, for all concentrations, up to an ion dose of 4.5×10^{13} ions/cm^2. Being able to detect the $(M + H)^+$ molecular ion of dopamine after these ion dosages may be the result of this ion being in a preexisting state and the protonated ion does not have to be formed during the SIMS process.

The question of ion beam effects or damage can be investigated by comparing the relative peak area of the various molecular ions versus ion dose. A comparison of the relative $(M + H - NH_3)^+/(M + H)^+$, $(M - 45)/(M + H)^+$, and $(M + Ag)^+/(M + H)^+$ peak area ratios for 5.0×10^{14} and 1.0×10^{15} L-DOPA molecules/cm^2 can be found in Figure 5. The peak area ratios for the two different concentrations were equivalent, within an combined relative standard deviation of ±15. These results would indicate no change in the rate of fragmentation occurred over the time of the SIMS experiment.

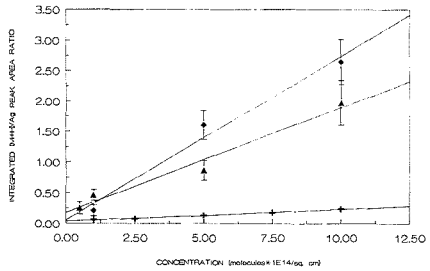

Figure 6. Plot of integrated $(M + H)^+/Ag^+$ peak area ratio versus initial concentration (molecules/cm^2 of Ag) of (+) L-DOPA (correlation coefficient, 0.9998), (◆) DHI (correlation coefficient, 0.9954), and (▲) dopamine (correlation coefficient, 0.9850).

The slight increase in the $(M - 45)^+/(M + H)^+$ peak area as a function of time is the result of a decrease in the absolute peak area of the protonated molecular ion of L-DOPA. Similar results were found for the $(M + H - H_2O)^+/(M + H)^+$ and $(M + Ag)^+/(M + H)^+$ peak area ratios of DHI and the $(M + H - NH_3)^+/(M + H)^+$ peak area ratio of dopamine.

The problems in obtaining quantitative information from static SIMS can easily be seen in Figures 2–4. The most problematic aspect of these figures is the variations in the peak area ratios with increased ion dose. The second problem illustrated in these figures is the nonlinearity of the peak area ratio as a function of concentration. The ability to obtain quantitative information from static SIMS by simply taking relative peak area ratios is very limited.

An alternative method of quantitation investigated in these studies is based on the dynamic SIMS model discussed in the Introduction. For these studies, the $(M + H)^+/Ag^+$ peak area ratio was integrated over a specific ion dosage and plotted as a function of the original concentration in molecules/cm^2. The $(M + H)^+/Ag^+$ peak area and not the absolute protonated molecular ion intensity was integrated in order to account for variations in the instrumental operating parameters. Because one does not obtain a sputter depth profile in static SIMS, as in dynamic SIMS, the peak area ratios were integrated over a known ion dosage rather than a known depth. The calibration curves obtained by using this method for L-DOPA, DHI, and dopamine can be seen in Figure 6. From these calibration curves, this method of quantitation yielded a linear relationship, within error limits, with a good correlation coefficient.

Unlike Benninghoven's study (*30*) this method of quantitation is not limited to submonolayer to monolayer coverages. In the previous study, linearity of the absolute secondary ion intensity was limited up to a complete monolayer coverage. Two reasons why the integrated method of quantitation gives linear results for multilayer coverages (i.e. up to 10 layers) involve surface roughness and surface area/molecule. Although equivalent sample preparations were used in Benninghoven's (*30*) and the present studies, the surface roughness of the silver substrates may be different. The surface prepared for this study may be rougher and, as a consequence, have a larger "true" surface area resulting in more material needed for a complete monolayer. Secondly, the surface area/molecule of the materials used in Benninghoven's and the present studies may be different, resulting in different concentrations needed to achieve monolayer coverages. In spite of these two possibilities, it appears the integrated method of quantitation overcome monolayer effects which limit the use of absolute secondary ion intensities, because of the large concentration range investigated. In particular, using the same criterion to define "monolayer" coverage as Benninghoven, i.e. saturation of the increase in absolute signal, we studied concentrations that were a factor of 10 greater. The integration technique appears to be successful.

The quantitative studies presented here were only preliminary results; however, they suggest quantitative information may be obtainable with static SIMS. A number of factors that may influence the secondary ion emission will have to be investigated to determine if this method of quantitation is feasible for a wide variety of compounds. Matrix effects (*37–39*), including composition, chemical state, and crystallographic orientation of the sample (*2*) affect ion yields. This system under a study provides a simple "ideal" substrate for production of molecular ions. The production of molecular ions is substrate dependent, and clearly, insulating nonchemically active substrates, which do not yield such ions, will still present the major difficulty to limit any quantification approach. Following this approach, which may be considered an application of an "external standard", we are investigating the use of internal standard methods via Langmuir–Blodgett films (*40*). Finally, the possibility of quantification may motivate chemical treatments to overcome matrix effects which drastically limit production of molecular ions.

CONCLUSIONS

The interest in obtaining quantitative information from static SIMS leads to a series of investigations to develop a possible method of achieving this information. The simple method of taking a molecular ion/substrate ion peak area ratio did not give this information. This method suffered from a nonlinear increase of the peak area ratio as a function of concentration and the peak area ratio varied with analysis time or ion dosage. A new method of obtaining quantitative information from static SIMs was also investigated in these studies. This method of quantitation involved integrating the total peak area ratio over a known ion dosage. By use of this method, linear calibration curves were constructed for L-DOPA, DHI, and dopamine.

LITERATURE CITED

(1) Pachuta, S. J.; Cooks, R. G. *Chem. Rev.* **19878** *87*, 647.
(2) Benninghoven, A.; Rudenauer, F. G.; Werner, H. W. In *Secondary Ion Mass Spectrometry: Basic Concepts, Instrumental Aspects, Applications and Trends*; Elving, P. J., Wineforder, J D., Kolthoff, I. M., Eds.; John Wiley & Sons: New York, 1987.
(3) Turner, N. H.; Colton, R. J. *Anal. Chem.* **1982**, *54*, 293R.
(4) Vickerman, J. C. *Chem. Br.* **1987**, October, 969.
(5) Benninghoven, A. *Z. Phys.* **1970**, *230*, 403.
(6) Benninghoven, A.; Jaspers, D.; Sichtermann, W. *Appl. Phys.* **1976**, *11*, 35.
(7) Benninghoven, A.; Sichtermann, W. K. *Org. Mass Spectrom.* **1977**, *12*, 595.
(8) Bletsos, I. V.; Hercules, D. M.; Magill, J. H.; vanLeyen, D.; Niehuis, E.; Benninghoven, A. *Anal. Chem.* **1988**, *60*, 938.
(9) Bletos, I. V.; Hercules, D. M.; vanLeyen, D.; Benninghoven, A. *Macromolecules* **1987**, *20*, 407.
(10) Briggs, D. *SIA, Surf. Interface Anal.* **1986**, *9*, 391.
(11) Briggs, D. *Org. Mass* spectrom. **1987**, *22*, 91.
(12) Brown, A.; Vickerman, J. C. *SIA, Surf. Interface Anal.* **1986**, *8*, 75.
(13) Eicke, A.; Anders, V.; Junack, M.; Sichtermann, W.; Benninghoven, A. *Anal. Chem.* **1983**, *55*, 178.
(14) Benninghoven, A.; Sichtermann, W. M. *Anal. Chem.* **1978**, *50*, 1180.
(15) Benninghoven, A.; Sichtermann, W. *Int. J. Mass Spectrom. Ion Phys.* **1981**, *38*, 351.
(16) Fakes, D. W.; Davis, M. C.; Brown, A.; Newton, J. M. *SIA, Surf. Interface Anal.* **1988**, *13*, 233.
(17) Lub, J.; Van Vroonhoven, F. C. B. M.; Brunix, E.; Benninghoven, A. *Polymer* **1989**, *30*, 40.
(18) Werner, H. M. *SIA, Surf. Interface Anal.* **1980**, *2*, 56.
(19) Rudat, M. A.; Morrison, G. H. *Anal. Chem.* **1979**, *51*, 1179.
(20) Andersen, C. A.; Hinthorne, J. R. *Anal. Chem.* **1973**, *45*, 1421.
(21) Simons, D. S.; Baker, J. E.; Evans, C. A., Jr. *Anal. Chem.* **1976**, *48*, 1341.
(22) Rudenauer, F. G.; Steiger, W. *Vacuum* **1976**, *26*, 537.
(23) Rudenauer, F. G.; Steiger, W.; Werner, H. M. *Surf. Sci.* **1976**, *54*, 533.
(24) Morgan, A. E.; Werner, H. M. *J. Chem. Phys.* **1978**, *68*, 3900.
(25) Pivin, J. C.; Roques-Carmes, C. *Int. J. Mass Spectrom. Ion. Phys.* **1978**, *26*, 219.
(26) Chu, P. K.; Morrison, G. H. *Anal. Chem.* **1982**, *54*, 2111.
(27) Leta, D. P.; Morrison, G. H. *Anal. Chem.* **1980**, *52*, 277.
(28) Galuska, A. A.; Morrison, G. H. *Anal. Chem.* **1983**, *55*, 2051.

(29) Harris, Jr., W. C.; Chandra, S.; Morrison, G. H. *Anal. Chem.* **1983**, *55*, 1959.
(30) Tamaki, S.; Sichtermann, W. K.; Benninghoven; A.; *Jpn. J. Appl. Phys.* **1984**, *2*, 544.
(31) Hearn, M. J.; Briggs, D.; Yoon, S. C.; Ratner; B. D. *SIA, Surf. Interface Anal.* **1987**, *10*, 524.
(32) Hues, S. M.; Colton, R. J.; Mowery, R. L.; McGrath, K. J.; Wyatt, J. R. *Appl. Surf. Sci.* **1989**, *35*, 507.
(33) Clark, M. B., Jr.; Gardella, J. A., Jr.; Schultz, T. M.; Salvati, L., Jr.; Patil, D. G. *Anal. Chem.*, in press.
(34) Clark, M. B., Jr. Ph.D. Thesis, State University of New York at Buffalo, 1989.
(35) Kurtz, S. K.; Schultz, T. M.; Wolfram, L. J. *Crystal Structure of Melanin Precursors*. Presented at the First Pan American Society for Pigment Cell Research Meeting; University of Minneapolis Medical School; Minneapolis, MN, June 1988.
(36) Roychowdhury, P.; Black, B. S. *Acta Crystallogr.* **1975**, *B31*, 1559.
(37) Busch, K. L.; Bih, H. H.; Ya-Xiang, X.; Cooks, R. G. *Anal. Chem.* **1983**, *55*, 1157.
(38) Lui, L. K.; Busch, K. L.; Cooks, R. G. *Anal. Chem.* **1981**, *53*, 109.
(39) Cooks, R. G.; Busch, K. L. *Int. J. Mass Spectrom. Ion. Phys.* **1983**, *53*, 111.
(40) Cornelio, P. A.; Clark, M. B., Jr.; Gardella, J. A., Jr. In *Secondary Ion Mass Spectrometry (SIMS) VII*, Benninghoven, A., Ed.; Springer Verlag, in press.

RECEIVED for review August 7, 1989. Accepted January 16, 1990. The authors thank the Lawrence M. Gelb Research Foundation and the National Science Foundation, Division of Materials Research (Polymer Program) Grant Number 8720650 for the financial support of this study.

CORRESPONDENCE

Reversible, Linear-Sweep Voltammetry of a Soluble Redox Couple: Effect of Initial Concentrations

Sir: Classical theoretical formulas are available to predict the peak current and potential at a planar electrode during linear-sweep voltammetry (LSV) for the reversible (Nernstian) reaction

$$O + ne^- \rightleftharpoons R \quad (1)$$

where O and R are soluble oxidized and reduced species, respectively, and n is the number of electrons transferred (*1*, *2*). Matsuda and Ayabe (*1*) and Nicholson and Shain (*2*) showed that if the reduced species is present initially in negligible amounts and the voltage is swept in the negative direction, the cathodic peak current is proportional to the absolute value of the sweep rate to the one-half power and the corresponding peak potential is sweep-rate independent. Matsuda and Ayabe (*1*) also demonstrated that if the sweep begins at the equilibrium potential, E_{eq}, the dimensionless peak current and potential depend only upon the product of two dimensionless ratios, $\gamma\theta^*$: the ratio of the square root of the diffusion coefficients of O and R, $\gamma \equiv (D_O/D_R)^{1/2}$, and the initial concentration ratio of O and R in the bulk electrolyte, $\theta^* \equiv (C_O^*/C_R^*)$. Matsuda and Ayabe (*1*) presented calculations for the case where $\gamma\theta^* \rightarrow \infty$. Left numerically unexamined was the influence of R when its concentration is not negligibly small. Farsang et al. (*3*), using the same formula as derived by Matsuda and Ayabe (*1*), examined the influence of $\gamma\theta^*$ on the peak values over the narrow range of $0.22 \leq \gamma\theta^* \leq 5.5$ and found a shift in the potential to more negative values and an increase in the dimensionless peak current as $\gamma\theta^*$ decreased.

Nicholson and Shain (*2*) considered the case of starting the sweep at a nonequilibrium potential, E_i, in the limit of the reduced species concentration equal to zero ($\theta^* = \infty$). They obtained a current–potential relationship which is a function of an analogous dimensionless grouping, $\gamma\theta$, where γ is the same as defined above, and θ is the concentration ratio at the *electrode surface* given by the Nernst equation immediately *after* E_i is applied. This nonequilibrium initial condition gives rise to a Cottrell current in the early portion of the sweep, which they showed does not significantly affect the peak current or potential as long as $\gamma\theta > 650$. This corresponds to starting the sweep at a potential that is at least $200/n$ mV ($T = 25$ °C) positive of the peak potential.

In what follows, the Matsuda and Ayabe (*1*) equation is applied to calculate the peak potential and current over the range of $\gamma\theta^*$ from zero to infinity. Also presented is an explicit heretofore unrecognized formula for the peak values in the limit of $\gamma\theta^* \rightarrow 0$. The peak values at the two limiting behaviors are used to deduce and develop an easy-to-apply empirical relationship which correlates the results as a function of $\gamma\theta^*$ over the entire range. The calculations are confirmed by experimental measurements. The effect of mistakingly applying the Nicholson and Shain (*2*) formula for regions of $\gamma\theta^*$ below its range of validity is also quantified.

PEAK CURRENT AND POTENTIAL CALCULATIONS

Matsuda and Ayabe (*1*) solved the one-dimensional transient diffusion equation for both soluble redox species and obtained the time-dependent surface concentrations for O and R in terms of the reaction current. Starting the sweep at the equilibrium potential, θ^* is related to E_{eq} by

$$\theta^* = \exp\left[\left(\frac{nF}{RT}\right)(E_{eq} - E^{\circ\prime})\right] \quad (2)$$

where $E^{\circ\prime}$ is the formal potential. For the case of reversible kinetics, substituting eq 2, the surface concentrations and the sweep rate, v, into the Nernst equation results in the integral equation for the current

$$\int_0^{at} \frac{\chi(z)\, dz}{(at - z)^{1/2}} = \frac{1 - \exp(-at)}{1 + \gamma\theta^* \exp(-at)} \equiv L(at) \quad (3)$$

where t is time, $a \equiv (nF/RT)v$ which is positive for a cathodic sweep, and $\chi(at)$ is the dimensionless current defined as

$$\pi^{1/2}\chi(at) \equiv \frac{i(at)}{nFAC_O^*(D_O a)^{1/2}} \quad (4)$$

where F is Faraday's constant, A is the electrode area, and $i(at)$ is the time-dependent reaction current that is positive for a cathodic reaction. The product (at) is the displacement of the dimensionless potential from the starting potential.

Equation 3 differs from the analogous formula given by Nicholson and Shain (eq 22 of ref 2) in that by their as-

0003-2700/90/0362-0875$02.50/0

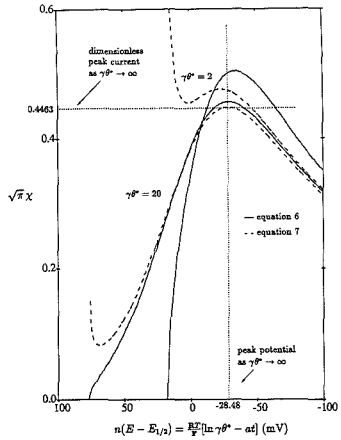

Figure 1. Predicted linear-sweep voltammograms from a planar electrode. The solid lines are the voltammograms generated from eq 6. The dashed lines are voltammograms generated from eq 7 with θ replaced by θ^*. The potentials, in mV, are for T = 298 K.

sumption of C_R^* is equal to zero, the numerator of $L(at)$ is equal to one, and θ^* is replaced by θ where θ is given by

$$\theta = \exp\left[\left(\frac{nF}{RT}\right)(E_i - E^{\circ\prime})\right] \tag{5}$$

Equation 3 is an Abel integral equation (5) for $\chi(at)$ with the solution

$$\pi^{1/2}\chi(at) = \frac{(1 + 1/\gamma\theta^*)}{4\pi^{1/2}} \int_0^{at} \frac{dz}{(at - z)^{1/2} \cosh^2 [(\ln \gamma\theta^* - z)/2]} \tag{6}$$

The analogous current–potential relationship derived by Nicholson and Shain (eq 33 of ref 2) from the solution of eq 3 with a unity numerator for $L(at)$ and θ replaced by θ^* is

$$\pi^{1/2}\chi(at) = \frac{1}{[\pi(at)]^{1/2}(1 + \gamma\theta)} + \frac{1}{4\pi^{1/2}} \int_0^{at} \frac{dz}{(at - z)^{1/2} \cosh^2 [(\ln \gamma\theta - z)/2]} \tag{7}$$

(For the calculations presented here, the integrals in eq 6 and 7 were numerically evaluated by using the IMSL (6) quadrature subroutine DQDAGS which accommodates integrands having end-point singularities.)

Although eq 6 as $\gamma\theta^* \to \infty$ is identical with the $\gamma\theta \to \infty$ limit of eq 7, θ^* and θ are not interchangeable. The leading term in eq 7 is a result of assuming the initial concentration of the reduced species is zero and predicts a Cottrell current upon application of E_i at the start of the sweep. This term can be significant when $\gamma\theta$ is not large. To illustrate this point, the effect on the voltammogram of erroneously replacing θ with θ^* in eq 7 is shown in Figure 1 with the potentials plotted relative to the half-wave potential, $E_{1/2} \equiv E^{\circ\prime} + (RT/nF) \ln \gamma$ (2). At $\gamma\theta^* = 20$, the dimensionless peak current and potential predicted from eq 6 both differ from those found by using eq 7 (with θ set equal to θ^*) by 2%, and at $\gamma\theta^* = 2$, the percentage difference is 6% and 33%, respectively.

The dimensionless peak current and potential may be determined as a function of $\gamma\theta^*$ by calculating the voltammogram using eq 6 to locate graphically the peak position.

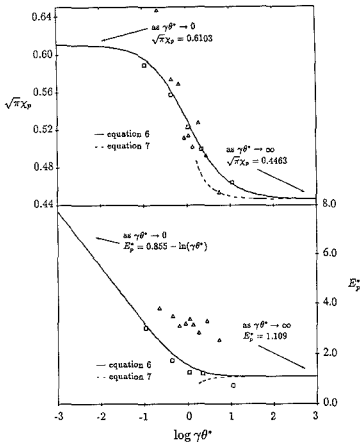

Figure 2. Dimensionless peak currents and potentials for linear-sweep voltammetry on a planar electrode as a function of $\gamma\theta^*$. The solid lines result from the use of eq 6, and the dashed lines result from the use of eq 7 with θ replaced by θ^*. For $\gamma\theta^* \leq 1.60$, eq 7 cannot predict peak values. The symbols are the peak values which were obtained experimentally using the $Fe(CN)_6^{4-}/Fe(CN)_6^{3-}$ redox couple. Key: □, present results; △, Tomcsanyi et al. (4) data.

However, a more convenient analytical procedure was derived by differentiating eq 6 with respect to (at) and setting the result equal to zero. The potential that satisfies the resulting expression is the peak potential which, when substituted into eq 6, specifies the peak current. Newton's method was used to solve the resulting nonlinear equation for the peak potential generated from this procedure. The same technique was applied to eq 7 (with θ replaced by θ^*) and the resulting dimensionless peak currents and potentials from the two predictions are compared in Figure 2 as a function of $\gamma\theta^*$. The dimensionless peak potential, E_p^*, is defined as

$$E_p^* \equiv [(at)_p - \ln \gamma\theta^*] \tag{8}$$

where $(at)_p$ is the dimensionless peak potential relative to the equilibrium potential.

Nicholson and Shain (2) report their results at $\gamma\theta$ = 650, and Matsuda and Ayabe report theirs at $\gamma\theta^*$ = 165 000, and from Figure 2 we see that θ and θ^* are interchangeable at these values; that is, no difference is found in the predicted peak values regardless whether eq 6 or 7 is used. Replacing θ^* with θ at smaller values of θ^*, however, will lead to differing results. Further, for values of $\gamma\theta^* \leq 1.60$, eq 7 does not predict a peak current because the Cottrell current dominates the transient response.

The dimensionless peak values ($\pi^{1/2}\chi_p$ = 0.4463 and E_p^* = 1.109) given by Matsuda and Ayabe (1) and Nicholson and Shain (2) are the limiting values as $\gamma\theta^* \to \infty$. Limiting values for the dimensionless peak current and potential can also be obtained for $\gamma\theta^* \to 0$ by taking the limit of eq 6 as $\gamma\theta^*$ approaches zero which, after some mathematical manipulation, results in

$$\pi^{1/2}\chi(at)|_{\gamma\theta^* \to 0} = \frac{1}{\pi^{1/2}} \int_0^{at} \frac{\exp(-z)}{(at - z)^{1/2}} dz \tag{9}$$

Following the analogous calculus procedure applied to eq 6 to calculate the peak potential, Newton's method was applied to determine numerically $(at)_p$ = 0.855 in the limit of $\gamma\theta^* \to 0$. The corresponding dimensionless peak current found from eq 9 is 0.6103.

EMPIRICAL CORRELATIONS

The following one parameter empirical relationship, motivated by the asymptotic trends seen in Figure 2, was fit to the theoretically predicted dimensionless peak currents from eq 6

$$\pi^{1/2}\chi_p(\gamma\theta^*) = \pi^{1/2}\chi_p(0) - [\pi^{1/2}\chi_p(0) - \pi^{1/2}\chi_p(\infty)]\left[\frac{\gamma\theta^*}{m + \gamma\theta^*}\right] \quad (10)$$

where $\pi^{1/2}\chi_p(0)$ and $\pi^{1/2}\chi_p(\infty)$ are the known dimensionless peak currents at the limits $\gamma\theta^* \to 0$ and $\gamma\theta^* \to \infty$, respectively, and m is an empirical parameter which was found by least-squares fit of eq 10 to the data in Figure 2. The resulting correlation is

$$\pi^{1/2}\chi_p(\gamma\theta^*) = 0.6103 - 0.164\left[\frac{\gamma\theta^*}{1.08 + \gamma\theta^*}\right] \quad (11)$$

The following one parameter empirical relationship, also motivated by the asymptotic trends seen in Figure 2, was fit to the theoretically predicted peak potentials from eq 6

$$E_p^*(\gamma\theta^*) = \ln \{[\exp E_p^*(0)]^m + [\exp E_p^*(\infty)]^m\}^{1/m} \quad (12)$$

where $E_p^*(0)$ and $E_p^*(\infty)$ are the known dimensionless peak potentials at the limits $\gamma\theta^* \to 0$ and $\gamma\theta^* \to \infty$, respectively. The parameter m was found by least-squares fit to the data in Figure 2. The resulting correlation is

$$E_p^*(\gamma\theta^*) = \ln\left[\left(\frac{2.35}{\gamma\theta^*}\right)^{1.19} + 3.74\right]^{0.84} \quad (13)$$

For $0 < \gamma\theta^* < \infty$, eqs 11 and 13 deviate from the exact values by at most 0.1% and 1%, respectively, differences which are visually indistinguishable in Figure 2. The maximum 1% error resulting from eq 13 (which occurs in the vicinity of $\gamma\theta^* = 3$) translates to less than a 0.5 mV ($n = 1$ and $T = 298$ K) error which is experimentally insignificant.

EXPERIMENTAL RESULTS

Linear-sweep voltammetry was conducted by using the ferro/ferricyanide redox couple in 1.0 M KCl at five different concentration ratios. The concentration of the ferricyanide was maintained at 0.010 M, and five different ferrocyanide concentrations were used: 0.0010 M, 0.0050 M, 0.010 M, 0.025 M, and 0.10 M. Cottrell experiments were run in order to determine γ by taking the ratio of the product of $(it^{1/2})$ for oxidation-to-reduction experiments, and $\gamma = 1.09$ was obtained which agrees within 1% of that calculated by using the diffusion coefficients for O and R given by Adams (7). Therefore, the $\gamma\theta^*$ values for the five concentrations ratios are 10.9, 2.18, 1.09, 0.436, and 0.109. All experiments were performed in a single-compartment cell at room temperature with a 1.6 mm diameter Pt disk as the working electrode which was not perfectly flush with the surface, and Ag/AgCl as the reference electrode. Voltammograms were generated at nine different sweep rates ranging from 4 to 150 mV/s and were run in duplicate. The *dimensionless* peak current, $\pi^{1/2}\chi_p$, was obtained by plotting the *dimensional* peak current, i_p, versus the absolute value of the sweep rate to the one-half power, $|v|^{1/2}$. The slope, $di_p/d|v|^{1/2}$, resulting from linear regression of these data was used to calculate $\pi^{1/2}\chi_p$ since from eq 4

$$\pi^{1/2}\chi_p(\gamma\theta^*) = \frac{(RT)^{1/2}}{(nF)^{3/2}C_O^* A D_O^{1/2}} \frac{di_p}{d|v|^{1/2}} \quad (14)$$

The unknown product $AD_O^{1/2}$ was determined by performing a series of linear sweeps at which only the oxidized species was present ($\gamma\theta^* = \infty$) and solving eq 14 for $AD_O^{1/2}$ using $\pi^{1/2}\chi_p = 0.4463$. The product $AD_O^{1/2}$ calculated in this manner was then used in eq 14 at the lower values of $\gamma\theta^*$ to obtain $\pi^{1/2}\chi_p(\gamma\theta^*)$. The peak potential, $(at)_p$, which is independent of the sweep rate, was read directly from the voltammogram for each value of $\gamma\theta^*$, and eq 8 was used to calculate E_p^*.

The experimental dimensionless peak currents and potentials (open squares) are compared to the theoretical values in Figure 2. The experimentally determined peak currents deviate from those theoretically predicted by at most 1%. The measured peak potentials also closely agree with those predicted, except for $\theta^* = 10$ at which a 10-mV deviation occurs. Also included in Figure 2 are the experimental data reported by Tomcsanyi et al. (4) (open triangles) from LSV run on a Pt electrode in 1.0 M KCl using the ferro/ferricyanide redox couple. The scatter is larger in these data, but the trend in $\pi^{1/2}\chi_p(\gamma\theta^*)$ is evident. The peak potentials obtained by Tomcsanyi et al. (4) were reported only to the nearest 10 mV and are 30–40 mV higher than the theory predicts.

Registry No. $Fe(CN)_6^{4-}$, 13408-63-4; $Fe(CN)_6^{3-}$, 13408-62-3.

LITERATURE CITED

(1) Matsuda, Hiroaki; Ayabe, Yuzo *Z. Elektrochem.* **1955**, *59*, 494–503.
(2) Nicholson, Richard S.; Shain, Irving *Anal. Chem.* **1964**, *36*, 706–723.
(3) Farsang, Gyorgy; Rozsondai, Bela; Tomcsanyi, Laszlo *Magy. Kem. Foly.* **1970**, *76*, 233–236.
(4) Tomcsanyi, Laszlo; Farsang, Gyorgy; Rozsondai, Bela *Magy. Kem. Foly.* **1970**, *76*, 236–240.
(5) Golberg, Michael A. *Solution Methods for Integral Equations: Theory and Application*; Golberg, Michael A., Ed.; Plenum Press: New York, 1976; Chapter 1.
(6) IMSL *MATH/LIBRARY, FORTRAN Subroutines for Mathematical Applications*; IMSL: Houston, TX, 1987.
(7) Adams, Ralph N. *Electrochemistry of Solid Electrodes*; Marcel Dekker: New York, 1969; Chapter 8.

* Author to whom correspondence should be addressed.

John W. Weidner
Peter S. Fedkiw*

Department of Chemical Engineering
North Carolina State University
Raleigh, North Carolina 27695-7905

RECEIVED for review October 31, 1989. Accepted January 29, 1990. This work was supported by a grant from the NASA-Lewis Research Center (NAG 3-649).

Detection of Mass 31 830 Ions with an External Ion Source Fourier Transform Mass Spectrometer

Sir: The analysis of high mass ions by Fourier transform mass spectrometry (FTMS) has been demonstrated in several laboratories (*1–5*). The highest m/z reported thus far is the cesium iodide cluster $[Cs(CsI)_{82}]^+$ at 16 241 daltons (*2*). The spectrometer used for these experiments had a 3-T magnet and a single section trapped ion analyzer cell. Ions were produced by bombarding a cesium iodide sample with a beam of 10-keV cesium ions. Other experiments (*3*) performed with a 7-T magnet and a dual trapped ion analyzer cell have demonstrated that laser desorption FTMS can provide high resolution mass spectra for potassium-attached oligomer ions of poly(ethylene glycol)-8000. A mass resolution of 60 000 was achieved for m/z 5922, and identifiable peaks were obtained up to m/z 9700.

In both of the studies just cited, a direct insertion probe was used to position the sample inside the magnetic field, adjacent to one of the trapping plates of the analyzer cell. Ions produced by a laser pulse or cesium ion bombardment were trapped and detected in the analyzer cell. This method of introducing samples works well in some cases, but the range of applications is limited because volatile components or impurities in the sample increase the pressure in the FTMS analyzer cell and cause a loss of resolution and sensitivity.

Recently, a number of laboratories have begun to work on an alternative approach that is far more flexible: the ion source is placed outside of the magnetic field and is separated from the FTMS analyzer cell by several stages of differential pumping (*4–14*). The first experiments of this type were reported by McIver and co-workers in 1983 (*6*). The ion source of their instrument was a conventional quadrupole mass spectrometer that was outside of the magnet, about a meter from the analyzer cell. A novel feature of the instrument was a second long radio frequency (rf) quadrupole lens that focused the ions and guided them through the fringing fields of the magnet. Without the focusing provided by this lens, ions were not transmitted efficiently to the FTMS analyzer cell because of the magnetic mirror effect (*7, 8*). The first experiments were done with an electron ionization source. Subsequent experiments, done in collaboration with D. F. Hunt and J. Shabanowitz at the University of Virginia, demonstrated that the method could be used for fast atom bombardment (FAB) ionization of small peptides (*9, 10*). Further improvements made by Hunt and co-workers resulted in the first FAB-FTMS mass spectra of porcine insulin at m/z 5777 and horse cytochrome *c* at m/z 12384 (*4*). External ion source FTMS experiments have also be performed by using electrostatic lenses, rather than a rf quadrupole lens, to inject the ions (*11–14*).

Recently, we completed the construction of a new external ion source FTMS instrument that uses a single, long rf quadrupole lens to inject the ions (*5*). This instrument is less complicated than the original external ion source design because only two controls (quadrupole rf voltage level and frequency) are needed to select the range of injected ions. Initial results with the new instrument showed very good sensitivity and a mass resolution of 53 000 at m/z 9746. By use of impulse excitation instead of rf chirp excitation, the upper mass limit of the instrument was extended to 13 000 daltons (*15–17*).

In the present study, we report on the factors that influence the upper mass limit and the range of masses that can be analyzed with the new instrument. With conventional quadrupole mass spectrometers both rf and dc voltages are applied to the rods. This produces a narrow-band mass filter that passes only one m/z value at a time. In contrast, the rf-only operating mode produces a band-pass mass filter that transmits a broad range of masses between certain high mass and low mass cut-offs. To determine these cut-off points, mass spectra of cesium iodide cluster ions have been acquired under various operating conditions.

EXPERIMENTAL SECTION

A schematic drawing and description of the new external ion source FTMS instrument has been published previously (*5*). Briefly, there are three differentially pumped regions that contain an ion source, a rf quadrupole lens, and a FTMS analyzer cell. Pumping restrictions between the regions produce a pressure gradient as large as 40000:1 between the ion source and the analyzer cell. The analyzer cell is centered in the homogeneous region of a horizontal bore, 6-T superconducting magnet manufactured by Oxford Instruments. Control pulses for the ion source, rf quadrupole lens, and FTMS analyzer cell were generated by an OMEGA data system manufactured by IonSpec Corp.

In a typical experiment, a thin layer of cesium iodide is coated on a copper probe tip and inserted into the source region through a vacuum lock. The sample is ionized by a 100-ms pulse from a 10-keV cesium ion gun, and at the same time a 1000-V, 1-MHz sine wave signal is applied to the quadrupole rods. The coherent cyclotron image current signal produced by the ions in the analyzer cell is digitized at a rate of 200 kHz by using a 12-bit analog-to-digital converter. The FFT calculations are done with two zero fills to increase the number of data points across each peak and improve the mass measurement accuracy.

RESULTS AND DISCUSSION

The performance of the new instrument is demonstrated by the mass spectrum in Figure 1 of cesium iodide cluster ions from m/z 1000 to 32 000. The peaks are labeled by the cluster size number n, according to the general formula $[Cs(CsI)_n]^+$. The range from m/z 20 000 to 32 000 is shown expanded ×20 so that the low abundance, high mass peaks can be seen. Figure 2, which is an expanded section from the same mass spectrum, shows the results for the $n = 62$ cesium iodide cluster ion at m/z 16 241. This peak, which was the previous upper mass limit for FTMS, is easily detected by our instrument with quite good signal-to-noise ratio and resolution. The full width at half height is 37 u, giving a mass resolution of $M/\Delta M = 439$. Previously we reported that the narrow-band acquisition mode could be used to get a high-resolution spectrum for the peak at m/z 9746, but this method did not seem to work for the much lower abundance peak at 16 241. The reason for this is not understood at this time.

Figure 1 shows that the present instrument configuration has an upper mass limit of m/z 31 830, which corresponds to the cluster $[Cs(CsI)_{122}]^+$. Strong peaks for other high mass ions at $n = 82$, 87, 97, 102, and 112 are also apparent. Table I compares the measured m/z values for these and other peaks with the exact masses for the various clusters. Even for the high mass ions, the agreement is very good. The measured m/z values are calculated from the measured cyclotron frequencies by using a single calibration equation of the form

$$m = \frac{A}{f} + \frac{B}{f^2} + \frac{C}{f^3} \qquad (1)$$

This equation is applied across the full mass spectrum. The calibration constants A, B, and C are determined by a least-squares fit between the measured cyclotron resonance frequencies, f_i, and the exact masses, m_i, for 11 peaks in the spectrum. The last column in Table I shows that above m/z 20 000 the mass measurement error is a just a few mass units,

0003-2700/90/0362-0878$02.50/0

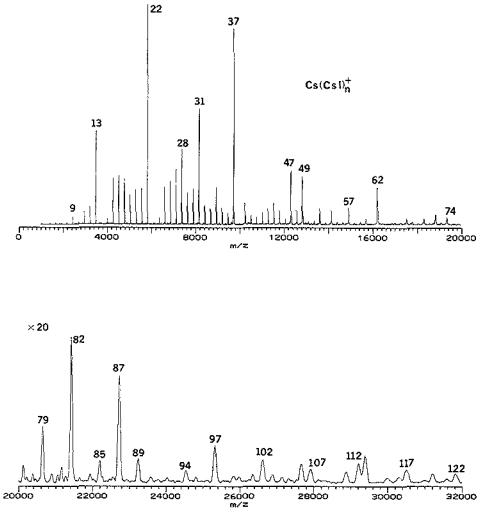

Figure 1. Mass spectrum of cesium iodide cluster ions obtained with an external ion source Fourier transform mass spectrometer. The peaks are labeled by the number of CsI units in the cluster, according to the general formula $[Cs(CsI)_n]^+$.

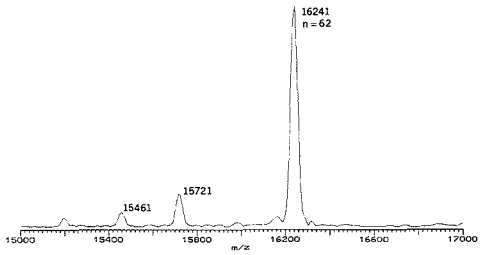

Figure 2. Improved mass resolution and sensitivity achieved for the peak at m/z 16 241, which was the previous upper mass limit for FTMS.

even though the peaks in this range are about 80 u wide. Ijames and Wilkins have shown that even higher mass measurement accuracy (8.59 ppm between m/z 5500 and m/z 6000) can be achieved with FTMS by using ion ejection and narrow-band detection (*3*).

Previous experiments have shown that the transmission efficiency of the rf quadrupole lens depends on the voltage and frequency of the signal that is applied to the rods (*5*). With a rf voltage of 300 V, the upper mass limit is about m/z 6000, and with 600 V, the upper mass limit is about m/z 13 000. The present results show that even higher rf voltage (1000 V) is needed to inject ions in the range 20 000 to 30 000 u. This effect is qualitatively similar to the results of Yost et al. for operation of the rf-only quadrupole that is used as a collision chamber in a triple quadrupole mass spectrometer (*18*). They calculated that the upper mass limit increases as $V^{5/2}$, where V is the rf voltage applied to the quadrupole rods. With the external ion source FTMS instrument, such a strong dependence on V is not observed, and it is likely that the fringing fields of the magnet interact with the quadrupole rf electric field to alter the trajectories of the ions.

Another feature of the quadrupole injection method is that the lower mass cut-off also increases as the rf voltage is increased. For example, in Figure 1 the abundant cesium iodide clusters below m/z 2000 are not seen in the spectrum because they are not transmitted by the quadrupole when a 1000-V, 1-MHz signal is used. This feature is useful for experiments that utilize a fast atom bombardment source because the intense low mass peaks that come from the liquid matrix are prevented from reaching the FTMS analyzer cell. To inject low mass ions, it is necessary to use lower voltages and/or higher frequencies for the rf quadrupole, but then the upper mass limit is also decreased.

Table I. Comparison of Measured Masses and Exact Masses for Cesium Iodide Cluster Ions: $[Cs(CsI)_n]^+$

cluster size, n	measured m/z	exact mass	error
5	1 431.97	1 431.95	0.02
9	2 471.20	2 471.19	0.01
13	3 510.33	3 510.43	−0.10
22	5 848.37	5 848.71	−0.34
31	8 186.83	8 187.00	−0.17
37	9 745.66	9 745.86	−0.20
47	12 343.99	12 343.95	0.04
49	12 864.13	12 863.57	0.56
57	14 939.98	14 942.05	−2.07
62	16 240.98	16 241.09	−0.11
74	19 360.33	19 358.81	1.52
79	20 655.84	20 657.86	−2.02
82	21 435.78	21 437.28	−1.50
87	22 734.50	22 736.33	−1.83
89	23 255.19	23 255.95	−0.76
97	25 336.12	25 334.43	1.69
102	26 633.71	26 633.48	0.23
112	29 229.04	29 231.57	−2.53
117	30 521.04	30 530.62	−9.58
122	31 831.96	31 829.67	2.29

Previous experiments on cesium iodide cluster ions using magnetic sector (*19–21*), time-of-flight (*22, 23*), and Wein filter (*24, 25*) mass spectrometers have shown that the ion currents and relative abundances of the high mass clusters are very low. One of the conclusions of the present study, therefore, is that the FTMS image current detection method has adequate sensitivity for the detection of low abundance, high mass ions up to m/z 30 000. Another conclusion is that the rf quadrupole lens functions like a filter so that a broad range of masses between certain low mass and high mass limits are transmitted to the FTMS analyzer cell. Preliminary experiments have shown that adding a small differential dc voltage to the quadrupole rods causes a narrower range of ions to be injected, just as expected. However, this also causes the injection efficiency to decrease substantially. Now that these general features of the quadrupole injection method have been identified, we plan to develop a quantitative model of the magnetic and electric fields so that ion trajectory calculations can be performed to optimize the design and performance of the instrument.

LITERATURE CITED

(1) Russell, D. H. *Mass Spectrom. Rev.* **1986**, *5*, 167.
(2) Amster, I. J.; McLafferty, F. W.; Castro, M. E.; Russell, D. H.; Cody, R. B., Jr.; Ghaderi, S. *Anal. Chem.* **1986**, *58*, 483.
(3) Ijames, C. F.; Wilkins, C. L. *J. Am. Chem. Soc.* **1988**, *110*, 2687.
(4) Hunt, D. F.; Shabanowitz, J.; Yates, J. R., III;, Zhu, N.-Z.; Russell, D. H.; Castro, M. E. *Proc. Natl. Acad. Sci. U.S.A.* **1987**, *84*, 620.
(5) Lebrilla, C. B.; Amster, I. J.; McIver, R. T., Jr. *Int. J. Mass Spectrom. Ion Processes* **1989**, *87*, R7.
(6) McIver, R. T., Jr.; Hunter, R. L.; Story, M. S.; Syka, J.; Labunsky, M. Presented at the 31st Annual Conference on Mass Spectrometry and Allied Topics, Boston, Massachusetts, May 8–13, 1983.
(7) McIver, R. T., Jr. Apparatus and Method for Injection of Ions into an Ion Cyclotron Resonance Cell, U.S. Patent 4,535,235, Aug. 13, 1985.
(8) McIver, R. T., Jr.; Hunter, R. L.; Bowers, W. D. *Int. J. Mass Spectrom. Ion Processes* **1985**, 64, 67.
(9) Hunt, D. F.; Shabanowitz, J.; McIver, R. T., Jr.; Hunter, R. L.; Syka, J. E. P. *Anal. Chem.* **1985**, *57*, 765.
(10) Hunt, D. F.; Shabanowitz, J.; Yates, J. R., III; McIver, R. T., Jr.; Hunter, R. L.; Syka, J. E. P.; Amy, J. *Anal. Chem.* **1985**, *57*, 2728.
(11) Kofel, P.; Allemann, M.; Kellerhals, H. P.; Wanczek, K. P. *Int. J. Mass Spectrom. Ion Processes* **1985**, *65*, 97.
(12) Kofel, P.; Allemann, M.; Kellerhals, H. P.; Wanczek, K. P. *Int. J. Mass Spectrom. Ion Processes* **1986**, *72*, 53.

(13) Alford, J. M.; Williams, P. E.; Trevor, D. J.; Smalley, R. E. *Int. J. Mass Spectrom. Ion Processes* **1986**, *72*, 33.
(14) Smalley, R. E. *Anal. Instrum.* **1988**, *17*, 1.
(15) McIver, R. T., Jr.; Hunter, R. L.; Baykut, G. *Anal. Chem.* **1989**, *61*, 489–491.
(16) McIver, R. T., Jr.; Hunter, R. L.; Baykut, G. *Rev. Sci. Instrum.*, **1989**, *60*, 400.
(17) McIver, R. T., Jr.; Baykut, G.; Hunter, R. L. *Int. J. Mass Spectrom. Ion Processes* **1989**, *89*, 343.
(18) Yost, R. A.; Enke, C. G.; McGilvery, D. C.; Smith, D.; Morrison, J. D. *Int. J. Mass Spectrom. Ion Phys.* **1979**, *30*, 127.
(19) Dunlap, B. I.; Campana, J. E.; Green, B. N.; Bateman, R. H. *J. Vac. Sci. Technol., A* **1983**, *1*, 432.
(20) Campana, J. E.; Colton, R. J.; Wyatt, J. R.; Bateman, R. H.; Green, B. N. *Appl. Spectrosc.* **1984**, *38*, 430.
(21) Hwang, H. J.; Sensharma, D. K.; El-Sayed, M. A. *J. Phys. Chem.* **1989**, *93*, 5012.
(22) Honda, F.; Lancaster, G. M.; Fukuda, Y.; Rabalais, J. W. *J. Chem. Phys.* **1978**, *69*, 4931.
(23) Ens, W.; Beavis, R.; Standing, K. G. *Phys. Rev. Lett.* **1983**, *50*, 27.
(24) Aberth, W. *Anal. Chem.* **1986**, *58*, 1221.
(25) Aberth, W. *Int. J. Mass Spectrom. Ion Processes* **1986**, *68*, 209.

[1]Current address: IonSpec Corporation, 17951 Skypark Circle, Suite K, Irvine, CA 92714.

Carlito B. Lebrilla
Diana T.-S. Wang
Richard L. Hunter[1]
Robert T. McIver, Jr.*

Department of Chemistry
University of California
Irvine, California 92717

RECEIVED for review September 25, 1989. Accepted January 24, 1990. Funding for the construction of the external ion source FTMS instrument was provided by a grant from the National Institutes of Health (GM34327). C.B.L. was supported by a postdoctoral fellowship from the University of California President's Fellowship Program.

New research grade GC/LC/MS/DS gives you more than you'd expect...

1. New MS Engine: *the* high performance, mid-priced quadrupole mass spectrometer. Its open structure keeps all your application options open.

2. Low picogram to low femtogram sensitivity, full-scan and SIM.

3. Research versatility with GC/MS, thermospray and particle beam LC/MS, EI, CI, NCI, DCI, DIP.

4. Autoswitching, programmable EI/CI source for ease of use.

5. Differential pumping for flexibility and optimum CI.

6. Optional 2000 amu mass range for high molecular weight analysis.

7. New thermospray source for higher sensitivity and increased fragmentation.

8. New higher sensitivity particle beam LC/MS for EI, CI and NCI spectra.

9. Multitasking MS ChemStation (HP-UX series) with X Window System based software for efficient operation and easy networking.

10. Top rated quality, reliability and support.

...for less than you'd expect.*

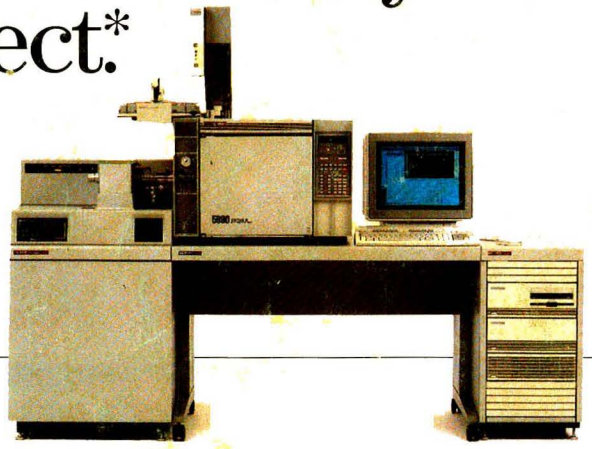

Our new MS Engine system brings you the highest performance in its class. At the lowest price in its class. Along with the sensitivity, reproducibility, versatility and reliability you need for demanding research, methods development and service laboratory applications. Add to this HP's acclaimed support, and the deal gets even better.

The MS platform for the 1990s, this flexible system combines HP's advanced GC and/or LC technologies plus our multitasking MS ChemStation with X-Windows. For information, call **1 800 556-1234, Ext. 10227.** In CA, call **1 800 441-2345, Ext. 10227.**

X Window System is a trademark of Massachusetts Institute of Technology

HEWLETT PACKARD

* Under $125,000 (U.S. list price) for a complete standard GC/MS/DS system, including EI/CI source.

CIRCLE 60 ON READER SERVICE CARD